BERICHTE
aus dem Fachbereich Geowissenschaften
der Universität Bremen

No. 249

Krastel, S., M.J. Beld, I. Bouimetarhan, M. Brüning, K. Enneking,
J.A. Felzenberg, G. Fischer, J. Geersen, T.J.J. Hanebuth, R. Henrich,
D.C. Heslop, M. Höcker, J. Hoffmann, C. Holz, A. Hübner, B. Kockisch,
M. Kölling, K.M. Mara, N. Nowald, R. Pierau, U. Proske, C. Reuter,
L. Schnieders, H.D. Schulz, T. Truscheit, M. Urlaub, T. Vogt,
R.B. Wynn, L. Zühlsdorff

REPORT AND PRELIMINARY RESULTS OF RV METEOR CRUISE M65/2, DAKAR - LAS PALMAS, 04.07. - 26.07.2005.

Berichte, Fachbereich Geowissenschaften, Universität Bremen, No. 249, 185 pages,
Bremen 2006

ISSN 0931-0800

Die "Berichte aus dem Fachbereich Geowissenschaften" werden in unregelmäßigen Abständen vom Fachbereich 5, Universität Bremen, herausgegeben.

Sie dienen der Veröffentlichung von Forschungsarbeiten, Doktorarbeiten und wissenschaftlichen Beiträgen, die im Fachbereich angefertigt wurden.

Die Berichte können bei:

Frau Monika Bachur

Forschungszentrum Ozeanränder, RCOM

Universität Bremen

Postfach 330 440

D 28334 BREMEN

Telefon: (49) 421 218-65516

Fax: (49) 421 218-65515

e-mail: MBachur@uni-bremen.de

angefordert werden.

Diejenigen Titel, die nur online verfügbar sind, finden Sie unter:

http://elib3.suub.uni-bremen.de/publications/diss/html

Zitat:

Krastel, S. and cruise participants

Report and preliminary results of RV METEOR Cruise M65/2, Dakar - Las Palmas, 04.07. - 26.07.2005.

Berichte, Fachbereich Geowissenschaften, Universität Bremen, No. 249, 185 pages, Bremen 2006.

ISSN 0931-0800

BERICHTE
aus dem Fachbereich Geowissenschaften
der Universität Bremen

No. 249

Krastel, S., M.J. Beld, I. Bouimetarhan, M. Brüning, K. Enneking,
J.A. Felzenberg, G. Fischer, J. Geersen, T.J.J. Hanebuth, R. Henrich,
D.C. Heslop, M. Höcker, J. Hoffmann, C. Holz, A. Hübner, B. Kockisch,
M. Kölling, K.M. Mara, N. Nowald, R. Pierau, U. Proske, C. Reuter,
L. Schnieders, H.D. Schulz, T. Truscheit, M. Urlaub, T. Vogt,
R.B. Wynn, L. Zühlsdorff

REPORT AND PRELIMINARY RESULTS OF RV METEOR CRUISE M65/2, DAKAR - LAS PALMAS, 04.07. - 26.07.2005.

Berichte, Fachbereich Geowissenschaften, Universität Bremen, No. 249, 185 pages,
Bremen 2006

ISSN 0931-0800

Table of Contents

1 Participants

Name	Discipline	Institution
Krastel, Sebastian, Dr.	Hydroacoustics, Chief-Scientist	GeoB / RCOM
Beld, Maaike Johanna	Micro-Paleontology	GeoB / RCOM
Bouimetarhan, Ilham	Micro-Paleontology	FSR
Brüning, Markus	Hydroacoustics	GeoB / RCOM
Enneking, Karsten	Geochemistry	GeoB / RCOM
Felzenberg, Janice Ann	Hydroacoustics	WU
Fischer, Gerhard, Dr.	Marine Geology	GeoB / RCOM
Geersen, Jacob	Hydroacoustics	GeoB / RCOM
Hanebuth, Till J.J., Dr.	Sedimentology	GeoB / RCOM
Henrich, Rüdiger, Prof. Dr.	Sedimentology	GeoB / RCOM
Heslop, David Christopher, Dr.	Marine Geophysics	GeoB / RCOM
Höcker, Mathias	Marine Geophysics	GeoB / RCOM
Hoffmann, Jan	Geochemistry	GeoB / RCOM
Holz, Christine, Dr.	Sedimentology	GeoB / RCOM
Hübner, Anne	Micro-Paleontology	GeoB / RCOM
Kockisch, Brit	Sedimentology	GeoB / RCOM
Kölling, Martin, Dr.	Geochemistry	GeoB / RCOM
Mara, Karim Moulaye	Observer Senegal	Sen. Navy
Nowald, Nicolas, Dr.	Marine Geology	GeoB / RCOM
Pierau, Roberto	Sedimentology	GeoB/RCOM
Proske, Ulrike	Sedimentology	GeoB / RCOM
Reuter, Christian	Sedimentology	GeoB / RCOM
Schnieders, Luzie	Geochemistry	GeoB / RCOM
Schulz, Horst D., Prof. Dr.	Geochemistry	GeoB / RCOM
Truscheit, Thorsten	Meteorology	DWD
Urlaub, Morelia	Hydroacoustics	GeoB / RCOM
Vogt, Thomas	Hydroacoustics	GeoB / RCOM
Wynn, Russell B., Dr.	Sedimentology	NOC
Zühlsdorff, Lars, Dr.	Hydroacoustics	GeoB / RCOM

GeoB/RCOMFachbereich Geowissenschaften /Forschungszentrum Ozeanränder, Universität Bremen

FSR Mohammed V – Agadal University, Rabat, Morocco

WU Wesleyan University, Wesleyan Station, Middletown, Connecticut, USA

DWD Deutscher Wetterdienst, Geschäftsfeld Seeschiffahrt

NOC National Oceanographic Centre, Southampton, UK

2 Research Program

Research Objectives

The continental margin off Northwest Africa is largely shaped by a complex interplay of sediment transport processes directed both downslope and along-slope. Where and how sediment 1) is exported from the shelf, 2) is deposited on the continental slope or 3) reaches the deep-sea basin depends on a wide variety of relevant factors such as seabed morphology, climate, sea level fluctuations, slope stability, oceanographic regime, and sediment sources. Sediment transport across slopes is quite variable and includes suspended bottom-current transport as well as mass wasting by slumps, slides, and debris flows. Sediment transport may occur in open-slope environments or might be confined in gullies, canyons or channels. The patterns can be further complicated by contour currents inducing along-slope sediment transport. Main target of Meteor-Cruise M65/2 is to develop sedimentary and evolutionary models for the sedimentation dynamics off NW-Africa and to establish quantitative sediment budgets in relation to climate controlled variable sediment supply. The investigations are carried out by the DFG Research Center 'Ocean Margins' at the University of Bremen.

Sedimentation processes off Mauritania were already studied during Meteor-Cruise M58/1 in 2005. The data clearly show that even at the arid, presumably sediment-starved, continental margin off Mauritania with the Sahara in its hinterland, sediment transport operates with different rates and styles, including a significant transfer of land-derived terrigenous and hemipelagic sediments to the deep sea. During Meteor-Cruise M65/2 the investigations of sediment transport processes were expanded to the south. It was originally proposed to study the tropical areas off Senegal, The Gambia, Guinea-Bissau and Guinea, where large amounts of sediments were delivered by numerous rivers. Due to missing permissions for the waters of Guinea-Bissau, only the continental margin off Senegal and The Gambia was studied. Main scientific targets in this area are:

- To investigate the relationship of morphological structures and sedimentary deposits on a subtropical shelf on the one hand and pathways and deposits of gravity driven sediment transport on the upper and middle continental slope on the other hand.
- To develop a model, which describes the transport dynamics of the sediments from shallow water into the deep sea and which will extend the existing models for the subtropical aspect.
- To quantitatively evaluate the importance of sediment composition, amount of sediment input, the relief of the ocean margin as well as the oceanographic regime on lateral sediment transport by means of numerical modeling.

One of the most unexpected results of Meteor-Cruise M58/1 was the discovery of a spectacular meandering slope channel off Cap Timiris at ~19°45'N. The canyon was surveyed by us for ~215km from the shelf edge to ~3000m water depth. To further study the formation and evolution of the canyon, we continued our investigations especially at the shelf edge and the previously not studied distal canyon. The specific aims are:

- To study the geometry, age and sediment sources of the fluvial system, which relicts are preserved on the shelf.
- To analyze the sediment transport pathways based on a study of drainage-and currents systems on the shelf and on the upper continental margin.

To analyze the sedimentation processes of distal Cap Timiris Canyon

Another working area is located in the central upwelling zone off Cap Blanc with the objective of studying the seasonal and interannual variability of the particle flux. Additionally the dinoflagellate cyst distribution in surface sediments and surface waters as well as the isotopic composition of Thoracosphaera heimii cysts will be studied in all working areas.

Scientific Program

Hydroacoustics

Hydroacoustic data collected off Senegal and The Gambia will be used to map the extension of individual slide bodies and to estimate their volumes. A regional stratigraphy will be established to analyze temporal changes in number, frequency and size of mass wasting events. The structure of deltas, drift bodies and other sedimentary features will be investigated in a similar way. The acoustic data will be used to analyze sediment transport processes on a tropical continental margin. The data will provide the basis for the development of models describing the transport dynamics of sediments from shallow waters into the deep sea.

The acoustic data collected in the head region of Cap Timiris Canyon should help to reconstruct the formation and evolution of the canyon. This data will allow to study sediment transport pathways and their temporal variability.

Additionally, the acoustic data will provide the basis for selecting coring locations. The larger penetration of the seismic data allows to analyze near surface processes while taking into account an adequate temporal and structural framework.

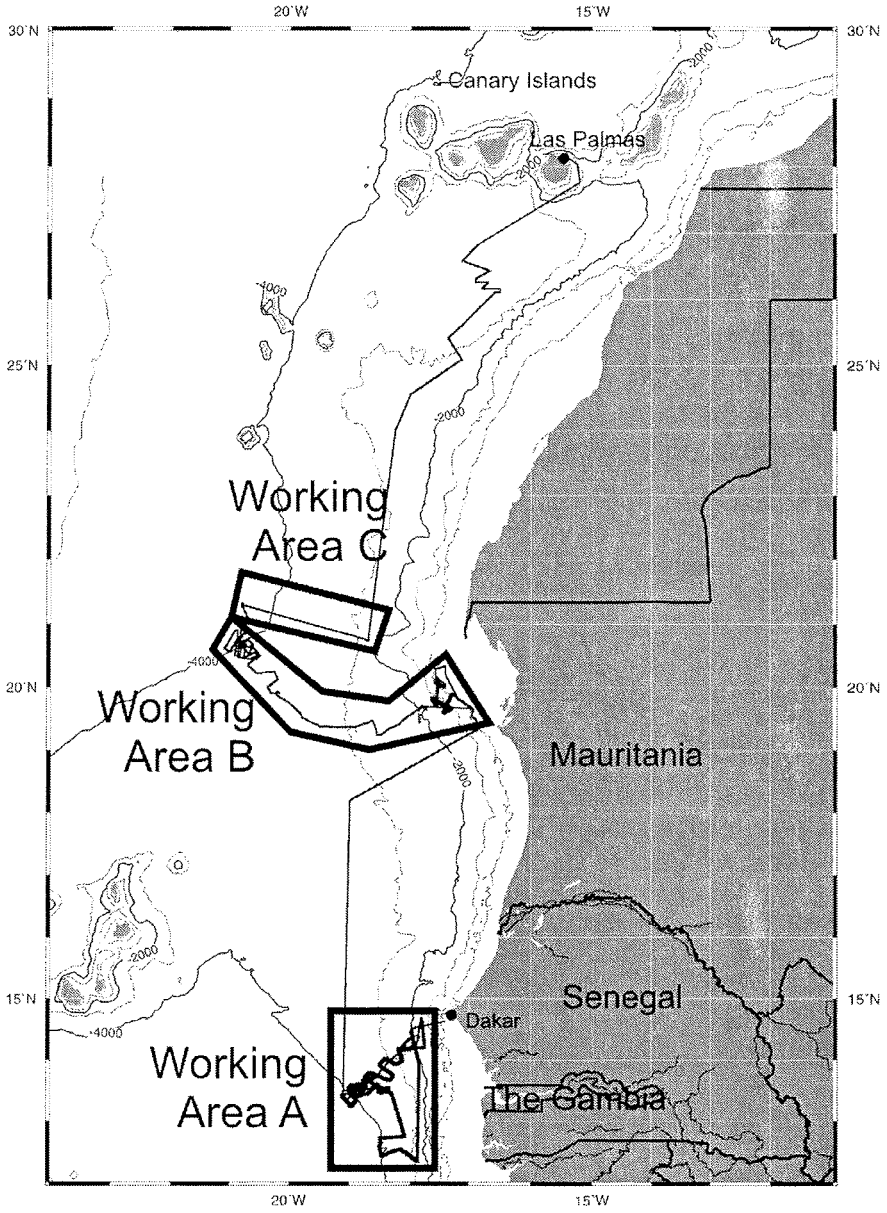

Fig. 2.1: METEOR Cruise M65/2, working areas and cruise track.

Sedimentology

The sedimentological program focuses on two main objectives: i) to investigate the sedimentation processes on the continental slope and ii) to link them to the sedimentary history of the associated shelf system. At the slope, deposits of individual mass wasting events will be mapped and interpreted with regard to their spatial and temporal distribution and reliable sediment accumulation budgets will be calculated. The study will specifically concentrate on the internal sedimentary structures of single events to distinguish between lateral (current-driven) and downslope (gravity-driven) transport mechanisms. In a next step, the different types of gravity mass movement deposits will be characterized to interpret the transport mechanism which was active during the event. Moreover, detailed analysis of the sediment composition will help to identify their original source region and material mixing processes along their transport path.

The sedimentological studies on the outer shelf and at the shelf break will use defined sedimentary structures that are typical for shelf systems such as ancient, now refilled incised valleys, mud belts and drowned coastlines. The stratigraphical position of these often laterally isolated deposits will be determined by age control and correlation. In the following, the depositional environment and sedimentary processes leading to these deposits will be interpreted to identify the sediment source, the kind of transport pathway and the reason of final deposition.

Geochemistry

The main goals of the geochemistry group on this leg are providing a preliminary stratigraphy from measuring the elementary composition of the solid phase using the well established portable XRF. We also plan a rough dating of young mass wasting events by measuring and modeling the pore water composition.

It has been shown that the elementary composition of undisturbed sequences of sedimentary records may be very successfully used for developing a fast offshore stratigraphic frame by correlation with oxygen isotope dated standard element profiles. A core characterized by deposition in the Cap Timiris Canyon (discovered on M58/1) was dated using this method. It could be shown that this part of the inner canyon even had a higher sedimentation rate than the levees.

As the specific characteristics of well understood early diagenetic processes can now be recognized in concentration profiles of the pore waters, it is possible to identify their disturbance by mass movements. In non-displaced sediments, the pore water concentration is determined by stationary conditions that result from concurrent early diagenetic reactions and diffusive transport processes. For example, sulfate profiles in pore waters of high productivity areas, typically show that sulfate and methane react at a depth of several meters below the sediment surface. At this depth, sulfate is completely consumed and recharged from the bottom water by diffusion. The resulting linear concentration gradient to the reaction horizon may be used to calculate the release of methane from the deeper sub-bottom strata. A displacement of material by mass wasting events massively modifies this concentration profile. After redeposition new stationary conditions will develop according to the geochemical environment. The readjustment gradually evolves and typically requires approximately 1,000 to 2,000 years to equilibrate. The intermediary stages of this process offer excellent possibilities to determine the age of sediment redeposition.

Marine Geophysics

Sedimentation on the shelf and the continental slope will be characterized by sediment physical data. Magnetic parameters are suitable to differentiate between different source areas and transport mechanisms of terrigenous material. Density and compressional wave velocity as basic parameters of acoustic methods will be used to compare local sediment characteristics as inferred from core data with results from profiling methods. This will give us the chance to transfer detailed local information into a larger area. On the other hand we are able to scrutinize the interpretation of profiling data with results from specific locations.

Additionally, color composition as well as structural anomalies (e.g. slumps, turbidites, sand layers, etc.) should be inferred from high-resolution imaging data determined with the Geotek multi-sensor core logger. Color changes may reflect variations in sediment input and deposition. As yet, investigations regarding the sediment color have been mainly performed with respect to the red/blue ratio, since the data were restricted to specific wave length bands. The now available digital images span nearly the complete color spectrum allowing a more detailed interpretation.

Some of the coring locations may not provide a continuous sedimentary sequence. Nevertheless, the listed methods should allow at least the characterization of contrasting sedimentation conditions.

Micro-paleontology

Organic- and calcareous-walled dinoflagellate cysts are useful tools in reconstructing past oceanographic conditions. They can be used to reconstruct surface water conditions such as sea-surface-temperature, sea-surface-salinity, stratification of the upper water column, and nutrient content. For accurate use of these cysts detailed information is needed about their biology and fossilisation of organic- and calcareous-walled dinoflagellate cysts in the water column and surface sediments.

Recently it has been discovered that individual dinoflagellate cyst species have different degradation constants and method has been developed that uses the difference in degradation rates of organic-walled dinoflagellate cysts, to separate degradation and productivity and quantify past upper ocean productivity changes and bottom/pore water oxygen concentration. This method has been successfully applied to solve previously existing discrepancies between productivity reconstructions of the Late Quaternary Benguela upwelling system by using the different degradation rates of organic-walled dinoflagellate cysts. To asses the species-specific degradation constants of individual cyst species, it is essential to have information about the degradation rates of the cysts in relation to the exposed oxygen concentration, oxygen exposure time (sedimentation

rates) and bioproductivity in the upper water column.

Another recent discovery is that the isotopic composition of the wall of the calcareous dinoflagellate cyst Thoracosphaera heimii reflects the temperature conditions of the upper water column where it is formed; the deep chlorophyll maximum. To use the stable isotope composition of calcareous dinoflagellate cysts for estimating the role and influence of tropical surface water masses as well as the variability of the intermediate and deep water circulation of the region on climate change, detailed information of the cyst distribution in surface sediments, surface waters as well as the isotopic composition of T.heimii cysts in situ, is required.

Particle flux

Another major topic of the scientific program are investigations of particle fluxes and particle transport in the water column. During the cruise, mooring CB located about 200 nm off Cap Blanc (Mauritania) shall be recovered and redeployed. This site operated since 1988 is located at the edge of the Cap Blanc filament in about 4100 m water depth. One additional mooring CBi, located about 80 nm closer to the coast shall be recovered and redeployed. This eutrophic site located in 2600 m water depth in the coastal upwelling off Mauretania is operated since about two years. Both sites are influenced by the NE trade winds being part of the North Atlantic climate system. They are characterized by enhanced supply of terrigenous material, mainly dust particles which may be important as ballast for the transfer of organic carbon to the deep sea. The spatial and temporal distribution of productivity and biomass and the supply of dust particles to the ocean will be monitored by satellite imagery (SeaWIFS) and shall be compared to the patterns of particles fluxes. In addition to the sediment trap mooring work, a profiling digital particle camera will be used on a transect off Cap Blanc to document the distribution of larger particles in the water column. Repeated sampling at the projected stations will allow to record temporal changes in particle distributions and vertical and horizontal particle transport processes. These studies will be complemented by CTD profiles and sampling of larger particles with NISKIN bottles.

3 Summarized Cruise Report

The main group of the scientific party arrived in Dakar on July 2nd in the evening. All containers were already stored on Meteor and July 3rd was used for setting up the equipment. We left the port of Dakar as scheduled on July 4th at noon heading west. The scientific crew of Meteor-Cruise M65/2 included 24 scientists from the DFG Research Center Ocean Margins and the Department of Geosciences at Bremen University, one scientist each from National Oceanographic Centre, Southampton (UK), Wesleyan University (US), and Mohammed-V Agdal University (Rabat, Morocco), as well as a technician from the German Weather Service, and a Senegalese Observer.

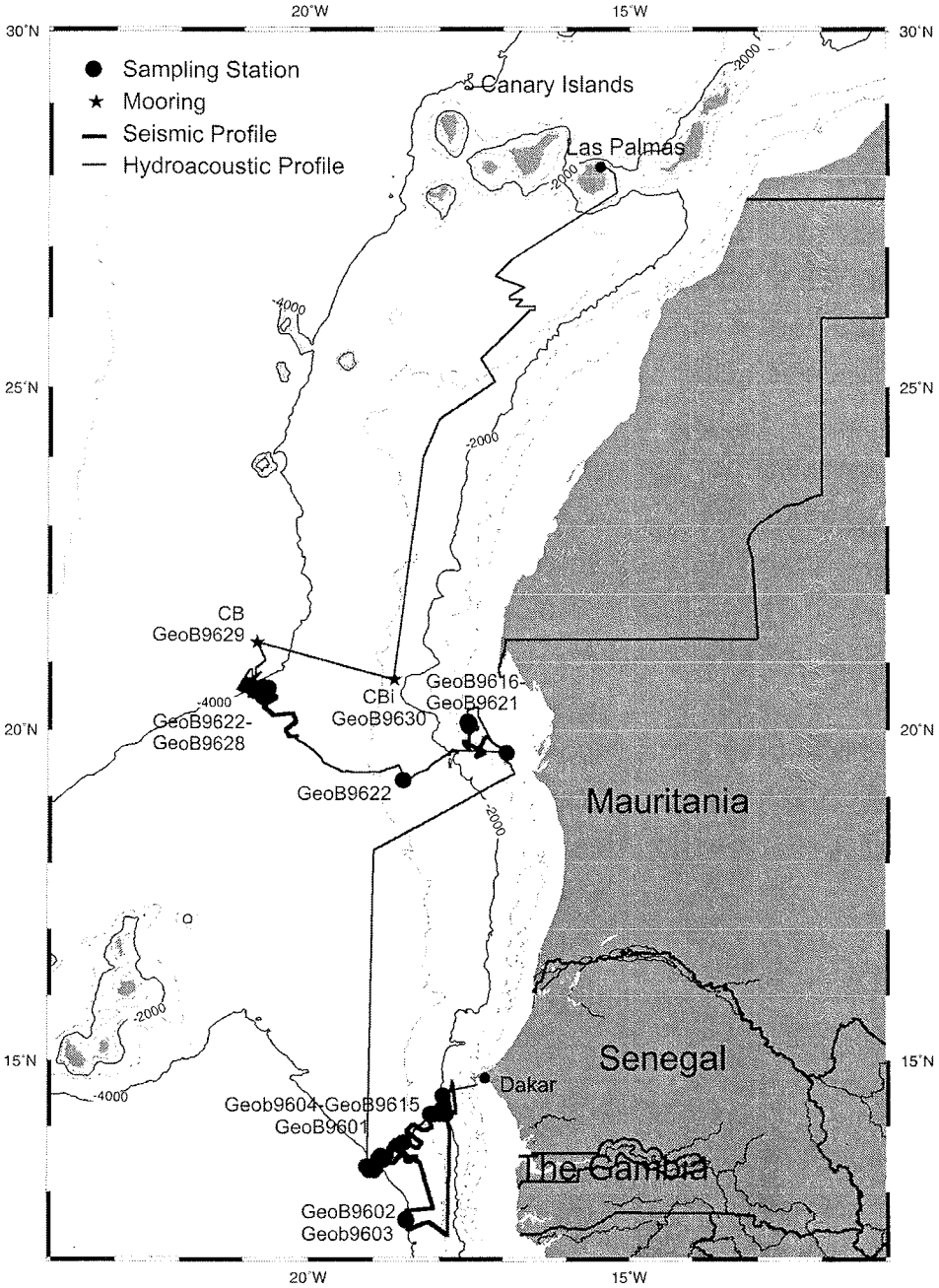

Fig. 3.1: Meteor Cruise M65/2, cruise track and core- and mooring locations.

As we did not receive permission for the waters of Guinea Bissau, which was one of our proposed main working areas, we decided to concentrate our work off the coast of Senegal and The Gambia for the first half of the cruise. After leaving the 3-mile-zone we started the scientific work at 13:25h on July 4th by switching on the hydroacoustic systems Parasound and Hydrosweep in order to search for a first sediment sampling station. On our first profile we crossed a small slump in 1500m water depth. At ~2000m water depth we changed our course to the south following the 2000m contour. On this profile we had our first crossing of Dakar Canyon, which is ~350m deep and 5km wide at this location. We decided to have our first station (GeoB9601) immediately north of Dakar Canyon, where we used a water sampler, a multicorer, and a gravity-corer. The 740cm-long gravity core shows undisturbed hemipelagic sediments throughout the core.

Thereafter, we deployed the multichannel seismics. Recording of seismic data started on July 5th at 2:38h along a profile running south parallel to the coastline in ~2000m water depth as far as we were allowed to go without entering the waters of Guinea-Bissau. On our way we crossed a slump in direct vicinity of Dakar canyon but most parts of the profile show well-stratified sediments without any indications of large scale downslope sediment-transport. Even off the Gambia-River with its supposed large fluvial sediment input we neither see indications for significant sediment transport on the open slope nor in a submarine channel. A number of small diapers and submarine canyons (including Diola and Mandingo canyons) were imaged further to the south. On July 6th early in the morning we changed course to the west and ran two profiles downslope up to ~4000m water depth. On these profiles we passed a very powerful cloud cluster with very heavy rain showers and a thunderstorm, which was accompanied by gusts of Beaufort 12 (up to 70kts). This cloud cluster developed during its way to the Caribbean Sea to the Hurricane Emily. Luckily the heavy gusts were short and seismic profiling was not interrupted. While the margin off southern Senegal is relatively stable up to a water depth of ~3000m, several deposits of mass wasting events were imaged seaward of the diapers imaged before in water depths >3000m. However, these deposits are too thick for sampling; hence, we turned to the north and collected an additional seismic profile across Diola Canyon in ~4000m water depth, which is only ~70m deep at this location. After crossing the canyon we retrieved the seismic gear and cored the northern levee of the canyon (Station GeoB9602). A 483cm-long gravity core shows a number of turbidites intercalated in hemipelagic sediments. The attempt to recover a core from the canyon thalweg was not successful (Station GeoB9603).

The seismic and bathymetric data indicate that the locations of the canyons off southern Senegal are structurally controlled and that the depth of the canyons is quickly decreasing with increasing distance from the coast. This indicates that these canyons are not of key importance for downslope sediment transport but we speculate that

sediments delivered by the Gambia River and the numerous smaller rivers further south might be transported on the shelf to the north and than enter the wide and deep Dakar Canyon. Hence, we decided to concentrate our efforts for the next week on Dakar Canyon.

We deployed the seismics on July 7th early in the morning and ran a profile back from the area off southern Senegal to Dakar-Canyon along the 3500m-contour. In contrast to the parallel profile further upslope the lower margin shows clear indication for large scale mass wasting. Very thick transparent units were imaged along large parts of this line. We crossed Dakar Canyon with the seismic system in ~3600m water depth on July 8th ~00:30h and continued the seismic survey with additional crossings of the canyon further upslope until July 9th around noon. In 3600 m water depth the canyon is incised into hemipelagic sediments for ~150m. The incision depth increases to >400m further upslope. The course of the canyon is relatively straight and several terraces were imaged at the canyon flanks. Average canyon width is 3-4km. The canyon floor is almost flat but usually shows a small V-shaped depression indicating young sediment transport through the canyon. The upper most part of the canyon shows a complex pattern with some smaller tributaries and older buried canyons.

Coring around Dakar Canyon started on July 9th in the afternoon. We started with coring a slide mass located close to the canyon. Station GeoB9604 was located inside the slide mass (831cm recovery), Station 9605 north of the slide mass (790cm recovery), and Station GeoB9606 (951cm recovery) was located a little bit further downslope where the Parasound records show thicker slide deposits.

The night was used for collecting additional bathymetric data of the canyon and coring was continued on July 10th at 08:00h with a transect across the canyon. The first core (GeoB9607) was taken at the thalweg of the canyon. As we expected sandy sediments at the thalweg, we decided to use a 3-m-long core barrel, which overpenetrated into the sediments up to the top of the weight. Therefore we used a 12-m long core barrel for the second try and we recovered a 784cm-long very interesting core. The uppermost section of the core (~50cm) shows undisturbed hemipelagic sediments; from there on the frequency and the thickness of turbidites increase, which are overlying a thick slump deposit. The uppermost undisturbed sediments probably represent the Holocene indicating that no significant sediment transport through the canyon occurred in the Holocene, but the canyon was active during Pleistocene times. Thereafter, we took a core on the northern levee (GeoB9608, 908cm recovery), which only showed thin mud turbidites, while some sandy turbidites were found in a 542cm-long core (GeoB9609) on a terrace of the canyon.

The night was used for collecting additional bathymetric data especially of the lower canyon, which were the basis for selecting additional seismic profiles. Seismic profiling

started on July 11th ~10.00h with a profile across the distal canyon in >4000m water depth. The canyon is almost absent on this profile and only some remnants of a levee were identified. Additional seismic profiles show that the canyon is getting shallower very quickly at water depth >3800m. The reason for the sudden decrease of canyon depth is a large slide mass south of the canyon, which filled and therefore destroyed the distal part of the canyon. The last seismic profile of the distal canyon was completed on July 12th at 06:00h and the day was used for taking cores of distal Dakar Canyon. Station GeoB9610 was taken at the thalweg ~60km downslope of the transect described above This core is only 254cm long but again shows a number of turbidites with a coarse grained sandy base. Another 50km downslope two additional cores were taken at the thalweg (GeoB9611) and on the northern levee (GeoB9612), which are 147cm and 878cm long, respectively. Both cores show similar features as described before. The set of three cores of the thalweg of the canyon might allow correlating the individual turbidites between the stations.

The following night was used for collecting additional seismic profiles of the slide, which destroyed the distal canyon. The width of the slide might be >100km. A 30-50m high headwall can be easily identified on several profiles in water depths around 3500m. This is unusually deep for a large mass wasting event. As we identified additional slide deposits in water depth >3000m and slope gradients <0.5° further to the south, slides in great water depth might to be more important than previously estimated.

On July 13th we tried to core the slide (Station GeoB9613) at a location where the cover seems to be thin. A 6-m-long core overpenetrated into the sediments up to the top of the weight; with the following 12-m-core barrel we recovered 980cm of sediments. A first visual inspection suggested that we did not reach the slide, though we cannot exclude that we hit a relatively intact slide block. The rest of the day was used for two additional gravity-cores (Stations GeoB9614 and 9615). One station was located at a depression of the slide which seems to be filled with turbidites and the second core was in the prolongation of Dakar Canyon. Both cores show a large number of turbidites suggesting that the confined flows travelling downslope in Dakar Canyon spread over a large area further downslope once they canyon was destroyed by the slide described above.

On July 14th at 02:16 we completed our work off Senegal and started our transit to Cap Timiris Canyon off Mauritania. For the first part of the transit we chose a northerly course along 19°W longitude. This track allowed us to extend existing hydroacoustic data collected during Meteor-Cruise M58/1 to greater water depth. On this transit we crossed a number of interesting seafloor structures, such as numerous canyons (some of them with exceptionally well developed terraces) and the distal Mauritania Slide Complex. The width of the youngest debris flow of this slide complex is ~30km in 3500m

water depth, while its thickness exceeds 20m. The southern and the northern edge of the debris flow are clearly identified on the Parasound records as depositional boundaries.

At 18°12'N, 19°00'W we changed course to NE and headed for the source area of Cap Timiris Canyon. Cap Timiris Canyon was discovered by us during Meteor-Cruise M58/1. The Cap Timiris Canyon runs westwards from the shelf break to a depth of at least 4000 m and is ~500 km long. The dominantly V-shaped and deeply entrenched canyon exhibits many fluvial features including dendritic, meander, and braiding patterns, a cut-off loop and terraces, and is presently incising. We ascribe canyon origin to an ancient river system in the adjacent presently arid Sahara Desert that breached the shelf during a Plio/Pleistocene sea level lowstand and delivered sediment directly into the slope area. To further prove this hypothesis we collected additional seismic data and took sediment cores in the head region of the canyon.

On July 15th at 17:00h we started a Parasound survey of the shelf, thereby also crossing a structure north of the head region of the canyon, which was previously interpreted as mud belt. The following morning was used for taking 5 giant box corers and a number of water samples (Stations GeoB9616-9620) in an area of a sediment wedge and an erosive feature identified on the Parasound records. The giant box corers mainly contained fine sand and numerous shells and shell fragments. As we also wanted to recover longer cores from the shelf we took a 3m-long Kastenlot (Station GeoB9618) but unfortunately the Kastenlot bent caused by a massive layer of shells in ~1.5m subbottom depth.

On July 16th in the evening we started to collect seismic data of the proximal part of the canyon from the shelf up to ~1500m water depth. The new seismic data show numerous V- and U-shaped canyons up to 500m deep but also some buried channels and erosional unconformities. This data will help to reconstruct the evolution of the proximal canyon. The seismic gear was recovered on July 17th around noon. Thereafter one additional station (GeoB9621) for sediment and water sampling was chosen on the shelf in the area of the mud belt. A 6m-long core-barrel was filled to the top with a homogenous fine sand including shell fragments and hence contradicting the existence of a mud belt in this area.

The next core (GeoB9622, 10.8m recovery) was taken in 2880m water depth in a cut off loop identified during Meteor-Cruise M58/1. As for all cores pore water was extracted using rhizomes immediately after the core was on deck. The pore water profile shows that the upper 4m of sediments slid less than 20 years ago. Additionally the increasing hydrogen sulphide smell with increasing sediment depth indicates the decay of organic matter under the condition of sulphate reduction. We assume the existence of organic rich clays in deeper layers, which were transported through the canyon from the high

production area at the shelf break. The fact that only a relatively small portion of the clay is deposited in the cut off loop demonstrates the importance of transfer of organic rich matter through the canyon into the deep sea.

Thereafter (18.07 in the morning), we continued the bathymetric survey of Cap Timiris Canyon by following the canyon with a single Hydrosweep profile. The prolongation of the area mapped during Meteor-Cruise M58/1 shows a small section with a tortuous meander pattern but most of the canyon is relatively straight and has a north-westerly direction. Unfortunately, the wind increased to force 7 resulting in a poor quality of the Hydrosweep data. Therefore, we decided to stop the Hydrosweep survey and to collect some seismic lines crossing the canyons instead. Seismic profiling started on July 18th at 21:00h. The seismic data show a deeply incised canyon with well developed terraces and right-hand levees but ~500km off the shelf break the depth of the canyons decreases suddenly and the canyon shows some distributaries. We retrieved the seismic gear on July 20th at 4.00h and took four gravity cores across the canyon and a distributary. Core GeoB9623 was located on a well developed broad terrace ~50m above the canyon floor. The core bent but we recovered a 2-m-long section showing several turbidites covered by ~20cm of hemipelagic sediments. The thickest turbidite has a coarse grained base consisting of sands and shell fragments. The only possible source area of this turbidite is the shelf demonstrating that coarse grained sediments are transported through the canyon into the deep sea. The 11.33m-long core GeoB9624 is located on the well developed northern levee. This core shows numerous overspill turbidites intercalated in hemipelagic sediments. This core will allow to reconstruct major phases of active sediment transport through the canyon. The attempt to recover a core from the canyon thalweg (Station GeoB9625) failed and the core was empty, but another core (Station GeoB9626) was successfully taken in one of the small distributaries. This 4m-long core shows numerous turbidites indicating that the distributaries are also important pathways for turbidity currents.

During the night from July 20th to July 21st we collected some additional Parasound lines with the aim to analyze the sudden change of the canyon depth and the depositional pattern. The idea that the Canyon was destroyed by the 170ka-old Cap Blanc Slide was not approved by our new data. They clearly show that the slide terminates on the levees and no slide material is found in the canyon itself. The termination of the slide on the levees gives a minimum age of 170ka for the canyon but the occurrence of levee sediments beneath the slide indicates a significant older age of the canyon. July 21st was used for two additional stations. Station GeoB9627 was taken in the most distal part of the canyon and the 3.12m-long core contains numerous turbidites. Station GeoB9628 was located in the area of the Cap Blanc Slide. The 10.68m-long core is characterized by hemipelagic sediments on top of a massive

debrite. This station was also used for a test run of the particle camera up to a depth of 1000m.

The last two days of the scientific program were mainly used to exchange two moorings off Cap Blanc. Work at the mooring station CB ~200nm off Cap Blanc started on July 22nd at 04:00h with a run of the particle camera up to 2000m depth. The mooring CB15 consisting of two sediment traps and one current meter was released at 07:15h. The top buoy was sighted at 07:45h but due to an unfavourable current situation it took until 09:42h to get the top buoy on deck. The mooring was fully recovered at 12:22h. The mooring was in a good condition and the sediment traps and the current meters worked continuously since their deployment in April 2004. Deployment of mooring CB16 with the same design as the recovered mooring started at 14:30h. The time between recovery of the old mooring and deployment of the new mooring was used for a 2000m deep CTD station. The top buoy of the new mooring dived down at 17:49h. The night was used for the transit to mooring station CBi ~80nm to the east. The operation at this station was identical as described above, i.e. a run of the particle camera, a CTD run, and the exchange of mooring CBi2 with CBi3. The top buoy of mooring CBi3 dived on July 23rd at 14:37h. Immediately afterwards we started our transit to Las Palmas. On our way we collected some Parasound data of the headwall region of the Saharan Debris Flow. The second leg of Meteor-Cruise M65/2 ended on July 26th at 07:00h with the arrival in Las Palmas, Spain.

4 Preliminary Results

4.1 Parasound, Hydrosweep and Navigation

(S. Krastel, M. Brüning, J. Felzenberg, J. Geersen, M. Urlaub, T. Vogt, L. Zühlsdorff)

4.1.1 Technical Description and Data Processing

All seismic profiling activities during R/V Meteor Cruise M65/2 as well as most transit passages included continuous operation of two hydro-acoustic systems (Parasound sediment echo sounder and Hydrosweep swath sounder) to determine the sea floor morphology, to characterize and analyze sediment deposition processes and sediment structures, and to provide information about potential coring sites. Both hydro-acoustic data sets were acquired digitally.

The Parasound system works both as a high-frequency narrow beam sounder to determine the water depth and as a low-frequency sediment echo sounder. It uses the parametric effect, which produces additional frequencies through nonlinear acoustic interaction of finite amplitude waves. If two sound waves of a certain frequency (e.g. 18 kHz and 22 kHz) are emitted simultaneously, a signal of the difference frequency (e.g. 4 kHz) is generated. The new signal component is traveling within the emission cone of the original high frequency waves, which are limited to an angle of only 4° for the equipment used. Therefore, the footprint size of 7% of the water depth is much smaller than for conventional systems and both vertical and lateral resolution is significantly improved.

The Parasound system is permanently installed on the ship. The hull-mounted transducer array has 128 elements on an area of ~ 1 m^2. It requires up to 70 kW of electric power due to the low degree of efficiency of the parametric effect. In 2 electronic cabinets, beam forming, signal generation and the separation of primary (18, 22 kHz) and secondary frequencies (4 kHz) is carried out. With the third electronic cabinet in the echo sounder control room, the system is operated on a 24 hour watch schedule.

Since the two-way travel time in the deep sea is long compared to the length of the reception window of up to 266 ms, the Parasound System sends out a burst of pulses at 400 ms intervals, until the first echo returns. The coverage of this discontinuous mode depends on the water depth and produces non-equidistant shot distances between bursts. On average, one seismogram is recorded about every second providing a spatial resolution on the order of a few meters on seismic profiles at 5.0 knots.

The main tasks of the operators are system and quality control and the adjustment of the start of the reception window. Because of the limited penetration of the echo sounder signal into the sediment, only a short window close to the sea floor is recorded.

The Parasound System was equipped with the digital data acquisition system PARADIGMA, which was developed at the University of Bremen [Spieß, 1993]. The data were stored on four exchangeable disc drives of 1.2 GigaByte capacity, allowing continuous recording between 3 and 6 days dependent on water depth and shot rate. The Pentium-processor based PC allows the buffering, transfer and storage of the digital seismograms at very high repetition rates. From the emitted series of pulses usually every second pulse is digitized and stored, resulting in recording intervals of 800 ms within a pulse sequence. The seismograms were sampled at a frequency of 40 kHz with a typical registration length of 266 ms for a depth window of ~200 m. The source signal was a band limited, 2-6 kHz sinusoidal wavelet of 4 kHz dominant frequency with a duration of 2 periods (~500 µs total length).

Already during the acquisition of the data, an online processing was carried out. For all profiles, Parasound sections were plotted with a vertical scale of 200 m. From these plots, first information about variations in sea-floor morphology, sediment coverage and sedimentation patterns along the ship track was provided. To improve the signal-to-noise ratio, the echogram sections were filtered with a wide band pass filter (2.5-5.5 kHz). In addition, the data were normalized to a constant value much smaller than the average maximum amplitude, to amplify in particular deeper and weaker reflections.

During the entire cruise, the combined Parasound/PARADIGMA system worked without significant problems. The storage procedure with exchangeable hard discs worked successfully and data backups could be efficiently produced.

The multibeam echo sounder Hydrosweep on R/V Meteor was routinely used during the cruise. Sounding 59 pre-formed beams over an opening angle of 90 degrees, the hull-mounted system provides an image of the sea floor topography with a path width of twice the water depth. The system operates at a frequency of 15.5 kHz. To compress refraction effects on the outer beams, the system uses a calibration mode to compare depth values of the central and outer beams in order to calculate a mean sound velocity by producing the best fit between both values. This configuration minimizes residual errors to values smaller than 0.5% of water depth [Grant and Schreiber, 1990]. Although data quality partly depends on course, heading, and weather conditions, the Hydrosweep system generally worked very well during the complete cruise.

During the entire cruise, GPS was available and provided high quality navigation data

4.1.2 Preliminary Results

PARASOUND and HYDROSWEEP data were collected along all seismic profiles and transits between stations. The quality of the data is best along the seismic profiles,

because the ship speed of ~5 knots during seismic profiling results in a better lateral resolution and a reduced noise level. No systematic bathymetric mapping was carried out with the HYDROSWEEP system resulting in isolated stripes of bathymetric data along the tracks. As we have not processes the HYDROSWEEP data while being onboard we only present PARASAOUND data of the different working areas in this chapter.

The first main working area was located off the south coast of Senegal (Fig. 3.1). In general we only identified minor indications for gravity controlled sediment transport on the upper slope in this working area. This pattern changes at the lower slope in water depth deeper than ~3000m. Thick deposits of mass wasting events can be found on the PARASOUND data. These deposits, however, are too thick for sampling; hence we decided not to investigate them in detail.

Additionally we identified a number of small diapers and several submarine canyons. Some of the canyons are ~500m deep on the upper slope but their depth decreases quickly with increasing distance from the coast. An example of a Parasound profile crossing the Diola Canyon on the lower slope in~4000m water depth is shown in Fig. 4.1.1.The canyon shows an asymmetrical profile with a gentle dipping ~70m-high southern flank and a steeper >100m-high northern flank. The southern flank shows some terraces. The width of the canyon is ~4km. The higher northern flank is probably a result of overspill turbidites, which are mainly deposited on the right hand flank of the canyon due to the Coriolis force. The sediments south of the canyon are characterized by a wavy subparallel reflection pattern. Transparent layers might indicate slide or slump deposits. Sediment core GeoB9602 was taken on the northern levee of the canyon. The 7-m-long gravity core shows a number of turbidites intercalated in hemipelagic sediments. The attempt to recover a core from the canyon thalweg (Station GeoB9603) was not successful. The quickly decreasing depth of the canyon with increasing distance from the coast indicates that the canyons are not a major pathway for sediment transport to the deep sea. The location of the canyons is probably structurally controlled. From a first profile across Dakar Canyon on our way to the south we had the impression that Dakar Canyon is more important for sediment transport in this region. Therefore Dakar Canyon and its surrounding was our main working area off Senegal.

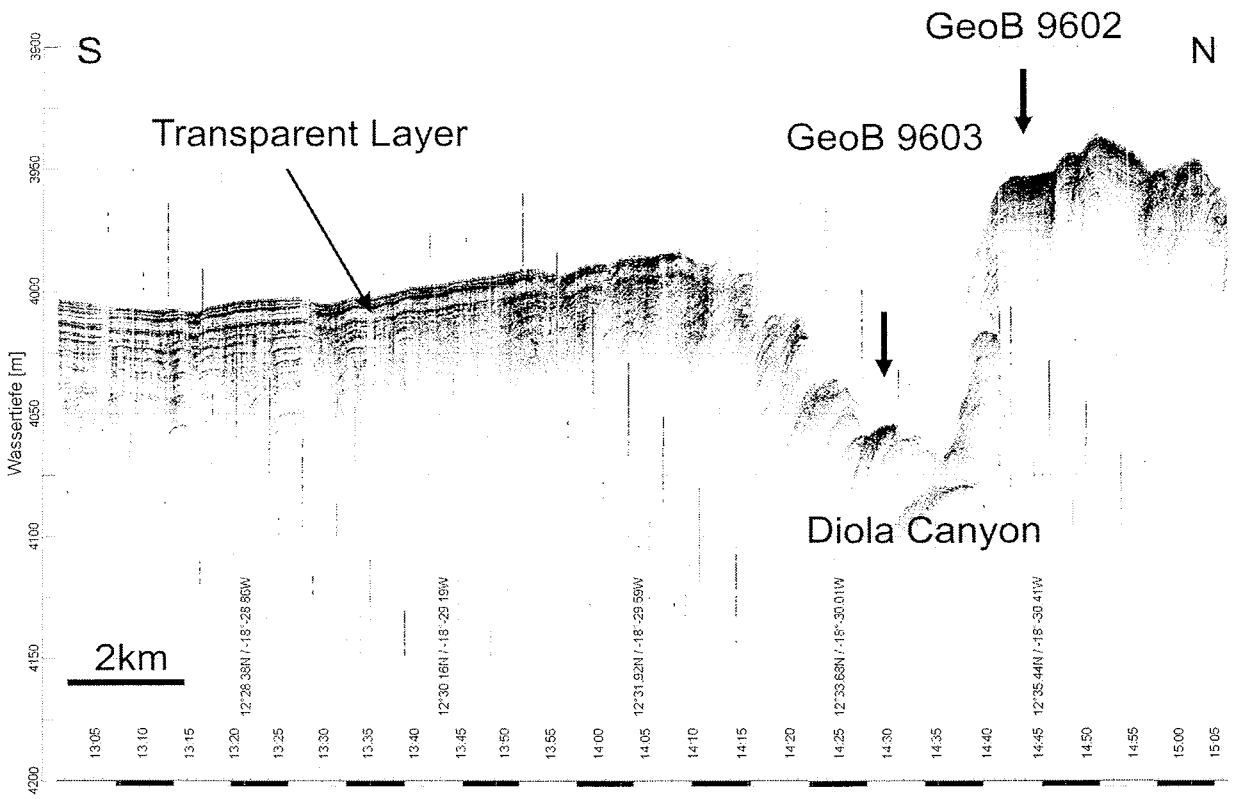

Fig. 4.1.1: PARASOUND Profile GeoB05-053 crossing lower Diola Canyon. See Fig. 4.2.5 for the location of the profile.

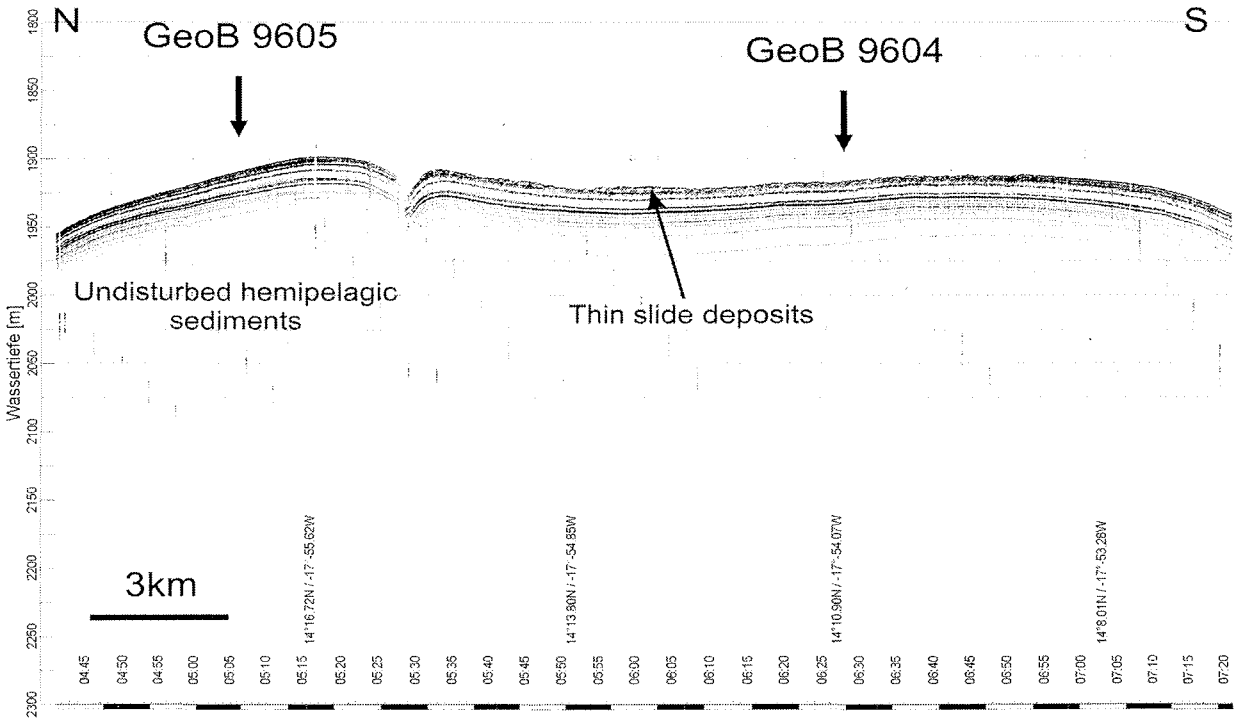

Fig. 4.1.2: Part of Parasound Profile GeoB05-049 crossing a small slide south of Dakar Canyon. See Fig. 4.2.8 for the location of the profile.

PARASOUND Profile GeoB05-049 (Fig. 4.1.2) was collected immediate to the south of Dakar Canyon. The northern part of this profile is characterized be continuous well-stratified reflectors. Thin slide deposits were imaged south of a small gully. A closer inspection of the slide deposits shows that parts of the uppermost sediments are missing, while thin slide deposits are deposited on an older surface. The slide can be traced further downslope, where the deposits become thicker. Parts of the slides seem reach the large Dakar Canyon.

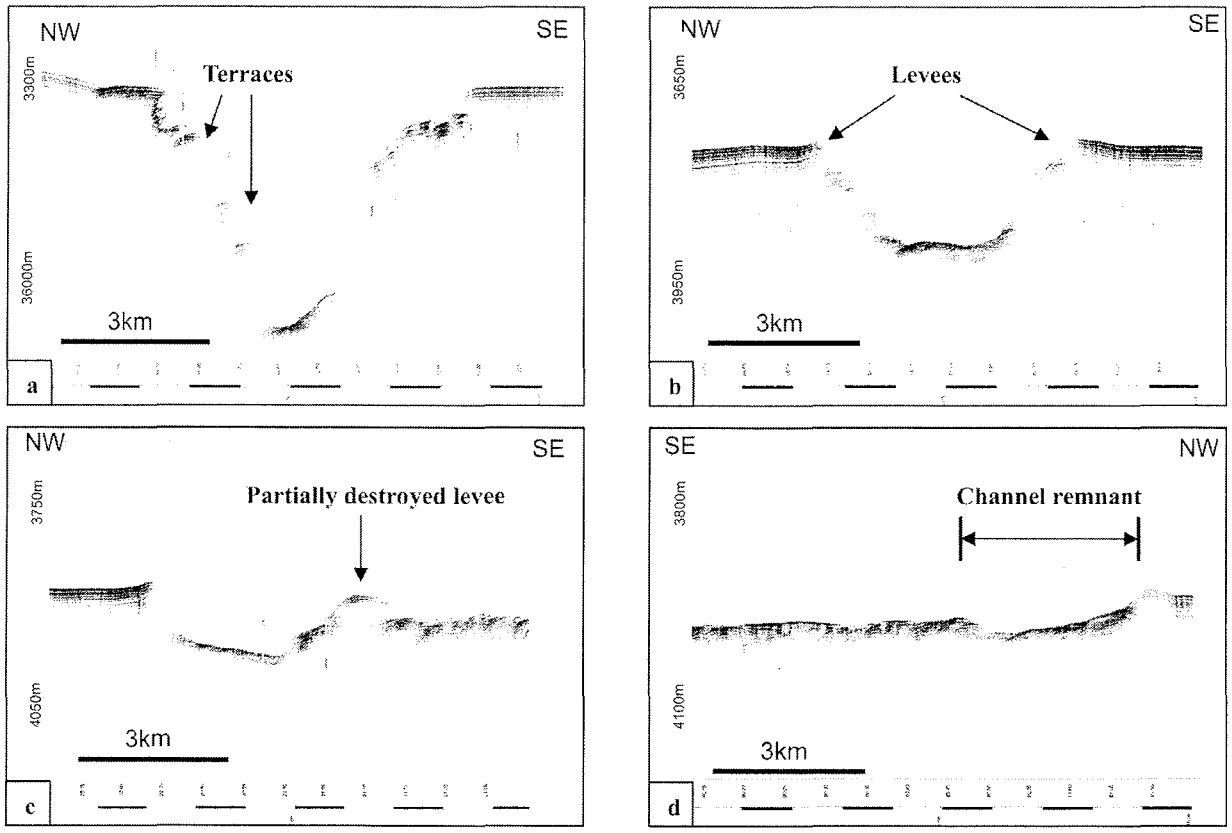

Fig. 4.1.3: Parasound profile crossing Dakar Canyon. Note increasingly drastic changes in canyon morphology towards distal end of Dakar Canyon system. (a) Profile 05-061 (proximal). (b) Profile 05-079. (c) Profile 05-073. (d) Profile 05-075 (plotted in reverse direction).

Numerous PARASOUND profiles were collected across Dakar Canyon. The upper part of the canyon is deeply incised in the slope sediments. Canyon depth reaches ~500m at the upper slope and is still ~300m at 3300m water depth at the lower slope. From there on drastic changes in canyon morphology are visible through the distal Dakar Canyon system (Fig. 4.1.3). The canyon quickly shallows below 3300m water depth. At 3750m water depth (Fig. 4.1.3b) the canyon is ~150m incised into the lower slope sediments, at 3900m water depth the incision depth is <100m (Fig. 4.1.3c), and the channel

disappears completely at 4100m water depth (Fig. 4.1.3d). Canyon width is variable through much of the canyon and generally varies between 3km and 5km though there is an abrupt narrowing beyond 3950m water depth. A number of features typically associated with deep-water canyons, such as levees and terraces, appear in various canyon profiles. In general, terraces are commonly found within the deep, V-shaped proximal canyon, while levees are well-developed in the shallower, U-shaped distal canyon.

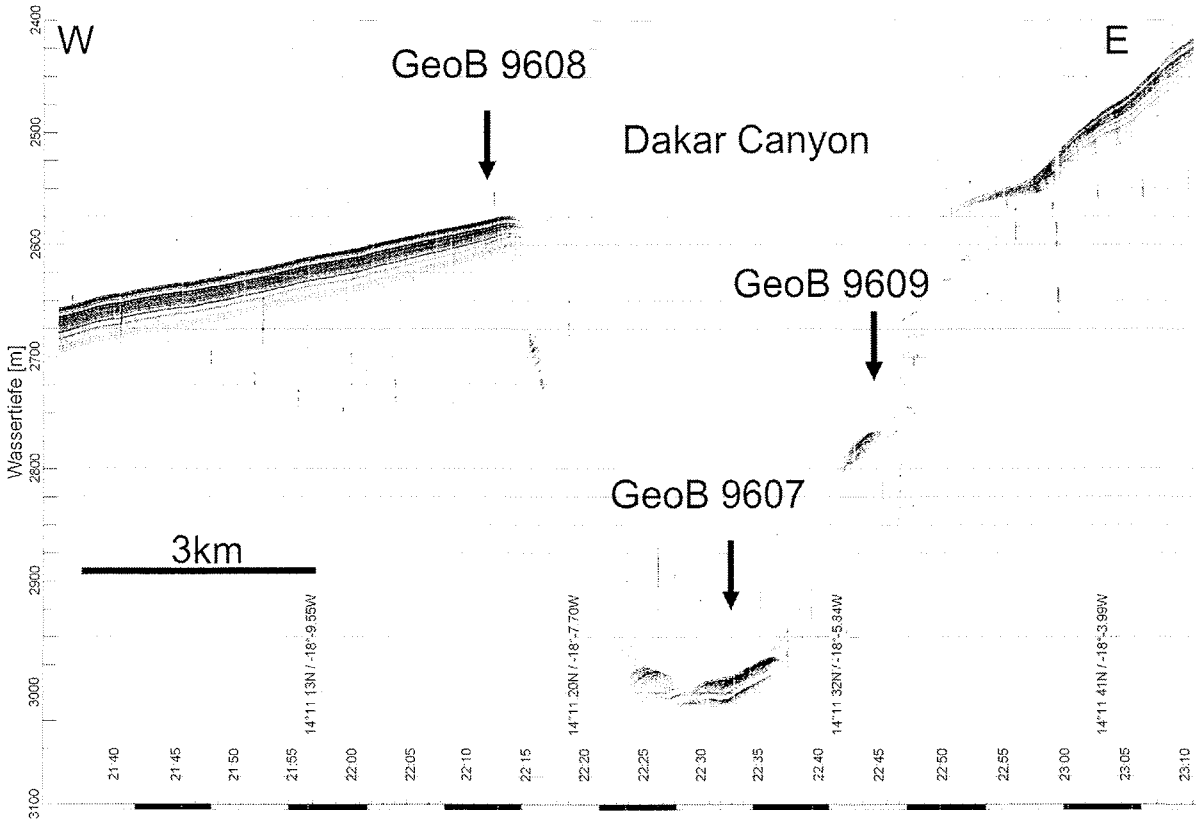

Fig. 4.1.4: Part of PARASOUND Profile GeoB05-066 with stations GeoB9607-9609. Note that the profile crosses the canyon obliquely. The profile crosses upper Dakar Canyon. See Fig. 4.2.8 for the location of the profile.

The PARASOUND data were the basis for selecting coring locations at different parts of the canyons. Parasound Profile GeoB05-066 (Fig. 4.1.4) shows a cross section of proximal Dakar Canyon. The generally U-shaped canyon is ~400m deep and ~5km wide at this location. A small V-shaped depression is found at the canyon floor. The western part of the canyon floor shows a transparent unit indicating slide deposits. This transparent unit was cored at Station GeoB9607. The 784cm-long gravity core show thick slump deposits which are overlain by numerous turbidites intercalated into

hemipelagic sediments. The uppermost ~50cm of the core show undisturbed hemipelagic sediments probably of Holocene age. The eastern flank shows a number of terraces. Station GeoB9609 was located on a terrace ~200m above the canyon floor. This core includes numerous sandy turbidites. The western flank of the canyons is too steep to be imaged by the PARASOUND system. The canyon is incised in well stratified hemipelagic sediments. The PARASOUND data do not show well developed levees. The sediment rates are even slightly reduced in direct vicinity to the canyon. Core GeoB9608 was taken at such a location. This core mainly consists out of hemipelagic sediments and only shows some thin mud turbidites.

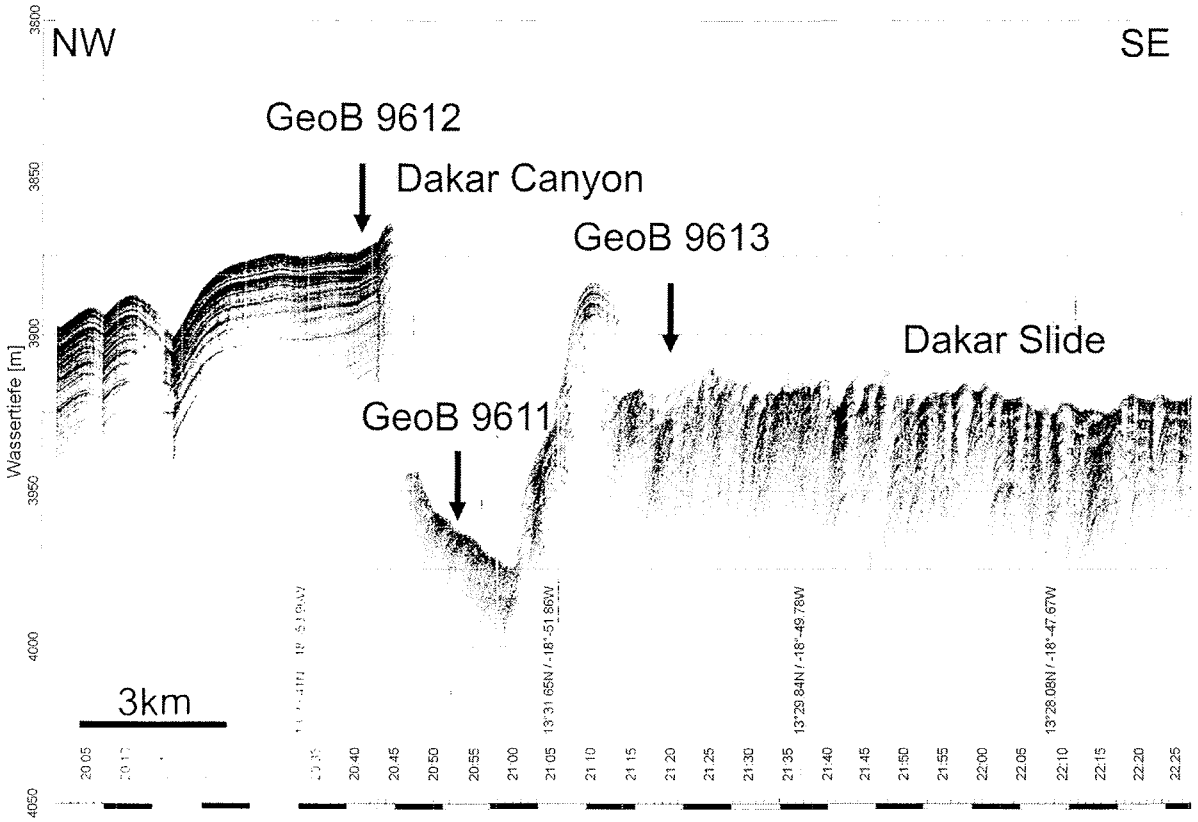

Fig. 4.1.5: Part of PARASOUND Profile GeoB05-073 with stations GeoB9611-9613. The profile crosses lower Dakar Canyon. See Fig. 4.2.8 for the location of the profile.

PARASOUND Profile GeoB05-073 (Fig. 4.1.5) is located ~100km downslope of Profile GeoB05-066. Canyon width is ~4km. The canyon is characterized by a highly asymmetrical V-shaped cross section. The north-western flank has a height of ~100m; the south-eastern flank is only ~60m high. The greater height of the north-western flank might be the result of higher sedimentation rates caused by overspill turbidites which are preferably deposited on the right-hand (north-western) side of the canyon. Station

GeoB9612 is located on the north-western levee in direct vicinity to the canyon. Some remnants of a levee are also visible on the south-eastern side of the canyon, but this area is generally characterized by a hummocky irregular reflection pattern. The hummocky topography is probably caused by a slide. This is supported by the seismic data (see Chapter 4.2), which show thick transparent units in this area. The slide was named Dakar slide during the cruise. A closer look at the Parasound data show some internal stratification of individual blocks, which can be explained by a hemipelagic cover of the slide or by relatively intact slide blocks, which have not moved very far. We tried to core the slide deposits are Station GeoB9613 but we do not see any obvious slide deposits in this 980cm-long core. Further analysis of the core will show, whether we hit a relatively intact slide block or if the slide is covered by hemipelagic deposits of more than 10m.

The canyon floor is characterized by a single prolonged high-amplitude reflector indicating sandy sediments. Turbidites with a coarse grained sandy base were sampled at Station GeoB9611 from the canyon floor.

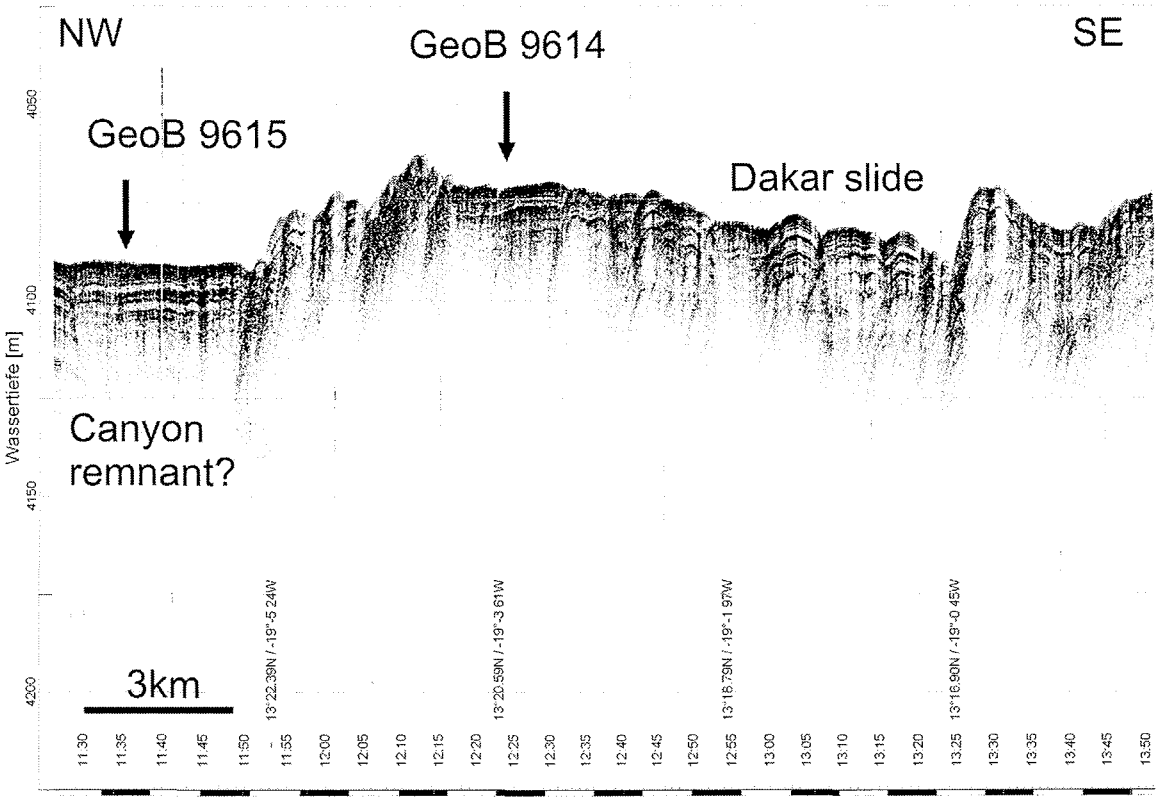

Fig. 4.1.6: PARASOUND Profile GeoB05-069 with stations GeoB9614 and GeoB9615. Only canyon remnants are visible on the profile. See Fig. 4.2.8 for the location of the profile.

PARASOUND Profile GeoB05-069 (Fig. 4.1.6) is located only 30km downslope of the previous profile but only remnants of the canyon are visible on the profile. The seismic data (see chapter 4.2) indicate that the canyon was destroyed by the slide. The destruction of the canyon results in a major change of sediment transport processes in this area. A small depression ~25m deep probably represents the prolongation of the canyon. This depression is characterized by subparallel continuous reflectors. Station GeoB9615 is located in this depression. Several turbidites were found in this core. The area south-east of this depression is characterized by a hummocky topography and represents the Dakar slide. As already described for the previous profile some internal stratification of individual blocks can be seen in the PARASOUND data. Core GeoB9614 was taken in a small depression of the slide which shows relatively continuous reflectors. Several turbidites were found in this core as well.

The second main working area was the Cap Timiris Canyon off Mauritania. This canyon was discovered during Meteor-Cruise M58/1 in 2003 (Schulz et al., 2003; Krastel et al., 2004). Additional PARASOUND data of the shelf and uppermost slope as well as the distal canyon were collected during Meteor-Cruise M65/2.

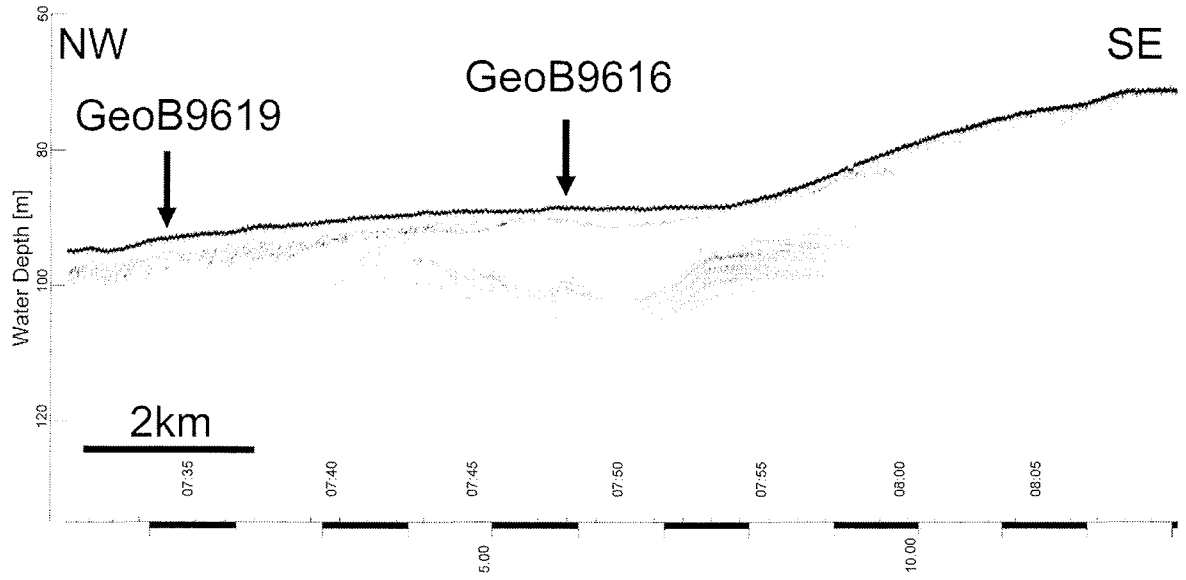

Fig. 4.1.7: PARASOUND profile of the shelf in the head region of Cap Timiris Canyon. See Fig. 4.2.15 for the location of the profile.

Fig. 4.1.7 shows a PARASOUND profile of the shelf in the head region of Cap Timiris Canyon. The seafloor is characterized by a strong sharp reflector. The profile can be divided in three parts. The north-western part mainly shows some diffuse subbottom returns, while the central part is characterized by a transparent unit beneath the

seafloor, which is underlain by a wavy parallel continuous reflector packet. Some reflectors of the packet are truncated by the transparent unit. The south-eastern part of the profile does not show any significant subbottom returns. Two giant box corers were taken on this profile, which mainly recovered fine sand and numerous shells and shell fragments. We do not have any information about deeper sediments. The central part of the profile might represent an incised valley fill. As we identified similar features only on the outermost shelf and as we cannot trace them further landward these features can be interpreted as local structures as well. The analysis of all PARASOUND profiles in this area will allow to analyze the dimension and the shape of the identified features in detail.

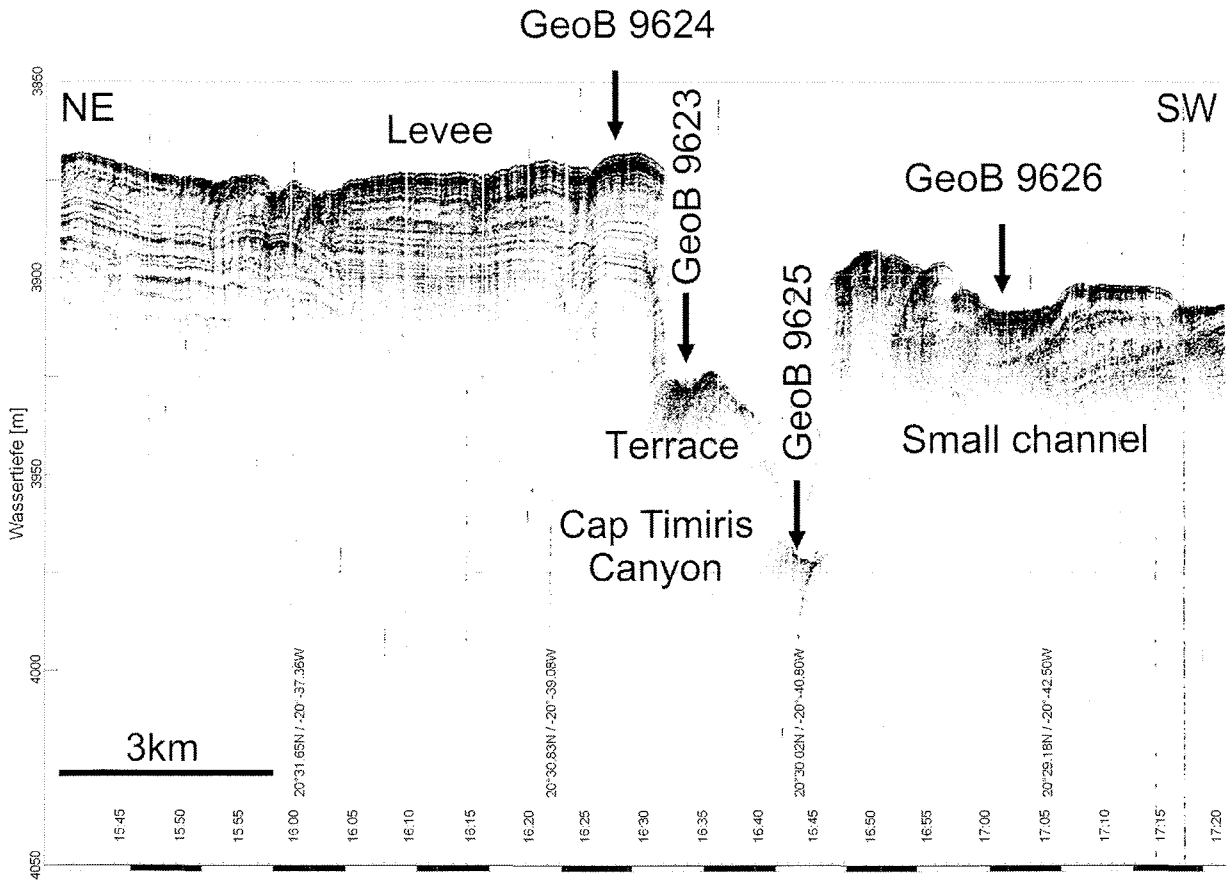

Fig. 4.1.8: PARASOUND profile GeoB05-101 with stations GeoB9623-9626. Note that the profile is plotted in reverse direction. See Fig. 4.2.17 for the location of the profile.

A second aim related to Cap Timiris Canyon was to survey and sample the distal Cap Timiris Canyon. The prolongation of the area mapped during Meteor-Cruise M58/1 (Schulz et al., 2003, Krastel et al., 2004) shows a small section with a tortuous meander pattern but most of the canyon is relatively straight and has a north-westerly direction. Fig. 4.1.8 shows a typical PARASOUND profile crossing distal Dakar Canyon. The 2km-

wide canyon shows an asymmetrical shape with a 100m-high north-eastern flank and a 70m-high south-western flank. A very prominent 1km-wide terrace is imaged at the north-eastern flank ~50m above the thalweg. The terrace is characterized by a prolonged seafloor echo without any significant subbottom reflectors. Station GeoB9623 was located on this terrace and a 2-m-long section shows several turbidites covered by ~20cm of hemipelagic sediments. The attempt to recover a core from the canyon thalweg (Station GeoB9625) was not successful. The areas on both sides of the canyons differ significantly. The north-eastern side is characterized by typical levee-sediments with some indications for sediment waves. Station GeoB9624 is located on the levee and the 11.33m-long core shows numerous overspill turbidites intercalated in hemipelagic sediments. The south-western side is characterized by an irregular reflection pattern with a strong prolonged seafloor return and a number of diffuse subbottom reflectors. A small depression (location of Station GeoB9626) in this area shows very high amplitudes. Bathymetric data indicate that this depression represents a small channel, which enters the main canyon further downslope. The 4m-long core GeoB9626 contains numerous turbidites indicating that this small channel is also an important pathway for turbidity currents.

Downslope of the above described profile the canyon shape changes significantly. Fig. 4.1.9 shows a Parasound profile located ~30km west of Profile GeoB05-101 (Fig. 4.1.8). On this profile the main canyon is only ~40m deep. A distributary canyon of similar size is observed ~10km to the north. The distributary canyon is bordered to the north by a well developed levee. The area between the two canyons is characterized by a strong prolonged seafloor return indicating sandy deposits. The reduced depth of the canyon might result in turbidity currents spreading over a larger area and thereby forming depositional lobes. Core GeoB9627 was taken between the canyons and contains numerous turbidites.

The reason for the sudden change of the morphological characteristics of the canyon remains unclear at the present stage. A first idea was that the 170ka-old Cap Blanc Slide, which was identified on a single previously available Parasound line and old GLORIA Sidescan sonar records in this area, destroyed the canyon. This idea, however, is not in agreement with our data. Fig. 4.1.10 shows levee sediments north of Cap Timiris Canyon. The transparent unit onlaping the levee sediments are the deposits of the Cap Blanc Slide. The data clearly show that the slide deposits terminate on the levee and we have not identified any slide deposits in the canyon itself. The same relationship between slide deposit and levee sediments is found on all available profiles. The Cap Blanc slide reaches a thickness of 10m-20m; the PARASOUND data also indicate a thin hemipelagic cover of the slide, what is in good agreement with the estimated age of the slide. This is also confirmed by Core GeoB9628, which is characterized by hemipelagic sediments on top of a massive debrite.

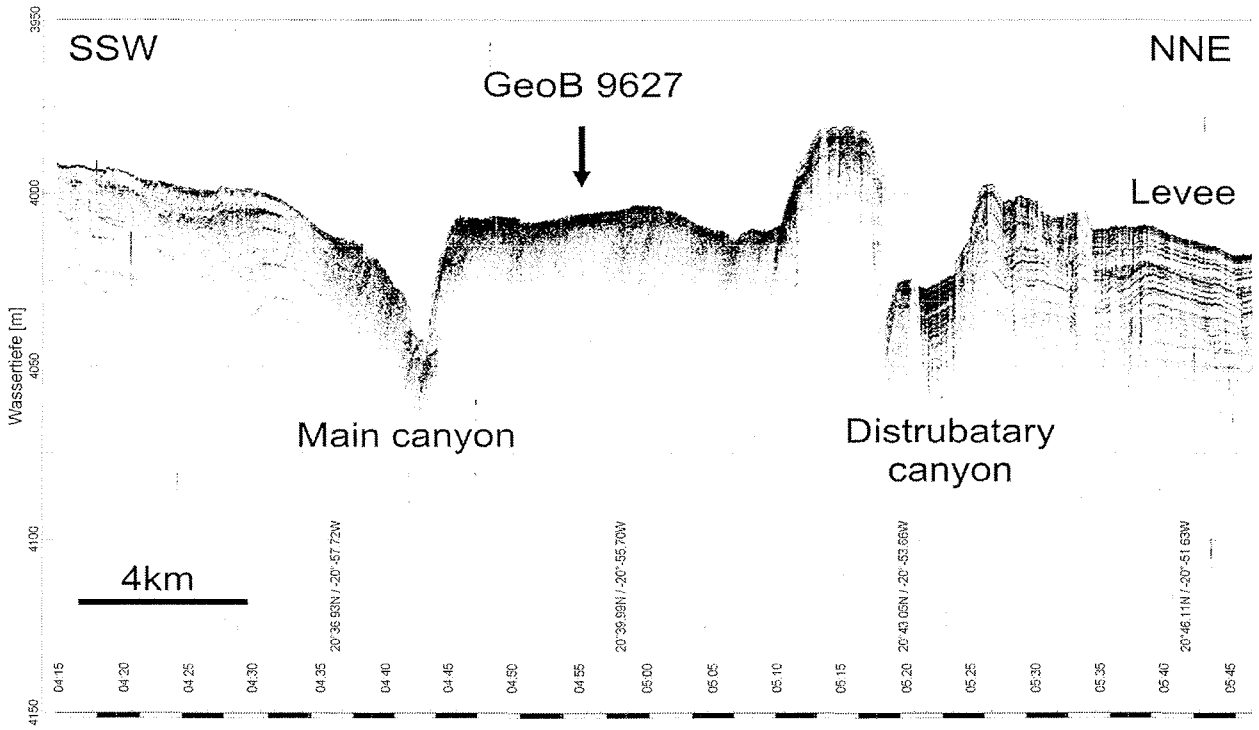

Fig. 4.1.9: PARASOUND profile with station GeoB9627. See Fig. 4.2.17 for the location of the profile.

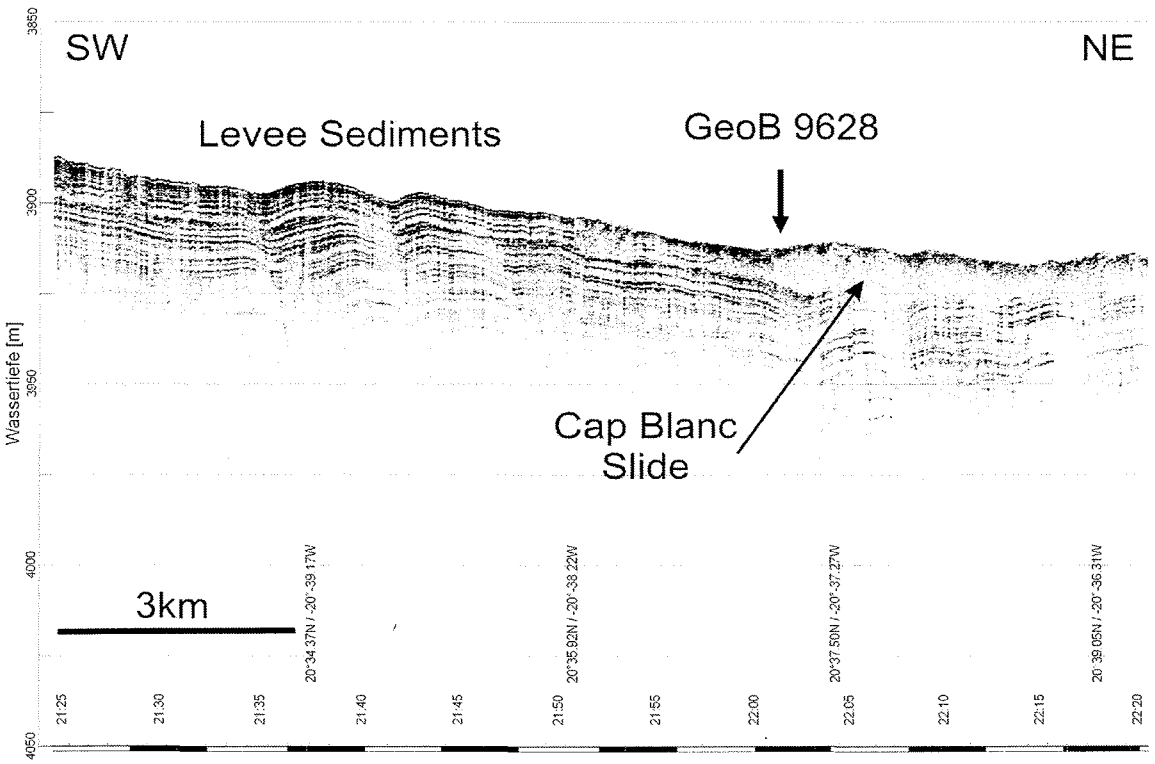

Fig 4.1.10: Parasound profile with station GeoB9628. See Fig. 4.2.17 for the location of the profile.

4.2 High-Resolution Multichannel Reflection Seismics

(S. Krastel, L. Zühlsdorff, M. Brüning, J. Felzenberg, J. Geersen, M. Urlaub, T. Vogt)

4.2.1 Introduction

With the GeoB high-resolution multichannel seismic equipment, small scale sedimentary structures and closely spaced layers can be imaged on a meter to sub-meter scale, which can usually not be resolved with conventional seismic systems. During R/V Meteor Cruise M65/2, a Generator-Injector (GI) airgun with normal chamber volume (2 x 1.7 L, 30-200 Hz) was used as the main seismic source. On some seismic lines, also a small chamber watergun (0.16 L, 200-1600 Hz) was operated. Along such lines, the alternating operation of those two guns provided two seismic data sets simultaneously, which are characterized either by greater depth penetration (GI-Gun source) or higher vertical resolution (watergun source).

Fig. 4.2.1 gives an outline of the system setup as it was used during R/V Meteor Cruise M65/2.

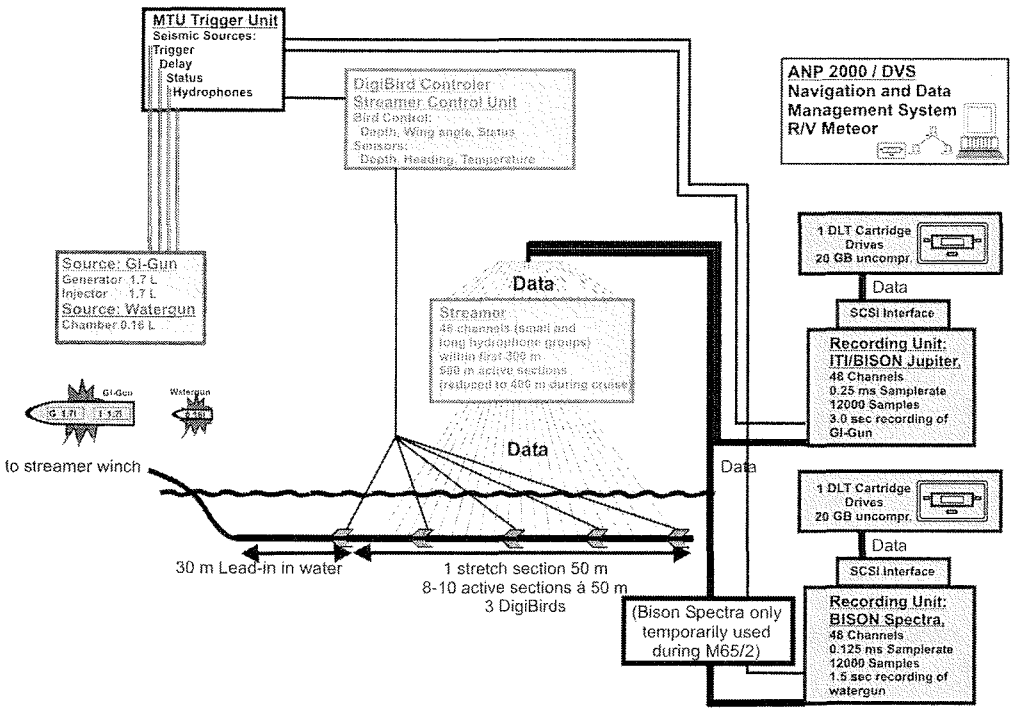

Fig. 4.2.1: Seismic system setup during R/V Meteor Cruise M65/2.

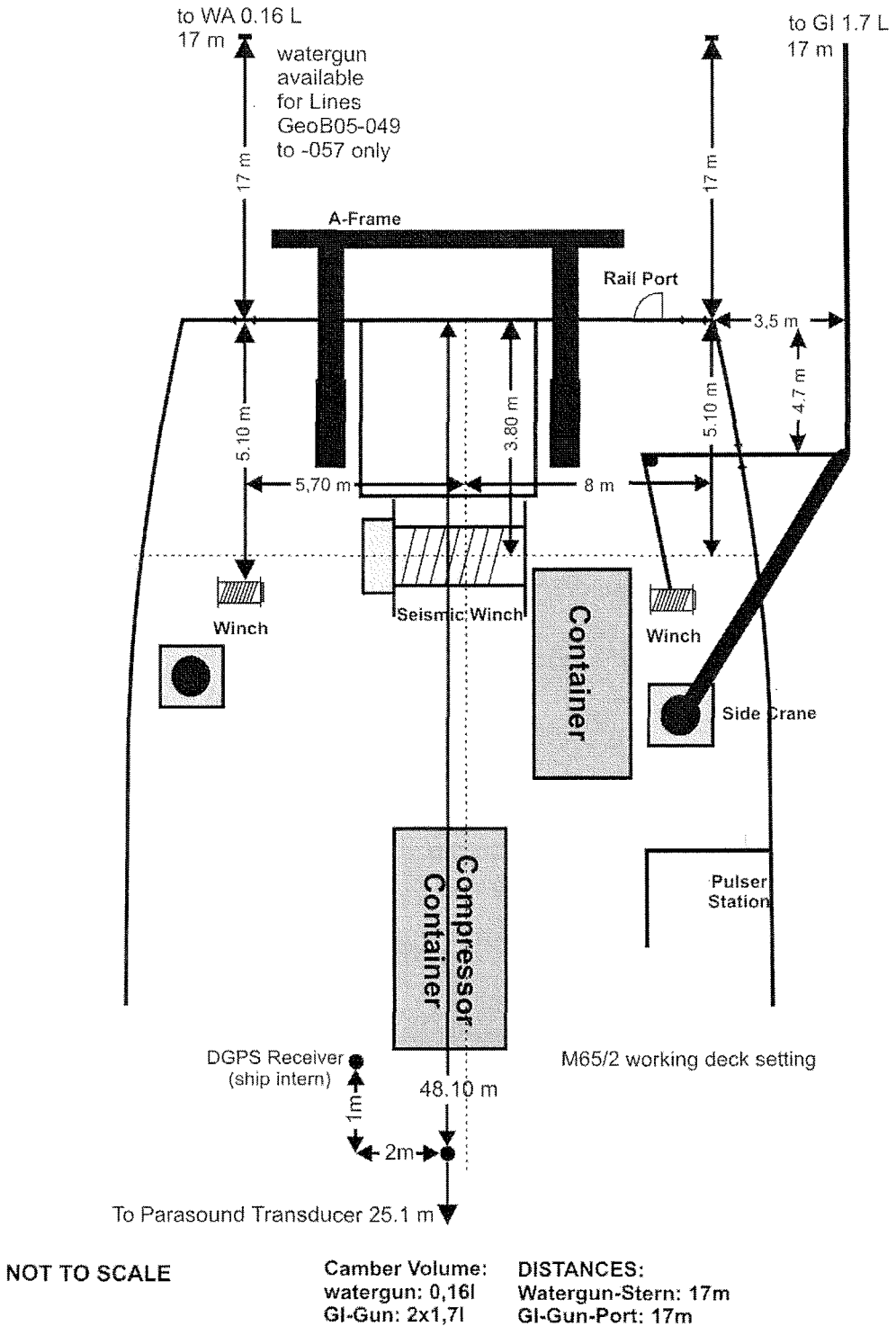

Fig. 4.2.2: Deck and seismic gun setting during Cruise M65/2. Watergun was only used starting with GeoB05-049 until the first half of GeoB05-057.

4.2.2 Seismic Sources

During seismic surveying, one GI-Gun (on all seismic lines) and one additional watergun (on Lines GeoB05-049 to the first half of GeoB05-057) were used. Whenever both guns were operated, they were triggered in a quasi-simultaneous mode at a time

interval of 9 s (see also trigger unit). Owing to an average ship speed of 5.0 kn, a shot distance of approximately 20 m to 25 m was thus obtained for the alternating mode operation of each gun type. Each source type was shot at an air pressure of about 150 bar.

The geometry of source and receiver systems during the measurements is shown in Fig. 4.2.2. Ship velocity during deployment and retrieval was between 1.5 and 2.5 kn.

One standard GI-Gun (Generator-Injector gun; Sodera) with normal chamber volume (2 x 1.7 L) at port side was towed from the port side crane and approximately 17 m behind the ship's stern (Fig. 4.4.2). The gun was connected to a bow with the GI-Gun hanging on two chains 40 cm beneath. An elongated buoy, which stabilized the guns in a horizontal position at a water depth of ~1.5 m, was connected to the bow by two rope loops. The Injector was triggered with a delay of 50 ms with respect to the Generator signal, which basically eliminated the bubble signal.

The second source was a S15 watergun (Sodera) with a volume of 0.16 L, which was towed on starboard side (Figure 4.4.2). The distance to the ship's stern was about 17 m. The umbilicals were secured by strong ropes to avoid damage of pressure lines and electric cables due to rubbing or bending. A steel frame held the watergun in a tight position parallel to the elongated buoy in a depth of approximately 0.5 m.

4.2.3 Streamer

The multichannel seismic streamer (SYNTRON) used during R/V Meteor Cruise M65/2 included a tow-lead (30 m of which was towed in water), one stretch section of 50 m, and eight to ten active sections of 50 m length. A 50 m long Meteor rope with a buoy at the end was connected to the tail swivel. A 30 m long deck cable connected the streamer to the recording system.

Active 50-m-sections are subdivided in 8 hydrophone groups (Fig. 4.2.3). Each of the 6.25 m long hydrophone groups is again subdivided into 5 subgroups of different length. One of the subgroups is a high-resolution hydrophone with pre-amplifier. A programming module distributes the subgroups of 4 hydrophone groups, i.e. a total of 20 groups, to 5 channels. Every second 6.25 m hydrophone subgroup was completely used with all 13 hydrophones, whereas the two additional channels were reduced in length to 2.2 m and 3.3 m, respectively. Locations of individual hydrophone groups are given in Tab. 4.2.1. For most part of Cruise M65/2 (see below), output channels 1 to 48 (all hydrophone groups of 300 m active sections) were connected to the Jupiter recording system, independent of the hydrophone group length. Single hydrophones were not recorded.

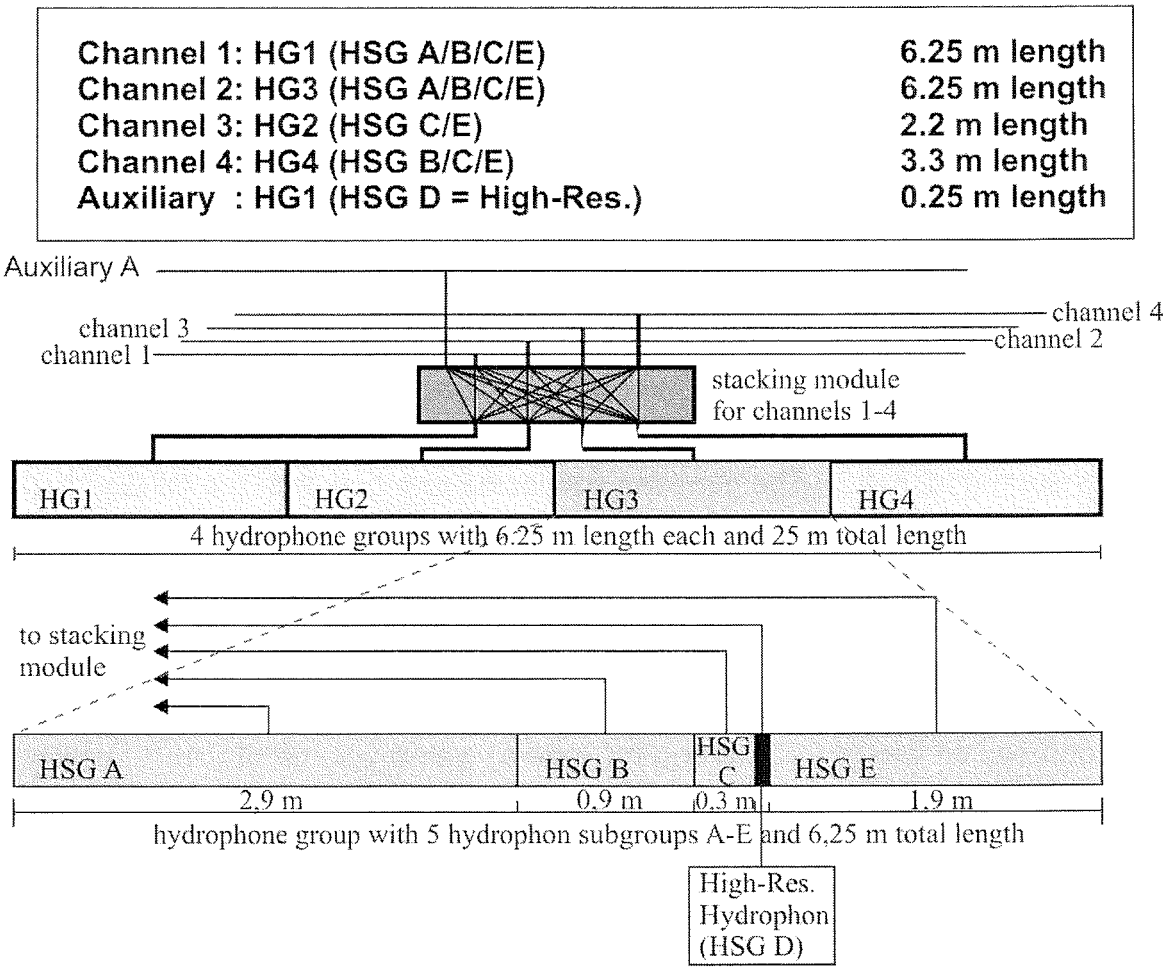

Fig. 4.2.3: Streamer configuration.

Table 4.2.1: Channel assignment and midpoint distances of hydrophone groups from begin of each active section.

Segment of 25 m length	Hydrophone Group No.	Channel No. In Section	Midpoint Distance
A (0-25 m)	1	1	3.1 m
A	2	3	11.3 m
A	3	2	15.6 m
A	4	4	23.3 m
B (25-50 m)	1	5	28.1 m
B	2	7	36.3 m
B	3	6	40.6 m
B	4	8	48.3 m

Between seismic Lines GeoB05-049 to GeoB05-053, ten active sections were deployed (500 m) but only data from the first 24 channels (300 m) could be recorded and channel 25 to 40 (300–500 m) turned out to be pure noise. Assuming that the problem was located at one of the streamer plugs behind 300 m, the seventh section was removed, leaving nine active sections (450 m) for seismic Lines GeoB05-054 to GeoB05-067. However, the problem could not be solved that way. Furthermore, the last (ninth) section had to be removed as well due to a severe leakage of oil, leaving only eight active sections (400 m), i.e. 32 channels, for all remaining seismic lines starting with GeoB05-068. Of the remaining 32 channels, still only 24 showed seismic data. Thus, several alternative plug configurations were tested in the seismic lab, eventually resulting in a win of a few additional seismic records on some channels between numbers 25 and 32. By then, however, the Bison Spectra watergun recording unit was already lost due to a main board failure (see below), leaving the choice of recording both watergun and GI-Gun on Bison Jupiter or increasing the data quality (i.e. the number of good channels) of GI-Gun recordings by using both small groups and long groups of the first 300 m of the streamer. The latter turned out to be most efficient. Since only three birds could be installed on the streamer (see below), they were thus located within the first 300 m in order to provide maximum control of those sections used for recording.

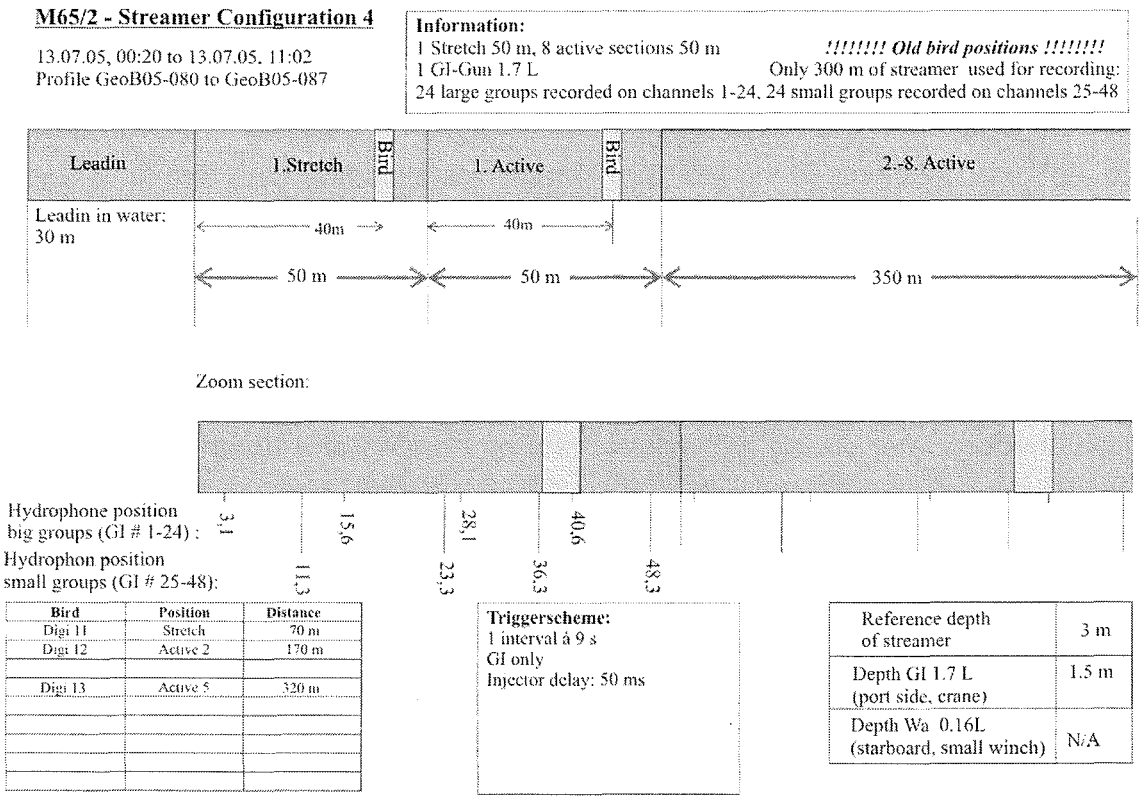

Fig. 4.2.4: Streamer setting during R/V Meteor Cruise M65/2.

Thus, in summary, watergun data (40 channels or 32 channels, respectively) were recorded until the first half of Line GeoB05-057 only. Until Line GeoB05-079, only 24 channels of GI-Gun data were recorded. Starting with Line GeoB05-080 and left unchanged for the rest of the cruise, GI-Gun data were recorded on 48 channels: the long streamer groups within the first 300 m of the streamer were recorded on channels 1-24 and the short streamer groups within the first 300 m of the streamer were recorded on channels 25-48. The streamer configuration used as a standard starting with GeoB05-080 is given in Fig. 4.2.4.

4.2.4 Bird Controller

Five DigiBird Remote Units (RUs 5, 6, 11, 12, 13) were available and could be configured using the bird controlling unit. In operation, however, only DigiBirds Number 11, 12, 13 could be attached to the streamer due to problems with the bird collars. The standard positions of all RUs are given in Figure 4.2.4 (only changed between Lines GeoB05-068 to GeoB05-079 where RUs 12 and 13 were both located 50 m closer to the ship). Each RU includes a depth and a heading sensor as well as adjustable wings. The RUs are controlled by a bird controller in the seismic lab. Controller and RUs communicate via communication coils nested within the streamer. A twisted pair wire within the deck cable connects controller and coils.

Each shot trigger started the bird scan of water depth, wing angle and heading data. The current location of the streamer can be displayed as a depth profile on a monitor. Due to technical problems in the lab, bird parameters including date and time were only digitally stored on the controller PC starting with Line GeoB05-068.

Before the streamer was deployed, each RU was programmed in the seismic lab to keep an operating depth of 3 m. The RUs thus forced the streamer to the chosen depth by adjusting the wing angles accordingly. Possible depth variations of the streamer could be checked later during preliminary data processing and depth control appeared to be successful.

4.2.5 Data acquisition system

A 48 channel Jupiter/ITI/Bison seismograph, which allows a maximum sampling frequency of 4 kHz at 24 bit resolution, is based on a Pentium PC (200 MHz; 64 MB RAM) with a Windows NT 4.0 operating system. The seismograph allows online data

display (shot gather), online demultiplexing and storing in SEG-Y format on DLT4000 cartridge tape with 20 GByte uncompressed capacity. Data were recorded at a sampling frequency of 4 kHz over an interval of 3 seconds, resulting 48 x 12000 samples of 4 bit per shot. Pre-amplifiers were set to 48 dB, low cut filter to 4 Hz. Despite some minor software problems, the instrument worked very reliable and data were routinely collected from the beginning of the seismic survey.

A 48 channel Spectra Bison seismograph, based on a Pentium PC with a Windows NT 3.51 operating system, allowed for a sample rate of 0.000125 s and was used to record watergun data during the first part of the cruise (48 x 12000 samples at 1.5 s recording length, 60 dB pre-amplifiers). During the course of Line GeoB05-057, however, there was a severe failure of the system main board that could not be fixed onboard. It was decided to increase GI-Gun data quality by increasing the channels recorded on the Jupiter Bison and to not deploy the watergun anymore for the rest of the cruise.

On both Bisons, 48 channels were recorded, even though only 40 or 32 channels, respectively, were available until Line GeoB05-079. This was to avoid known software problems. For backup, only channels containing seismic data were read.

4.2.6 Trigger unit

The custom trigger unit used during R/V Meteor Cruise M65/2 controls seismic sources, seismographs, online printer, and bird controller. The unit is set up on an IBM compatible PC with a Windows NT 4.0 operating system and includes a real-time controller interface card (SORCUS) with 16 I/O channels, synchronized by an internal clock. The unit is connected to an amplifier unit and a gun amplifier unit. The PC runs a custom software, which allows to define arbitrary combinations of trigger signals, which were used to optimize the available recording time for two seismic sources and to minimize shot distance.

Trigger times can be changed at any time during the survey. Through this feature, the recording delay can be adjusted to water depth without interruption of data acquisition. The amplifier unit converts the controller output to positive or negative TTL levels. The gun amplifier unit, which generates a 60V/8 Amp. trigger level, controls the magnetic valves of the individual seismic sources. It was placed in the pulser station close to the gun pressure controls for immediate shutdown of gun operation.

The quasi-simultaneous trigger scheme for one or two recording systems and one or two guns was kept simple and consisted of one trigger interval of 9 s only (only

extended at great water depth or in the few cases of continuous memory problems on the jupiter Bison). The GI-Gun was shot 1.5 seconds after the watergun and recording units were triggered accordingly taking the required recording delay into account. The bird controller was usually triggered right at the beginning of the trigger period to avoid interference with seismic recording. The online printer was triggered such that GI-Gun signals could be displayed within a 2 s window and with continuous seafloor reflection after delay changes whenever possible.

4.2.7 Onboard Seismic Data Processing

For an immediate evaluation of data quality, brute stacks of the GI-Gun data were produced for each multichannel seismic line. Processing was done with the Vista software (Seismic Image Software Ltd) on a PC with. The field traces 1-5 were chosen for the brute stacks due to a good signal to noise ratio of these traces. The data were filtered with a wide bandpass (55/110 – 600/800 Hz) and thereafter simply summed up. These images were used for preliminary analyses of the seismic data.

For some selected lines CMP-stacks were carried out on board. The processing procedure included trace editing, setting up geometry, static corrections, velocity analysis, normal moveout corrections, bandpass frequency filtering (frequency content: 55/110 - 600/800 Hz), stack and time migration. A common midpoint spacing of 10 m was applied throughout.

4.2.8 Preliminary results of the seismic survey off Senegal

As already described for the PARASOUND Data, our investigations off Senegal were concentrated around Dakar Canyon (Fig. 4.2.5). This decision was mainly based on two profiles parallel to the coast along the ~2000m, and ~3500m contour, respectively (Figs. 4.2.6, 4.2.7), which were collected to get a general picture of the sedimentary deposits south of Dakar up to the boarder to Guinea-Bissau. Interestingly the profiles in different water depths show very different reflection patterns. The central part of Profile GeoB05-050 (Fig. 4.2.6) is characterized by parallel reflectors with a very good continuity. A small gully is imaged around SP 5100 but no further indications for gravity driven sediment transport is visible on this part of this profile. The picture slightly changes further to the south along Profile GeoB05-050. We did not identify any mass wasting events on the slope shallower than 3000m water depth but the number of

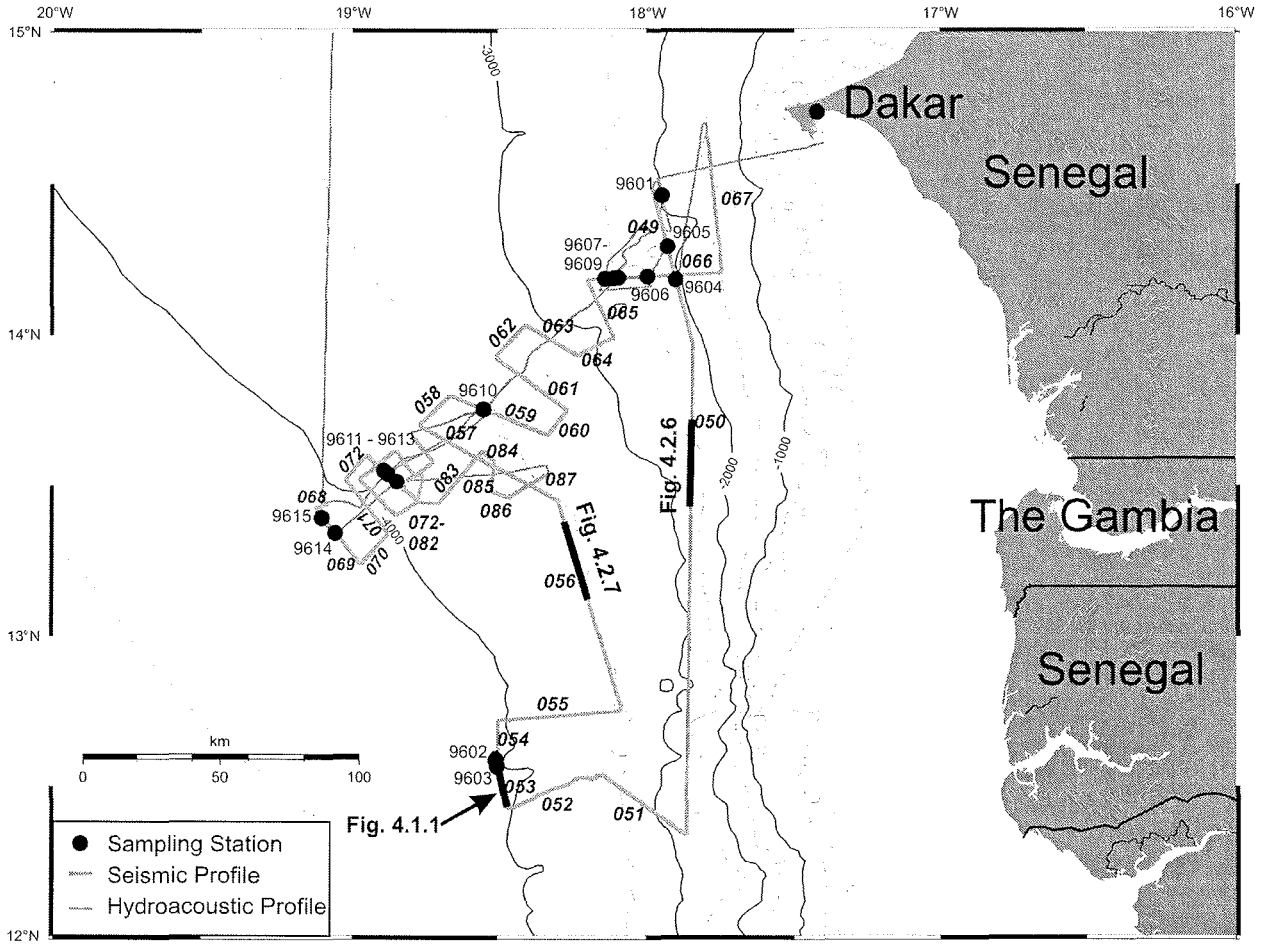

Fig. 4.2.5: Track chart of seismic and hydroacoustic survey off Senegal.

canyons and gullies increases. Some of the canyons are ~500m deep on the upper slope but their depth decreases quickly with increasing distance from the coast. The seismic data indicate that their location is structurally controlled. The structural control of canyon locations and the rapid decrease of depth with increasing distance from the coast suggest that the canyons off southern Senegal are not of key importance for the understanding of sediment transport processes at this margin.

A different picture shows Profile GeoB05-056 (Fig. 4.2.7). The upper 50-100 ms TWT beneath the seafloor are characterized by some internal reflectors with a blocky structure but individual reflectors cannot be traced over longer distances. These reflectors are underlain by an up to 200ms-TWT-thick transparent layer. Deeper intervals show an interlayering of well stratified reflectors and chaotic to transparent units. This reflection pattern, especially the thick transparent unit representing a large slide/slump deposit (Dakar Slide), demonstrates the importance of large scale mass wasting on the lower slope off Senegal. Indications for large scale mass wasting are found off the entire coast south of Dakar in water depths deeper than 3000-3500m with slope gradients <0.5°. Such a setting with a very stable upper slope and an unstable lower slope and continental rise is atypical for most continental margins. The reason for

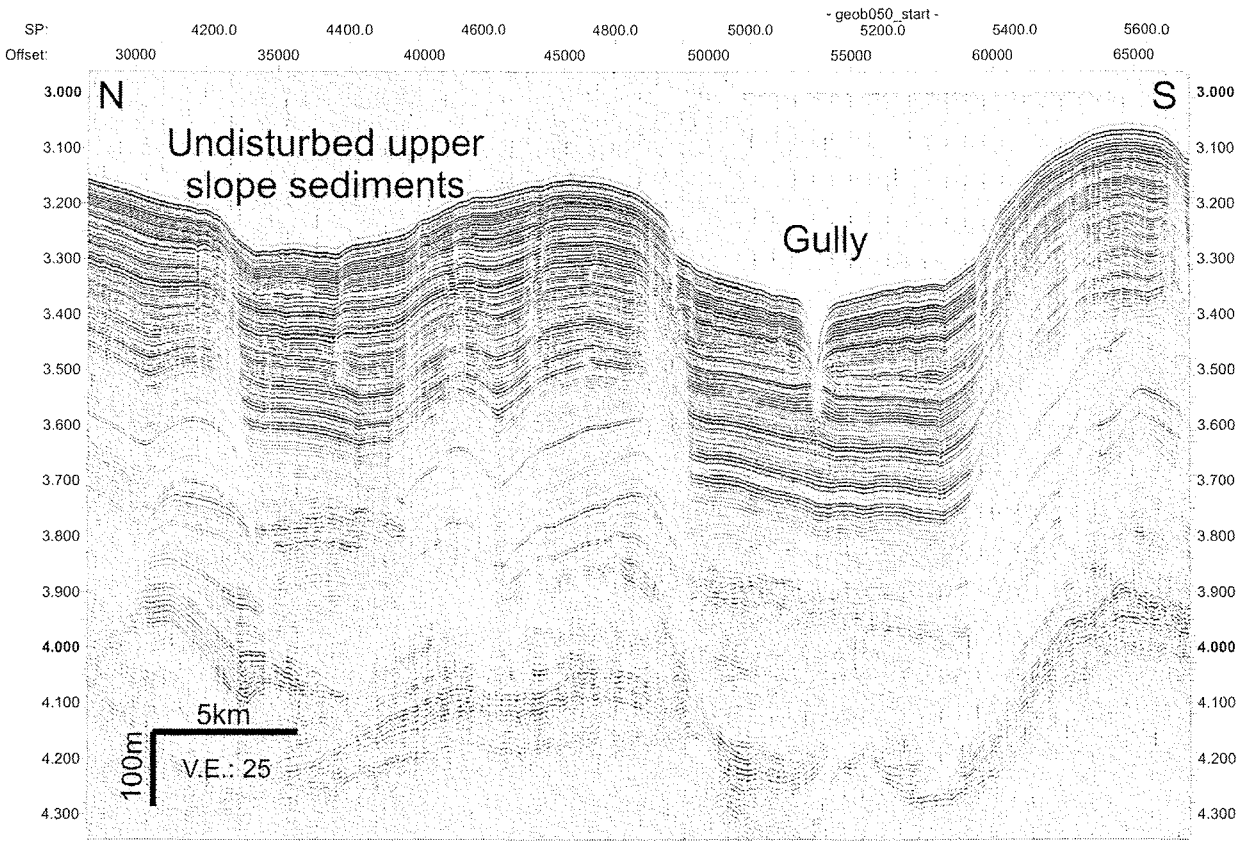

Fig. 4.2.6: Brute stack of a part of seismic Profile GeoB05-050. See Fig. 4.2.5 for location of the profile.

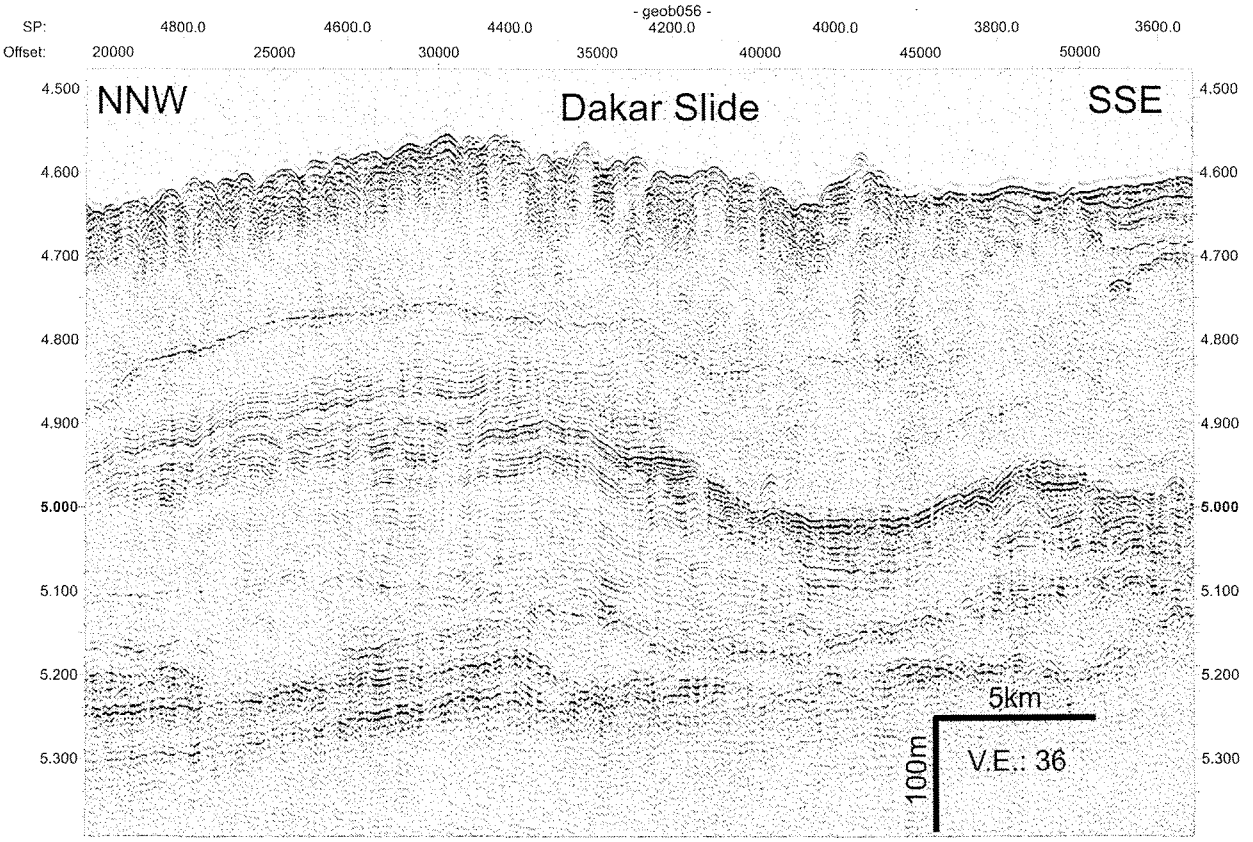

Fig. 4.2.7: Brute stack of a part of seismic Profile GeoB05-056. See Fig. 4.2.5 for location of the profile.

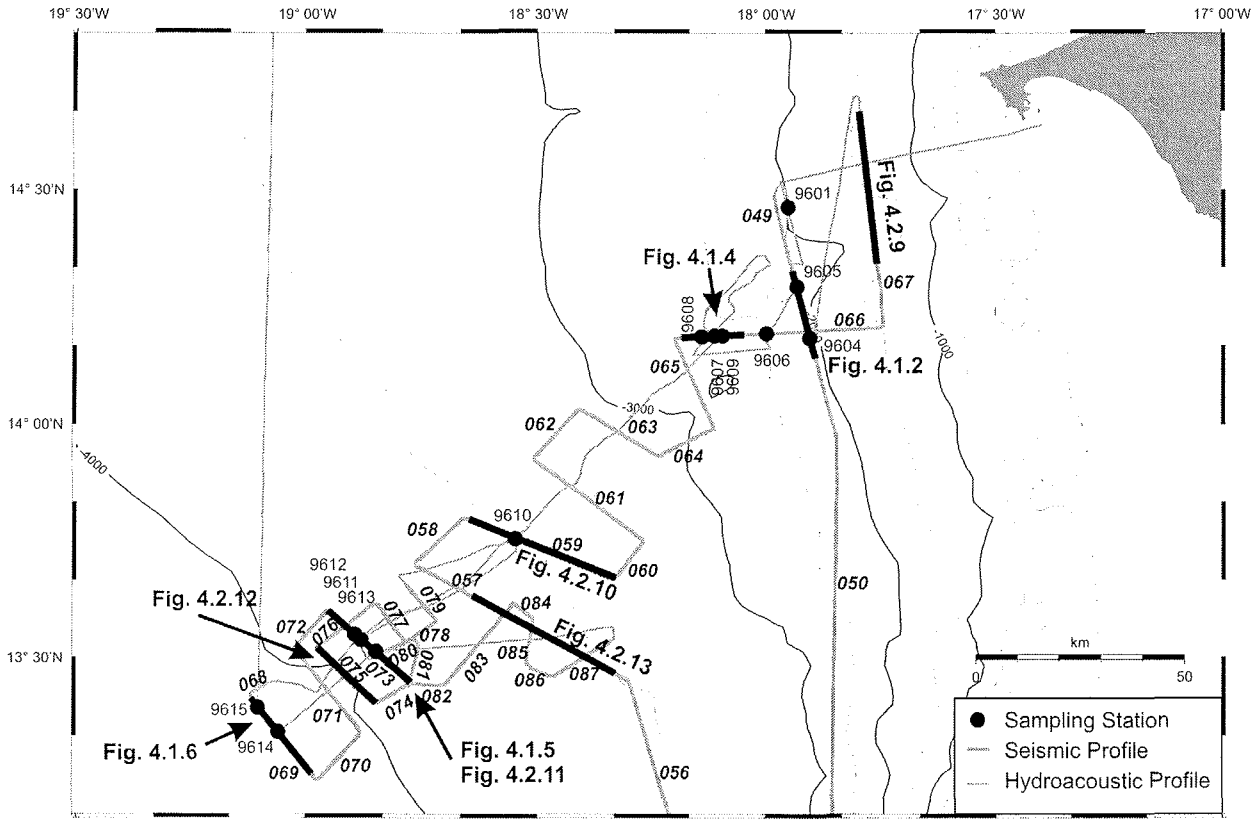

Fig. 4.2.8: Track chart of seismic and hydroacoustic survey of Dakar Canyon.

the occurrence of large scale mass wasting at great water depth and low slope gradients will be further investigated based on the new seismic data.

The interaction between large scale mass wasting in an open slope environment and confined sediment transport in a canyon was studies around Dakar Canyon, the main survey area off Senegal during Cruise M65/2 (Fig. 4.2.8). Figs 4.2.9-4.2.12 show seismic sections crossing Dakar Canyon at different locations. Seismic Profile GeoB05-067 (Fig. 4.2.9) is the most proximal profile of Dakar Canyon. It crosses the canyon in ~1300m water depth and a distance of ~40km off the coast. The canyon is almost 700m incised in upper slope sediments; canyon width of the main canyon is ~10km. Some terraces can be seen especially on the northern canyon flank. At least some of the terraces are probably formed by gravitational sliding of large blocks. A much smaller tributary canyon is imaged south of the main canyon. Its depth is only ~150m. The seismic data show a complex pattern of the upper slope sediments. Smaller buried canyons are imaged especially north of the main canyon. These buried channels usually do not show any indications for levees except for a system at the northern end of the profile. All buried canyons are relatively small compared to the present main canyon. The continuous parallel to subparallel units are separated by erosional unconformities, which are imaged in different depth intervals. One of the erosional

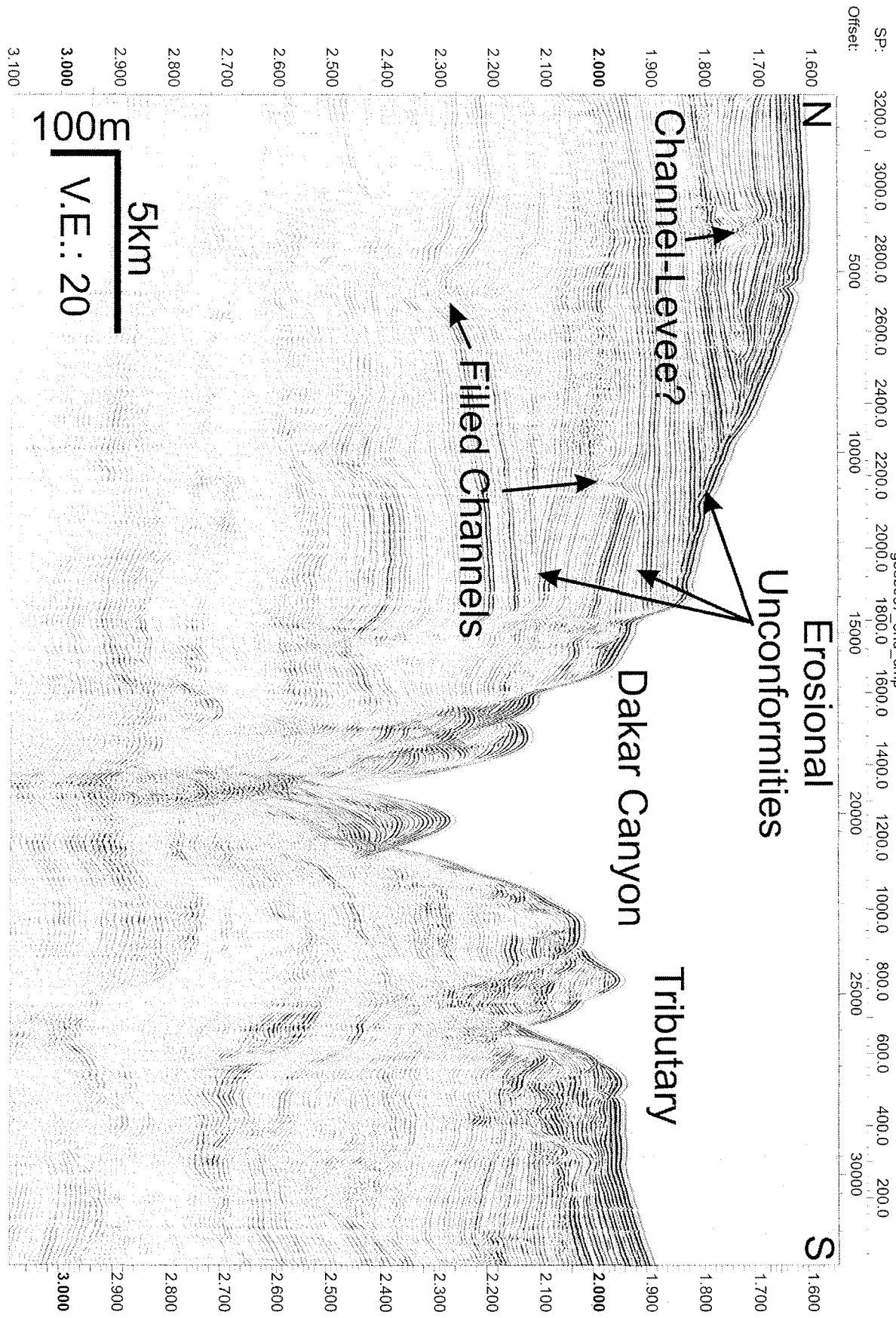

Fig. 4.2.9: Part of CMP-Stack of Profile GeoB05-067. See Fig. 4.2.8 for location of profile.

unconformities is located close to the surface but the seismic data suggest a thin hemipelagic drape on top of the erosional surface. The sedimentary pattern suggests a complex evolution of Dakar Canyon and the upper slope sediments. While no indications for a buried canyon of a similar size of the present Dakar Canyon are found in the data, the buried smaller canyons show a reorganization of sediment transport pathways during the evolution of the continental margin. The pronounced unconformities must been formed during periods of intense erosion by water or turbidity currents, while thick units of continuous subparallel to parallel reflectors were formed during periods of undisturbed hemipelagic sedimentation.

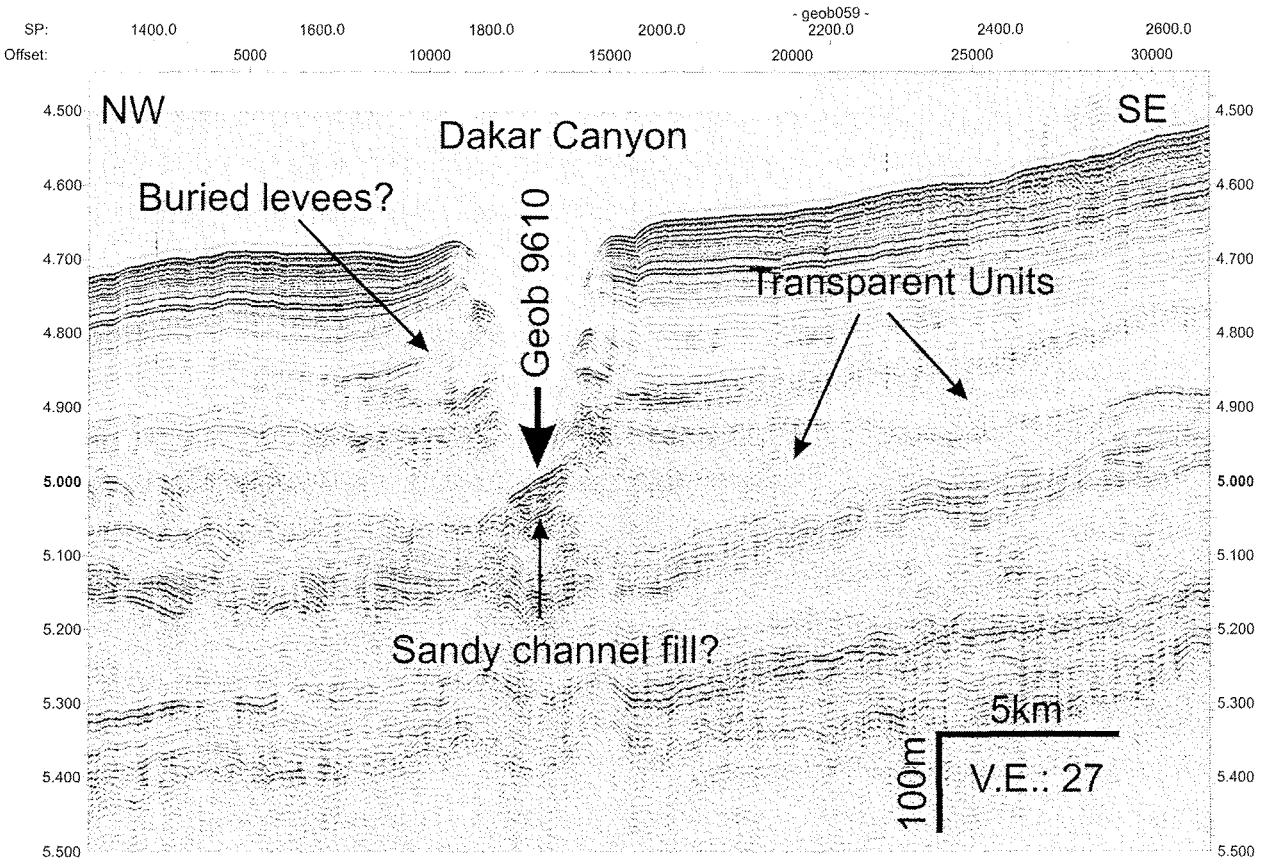

Fig. 4.2.10: Brute-Stack of Profile GeoB05-059. See Fig. 4.2.8 for location of profile.

Seismic Profile GeoB05-059 (Fig. 4.2.10) shows a typical profile crossing Dakar Canyon at the continental rise at a water depth of ~3500m. Similar profiles were also collected at the middle and lower continental slope. The canyon is incised in well stratified sediments though some transparent units are also found beneath the well stratified upper sedimentary unit. Canyon depth is ~250m; canyon width is ~3km. The canyon floor is characterized by irregular reflectors of high amplitude. They might represent a sandy channel fill. Core GeoB9610 was taken at the canyon thalweg. This core is only 254cm long but shows a number of turbidites with a coarse grained sandy base. Only

minor terraces were found at the canyon flanks. The upper ~100ms TWT of sediments show high amplitudes, subparallel to parallel reflectors with a good continuity. The reflection pattern does not show indications for present levee formation though an upbending of the uppermost reflectors at the north-western side of Dakar Canyon is visible in the data. The upbending is caused by a divergent reflection pattern beneath the upper most well stratified unit. This divergent reflection configuration with greatest thickness in immediate vicinity to the canyon might represent an old levee. The ~100ms TWT (75m) thick cover on top of such a levee would mean that canyon must be relatively old (several 100ka) and that the canyon was stable for this period of time. Buried Canyons were found in none of the seismic profiles of the lower slope and continental rise. Missing young levee sediments can be explained by the great canyon depth which prevents overspill of turbidity currents in the younger past. Though the canyon is probably inactive at present times as indicated by ~40-50cm thick hemipelagic sediments in the core data, numerous turbidites were found beneath the upper hemipelagic layer demonstrating the importance of sediment transport during the last glacial period. However, these turbidites were probably too small to form major levee deposits.

Seismic Profile GeoB05-073 (Fig. 4.2.11) is collected in 3900m water depth. Incision depth of the canyon is only ~80m. The canyon floor is characterized by strong reflector patches of about 100ms TWT thickness representing a major canyon fill. The sediments on both sides of the canyon show significant differences. The north-western flank is characterized by continuous reflectors with a slightly divergent reflection pattern, which is typical for levee sediments. Due to the reduced incision depth of the canyon a well developed right hand levee was formed as a result of overspill turbidites. The south-eastern flank shows some levee remnants but the upper ~120 ms TWT of sediments are generally imaged as a transparent unit. This unit is underlain by strong reflectors with medium continuity. The transparent unit represents a major slide, which we named Dakar Slide during the cruise (see below). No slide deposits were found in the canyon axis suggesting that the slide was stopped by the south-eastern levee at this location.

Seismic profile GeoB05-075 (Fig. 4.2.12) is located only ~10km further downslope of Profile GeoB05-073 (Fig. 4.2.11) but shows a significantly different picture. Only remnants of the channel are visible on the profile as a ~3km wide and ~20m deep depression. The north-western (right-hand) side of the channel is characterized by levee sediments while no indications for levees were found on the south-eastern flank. The above described Dakar Slide is imaged as transparent unit south-east of the channel remnants. It is interesting to note that the Dakar Slide seems to fill a ~80m-deep depression beneath the small depression on the seafloor. This suggests that the

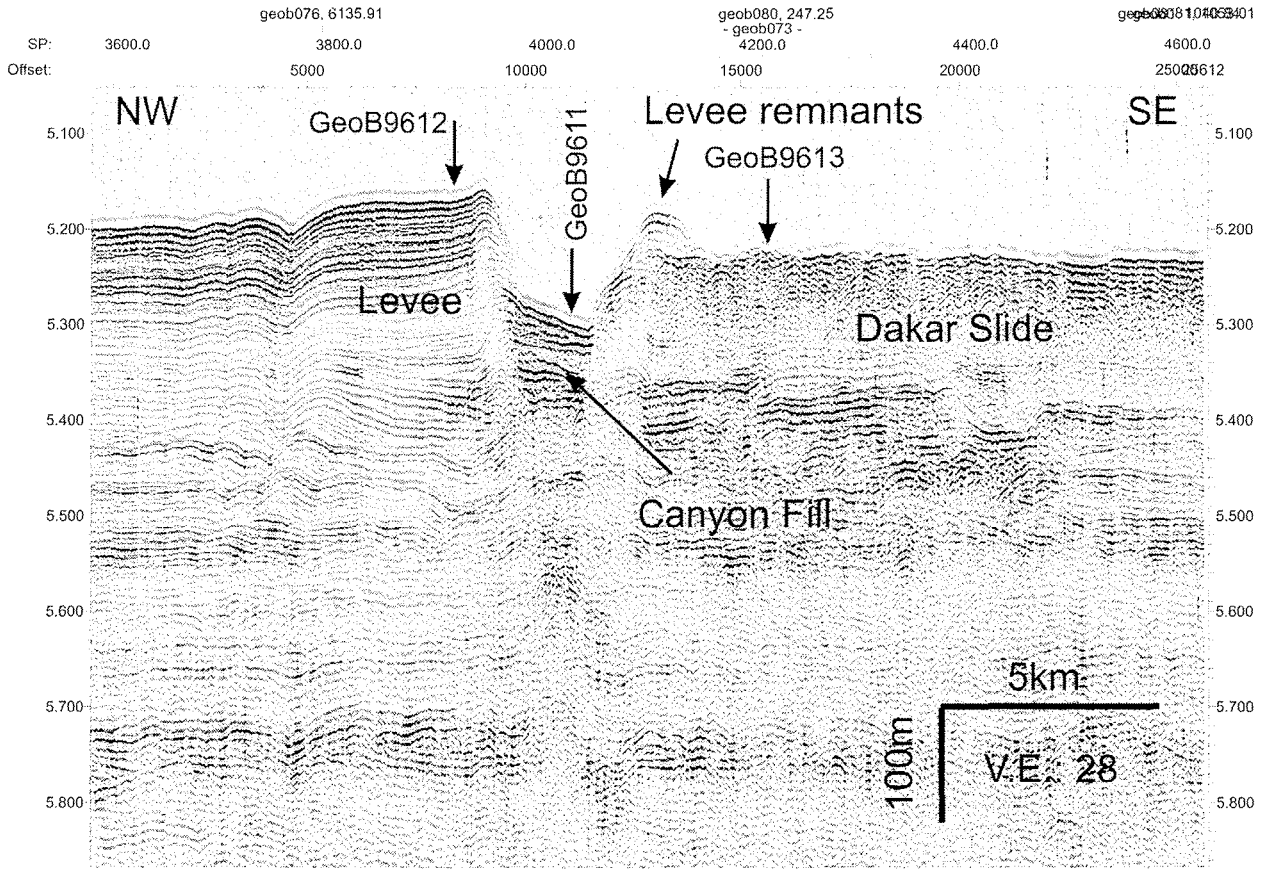

Fig. 4.2.11: Brute-stack of Profile GeoB05-073. See Fig. 4.2.8 for location of profile.

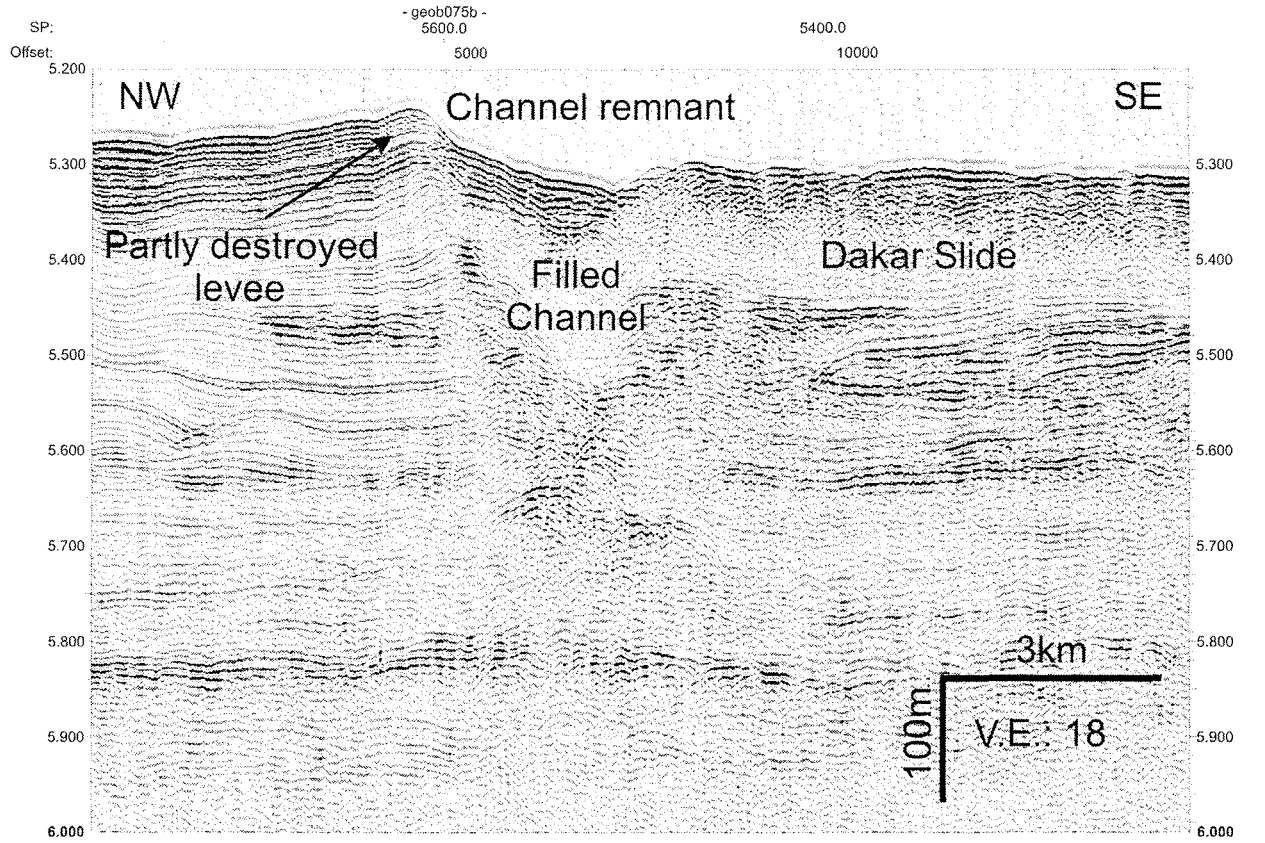

Fig. 4.2.12: Brute stack of Profile GeoB05-075. See Fig. 4.2.8 for location of profile.

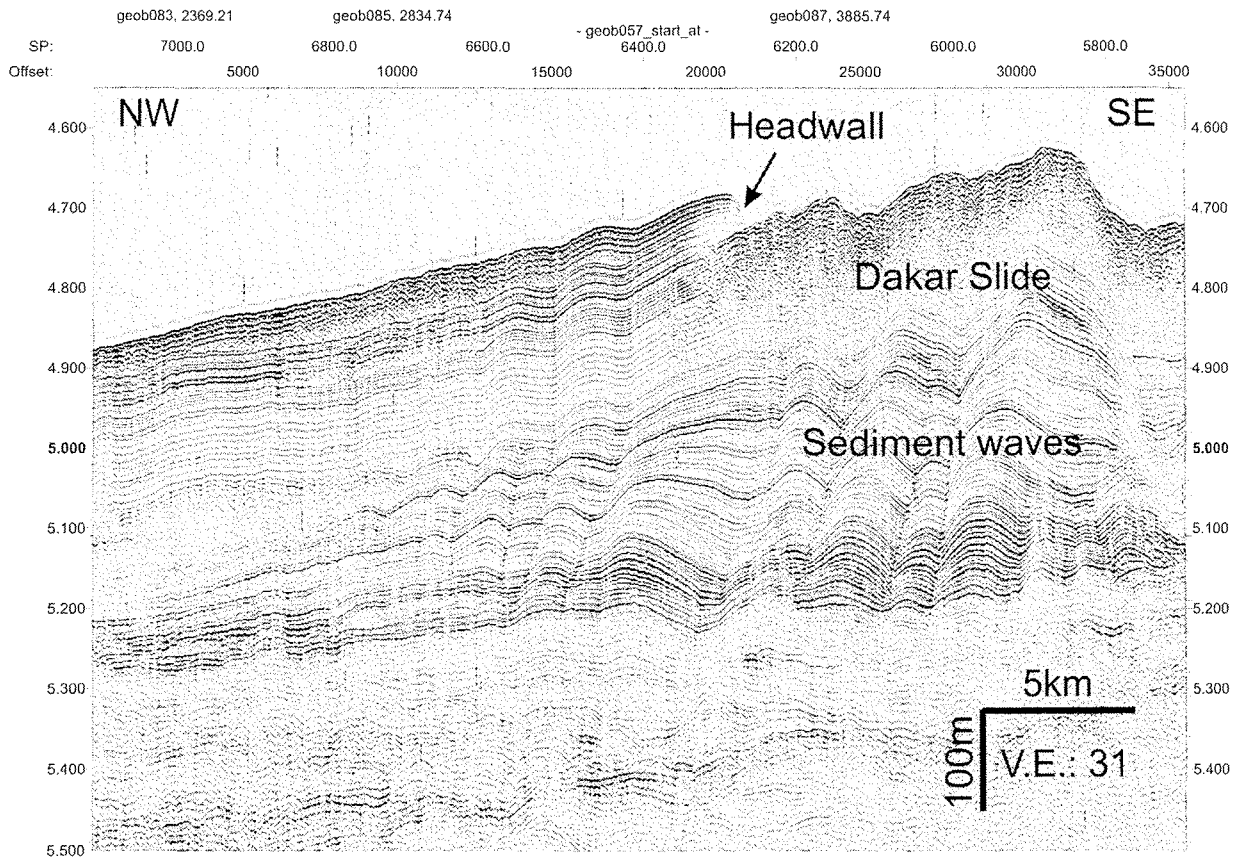

Fig. 4.2.13: Brute stack of Profile GeoB05-057. See Fig. 4.2.8 for location of profile.

canyon was significantly deeper prior to the initiation of the Dakar Slide and that the slide destroyed the canyon at water depths >3500m.

The large dimension of the Dakar Slide is illustrated by profiles collected south-east of Dakar Canyon. A typical example of the slide deposits and the sidewall area of the slide shows Profile GeoB05-057 (Fig. 4.2.13). A ~30m-high step in the morphology marks the headwall of the slide. The slope gradient in the headwall area is ~0.5°. Beneath the headwall the slide deposits are imaged for ~150ms-TWT. The slide deposits can be divided into two units. The upper unit is characterized by chaotic high amplitude reflector patches, while the lower unit shows acoustic transparency. It is unclear whether the slide is draped by a hemipelagic cover. Cores taken in the area of the Dakar Slide do not show clear indications for redeposited material, but we might have hit a relatively intact slide block, which have not moved very far. The deposits beneath the slide and north-west of the headwall are general characterized by parallel to subparallel reflectors with very good continuity. The sediments directly beneath the slide show a wavy pattern typical for large scale sediment waves. The sediment waves might be the result of contour parallel sediment transport due to bottom currents.

The Dakar Slide is an atypical slide in terms of water depth and slope gradient of the headwall area. A headwall in 3500m water depth is unusually deep and slope gradients of only 0.5° are very low. It is also a very large slide. Our profiles indicate that the diameter of the slide is >100km. Slides in water depths around 3500m were also imaged off the southern edge of the Senegal suggesting that large scale mass wasting in water depths >3000m is more important at this margin than previously suggested.

4.2.9 Preliminary results of the seismic survey of Cap Timiris Canyon

Cap Timiris Canyon was discovered during Meteor-Cruise M58/1 in spring 2003 (Schulz et al, 2003). During this cruise the canyon was surveyed for ~215km from the shelf edge to ~3000m water depth (Krastel et al., 2004, Antobreh and Krastel, 2005). During Cruise M65/2 additional seismic data were collected in the head region of Cap Timiris Canyon and the previously not mapped distal canyon (Fig. 4.2.14)

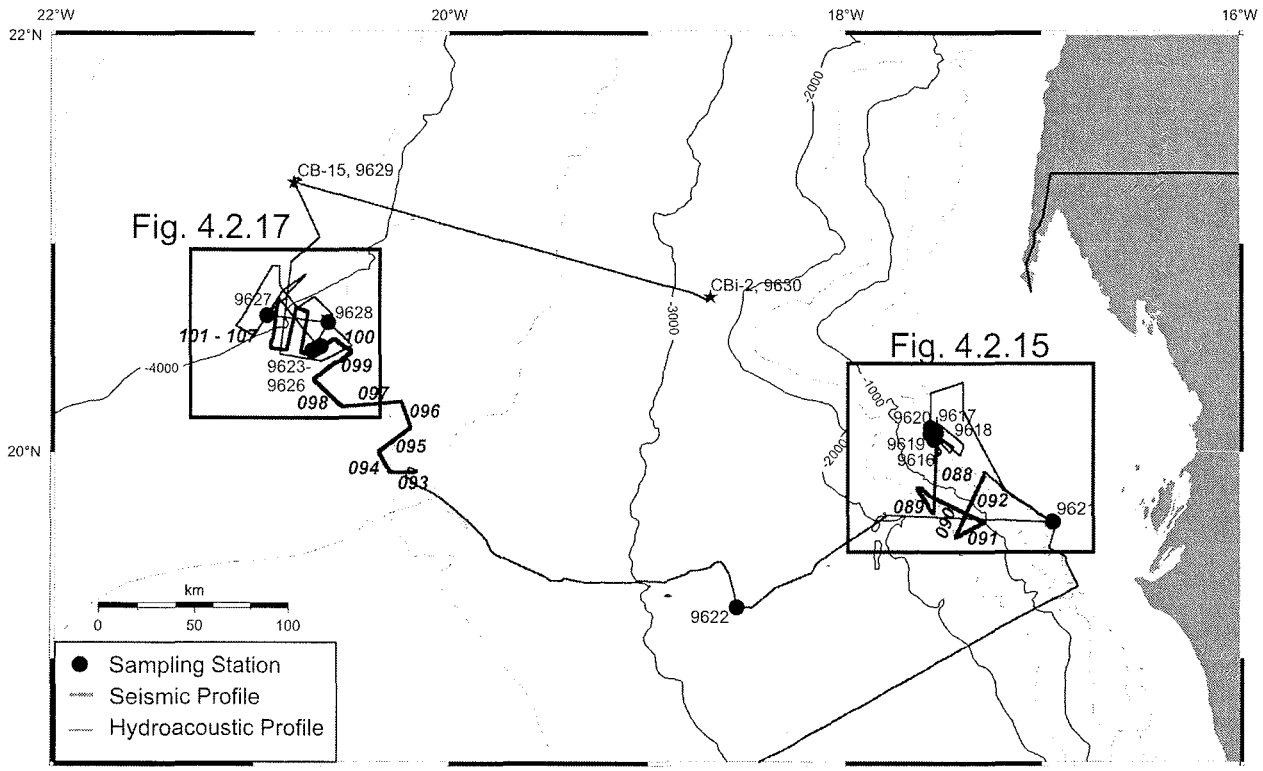

Fig. 4.2.14: Track chart of seismic and hydroacoustic survey of Cap Timiris Canyon.

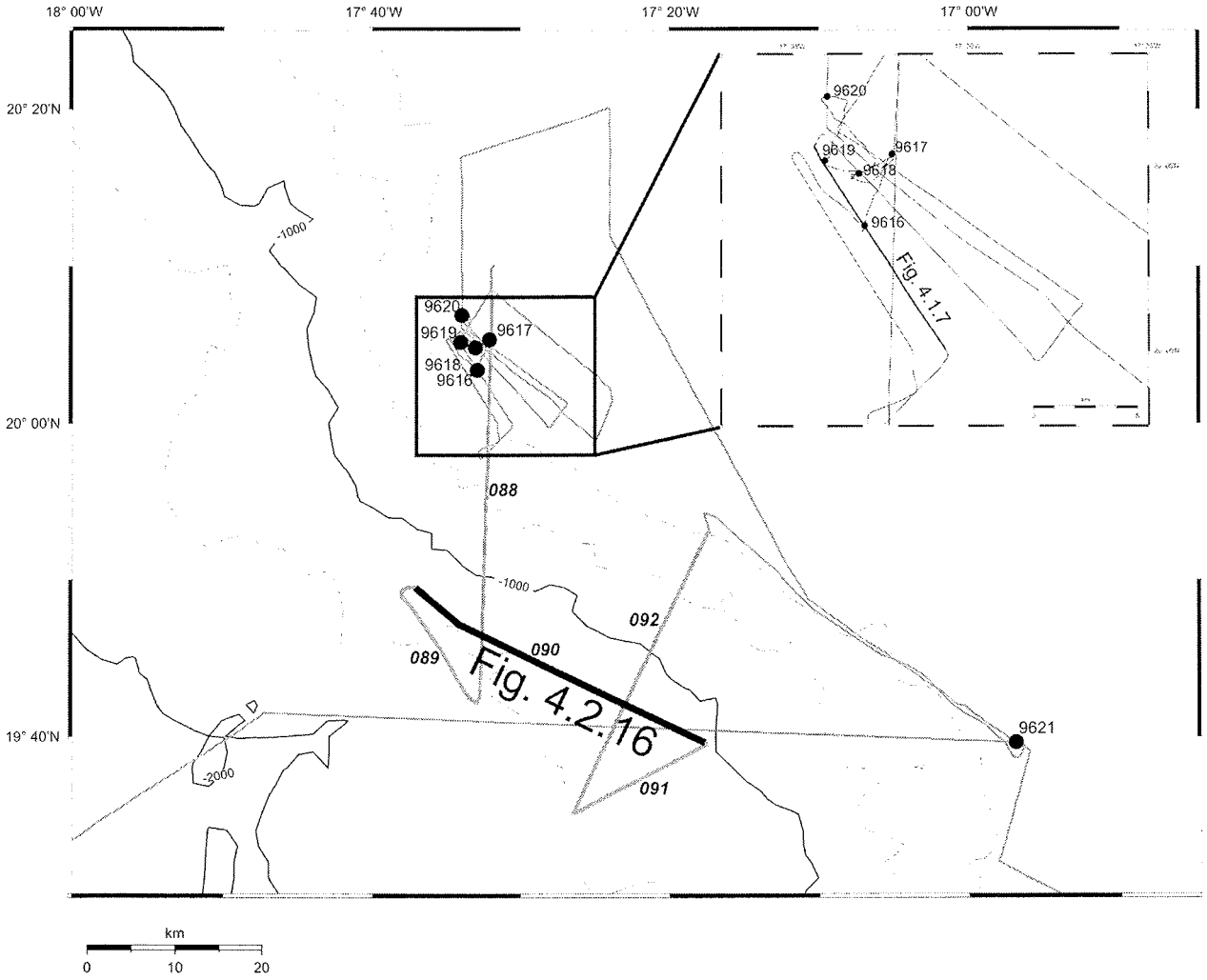

Fig. 4.2.15: Track chart of seismic and hydroacoustic survey of upper Cap Timiris Canyon.

Upper Timiris Canyon

Two slope perpendicular and one slope parallel seismic profile were collected in the head region of Cap Timiris Canyon (Fig. 4.2.15). Seismic Profile GeoB05-090 (Fig. 4.2.16) runs slope parallel in a water depth of ~1200m. Four main tributary canyons are visible on the profile. Each of these canyons is >250m deep. The seismic data do not show a major sediment fill of any canyon, hence suggesting that all canyons were active in the younger past though thin (<10m) layers cannot be detected by the used seismic system. The tributary canyons collect sediments from a large area, which might be the explanation for sediment transport through the canyon in the Holocene. Missing levees indicate that the turbidity currents are confined in the canyon. The tributary canyons show some terraces which are probably mainly the result of sliding and slumping. Despite the deeply incised tributary canyons some buried canyons are

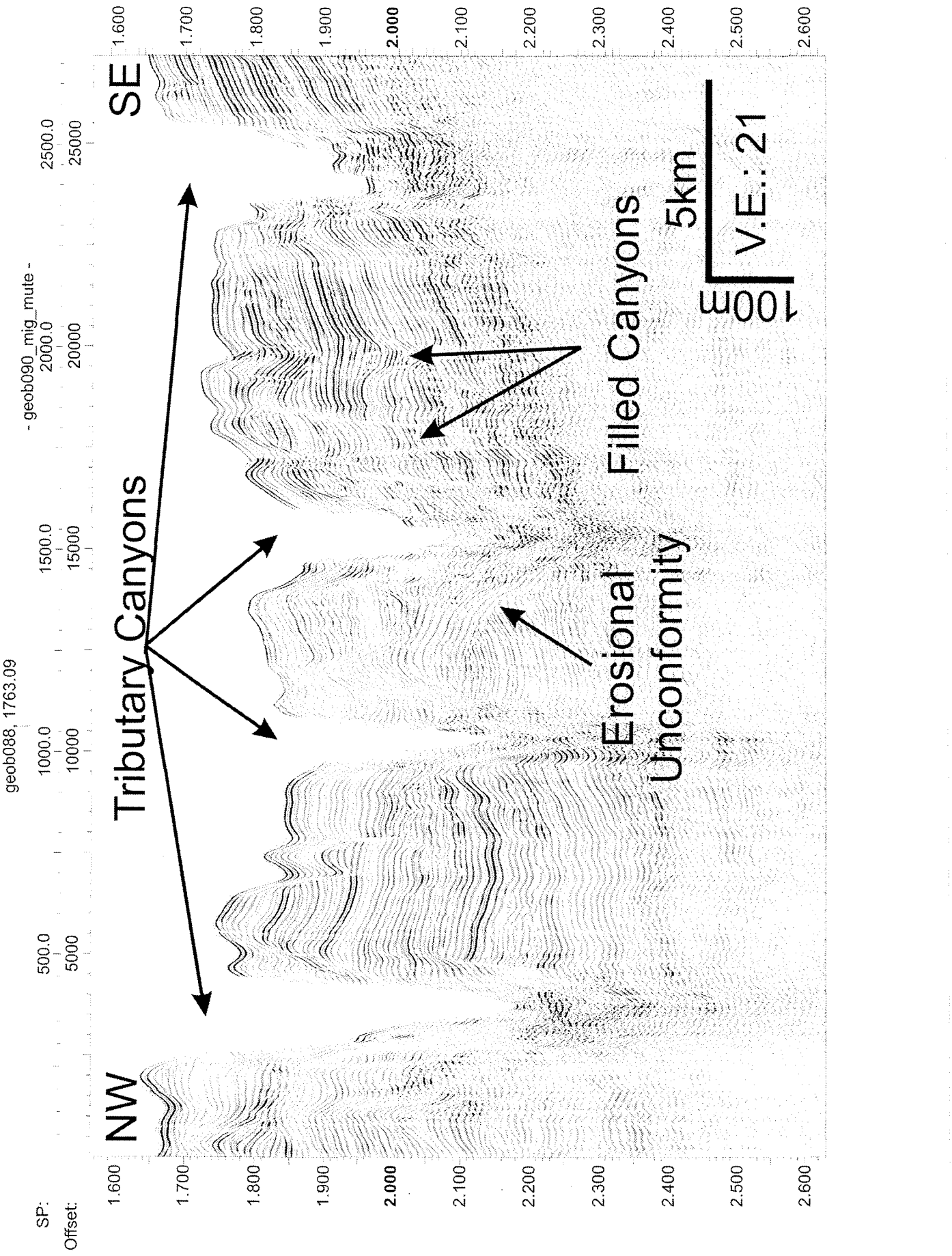

Fig. 4.2.16: CMP-Stack of Profile GeoB05-090. See Fig. 4.2.15 for location of profile.

imaged by the seismic data as well. Some of these buried canyons are relatively small but one of the buried canyons has a similar dimension as the presently active tributary canyons. A major erosional unconformity is found in the central part of the profile but cannot be traced further to the north-west or south-east. The erosional unconformity probably formed during a period of intense erosion by water or turbidity currents. As we cannot trace this unconformity over larger areas, such currents probably occur only locally and did not affect a larger area. The structure of the head region of Cap Timiris Canyon suggests a relatively complex evolution of the head region of the canyon. While no major shifts of the canyon were found on the middle and lower slope (Antobreh and Krastel, 2005), major changes of the main sediment transport pathways have occurred in the head region of the canyon.

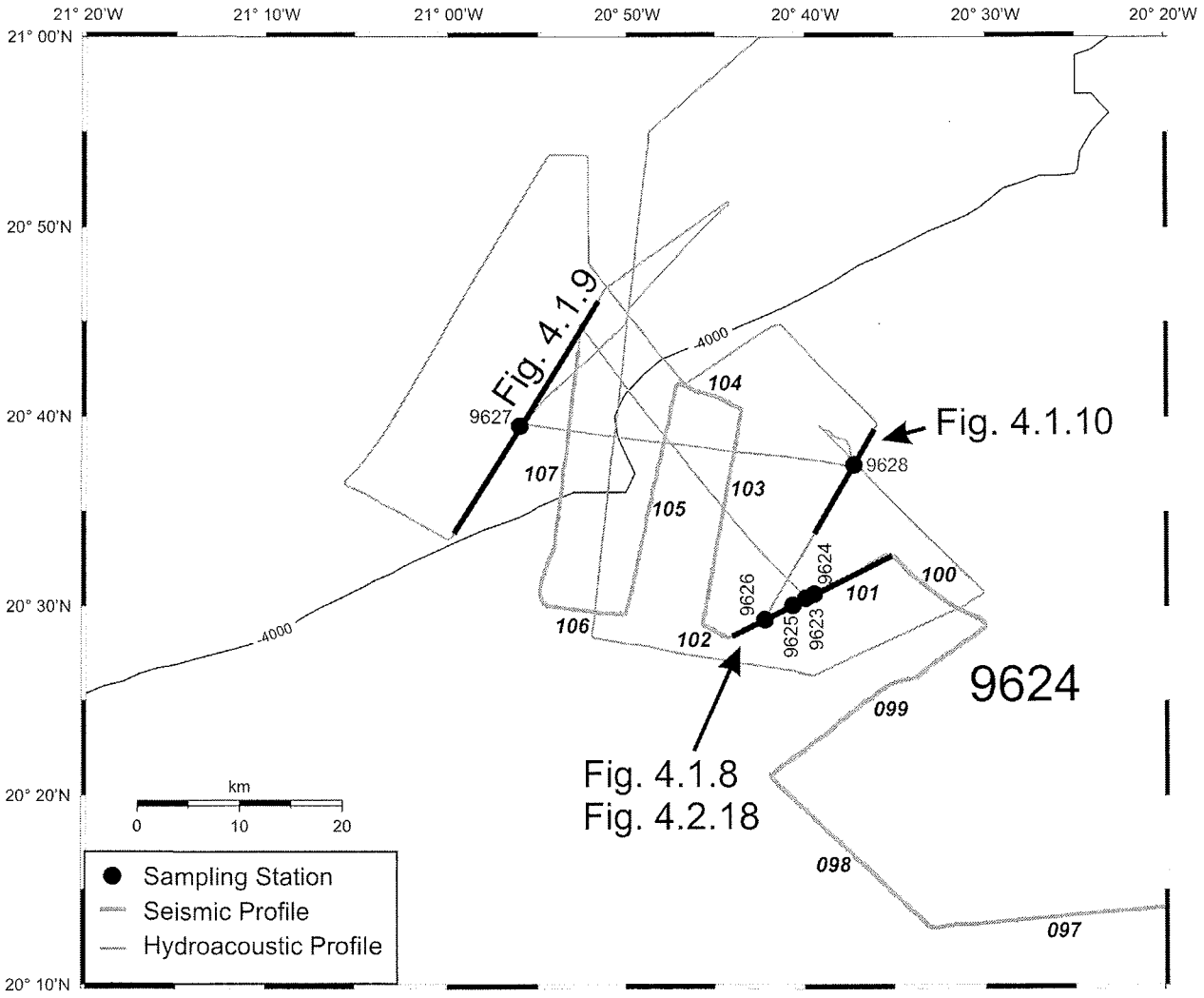

Fig. 4.2.17: Track chart of seismic and hydroacoustic survey of distal Cap Timiris Canyon.

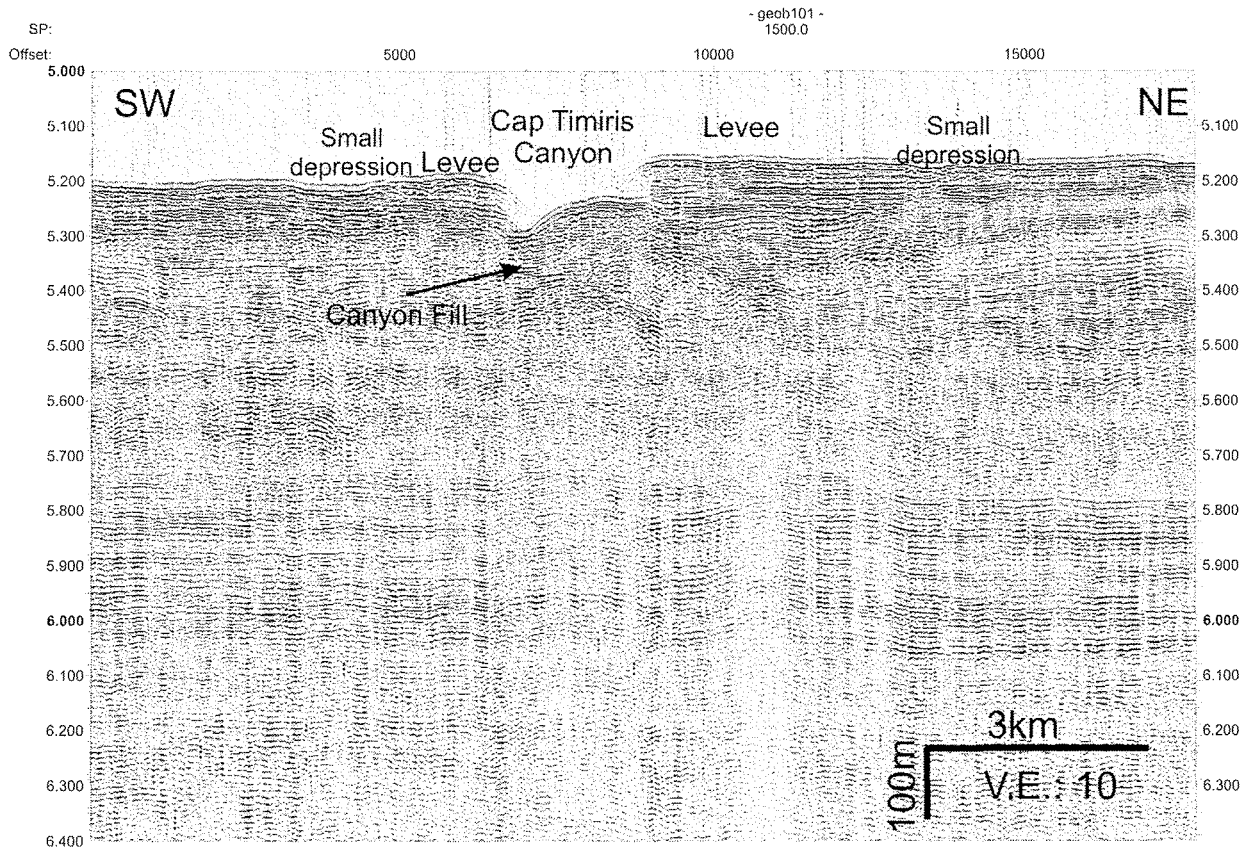

Fig. 4.2.18: Brute stack of Profile GeoB05-101. See Fig. 4.2.17 for location of profile.

Distal Timiris Canyon

Several seismic profiles crossing the canyon were collected at distal Timiris Canyon (Fig. 4.2.17). Seismic Profile GeoB05-101 (Fig. 4.2.18) shows a typical example. At this location the canyon is ~2km-wide and shows an asymmetrical shape with a 100m-high north-eastern flank and a 70m-high south-western flank. The canyon floor is characterized by short patches of parallel high-amplitude reflectors which probably represent a sandy canyon fill. A major terrace is imaged at the north-eastern flank of the canyon. This terrace is also characterized by parallel high amplitude reflectors. Levees are developed on both sides of the canyon though the right-hand north-western levee is higher and much better developed than the south-western levee. The occurrence of levees at distal Cap Timiris Canyons proves that overspill is becoming more important with decreasing incision depth and increasing distance from the shelf edge. The better developed north-eastern levee indicates preferred overspill of turbidity currents on the right-hand side of the canyons as a result of the Coriolis force. Some very small depressions are found on both sides of the main canyon but no major buried channels can be identified on the seismic section. Distal Cap Timiris Canyon was relatively stable

since its formation more than 170ka ago. The upper 100-200ms TWT sediments on both sides of the canyon are characterized by relatively high amplitude reflectors while the sediments beneath are imaged as medium amplitude reflectors with varying continuity. The high amplitude reflectors might be caused by sand rich turbidity currents, while the lower part of the section probably represents pelagic sediments.

4.2.10 List of seismic profiles

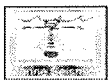

MTU Seismic Survey FG MeeresTechnik/Umweltforschung **M65/2**

Seismic Line GeoB

	Start						End					
Number of profile GeoB 05-	Date	Time UTC	Latitude north xx° xx.x'	Longitude west xx° xx.x'	Bison-1 FFN	Bison-2 FFN	Date	Time UTC	Latitude north xx° xx.x'	Longitude west xx° xx.x'	Bison-1 FFN	Bison-2 FFN
49	5.7.05	2:38	14°29,35	17°58,83	336	227	5.7.05	9:05	13°57,84	17°50,70	2934	2796
50	5.7.05	9:05	13°57,84	17°50,70	2934	2796	6.7.05	4:52	12°20,39	17°52,19	2861	2658
51	6.7.05	4:55	12°20,39	17°52,42	2889	2681	6.7.05	8:51	12°38,08	18°08,52	4459	4249
52	6.7.05	9:06	12°32,08	18°9,86	4555	4350	6.7.05	12:26	12°25,68	18°26,75	5892	5690
53	6.7.05	13:00	12°26,56	18°28,69	6105	5903	6.7.05	15:04	12°37,09	18°30,65	6933	6730
54	7.7.05	6:10	12°36,61	18°29,99	116	12	7.7.05	7:21	12°42,62	18°29,99	589	485
55	7.7.05	7:30	12°43,02	18°29,66	641	537	7.7.05	12:11	12°44,98	18°05,85	2523	2421
56	7.7.05	12:32	12°46,23	18°05,27	2658	2555	7.7.05	20:20	13°27,04	18°18,06	5780	5675
57	7.7.05	20:25	13°27,14	18°18,22	5802	5697	8.7.05	2:11	13°41,67	18°45,45		516
58	8.7.05	2:30	13°42,47	18°45,61		638	8.7.05	4:05	13°47,97	18°39,49		1288
59	8.7.05	4:10	13°47,91	18°39,33		1308	8.7.05	8:12	13°40,06	18°20,18		2908
60	8.7.05	8:20	13°40,29	18°19,69		2961	8.7.05	9:25	13°44,72	18°16,21		3401
61	8.7.05	9:35	13°45,27	18°16,36		3450	8.7.05	12:56	13°55,24	18°30,14		4766
62	8.7.05	13:08	13°55,87	18°30,19		4844	8.7.05	14:43	14°01,61	18°24,84		5465
63	8.7.05	14.56	14°01,61	18°24,04		5549	8.7.05	17:22	13°55,93	18°14,12		6502
64	8.7.05	17 27	13°55,96	18°13,83		6530	8.7.05	18:59	13°59,47	18°06,74		7135
65	8.7.05	19 02	13°59,62	18°06,76		7151	8.7.05	21:25	14°08,97	18°11,82		810
66	8.7.05	21 35	14°11,03	18°11,40		865	9.7.05	2:38	14°12,31	17°45,29		2839
67	9.7.05	2 58	14°13,12	17°44,75		2972	9.7.05	8:24	14°20,02	17°47,74		1262
68	11.7.05	10 31	13°26,67	19°05,04		138	11.7.05	11:09	13°25,39	19°07,17		312
69	11.7.05	11 14	13 24,97	19°07,23		349	11.7.05	13:59	13°14,66	18°58,72		1378
70	11.7.05	14 10	13 14,53	18°58,10		1439	11.7.05	15:34	13°19,83	18°53,15		1979
71	11.7.05	15 48	13 20,73	18°52,96		2066	11.7.05	18:24	13°30,98	19°01,35		3049
72	11.7.05	18 30	13 31,53	19°01,16		3093	11.7.05	19:43	13°36,03	18°57,03		3550
73	11.7.05	19 47	13 35,87	18°56,74		3583	11.7.05	22:27				
74	11.7.05	22 34	13 26,68	18°46,59		4630	11.7.05	23:30	13°24,25	18°50,60		4986
75	11.7.05	23 37	13 24,41	18°51,24		5038	12.7.05	1:34	13°31,10	18°58,42		5767
76	12.7.05	1 43	13 31,72	18°58,12		5826	12.7.05	3:21	13°36,65	18°51,45		6457
77	12.7.05	3 34	13 36,78	18°50,57		6544	12.7.05	4:43	13°32,07	18°47,05		7004
78	12.7.05	4 47	13 32,10	18°46,74		7003	12.7.05	5:38	13°34,71	18°43,07		7378
79	12.7.05	5 42	13 34,84	18°34,14		7400	12.7.05	6:52	13°39,42	18°47,02		7858
80	13.7.05	0 4	13 24,98	18°50,88		198	13.7.05	1:47	13°32,27	18°46,35		565
81	13.7.05	2 [illegible]	13 [illegible]	18°45,36		705	13.7.05	3:03	13°07,20	18°46,40		1056
82	13.7.05	3 21	13 26,60	18°45,11		1179	13.7.05	3:56	13°26,48	18°42,06		1417
83	13.7.05	4 06	13 26,59	18°41,93		1435	13.7.05	6:43	13°36,92	18°33,04		2494
84	13.7.05	6 49	13 36,84	18°32,82		2513	13.7.05	7:19	13°35,06	18°30,58		2723
85	13.7.05	7 2[illegible]	13 34,77	18°30,55		2758	13.7.05	8:28	13°29,39	18°31,41		3186
86	13.7.05	8 2[illegible]	13 26,76	18°30,89		3258	13.7.05	9:14	13°27,49	18°28,24		3484
87	13.7.05	9 19	13 27,61	18°27,86		3518	13.7.05	11:02	13°32,16	18°20,38		4193
88	16.7.05	18 [illegible]	20 06,22	17°33,02		50	16.7.05	23:24	19°42,64	17°32,79		2040
89	16.7.05	23 40	19 42,36	17°33,34		2180	17.7.05	1:24	19°48,79	17°37,88		2765
90	17.7.05	1 48	19 48,45	17°36,96		2917	17.7.05	5:57	19°39,55	17°17,62		4466
91	17.7.05	6 [illegible]	19 [illegible]	17°17,76		4491	17.7.05	7:51	19°35,10	17°26,33		5189
92	17.7.05	7 [illegible]	19 [illegible]	17°26,26		5224	17.7.05	12:07	19°53,27	17°17,43		6822
93	18.7.05	22 [illegible]	19 53,90	20°10,37		270	18.7.05	23:44	19°54,10	20°18,39		894
94	18.7.05	23 48	19 54,26	20°18,61		923	19.7.05	1:05	19°59,83	20°21,90		1432
95	19.7.05	1 [illegible]	20 [illegible]	20°21,37		1474	19.7.05	3:22	20°06,68	20°12,41		2348
96	19.7.05	3 2[illegible]	20 07,28	20°12,14		2416	19.7.05	5:22	20°14,49	20°15,01		3165
97	19.7.05	5 27	20 14,52	20°15,23		3177	19.7.05	8:47	20°12,98	20°32,76		4514
98	19.7.05	8 59	20 [illegible]05	20°33,05		4541	19.7.05	11:11	20°20,87	20°41,81		5480
99	19.7.05	11 16	20 21,11	20°41,80		5507	19.7.05	14:15	20°28,84	20°30,08		690
100	19.7.05	14.23	20 29,24	20°30,20		742	19.7.05	15:31	20°32,51	20°34,91		1191
101	19.7.05	15.39	20 32,60	20°35,66		1242	19.7.05	17:27	20°28,33	20°44,30		1961
102	19.7.05	17.30	20 26,39	20°44,49		1980	19.7.05	17:41	20°28,89	20°45,36		2055
103	19.7.05	17.47	20 29,21	20°45,67		2099	19.7.05	19:59	20°40,12	20°43,58		2986
104	19.7.05	20:03	20 40,33	20°43,55		3002	19.7.05	20:45	20°41,72	20°46,90		3267
105	19.7.05	20:51	20 41,45	20°47,21		3306	19.7.05	23:19	20°29,66	20°50,02		4271
106	19.7.05	23:23	20 29,55	20°50,23		4295	20.7.05	0:10	20°29,96	20°54,25		4608
107	20.7.05	0:23	20 30,40	20°54,84		4686	20.7.05	3:26	20°43,48	20°52,74		5889

4.3 Sediment Sampling

(T.J.J. Hanebuth, R. Henrich, C. Holz, B. Kockisch, R. Pierau, U. Proske, C. Reuter, R.B. Wynn)

4.3.1 Sediment Sampling and Methods

The cruise has covered different environmental settings such as the usually fine-grained upper to lower portions of the continental slope on the one hand, and the commonly coarser-grained basal parts of canyons and the shelf on the other. Therefore, we have used the Multicorer (*Multilot*) and Giant Box Corer (*Großkastengreifer*) for sampling of seafloor sediments and the Gravity Corer (*Schwerelot*) and Kasten Corer (*Kastenlot*) for deeper penetration. In the following the different sampling strategies are briefly presented, the individual core descriptions are shown and a preliminary discussion of the first results is given.

Tab. 4.3.1: M65-2 station list.

GeoB #	Ship's #	Date 2005	Time (UTC)	Lat (°N)	Long (°W)	Water depth (m)	Gear	Recovery Remarks
9601-1	333	4. Jul		14°27,80	17°57,04	1924	Rosette/CTD	150 m WD
9601-2	333	4. Jul	20:46	14°27,79	17°57,01	1924	Multicorer	8/4 20-24 cm recovery
9601-3	333	4. Jul	22:37	14°27,81	17°59,98	1920	Gravity corer	740 cm
9601-4	333	4. Jul	23:50	14°27,89	17°57,07	1924	Rosette	60 m WD
9602-1	335	6. Jul	16:29	12°35,27	18°30,39	3981	Rosette/CTD	400 m WD
9602-2	335	6. Jul	18:34	12°35,23	18°30,36	3986	Multicorer	8/4 34-38 cm recovery
9602-3	335	6. Jul	21:35	12°35,26	18°30,37	3981	Gravity corer	483 cm
9603-1	336	6. Jul	23:21	12°34,03	18°30,07	4087	Rosette/CTD	
9603-2	336	7. Jul	0:55	12°34,02	18°30,08	4083	Multicorer	0/1 40 cm recovery
9603-3	336	7. Jul	3:56	12°34,11	18°30,10	4085	Gravity corer	core bent
9604-1	338	9. Jul	12:31	14°11,14	17°54,05	1921	Rosette/CTD	
9604-2	338	9. Jul	14:11	14°11,07	17°54,04	1920	Multicorer	0/1 33 cm recovery
9604-3	338	9. Jul	16:12	14°11,01	17°54,10	1925	Gravity corer	831 cm
9605-1	339	9. Jul	18:12	14°17,60	17°55,80	1912	Gravity corer	790 cm
9605-2	339	9. Jul	19:58	14°17,60	17°55,80	1915	Multicorer	8/4 30 cm recovery
9606-1	340	9. Jul	22:37	14°11,65	17°59,85	2286	Multicorer	8/4 34 cm recovery
9606-2	340	10. Jul	0:41	14°11,03	17°59,82	2287	Gravity corer	951 cm
9607-1	342	10. Jul	8:03	14°11,29	18°06,65	2999	Gravity corer	350 cm
9607-2	342	10. Jul	10:18	14°11,23	18°06,63	3000	Multicorer	8/4 48 cm recovery
9607-3	342	10. Jul	12:56	14°11,29	18°06,65	3004	Gravity corer	784 cm
9608-1	343	10. Jul	14:41	14°11,22	18°08,25	2589	Rosette/CTD	
9608-2	343	10. Jul	16:01	14°11,29	18°08,29	2586	Gravity corer	908 cm
9608-3	343	10. Jul	18:10	14°11,18	18°08,28	2590	Multicorer	8/4 35-43 cm recovery
9609-1	344	10. Jul	20:48	14°11,32	18°05,62	2776	Multicorer	8/4 35-39 cm recovery
9609-2	344	10. Jul	23:08	14°11,35	18°05,63	2785	Gravity corer	542 cm
9610-1	347	12. Jul	9:47	13°45,27	18°32,68	3752	Gravity corer	254 cm
9611-1	348	12. Jul	15:18	13°32,30	18°52,60	3983	Gravity corer	147 cm
9612-1	349	12. Jul	17:08	13°32,96	18°52,70	3956	Rosette/CTD	
9612-2	349	12. Jul	19:14	13°32,98	18°53,50	3922	Multicorer	1/3 10-11 cm recovery

Tab. 4.3.1: M65-2 station list (continued).

GeoB #	Ship's #	Date 2005	Time (UTC)	Lat (°N)	Long (°W)	Water depth (m)	Gear	Recovery Remarks
9612-3	349	12. Jul	22:15	13°33,01	18°53,50	3893	Gravity corer	878 cm
9613-1	351	13. Jul	15:33	13°30,79	18°50,80	3937	Gravity corer	over penetrated
9613-2	351	13. Jul	17:57	13°30,80	18°50,80	3936	Gravity corer	982 cm
9614-1	352	13. Jul	22:21	13°20,54	19°03,56	4090	Gravity corer	478 cm
9615-1	353	14. Jul	1:14	13°23,65	19°06,25	4108	Gravity corer	944 cm
9616-1	355	16. Jul	10:12	20°03,37	17°32,96	90	Box Corer	25 cm
9617-1	356	16. Jul	10:55	20°05,32	17°32,17	80	Rosette/CTD	winch problems
9617-2	356	16. Jul	11:15	20°05,32	17°32,15	10	Rosette/CTD	
9617-3	356	16. Jul	11:50	20°05,32	17°32,15	80	Box Corer	39 cm
9618-1	357	16. Jul	12:37	20°04,79	17°33,08	90	Box Corer	36 cm
9618-2	357	16. Jul	15:17	20°04,75	17°33,16	90	Kastenlot	core bent
9619-1	358	16. Jul	13:16	20°05,16	17°34,06	84	Box Corer	39 cm
9620-1	359	16. Jul	14:00	20°06,89	17°34,07	92	Rosette	
9620-2	359	16. Jul	14:10	20°06,88	17°34,01	91	Box Corer	41 cm
9621-1	362	17. Jul	15:35	19°39,37	16°56,37	53	Rosette/CTD	
9621-2	362	17. Jul	16:01	19°39,37	16°56,37	53	Multicorer	8/4 32-34 cm recovery
9621-3	362	17. Jul	16:31	19°39,37	16°56,36	52	Gravity corer	574 cm
9622-1	364	18. Jul	3:12	19°14,84	18°33,19	2879	Rosette/CTD	400 m WD
9622-2	364	18. Jul	4:45	19°14,87	18°33,20	2878	Multicorer	8/4 32-39 cm recovery
9622-3	364	18. Jul	7:16	19°14,87	18°33,24	2881	Gravity corer	1045 cm
9623-1	367	20. Jul	6:17	20°30,48	20°40,06	3940	Rosette/CTD	400 m WD
9623-2	367	20. Jul	8:12	20°30,38	20°39,96	3940	Gravity corer	196 cm / core bent
9623-3	367	20. Jul	9:42	20°30,43	20°39,98	3938	Partikelcamera	
9624-1	368	20. Jul	11:08	20°30,64	20°39,53	3894	Gravity corer	1133 cm
9624-2	368	20. Jul	13:59	20°30,64	20°39,55	3890	Multicorer	3/3 8-10 cm recovery
9625-1	369	20. Jul	17:04	20°30,06	20°40,74	3990	Gravity corer	empty
9626-1	370	20. Jul	19:33	20°29,31	20°42,24	3926	Gravity corer	431 cm
9627-1	372	21. Jul	9:14	20°39,50	20°56,03	4028	Gravity corer	312 cm
9628-1	373	21. Jul	13:27	20°37,45	20°37,33	3928	Gravity corer	1068 cm
9628-2	373	21. Jul		20°38,55	20°37,62	3941	Partikelcamera/ CTD	1000 m WD
9629-1	375	22. Jul		21°16,85	20°47,29	4177	Partikelcamera/ CTD	2000 m WD
9629-2	375	22. Jul	7:17	21°17,75	20°47,35	4170	CB 15	
9629-3	375	22. Jul		21°18,76	20°45,94	4177	Rosette	600 m WD
9629-4	375	22. Jul		21°18,96	20°46,34	4177	Rosette	45 m WD
9629-5	375	22. Jul	17:30	21°18,10	20°47,80	4170	CB 16	
9630-1	376	23. Jul		20°43,71	18°42,00	2717	Partikelcamera/ CTD	
9630-2	376	23. Jul	7:24	20°44,20	18°42,10	2722	CBi-2	
9630-3	376	23. Jul	11:15	18°42,36	20°44,09	2730	Rosette	900 m WD
9630-4	376	23. Jul		18°42,64	20°44,17	2735	Rosette	500m WD
9630-5	376	23. Jul	14:30	20°45,72	18°41,10	2670	CBi-3	

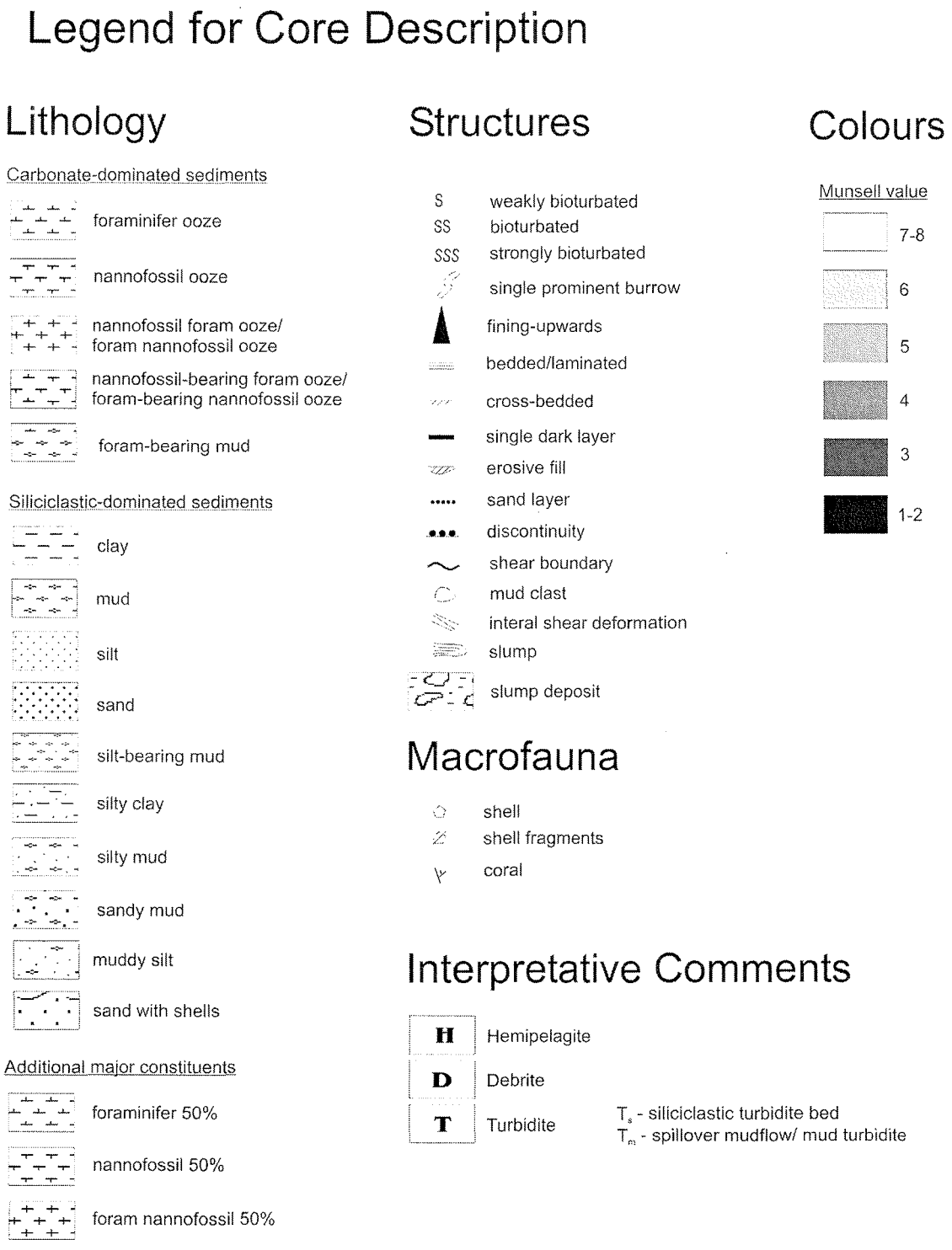

Fig. 4.3.1: Legend for the core descriptions following in this chapter.

4.3.1.1 Sampling procedure of Multicorer sediment profiles

During the cruise M65-2, we used the Multicorer to get undisturbed surface sediment profiles together with the overlying bottom water from soft-sediment stations in 8 large and 4 small (10 and 6 cm in diameter) 60-cm long plastic tubes. The Multicorer was used at 13 stations. Once the core was retrieved on the deck, the water temperature was measured and the overlying water was removed afterwards.

Tab. 4.3.2: Multicorer station list.

GeoB #	Date 2005	Time at sea floor	Lat (°N)	Long (°W)	Water depth (m)	Recovery	Temp. (°C) [*]
9601-2	4. Jul	20:46	14°27,79	17°57,01	1924	8xL, 4xS, 20-24 cm	11,1
9602-2	6. Jul	18:34	12°35,23	18°30,36	3986	8xL, 4xS, 34-38 cm	9,3
9603-2	7. Jul	00:55	12°34,02	18°30,08	4083	0xL, 1xS, 40 cm	13,1
9604-2	9.jul	14:11	14°11,07	17°54,04	1920	0xL, 1xS, 33 cm	-
9605-2	9.jul	19:58	14°17,60	17°55,80	1915	8xL, 4xS, 30 cm	9,5
9606-1	9.jul	22:37	14°11,65	17°59,85	2286	8xL, 4xS, 34 cm	9,6
9607-2	10.jul	10:18	14°11,23	18°06,63	3000	8xL, 4xS, 48 cm	8,1
9608-3	10.jul	18:10	14°11,18	18°08,28	2590	8xL, 4xS, 35-43 cm	8,3
9609-1	10.jul	20:48	14°11,32	18°05,62	2776	8xL, 4xS, 35-39 cm	8,5
9612-2	12.jul	19:14	13°32,98	18°53,50	3922	1xL, 3xS, 10-11 cm	10,2
9621-2	17.jul	16:01	19°39,37	16°56,37	53	8xL, 4xS, 32-34 cm	22
9622-2	18.jul	4:45	19°14,87	18°33,20	2878	8xL, 4xS, 32-39 cm	8,5
9624-2	20.jul	13:59	20°30,64	20°39,55	3890	3xL, 3xS, 8-10 cm	13,4

[*] The temperature was measured directly after opening the MUC and does not represent the original temperature on the seafloor.

The following standard scheme was applied for Multicorer sampling (in most cases):

<u>8 large tubes:</u>

Cut into 1 cm slices for organic purposes
Cut into 1 cm slices for planktonic and benthic foraminifer studies
Cut into 1 cm slices for planktonic and benthic foraminifer studies
Cut into 1 cm slices for sedimentological investigations
Cut along-core in two half pieces for detail description
Cut into 1 cm slices for paleontological purposes
Surface sampling for paleontological purposes
Cut into 1 cm slices for geochemical measurements

<u>4 small tubes:</u>

Cut into 1 cm slices for geomagnetic investigations
For geochemical/RFA purposes
Frozen in once for organic purposes
Frozen in once as archive core

Multicorer core descriptions:

GeoB 9602-2

Date: 06.07.05 Pos: 12°35.23' N 18°30.36' W
Water depth: 3986 m Core length: 38 cm

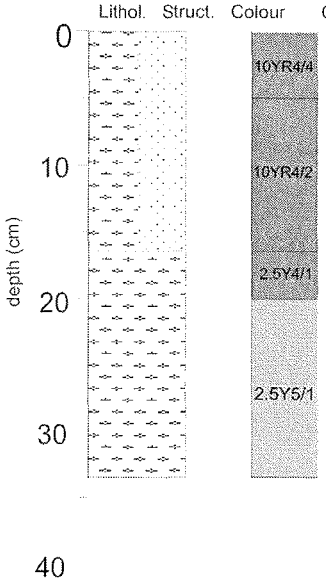

0 - 5 cm: dark yellowish brown foraminiferal silty mud, 10YR4/4

5 - 16 cm: dark greyish brown foraminiferal silty mud, 10YR4/2

16 - 20 cm: dark grey foram-bearing mud, 2.5Y4/2

20 - 33 cm: dark grey foram-bearig mud, 2.5Y5/1

GeoB 9603-2

Date: 06.07.05 Pos: 12°34.02' N 18°30.08' W
Water depth: 4083 m Core length: 40 cm

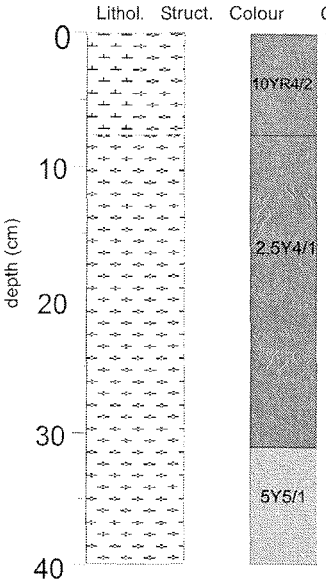

0 - 7 cm: dark yellowish brown to brown foraminiferal mud, 10YR4/2 to 10YR4/3

7 - 31 cm: dark grey mud, 2.5Y4/1

31 - 40 cm: grey mud, 5Y5/1

GeoB 9604-2

Date: 09.07.05 Pos: 14°11.07' N 17°54.04' W
Water depth: 1920 m Core length: 33 cm

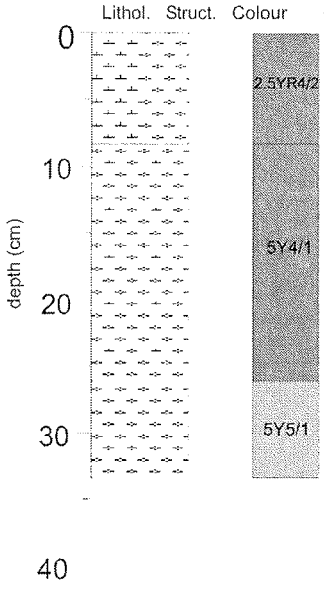

0 - 8 cm: dark greyish brown foraminiferal mud, 2.5YR4/2

8 - 26 cm: dark grey to olive grey foram-bearing mud, 5Y4/1 to 5Y4/2

26 - 33 cm: grey to dark grey mud, 5Y5/1 to 5Y4/1

GeoB 9605-2

Date: 09.07.05 Pos: 14°17.60' N 17°55.80' W
Water depth: 1915 m Core length: 31 cm

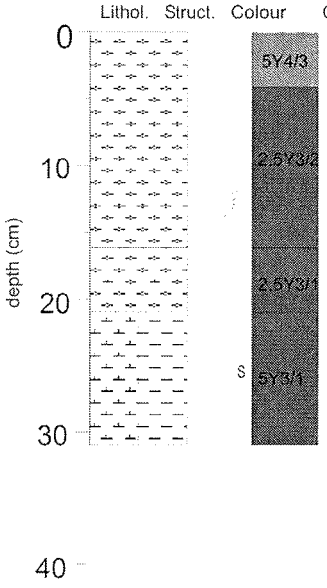

0 - 4 cm: olive very soft mud with open burrows, 5Y4/3

4 - 16 cm: very dark grayish brown very soft mud with open burrows, 2.5Y3/2

16 - 21 cm: very dark grey, foram-bearing mud with large burrows, transition zone, 2.5Y3/1

22 - 31 cm: very dark grey sticky, plastic foram-bearing clay, slightly bioturb., 5Y3/1

GeoB 9606-1

Date: 09.07.05 Pos: 14°11.65' N 17°59.85' W
Water depth: 2286 m Core length: 34 cm

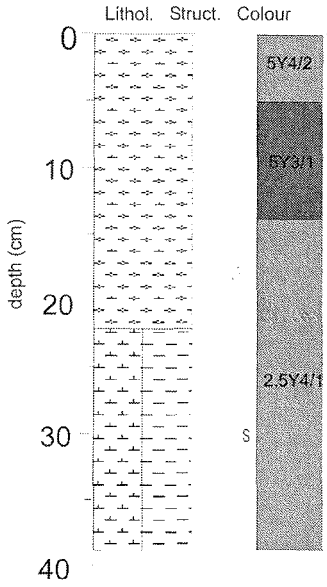

0 - 5 cm: olive grey very soft foram-bearing mud, 5Y4/2

5 - 14 cm: very dark grey, very soft foram-bearing mud, 5Y3/1

14 - 22 cm: dark grey, foram-bearing mud with open burrows, transition zone, 2.5Y4/1

22 - 38 cm: dark grey sticky, plastic foram-bearing clay, slightly bioturb.,2.5Y4/1

GeoB 9607-2

Date: 10.07.05 Pos: 14°11.23' N 18°06.63' W
Water depth: 3000 m Core length: 48 cm

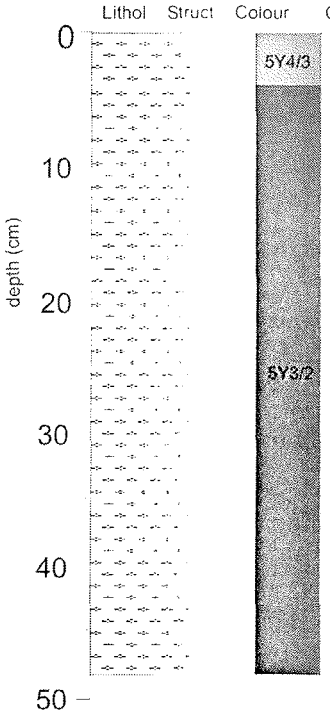

0 - 4 cm: olive very soft mud, 5Y4/3

4 - 48 cm: dark olive grey foram-bearing mud with large burrows filled with very soft mud, 5Y3/2

GeoB 9621-2

Date: 17.07.05 Pos: 19°39.37' N 16°56.37' W
Water depth: 53 m Core length: 29 cm

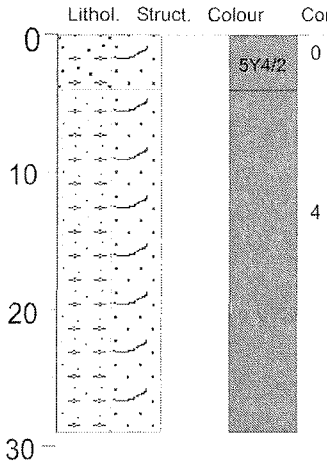

0 - 4 cm: olive grey sandy, silty mud with shell fragments, 5Y4/2

4 - 29 cm: dark grey silty to fine sand mud with shell fragments

GeoB 9622-2

Date: 18.07.05 Pos: 19°14.87' N 18°33.20' W
Water depth: 2878 m Core length: 43 cm

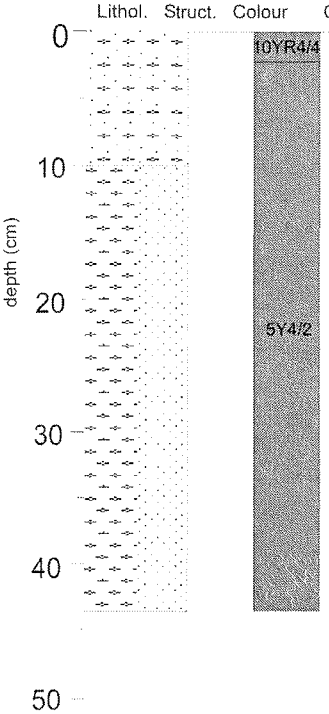

0 - 2 cm: dark yellowish brown
0 - 10 cm: olive grey very soft silty mud, some forams, pteropods at the surface, 5Y4/2

10 - 43 cm: olive grey foram-bearing silty mud, very homogenous, 5Y4/2

4.3.1.2 Sampling procedure of Giant Box Corer (Großkastengreifer) sediment profiles

The Giant Box Corer was used in areas where we expected a coarse-grained surface material, i. e. in shelf settings. The Giant Box Corer was applied at 5 stations (Tab. 4.3.3). The over-standing water has been removed and the sediment surface has been described and photographed. Then, the front wall has been opened and the downcore profile has been described, photographed and sampled.

Tab. 4.3.3: Giant Box Corer station list.

GeoB #	Date 2005	Time at sea floor	Lat (°N)	Long (°W)	Water depth (cm	Recovery
9616-1	16. Jul	10:12	20°03,37	17°32,96	90	3xL, 25 cm
9617-3	16. Jul	11:50	20°05,32	17°32,15	80	3xL, 39 cm
9618-1	16. Jul	12:37	20°04,79	17°33,08	90	3xL, 36 cm
9619-1	16. Jul	13:16	20°05,16	17°34,06	84	3xL, 39 cm
9620-2	16. Jul	14:10	20°06,88	17°34,01	91	3xL, 41 cm

Generally, the following standard scheme was applied for the Giant Box Corer sampling:

1. 1 *surface* sample for dinoflagellate analyses
2. 1 *surface* sample for sedimentological investigations
3. 1 *surface* sample for foraminifer studies
4. 1 sub-core (tube), cut into two halves for detailed description and radiography
5. 2 sub-cores (tubes) for archive purposes
6. 1 transparent archive box sample
7. 1 plastic bag sample (ca. 1 kg) for paleontological purposes
8. Continuous downcore sampling in plastic bags in 5-cm steps for sedimentological analysis

Giant Box Core descriptions:

GeoB 9616-1

Date: 16.07.05 Pos: 20°03.37' N 17°32.96' W
Water depth: 90 m Core length: 25 cm

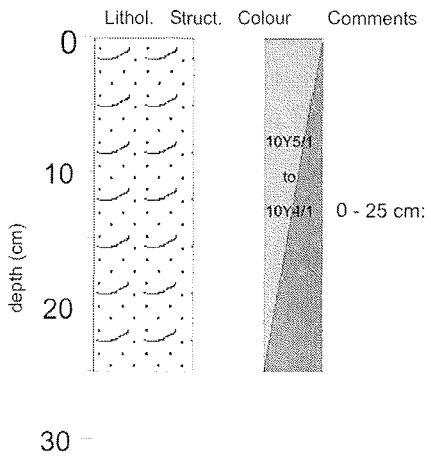

0 - 25 cm: greenish grey to dark greenish grey fine to medium quartz sand, admixed common fine shell debris of molluscs, 10Y5/1 to 10Y4/1

GeoB 9617-3

Date: 16.07.05 Pos: 20°05.32' N 17°32.15' W
Water depth: 80 m Core length: 24 cm

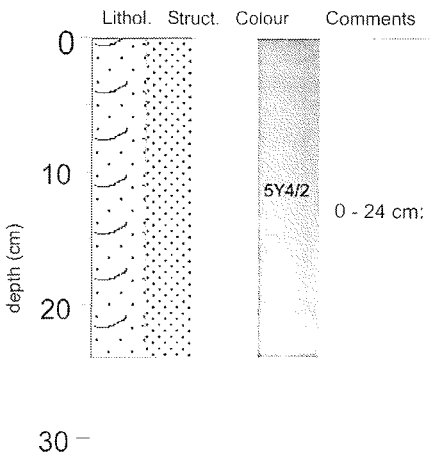

0 - 24 cm: olive grey fine to very fine quartz sand and sandy mud, mixed with fine shell debris of molluscs, few agglitunated (mm-sized) worm tubes, 5Y4/2

GeoB 9618-1

Date: 16.07.05 Pos: 20°04.79' N 17°33.08' W
Water depth: 90 m Core length: 28 cm

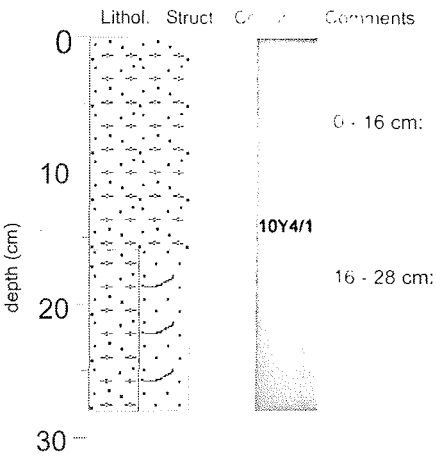

0 - 16 cm: olive grey fine sandy mud, common forams, 10Y4/1

16 - 28 cm: olive grey fine sand and sandy mud, mixed with abundant shell debris and intact shells of molluscs, 10Y4/1

GeoB 9619-1

Date: 16.07.05 Pos: 20°05.16' N 17°34.06' W
Water depth: 84 m Core length: 28 cm

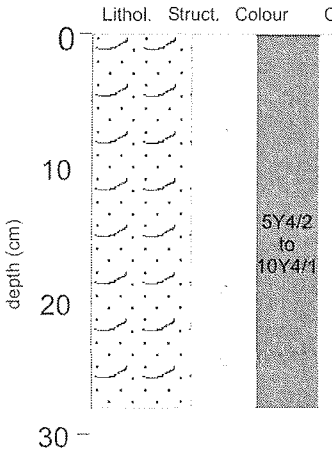

0 - 18 cm: olive grey to dark greenish grey fine quartz sand, admixed with sand sized shell fragments and forams, 5Y4/2 to 10Y4/1

18 - 28 cm: see above, large shells of bivalves and shell fragments

GeoB 9620-2

Date: 16.07.05 Pos: 20°06.88' N 17°34.01' W
Water depth: 91 m Core length: 28 cm

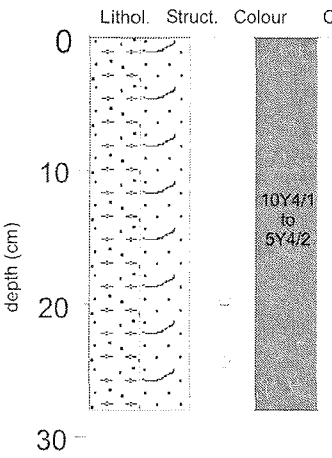

0 - 28 cm: dark greenish grey very fine sandy mud with shell drbris of molluscs, 10Y4/1 to 5Y4/2

17 - 28 cm: more shells

4.3.1.3 Sampling procedure of Gravity Corer sediment profiles

During the M65-2 cruise, 25 sediment cores from 26 stations were recovered using the Gravity Corers SL-3.5, SL-6 and SL-12 (Tab. 4.3.4). Once the core was retrieved on the deck, the core liners were cut into 1-m long segments, closed with caps and inscribed according to the GeoB scheme. All cores were cut along-core into two halves: one containing the *Work* and the other the *Archive* material.

Tab. 4.3.4: Gravity Corer station list.

GeoB	Lat (°N)	Long (°W)	Water depht (m)	Location	Recovery (cm)	Remarks
9601-3	14°27,81	17°59,98	1920	Senegal slope	740	
9602-3	12°35,26	18°30,37	3981	Senegal slope	483	
9603-3	12°34,11	18°30,10	4085	Senegal slope	0	core bent
9604-3	14°11,01	17°54,10	1925	Dakar Canyon	831	
9605-1	14°17,60	17°55,80	1912	Dakar Canyon	790	
9606-2	14°11,03	17°59,82	2287	Dakar Canyon	951	
9607-1	14°11,29	18°06,65	2999	Dakar Canyon	350	Overpenetrated
9607-3	14°11,29	18°06,65	3004	Dakar Canyon	784	
9608-2	14°11,19	18°08,29	2586	Dakar Canyon	908	
9609-2	14°11,35	18°05,63	2785	Dakar Canyon	542	
9610-1	13°45,27	18°32,61	3752	Dakar Canyon	254	
9611-1	13°32,30	18°52,60	3983	Dakar Canyon	147	
9612-3	13°33,01	18°53,50	3893	Dakar Canyon	878	
9613-1	13°30,79	18°50,80	3937	Dakar Canyon		Overpenetrated
9613-2	13°30,80	18°50,80	3936	Dakar Canyon	982	
9614-1	13°20,54	19°03,56	4090	Dakar Canyon	478	
9615-1	13°23,65	19°06,25	4108	Dakar Canyon	944	
9618-2	20°04,75	17°33,16	90	Mauritania shelf	135	Kasten corer, core bent
9621-3	19°39,37	16°56,36	52	Mauritania shelf	574	
9622-3	19°14,87	18°33,21	2881	Cap Timiris Canyon	1045	
9623-2	20°30,38	20°39,96	3940	Cap Timiris Canyon	196	core bent
9624-1	20°30,64	20°39,53	3894	Cap Timiris Canyon	1133	
9625-1	20°30,06	20°40,74	3990	Cap Timiris Canyon		Empty
9626-1	20°29,31	20°42,24	3926	Cap Timiris Canyon	431	
9627-1	20°39,50	20°56,03	4028	Cap Timiris Canyon	312	
9628-1	20°37,45	20°37,33	3928	Cap Timiris Canyon	1068	

The sediments have been described and documented by overview and detail photography. The preliminary lithology of the sediments retrieved by Gravity Coring is based on visual description and smear slides taken from distinct horizons (Figs. in the following). Colours have been identified according to the MUNSELL soil colour chart. Special efforts have been made for a detailed description of deposits resulting from gravity mass movement processes. In order to have a better understanding about the mechanism of sedimentation process, x-ray radiographs of 25-cm length have been taken continuously from all cores to resolve the internal sediment structures in highest quality.

Each visual core description is complemented by the results of the physical properties measurements (reflectance, red/blue ratio, porosity, magnetic susceptibility). The physical background and experimental techniques are described in section 4.4.1.

From the work-half, samples were taken routinely at 10-cm depth intervals (Fig. 4.3.2). Samples were taken for sedimentological, paleoceanographical, geochemical, and rock and paleomagnetic analyses. The hemipelagic portions ("background") of cores, which have been classified as of significant interest on the base of first observations, have been sampled in 5-cm intervals. Turbidites have been sampled in 1-cm steps over their full thickness. This means that the material of these gravity-driven deposits was completely sampled. In contrast, debrite deposits have not at all been sampled since sampling for stratigraphic purposes is meaningless and a later selective sampling strategy can be based on our radiography results.

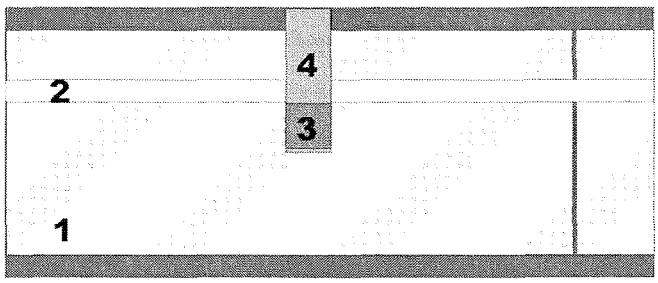

1. Radiography
2. RFA-Line
3. Magnetic Cubes
4. Sampling 50 cc

Fig. 4.3.2: Gravity Core sampling scheme.

Gravity Core descriptions:

GeoB 9601-3

Date: 04.07.05 Pos: 18°27.81'N 17°59.98'W
Water depth: 1920 m Core length: 740 cm

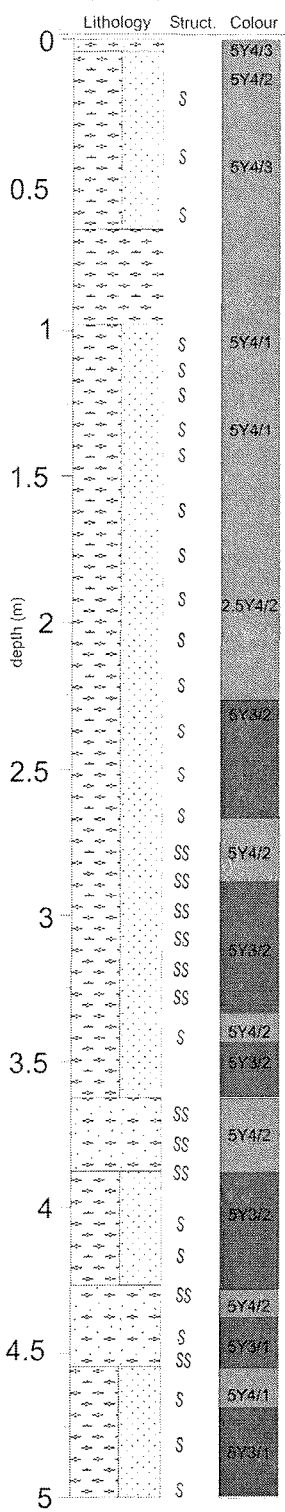

Comments	
0-4 cm:	olive foraminiferal silty mud, soft; 5Y4/3.
4-41 cm:	olive grey foram silty (quartz) mud, commonly cm-sized burrows, faint monosulfid tubes scattered throughout, few very fine shell debris admixed: 5Y4/2.
41-55 cm:	olive foram bearing silty (quartz) mud with common cm-sized burrows; 5Y4/3.
55-65 cm:	olive silty foram mud (silty quartz), weak bioturbation; 5Y4/3.
65-98 cm:	soft (more water) olive brown foram-bearing mud with some cm-sized, olive burrow fillings.
98-135 cm:	olive grey foram. silty (quartz) mud with rare to common faint burrows
135-168 cm:	dark grey foram silty (quartz) mud, faint monosulfid burrows troughout, some layer burrows, common very fine-grained shell debris admixed; 5Y4/1.
168-199 cm:	dark grey foram silty (quartz) mud, faint monosulfid burrows and undistinct larger burrows common throughout, some fine-grained shell debris admixed (less than above); 5Y4/1 (somewhat lighter than above).
199-226 cm:	dark greyish brown foram-bearing silty (quartz) mud with distinct large burrows filled from above; 2.5Y4/2.
226- 266 cm:	dark olive grey foram-bearing silty (quartz) mud with some very fine-grained shell debris admixed, faint monosulfid burrows throughout; 5Y3/2.
266-288 cm:	olive grey foram-bearing silty mud with faint monosulfid burrows throughout, some larger burrows, few fine shell debris admixed; 5Y4/2.
288-333 cm:	dark olive grey foram-bearing, silty (quartz) mud with common burrows throughout including faint monosulfid burrows, some fine-grained shell debris admixed: 5Y3/2.
333- 343 cm:	olive grey foram-bearing silty (quartz) mud, faint burrows and larger burrows common; 5Y4/2.
343-363 cm:	dark olive grey foram-bearing silt mud admixed with fine shell debris; 5Y3/2.
363-388 cm:	olive grey (at the base with brownish hue) silty (quartz) mud, few fine shell debris admixed, common cm-sized burrows; 5Y4/2.
388-427 cm:	dark olive grey foram-bearing silty (quartz) mud admixed with very fine shell debris, faint mm-sized monosulfid burrows throughout; 5Y3/2.
427-435 cm:	olive grey (at the base with brownish hue) silty (quartz) mud, few fine shell debris admixed, common cm-sized burrows; 5Y4/2.
435-455 cm:	very dark grey silty (quartz) mud, few fine shell debris admixed, common cm-sized burrows; 5Y3/1.
455-465 cm:	dark grey foram-bearing silty (quartz) mud with common large several cm-sized burrows; 5Y4/1.
465-509 cm:	very dark grey foram-bearing silty (quartz) mud with faint monosulfid burrows throughout, some very fine-grained shell debris admixed; 5Y3/1.

GeoB 9601-3

Date: 04.07.05 Pos: 18°27.81´N 17°59.92´W
Water depth: 1920 m Core length: 740 cm

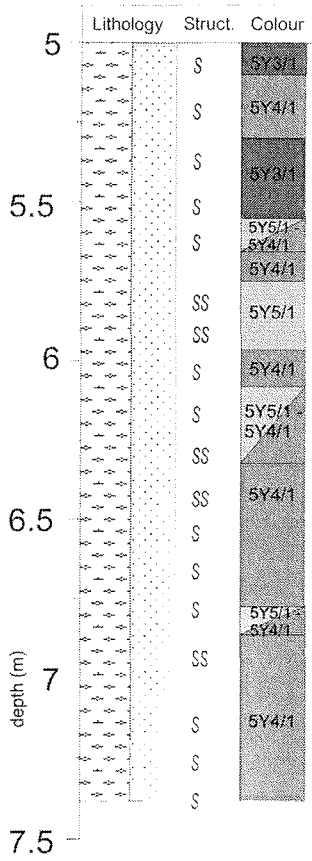

509-528 cm: dark grey foram-bearing silty mud with faint monosulfid burrows, some very fine-grained shell debris admixed; 5Y4/1.
528-554 cm: very dark grey foram-bearing silty (quartz) mud with faint monosulfid burrows throughout, some very fine-grained shell debris admixed; 5Y3/1.

554-568 cm: grey to dark grey foram-bearing silty mud with minor amounts of very fine-grained shell debris admixed; 5Y5/1 to 5Y4/1.
568-575 cm: dark grey foram-bearing silty (quartz) mud with faint monosulfid burrows throughout, common minor amount of fine shell debris admixed; 5Y4/1.
575-598 cm: grey to dark grey foram-bearing silty mud with minor amounts of very fine-grained shell debris admixed; 5Y5/1 to 5Y4/1.
598-610 cm: dark grey foram-bearing silty (quartz) mud with faint monosulfid burrows throughout, common minor amount of fine shell debris admixed; 5Y4/1.
610-634 cm: grey to dark grey foram-bearing silty mud with minor amounts of very fine-grained shell debris admixed; 5Y5/1 to 5Y4/1.

634-679 cm: dark grey foram-bearing silty (quartz) mud with common faint monosulfid burrows throughout, very minor amount of fine-grained shell debris admixed; 5Y4/1.

679-688 cm: grey to dark grey foram-bearing silty mud with minor amounts of fine-grained shell debris; 5Y5/1 to 5Y4/1.
688-740 cm: dark grey foram-bearing silty (quartz) mud with common faint monosulfid burrows throughout, very minor amount of fine-grained shell debris admixed; 5Y4/1.

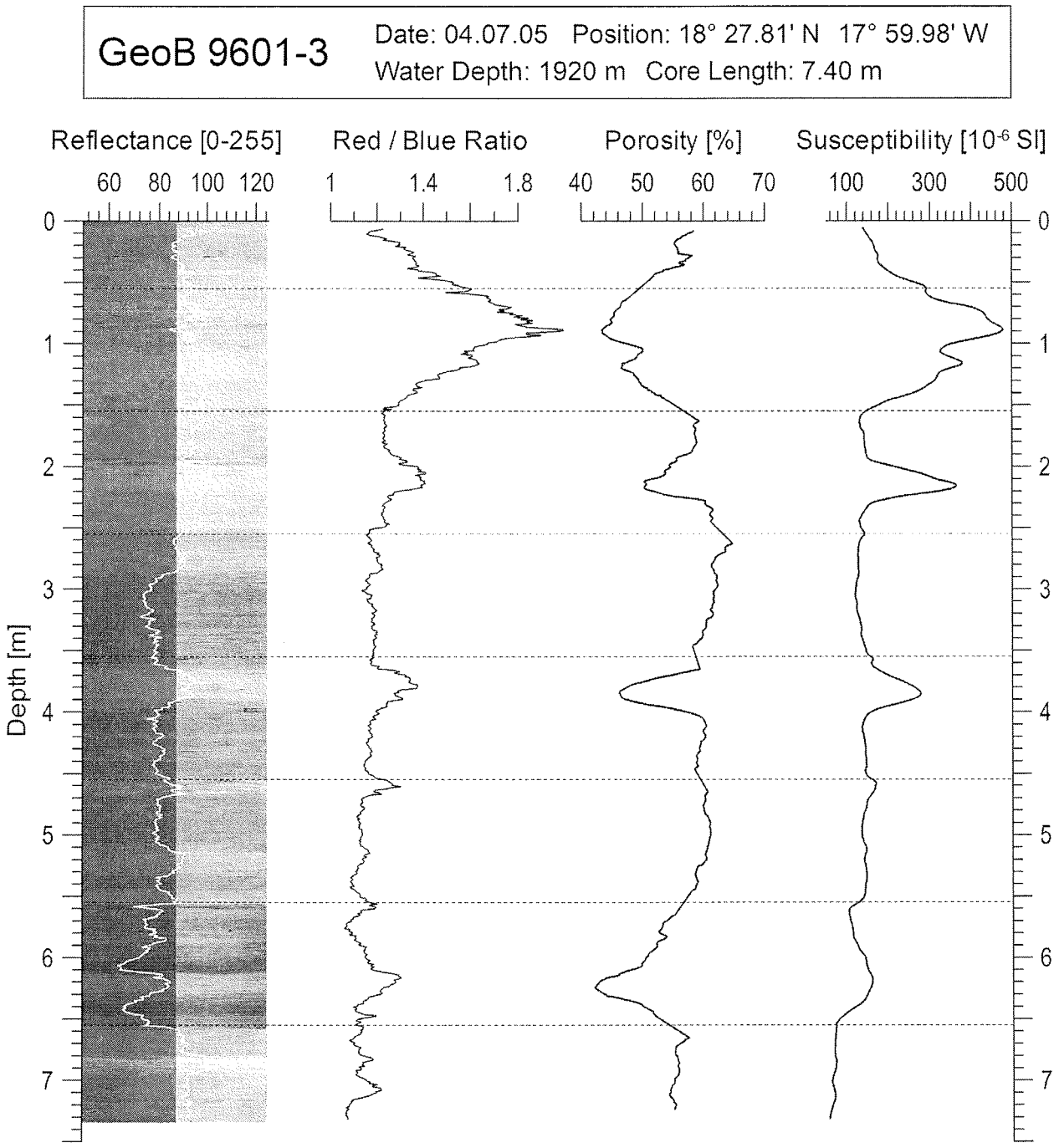

Physical properties of gravity core GeoB 9601-3. The dashed lines indicate the ends of the 1 m sections of the core.

GeoB 9602-3

Date: 06.07.2005 Pos: 12°35.25´ N, 18°30.4´W
Water depth: 3981 m Core length: 483 cm

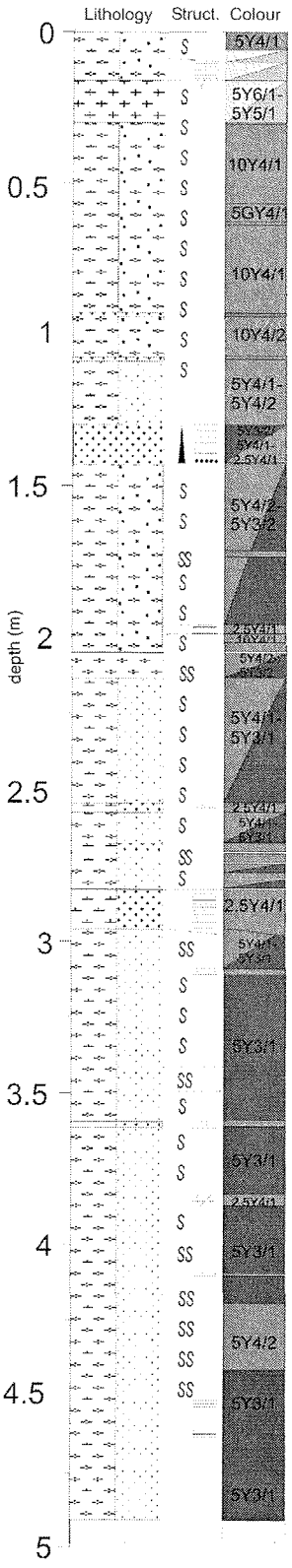

Comments

0-5.5 cm: dark grey foram. silty (qtz) sand mud, some shell debris. 5Y4/1
5.5-6 cm: dark grey to olive mud. 5Y4/1 to 5Y5/1
6-10 cm: grey, foram-nanno silty mud, weakly bioturbated. 2.5Y6/2 to2.5Y5/2.
10-16 cm: light brownish grey to brownish grey, laminated fine foram-bearing qtz sand, rare glauconite grains. 5Y6/1 to 5Y5/1. ***Turbidite (C/D, T_{s1})***
16-30 cm: grey, foram-nanno silty mud, weakly bioturbated. 2.5Y6/2 to2.5Y5/2.
30.5 cm: dark grey band of fine silt (2mm thick)
30-57 cm: dark greenish grey foram-bearing silty (qtz) mud, mod. bioturbated. 10Y4/1
57-63 cm: dark greenish grey foram-bearing silty mud, mod. bioturbated. 5gY4/1
63-64 cm: dark greenish grey colour band; 10gY4/1.
64-93 cm: dark greenish grey foram-bearing silty (qtz) mud, mod. bioturbated; 10Y4/1.
93-94 cm: dissiminated and bioturbate fine qtz sand; 10Y4/2. ***Turbidite (T_{s2})***
94-107 cm: dark greenish grey foram-bearing silty mud; 10Y4/2.
107-108 cm: dark grey to dark greyish brown, very fine sand with forams; 2.5Y4/1-2.5Y4/2. ***Turbidite (T_{s3})***
108-129.5 cm: dark grey-olive grey silty (qtz), foram-bearing mud, mod. bioturb.; 5Y4/1-5Y4/2.
129.5-142 cm: dark grey-dark olive grey, foram-bearing, coarse to fine qtz sand, base: abundant shell debris, typ. Bouma-seq.; 5Y3/2/5Y4/1 to 2.5Y4/1. ***Turbidite (B/C/D, T_{s4})***
142-201 cm: olive grey to dark olive grey foram-bearing silty (qtz) mud, mod. bioturbated.; 5Y4/2 to 5Y3/2.
intercalated by:
dark greenish grey to very dark greenish grey mud bands, mm-sized. at 148, 152, 158, 163-164, 167, 169/170, 173, 184 and 187cm, ***Turbidites T_{m1} to T_{m10}***; 5gY4/1 to 5gY3/1.
171-173 cm: dark greenish grey, foram-bearing, silty nanno mud, strongly bioturbated.; 10Y4/1.

195-198 cm: dark grey fine-very fine foram-bear. qtz sand (rare glauconite); 2.5Y4/1. ***Turbidite (T_{s5})***

201-203 cm: dark greyish green silty, foram-bearing nanno mud, mod. bioturbated. 10Y4/1
203-206 cm: see mud bands at 142-201 cm, ***Turbidites T_{m11} and T_{m12}***
206-214 cm: olive grey to dark olive grey foraminiferal silty (qtz) nanno mud. 5Y4/2 to 5Y3/2
214-255 cm: dark to very dark grey silt, foram-bearing mud, mod. bioturbated. 5Y4/1 to 5Y3/1
.intercalated by:
dark greenish grey to very dark greenish grey mud bands, mm-sized, at 216, 220, 223, 225, 227, 230, 233, 242 and 252 cm, ***Turbidites T_{m13} to T_{m21}***

255-258 cm: dark grey fine to very fine foram-bearing qtz sand, disseminated and bioturbated layer. 2.5Y4/1. ***Turbidite (T_{s6})***
258-268 cm: see 214-255 cm (without mud bands)
268- 271 cm: dark grey fine to very fine foram-bearing qtz sand. 2.5Y4/1. ***Turbidite (T_{s7})***
271-274 cm: dark greenish grey silty, foram-bearing mud, weakly bioturbated. 10Y4/1
274-277 cm: see 214-255 cm. (without mud bands)
277-279 cm: see 255-258 cm, 2.5Y4/1. ***Turbidite (T_{s8})***
279-282 cm: see 214-255 cm (without mud bands)
282-295/297 cm: see 255-258 cm. 2.5Y4/1.***Turbidite (T_{s9})***
297-308 cm: see 214-255 cm
295/297-308 cm: see 214-255 cm (without mud bands)
308-310 cm: dark grey, fine to very fine foram-bearing, qtz sand,2.5Y4/1. ***Turbidite (D, Ts_{10})***
310-340 cm: very dark olive grey, foraminiferal silty (qtz) mud with very fine shell debris admixed; 5Y3/1.
340-348 cm:
348-358 cm: very dark grey foram-bearing silty (qtz) mud, faint monosulf. burrow tubes throughout. 5Y3/1
358-360 cm: see 308-310 cm, ***Turbidite (D, T_{s11})***
360-382 cm: see 310-340 cm
382-386 cm: see 308-310 cm, ***Turbidite (C, T_{s12})***
386-418 cm: see 310-340 cm
410-411 cm: see 308-310 cm, ***Turbidite (C, T_{s13})***
417-418 cm: see 308-310 cm, ***Turbidite (C, T_{s14})***
418-440 cm: olive grey silty (qtz) foram-beariing mud, mod. bioturbated
440-465 cm: see 310-340 cm
451-453 cm: see 308-310 cm, ***Turbidite (C, T_{s15})***
459-460 cm: see 308-310 cm, ***Turbidite (C, T_{s16})***
460-483 cm: see 310-340 cm

T_s - siliciclastic turbidite bed
T_m - spillover mudflow/ mud turbidite

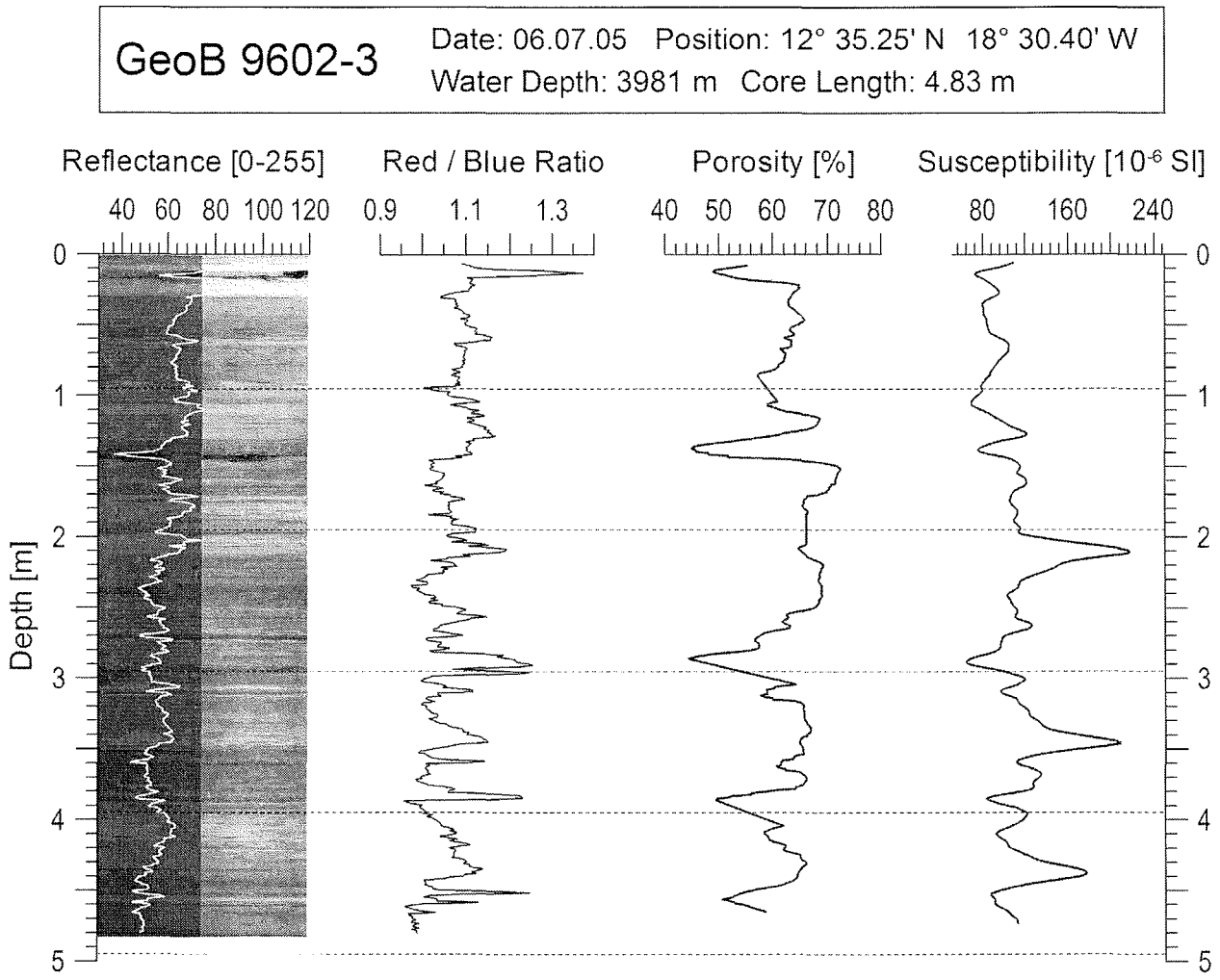

Physical properties of gravity core GeoB 9602-3. The dashed lines indicate the ends of the 1 m sections of the core.

GeoB 9604-03

Date: 09.07.2005 Pos: 14°11.01´N 17°54.10´W
Water depth: 1925 m Core length: 831 cm

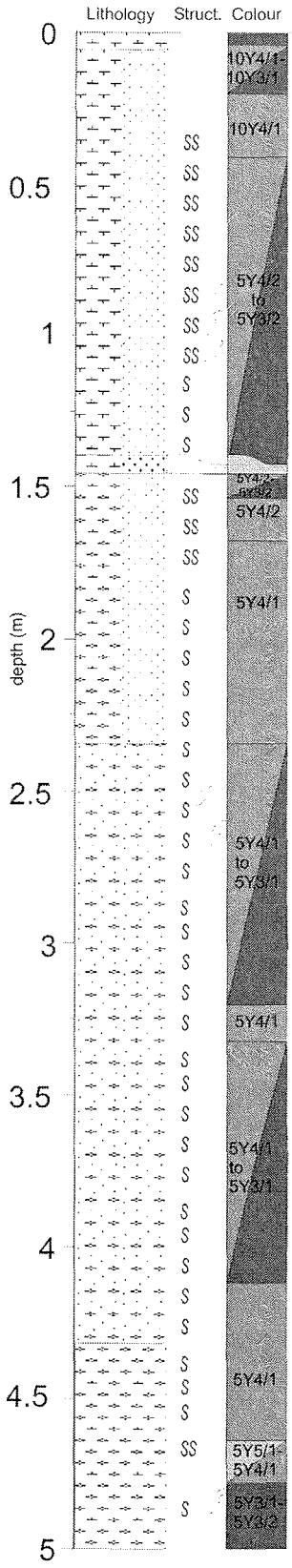

Comments

0-4 cm: dark greyish brown, silty, foram-nanno mud
4-20 cm: dark greenish grey-very dark greenish grey, silty (qtz) foram-nanno mud, some spicules; 10Y4/1 to 10Y3/1.
20-41 cm: dark greenish grey, silty (qtz), foram-nanno bearing mud, some spicules; 10Y4/1.
30-230 cm: strong smell of H_2S

41-139/142 cm: olive grey-dark olve grey siliceous (radiolarian, spicules), silty, foram-bearing mud, somelayers with fine shell debris; 5Y4/2 to 5Y3/2.

74-108 cm: weak bioturbation (*Zoophycos*)

below 108 cm: minor bioturbation

139/142-145 cm: grey-greyish brown, foram-rich qtz sand with gastropods and shell fragmts, some echinoid spines; 5Y5/1 to 5Y5/2. ***Turbidite*** ($T_{e,}$)
145-152 cm: olive grey-dark olive grey, silty (qtz), foram-bearing mud, mod. bioturb.; 5Y/2 to 5Y5/2.
152-166 cm: olive grey, siliceous (spicules), silty, foram-bearing mud, mod. bioturbated.; 5Y4/2.

166-233 cm: dark grey, siliceous, silty, foram-bearing mud, weakly bioturb.; 5Y4/1.

233-319 cm: dark grey to very dark grey, silicous, silty (qtz) mud, with some forams weakly bioturbated, some areas with very fine shell fragmts.; 5Y4/1 to 5Y3/1.
255-260 cm: huge burrow tube filled with fine foram/qtz sand

319-331 cm: dark grey, siliceous, silty mud, some forams.; 5Y4/1.

331-410 cm: dark grey-very dark grey, siliceous, silty mud, with forams.; 5Y4/1 to 5Y3/1.

410-430 cm: dark grey, siliceous, silty mud, with forams.; 5Y4/1.
430-462 cm: dark grey, siliceous, foram-bearing mud.; 5Y4/1.

462-476 cm: grey-dark grey, siliceous, foram-bearing mud, mod. bioturb.; 5Y5/1 to 5Y4/1.

476-531 cm: very dark grey-dark olive grey, siliceous, foram-bearing mud, faint monosulf. tubes *Planolites* type burrows.; 5Y3/1 to 5Y3/2.

GeoB 9604-3

Date: 09.07.2005 Pos: 14°11.01´N 17°54.10´W
Water depth: 1925 m Core length: 831 cm

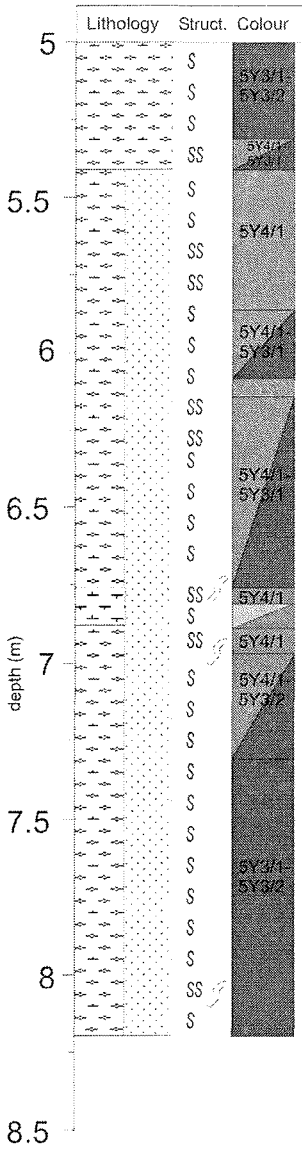

476-531 cm:	very dark grey-dark olive grey, siliceous, foram-bearing mud, faint monosulf. tubes *Planolites* type burrows.; 5Y3/1 to 5Y3/2.
530-540 cm:	moderately bioturbated
540-562 cm:	dark grey, siliceous, silty, foram-bearing mud, weakly bioturb.; 5Y4/1.
562-585 cm:	dark grey, siliceous, silty, foram-bearing mud, mod. bioturb.; 5Y4/1.
585-607 cm:	dark grey-very dark grey, silty, foram-bearing mud, mod. bioturb.; 5Y4/1 to 5Y3/1.
607-613 cm:	dark grey, silty, foram-bearing mud, mod. bioturb.; 5Y4/1.
613-631 cm:	dark grey-very dark grey, silty, foram-bearing mud, mod. bioturb.; 5Y4/1 to 5Y3/1.
631-676 cm:	dark grey-very dark grey, siliceous, silty, foram-bearing mud, mod. bioturb.; 5Y4/1 to 5Y3/1.
676-681 cm:	dark grey, silty, foram-bearing, nanno mud, mod. bioturb., weakly deformed burrows.; 5Y4/1.
681-689 cm:	grey to dark grey, silty, foram-bearing mud.; 5Y5/1 to 5Y4/1.
689-697 cm:	dark grey, silty, foram-bearing mud, strongly bioturb., large burows clearly stretched.; 5Y4/1.
697-731 cm:	dark grey-dark olive grey, siliceous, silty, foram-bearing mud, weakly bioturb.,
indications of:	shearing at thin dark layers and burrow tubes.; 5Y4/1 to 5Y3/2.
731-801 cm:	very dark grey-dark olive grey, siliceous, silty, foram-bearing mud, weakly bioturb.; 5Y3/1 to 5Y3/2.
797-801 cm:	sheared and stretched sediment
801-804 cm:	grey-dark grey, strongly stretched and sheared burrows
801-820 cm:	very dark grey-dark olive grey, siliceous, silty, foram-bearing mud, weakly bioturb.; 5Y3/1 to 5Y3/2.

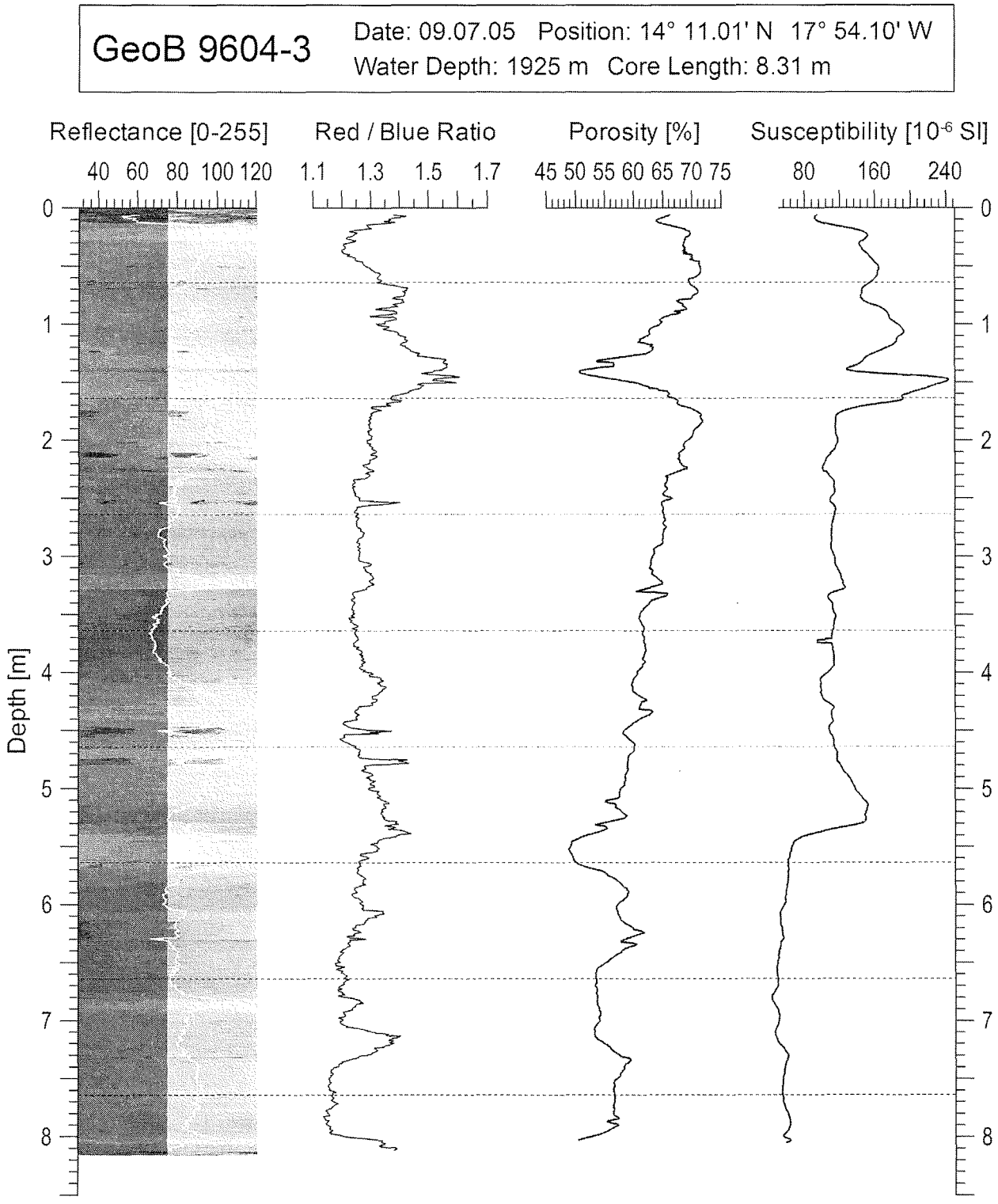

Physical properties of gravity core GeoB 9604-3. The dashed lines indicate the ends of the 1 m sections of the core.

GeoB 9605-1

Date: 09.07.05 Pos: 14°17.60´N 17°55.80´W
Water depth: 1912 m Core length: 790 cm

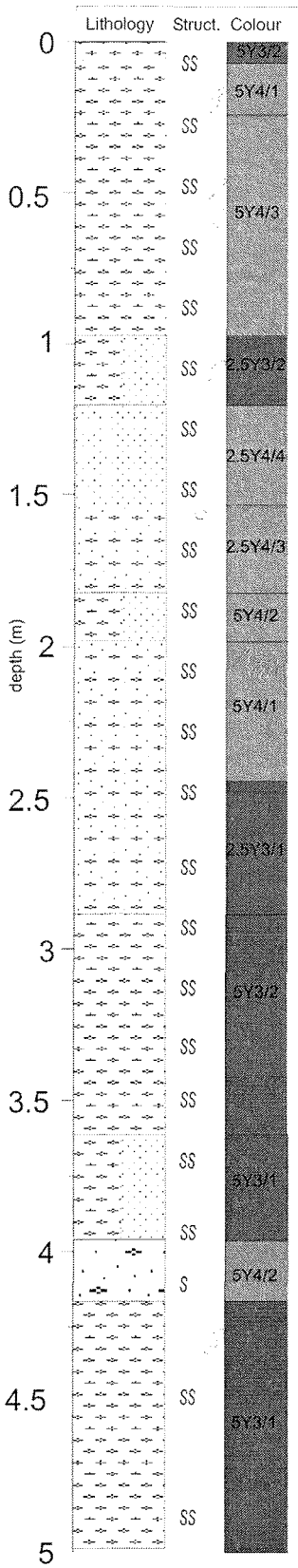

Comments

0-7 cm: dark olive grey, soft mud. 5Y3/2
7-24 cm: dark grey, foram-bearing mud, bioturb. 5Y4/1
24-97 cm: olive, foram-bearing mud, bioturb. (series of *Zoophycos* filled with upper mud, disperse, tiny monosulphid spots). 5Y4/3

97-120 cm: very dark greyish brown, silty, foram-bearing (enriched in 97-103 cm) mud, *Zoophycos* bioturb. 2.5Y3/2

120-153 cm: olive brown, silty, sof clay, bioturb., bare of forams, outpouring water. 2.5Y4/4

153-182 cm: olive brown, silty mud, bioturb., some forams, single mollusc fragmts. , faint monosulphide spots in lower part. 2.5Y4/3

182-198 cm: olive grey, silty, foram-bearing mud, bioturb. 5Y4/2

198-288 cm: dark grey-very dark grey, silty mud, abundant large forams (e.g. *Globorotalia*). 5Y4/1 Very dark grey lenses at 230-232, 245-247 and 260-262 cm. 5Y3/1

288-361cm: dark olive grey, foram-bearing mud, some faint monosulph. spots, bioturb., shell debris of pteropods. 5Y3/2, contains two layers of clayey silt at 321-323 and 340-342 cm.

361-396 cm: very dark grey, silty, foram-bearing mud, faint and some larger monosulph. spots. 5Y3/1

396-416 cm: olive grey, clayey silt, single pteropods. 5Y4/2

416-505 cm: very dark grey, foram-bearing mud, some large, dispers distrib. forams. 5Y3/1, contains large monosulph. spots at 437-439 and 461-463 cm.

GeoB 9605-1

Date: 09.07.05 Pos: 14°17.60´N 17°55.80´W
Water depth: 1912 m Core length: 790 cm

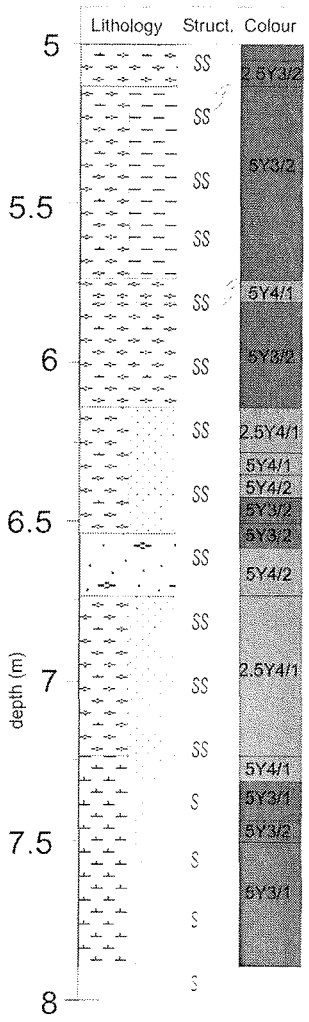

Comments

505-513 cm: very dark grey brown, foram-bearing mud, bioturb. 2.5Y3/2
513-574 cm: dark olive grey, clayey, foram-bearing mud, bioturb., faint monosulph. spots. 5Y3/2

574-581 cm: dark grey mud, bioturb., rare forams, faint monosulph. spots, one large borrow filled with large shell fragmts. 5Y4/1

581-614 cm: dark olive grey, foram-bearing mud, abundant monosulph. spots. 5Y3/2

614-658 cm: dark grey-olive grey-dark olive grey, silty, foram-bearing mud, medium sized burrows (become compressed and stretched in deeper parts, coring or gliding effect?), few tiny monosulph. spots. 2.5Y4/1 to 5Y4/1 to 5Y4/2 to 5Y3/2

658-673 cm: olive grey, clayey silt, almost bare of forams, faint monosulph. spots. 5Y4/2

673-724 cm: dark grey, silty, foram-bearing mud. 2.5Y4/1. contains an olive grey, silty clay layer with faint monosulph. spots at 691-694 cm (5Y4/2) and swarms of small burrows (Chondrites) of compressed and elongated shape at 695-698 and 700-702 cm.

724-732 cm: dark grey, slightly clayey, foraminiferal silt, numerous large forams, some monosulph. spots. medium-sized burrows (strongly stretched and laterally ripped). 5Y4/1
732-790 cm: very dark grey, clayes, foram-bearing silt, content of forams and clay decreasing upwards, abundant faint monosulph. spots. 5Y3/1. contains concretion (coral?) at 767-769 cm and and a dark olive grey layer of same material at 744-751 cm (5Y3/2)

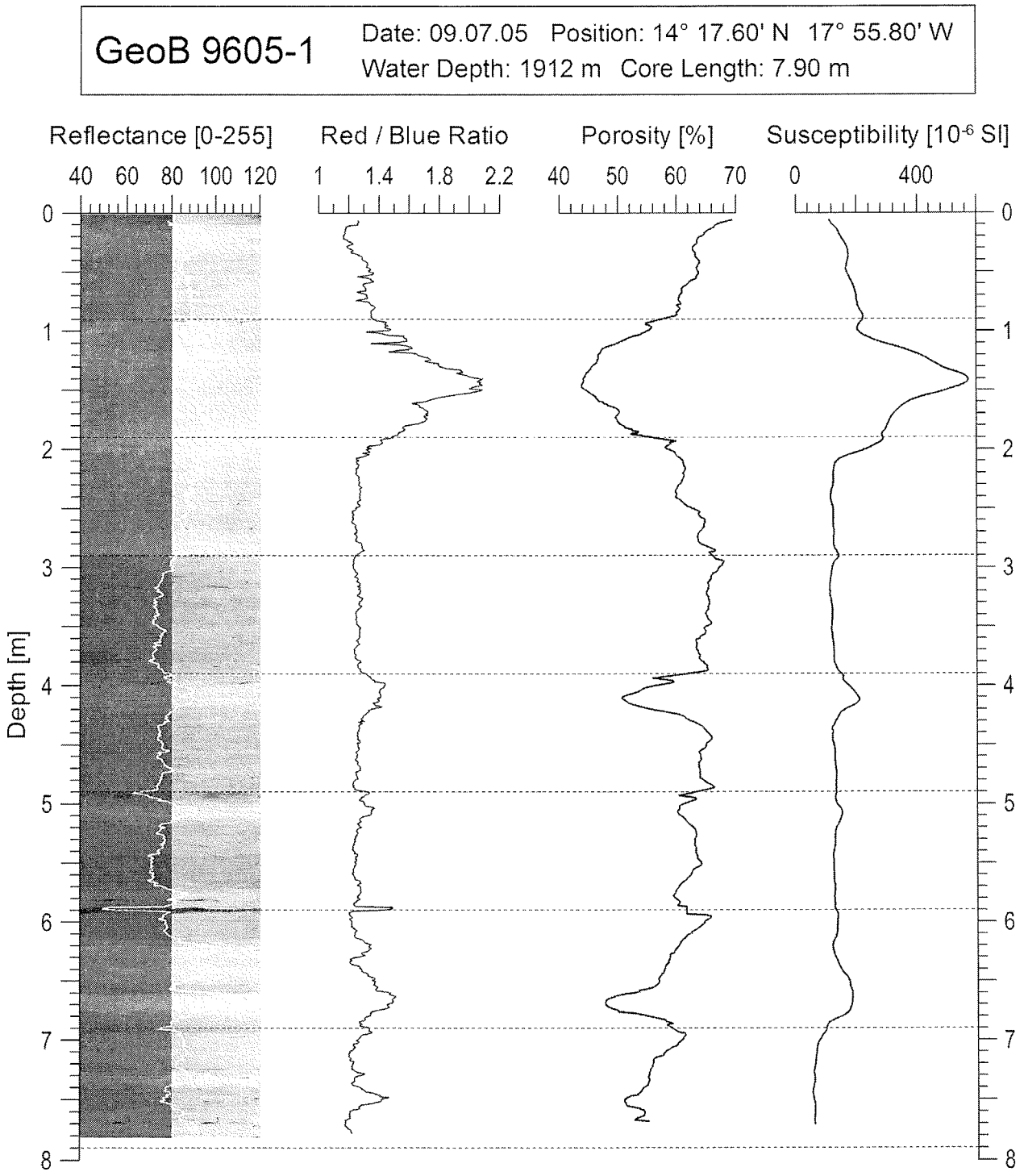

Physical properties of gravity core GeoB 9605-1. The dashed lines indicate the ends of the 1 m sections of the core.

GeoB 9606-2

Date: 10.07.05 Pos: 14°11.03´N 17°59.82´W
Water depth: 2287 m Core length: 951 cm

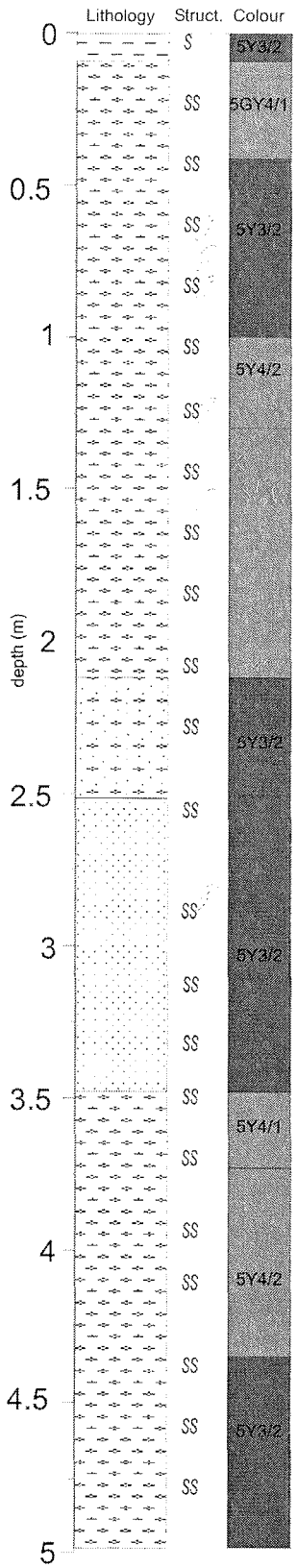

Comments

0-9 cm: dark olive grey, very soft, fluffy clay; 5Y3/2.
9-41 cm: dark greenish grey, foram bearing mud, bioturb. (open *Zoophycos* burrows); 5gY4/1.
41-130 cm: dark olive grey-olive grey foram-bearing mud, bioturb. (frequent Zoophycos burrows, some still open), some large forams, rare, tiny monosulph. spots; 5Y3/2.

130-212 cm: ?? , foram-bearing mud, faint tiny monosulph. spots.

212-251 cm: dark olive grey, silty mud, bioturb., faint tiny monosulph. spots, almost no forams; 5Y3/2.
251-348 cm: dark olive grey, silty, slightly foram-bearingmud, bioturb., abundant medium-sized tiny monosulph. spots; 5Y3/2.

348-373 cm: dark grey, foram-bearing mud, bioturb., abundant monosulph. spots; 5Y4/1.
373-435 cm: olive grey, foram-bearng mud, bioturb., abundant monosulph. spots; 5Y4/2.

435-520 cm: dark olive grey, foram-bearing mud, bioturb., abundant monosulph. spots; 5Y3/2.

GeoB 9606-2

Date: 10.07.05 Pos: 14°11.03´N 17°59.82´W
Water depth: 2287 m Core length: 951 cm

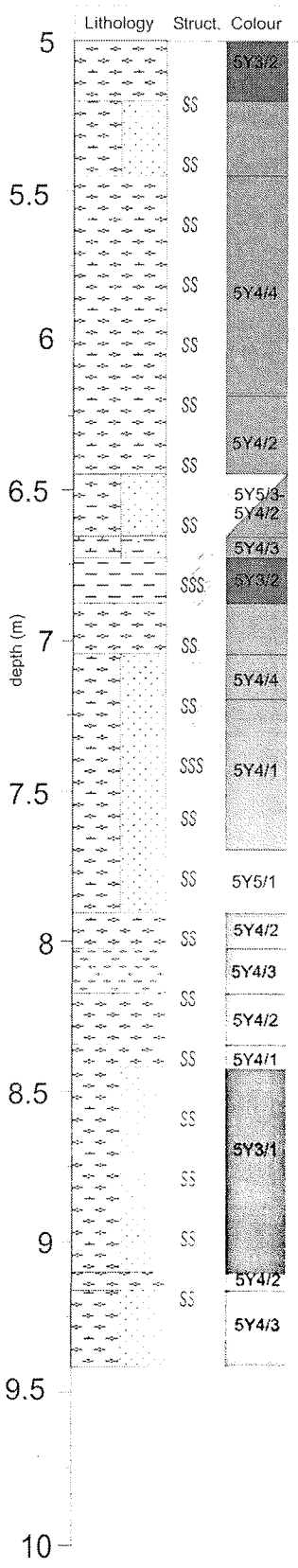

435-520 cm: dark olive grey, foram-bearing mud, bioturb., abundant monosulph. spots; 5Y3/2.

520-545 cm: olive grey, slightly silty, foram-bearing mud, bioturb., faint tiny and some larger monosulph. spots; 5Y4/2.

545-644 cm: olive-olive grey, foram-bearing mud, bioturb., frequent faint, tiny and some larger monosulph. spots; 5Y4/4 to 5Y4/2.

644-665 cm: olive-olive grey, silty, foraminiferal (>50%) mud, bioturb. (two burrows with soft foram. ooze + monosulph. material); 5Y5/3 to 5Y4/2.

665-672 cm: olive. clayey, foraminiferal silt, bioturb.; 5Y4/3.

672-687 cm: dark olive grey clay, highly bioturb. (like mud turbidites in CT-Canyon); 5Y3/2.

687-704 cm: olive mud, highly bioturb. (several *Zoophycos* burrows), bare of forams; 5Y4/3.

704-719 cm: olive, silty, foram-bearing. mud, bioturb., plenty monosulph. spots; 5Y4/4.

719-769 cm: dark grey, silty, foram-bearing mud, highly bioturb., many monosulph. spots; 5Y4/1.

769-790 cm: grey, silty, foram-bearing mud, bioturb., faint monosulph.spots; 5Y5/1.

790-802 cm: olive grey, foram-bearing mud (like mud turbidite of CT-Canyon); 5Y4/2.

802-817 cm: olive, clayey silt, bioturb., some monosulph. spots; 5Y4/3.

817-834 cm: olive grey mud, bioturb., rare forams, plenty monosulph. spots; 5Y/2.

834-842 cm: dark grey, foraminiferal mud, bioturb., some monosulph.spots; 5Y4/1.

842-910 cm: very dark grey, silty, foram-bearing mud, bioturb. (two burrows filled with with shells); 5Y3/1 contains a burrow-like spot with large gastropod (?) shell framgts. at 886 cm

910-916 cm: olive grey mud, bioturb., rare forams; 5Y4/2.

916-941 cm: olive,silty, foram-bearing mud, bioturb., some monosulph. spots; 5Y4/3.

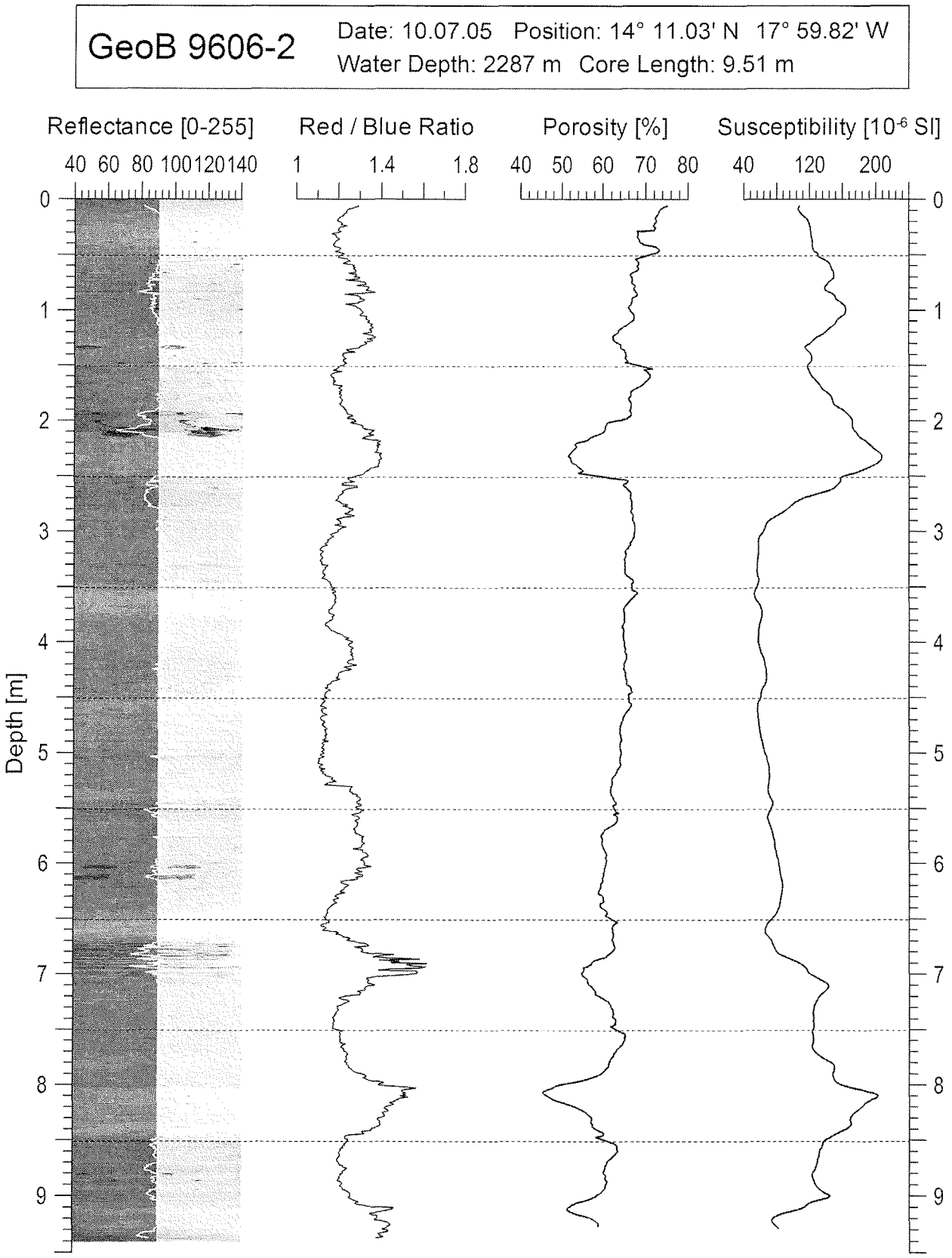

Physical properties of gravity core GeoB 9606-2. The dashed lines indicate the ends of the 1 m sections of the core.

GeoB 9607-1

Date: 10.07.05 Pos: 14°11.29´N 18°06.65´W
Water depth: 2999 m Core length: 333 cm

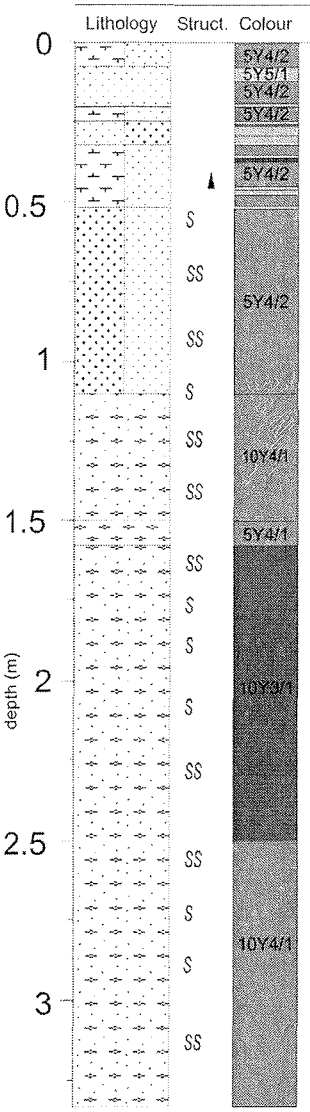

Comments

0-7.5 cm: olive grey, siliceous, silty, foram-nanno mud; 5Y4/2.
7.5-12cm: light olive brown silt; 5Y5/1. ***Turbidite (D, T_{s1})***
19-20 cm: light olive brown silt; 5Y5/1. ***Turbidite (D, T_{s2})***
20-24.5cm: olive grey, siliceous, silty, foram-nanno mud; 5Y4/2. contains lens at 22-23 cm. 5Y3/1.
24.5-25.5 cm: light olive brown silt; 5Y5/1. ***Turbidite (D, T_{s3})***
26-32 cm: olive grey, fine sand grading upwards into light olive brown, very fine sand and silt; 5Y5/1 to 5Y5/3. ***Turbidite (C,D, T_{s4})***
32-35 cm: olive grey, siliceous, silty, foram-nanno mud; 5Y4/2
35-36 cm: light olive brown silt; 5Y5/1. ***Turbidite (D, T_{s5})***
36-45 cm: olive grey, siliceous, silty, foram-nanno mud; 5Y4/2.
45-47.5 cm: light olive brown silt; 5Y5/1. ***Turbidite (C, D, T_{s6})***
47.5-51 cm: olive grey, siliceous, silty, foram-nanno mud. 5Y4/2
51-52 cm: olive grey, fine-very fine sand-silt; 5Y5/1. ***Tubidite (D, Ts_7)***
52-110 cm: see 36-45 cm. interrupted by olive grey, fine-very fine sand-silt at 54-58, 65-66 and 68-70 cm; 5Y5/3 to 5Y5/1. ***Turbidites (C (only the first), D, T_{s8} to T_{s10})***
70/72-88/91 cm: see 51-52 cm, erosive base, contains coarse shell fragmts (gastropods, bivalves, serpulids, scaphopods, cm-sized single coral colony), ***Turbidite (B, C, D, T_{s11})***
91/93-93/93.5 cm: see above. ***Turbidite (B, C/D, T_{s12})***
110-132 cm: dark greenish grey-very dark greenish grey, silty mud, clasts in slumped mud; 10Y4/1 to 10Y3/1.
132/136-132/140 cm: dark greenish grey mud clast, with two light greenish grey, strongly overconsolidated mud clasts and basal shel fragmts; 10GY4/3.
140-150 cm: dark greenish grey-very dark greenish grey, silty mud; 10GY4/3.
150-158 cm: very dark grey mud, with slide/slump and enrichment of large shell fragmts at the base (156-158cm); 5Y3/3 to 5Y4/1, at the base 5Y3/1.
158/160-250 cm: very dark greenish grey, silty mud, weakly bioturb.; 10Y3/1.
250-333 cm: dark greenish grey, silty mud, with faint burrow tubes (some *Zoophycos* and *Planolites*), undisturbed and uncompacted; 10Y4/1.

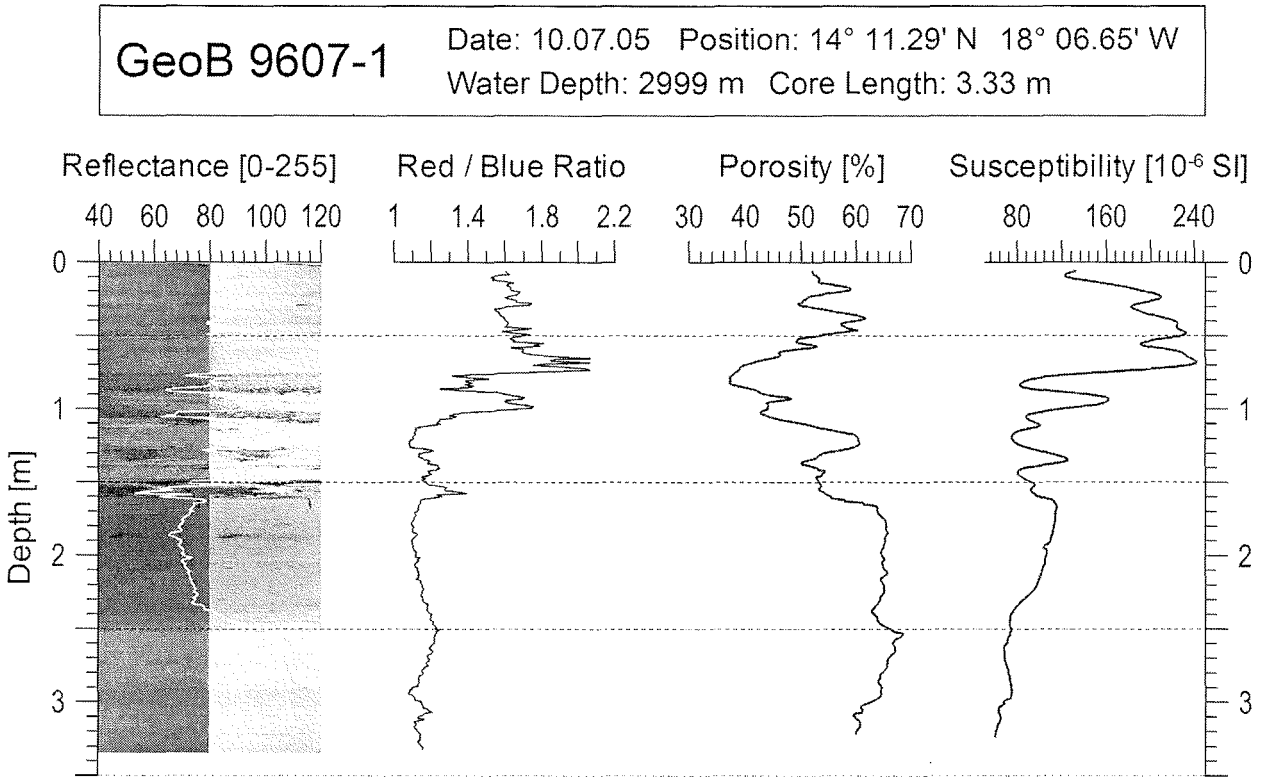

Physical properties of gravity core GeoB 9607-1. The dashed lines indicate the ends of the 1 m sections of the core.

GeoB 9607-3

Date: Pos: ´N ´W
Water depth: m Core length: 771 cm

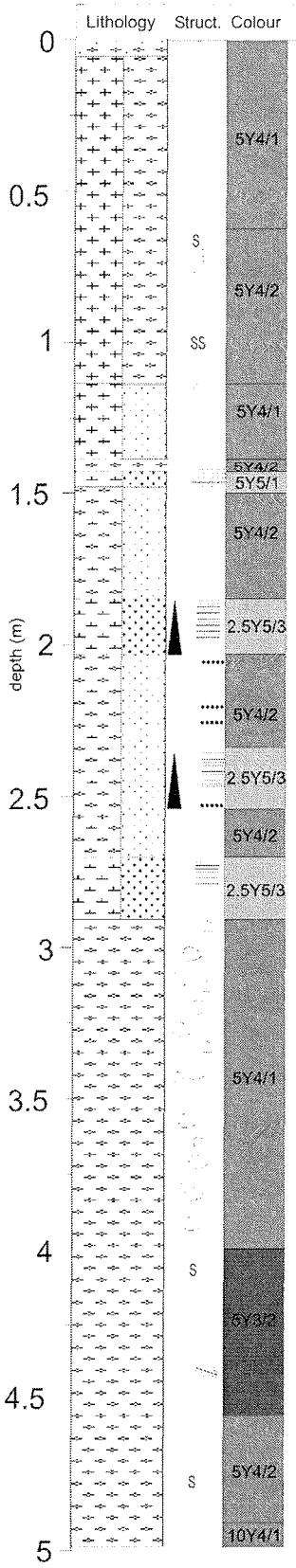

Comments

0-5 cm: dark grey-olive grey, siliceous, silty mud, with some forams. 5Y4/1 to 5Y4/2
5-62 cm: dark grey, siliceous, foram-nanno mud, weakly bioturb. 5Y4/1
62-113 cm: olive grey, siliceous, weakly silty, foram-nanno mud, weakly-mod. biotub., well developed *Zoophycos* beginning at 64 cm, *Chondrites* in upper part (62-64 cm). 5Y4/2

113-138 cm: dark grey, siliceous, silty, foram-nanno mud. 5Y4/1
138-142 cm: olive grey mud. 5Y4/2. ***Turbidite? (E?)***
142-147 cm: grey-olive grey, fine, quarz/foram-admixed sand, with echinoid spines, cross bedded and laminated. 5Y5/1 to 5Y4/2. ***Turbidite (T_{s1})***
147-189 cm: olive grey, siliceous, silty, foram-bearing mud, weakly bioturb. 5Y4/2
184-186 cm: light olive brown-dark greyish brown, fine, quartz-foram sand, laminated. 2.5Y5/3 to 2.5Y4/2. ***Turbidite (T_{s2})***
189-203 cm: light olive brown-dark greyish brown, fine, quartz-foram sand, laminated. 2.5Y5/3 to 2.5Y4/2. ***Turbidite (A/B,C,D, T_{s3})***

203-270 cm: olive grey, siliceous, silty, foram-bearing mud. 5Y/2 (bakground sedimentation)
205-205.5 cm: see 184-186 cm. ***Turbidite (T_{s4})***
207-207.5 cm: see 184-186 cm. ***Turbidite (T_{s5})***
216-217.5 cm: see 184-186 cm. ***Turbidite (T_{s6})***
223-225 cm: see 184-186 cm. ***Turbidite (T_{s7})***
226-227 cm :see 184-186 cm. ***Turbidite (T_{s8})***
231-232 cm: see 184-186 cm. ***Turbidite (T_{s9})***
237-256 cm: dark greyish brown, medium-coarse, qtz-foram sand, with shell fragments, grading upward into light olive brown, medium-fine, qtz-foram sand, parallel laminated. 2.5Y5/3 to 2.5Y4/2. ***Turbidite (A/B, C, D, T_{s10})***
260-263 cm: see 184-186 cm, slumped layer. ***Turbidite (T_{s11})***
270-286 cm: see 184-186 cm. ***Turbidite (C, D, T_{s12})***

286-384cm: dark grey-dark olive grey, shelly mud, partly with intact shells and shell/coral fragmts. 5Y4/1 to 5Y4/2. ***Matrix (M_1) of Debrite***
greenish grey mud, with dark striations. 10gY5/1. ***Matrix (M_2) of Debrite***
pale green, very stiff mud. 5gY7/2 to 5gY6/2. ***Clasts (C_1) of Debrite***
olive grey-dark olive grey, siliceous mud. 5Y4/2 to 5Y3/2. ***Clasts (C_2) of Debrite***
dark grey mud. 5Y4/1. ***Clasts (C_3) of Debrite***
384-401 cm: dark grey-dark olive grey, shelly mud, with commonly mud clasts of different colour. 5Y4/1 to 5Y4/2

400-625 cm: intakt block into debrite
401-436 cm: dark olive grey, siliceous mud, burrow tubes (weakly stretched and eformed at 412-418 cm). 5Y3/2
436-454 cm: dark greenish gray, fine qtz sand, laminated. ***Turbidite (T_{s13})***
454-484 cm: olive grey mud, weakly-mod. bioturb. 5Y4/2
455-462 cm: internal shearing as indicated by strongly sheared and stretched burrow tubes
484-495 cm: olive grey mud, weakly-mod. bioturb. 5Y4/2
495-504 cm: dark greenish grey mud, mod. bioturb (*Zoophycos*). 10Y4/1

GeoB 9607-3

Date: Pos: ´N ´W
Water depth: m Core length: 771 cm

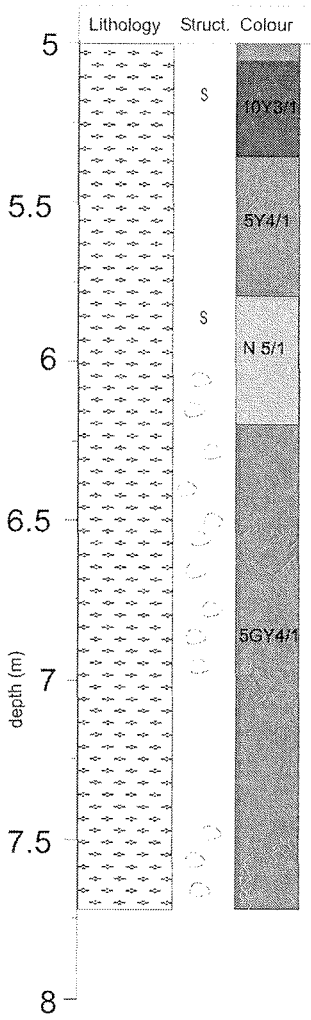

495-504 cm: dark greenish grey mud, mod. bioturb (*Zoophycos*). 10Y4/1
504-530 cm: very dark greenish grey mud, weakly. bioturb. 10Y3/1
530-580 cm: dark grey mud, weakly. bioturb. 5Y4/1
580-625 cm: greenish grey mud. N5/1

625-680 cm: greenish grey and dark olive grey, sheared clast carpet.
680-752 cm: dark greenish grey mud, with sheared clasts up from 708-745 cm. 5gY4/1

752-771 cm: greenish grey and dark olive clasts and layers, mud clast carpet.

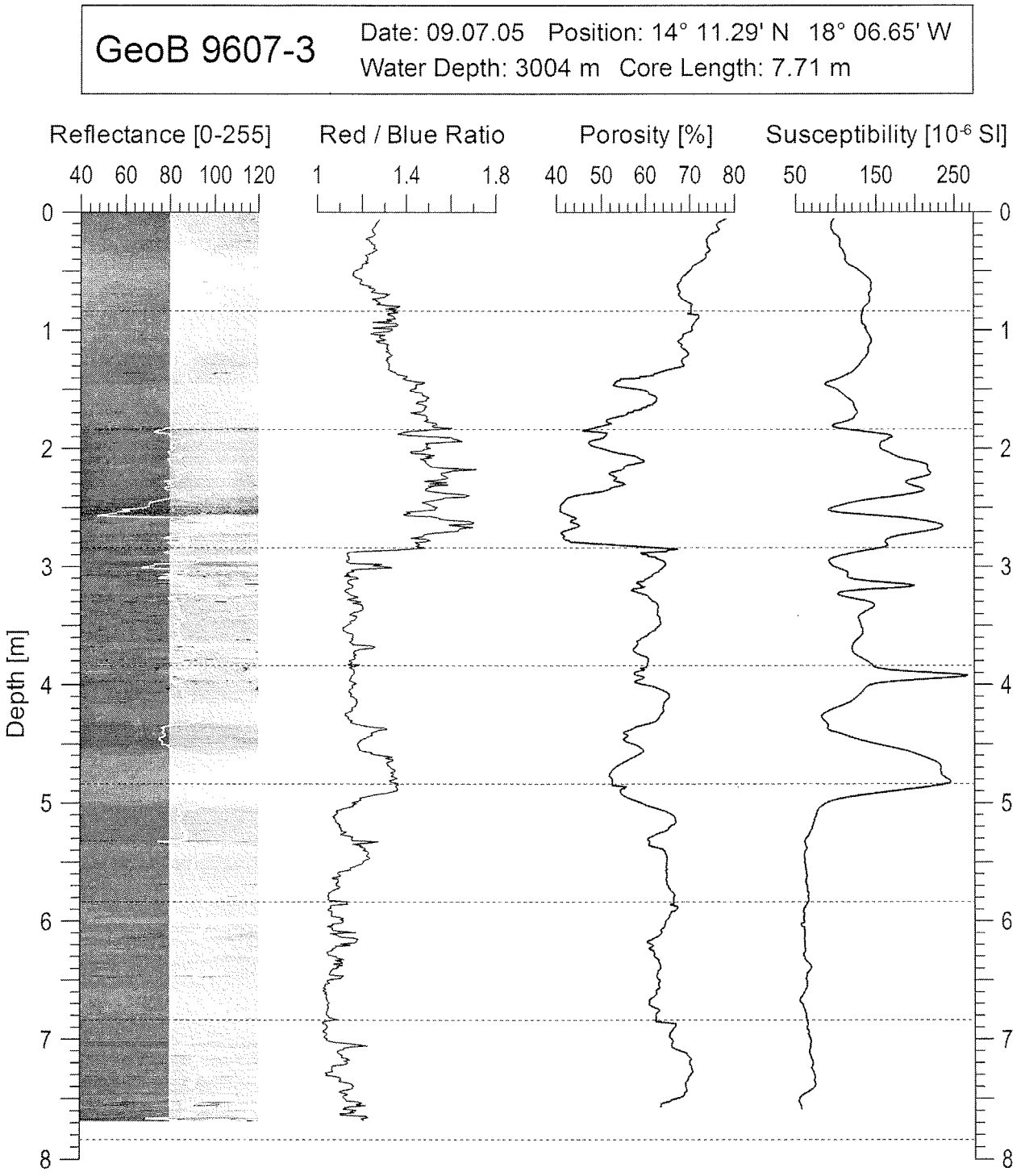

Physical properties of gravity core GeoB 9607-3. The dashed lines indicate the ends of the 1 m sections of the core.

GeoB 9608-2

Date: 10.07.05 Pos: 14°11.22´N 18°08.26´W
Water depth: 2585 m Core length: 893cm

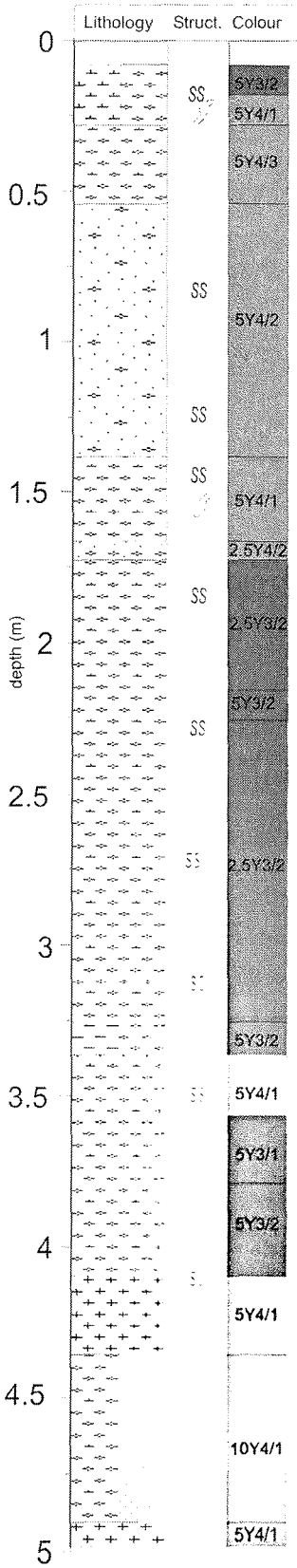

0-8 cm:	not opened	
8-17 cm:	dark olive grey, soft foraminiferal mud, bioturb., 5Y3/2.	
17-27 cm:	dark grey, soft foraminiferal mud, bioturb., some open burrows, 5Y4/1.	
27-53 cm:	olive, soft foram-bearing mud, bioturb., some open burrows, rare monosulphitic spots, single Zoophycos, 5Y4/3.	
53-137 cm:	olive grey to olive brown, soft muddy silt to slightly silty mud, bioturb., some Chondrites, some medium-sized monosulphitic spots from 78-100 cm, silt content strongly decreasing in the lower part, 5Y4/2.	
137-165 cm:	dark grey, foram-bearing mud, bioturb., a series of Zoophycos, some monosulph. spots, 5Y4/1.	
167-173 cm:	dark greyish brown, slightly silty mud, bioturb., some Zoophycos, 2.5Y4/2.	
173-216 cm:	very dark greyish brown, foraminiferal clayey mud, stiffer than the overlinging sediments, bioturb., faint tiny monosulph. spots, 2.5Y3/2.	
216-226 cm:	dark olive grey, foram-bearing mud, bioturb., some monosulph. spots, 5Y3/2.	
226-326 cm:	very dark grey, foram-bearing to foraminiferal mud, continuously bioturb.,faint monosulph. spots, 2.5Y3/1.	
275-308 cm:	frequent thin Zoophycos burrows	
326-335 cm:	dark olive grey, clayey mud, rare foraminifres, faint monosulph. spots, bioturb., 5Y3/2.	
335-355 cm:	dark grey, foram-bearing clayey mud, faint monosulph. spots, bioturb., 5Y4/1.	
355-377 cm:	very dark grey, foraminifreal clayey mud, faint to medium sized monosulph. spots, bioturb., 5Y3/1.	
377-408 cm:	dark olive grey, foraminiferal to foram-bearing mud, faint tiny monosulph. spots, bioturb.,	
408-434 cm:	dark grey, foram-nanno ooze, 5Y4/1.	
434-489 cm:	dark greenish grey, foram-bearing silty nanno mud, 10Y4/1	
489-501 cm:	dark grey, foram-nanno ooze, weakly bioturb., 5Y4/1	

GeoB 9608-2

Date: 10.07.05 Pos: 14°11.22´N 18°08.26´W
Water depth: 2585 m Core length: 893 cm

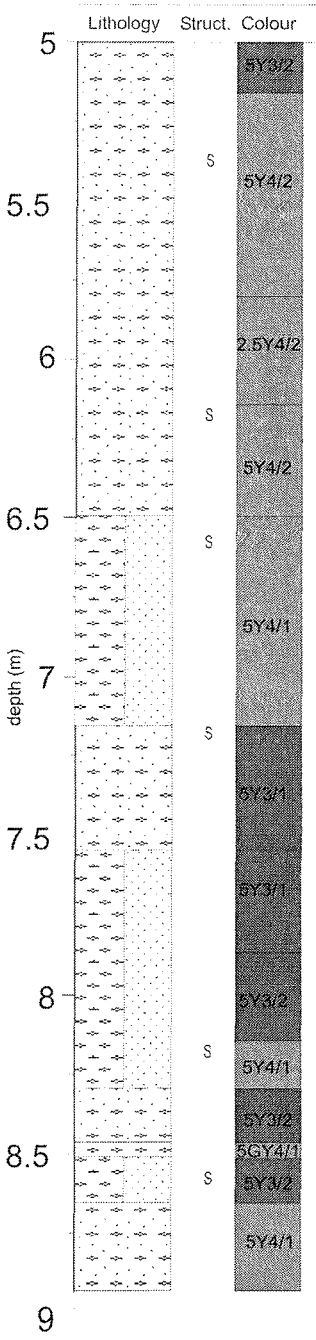

501-517 cm: dark olive grey, siliceous silty mud, moderately bioturb., 5Y3/2.

517-581 cm: olive grey, siliceous silty mud, weakly bioturb., 5Y4/2.

581-615 cm: dark greyish brown, silty mud, 2.5Y4/2.

615-650 cm: olive grey siliceous silty mud, weakly bioturb., 5Y4/2.

650-716 cm: dark grey, foram-bearing silty mud, weakly bioturb., 5Y4/1.

716-755 cm: olive grey, silty mud, weakly bioturb., few forams, 5Y3/1.

755-787 cm: very dark grey, foram-bearing silty nanno mud, weakly bioturb., 5Y3/1.

787-815 cm: dark olive grey, foram-bearing silty mud, weakly bioturb., 5Y3/2.

815-830 cm: grey to olive grey, foram-bearing slightly silty and siliceous nanno mud, 5Y4/1.

830-847 cm: dark olive grey, silty mud with some forams, weakly bioturb., 5Y3/2.
847-852 cm: greenish grey, foram-bearing nanno mud, weakly bioturb., 5GY4/1.
852-866 cm: dark olive grey, foram-bearing silty mud, weakly bioturb., 5Y3/2.

866-893 cm: dark grey to olive grey, silty mud wirh some forams, weakly bioturb., 5Y4/1 to 5Y4/2.

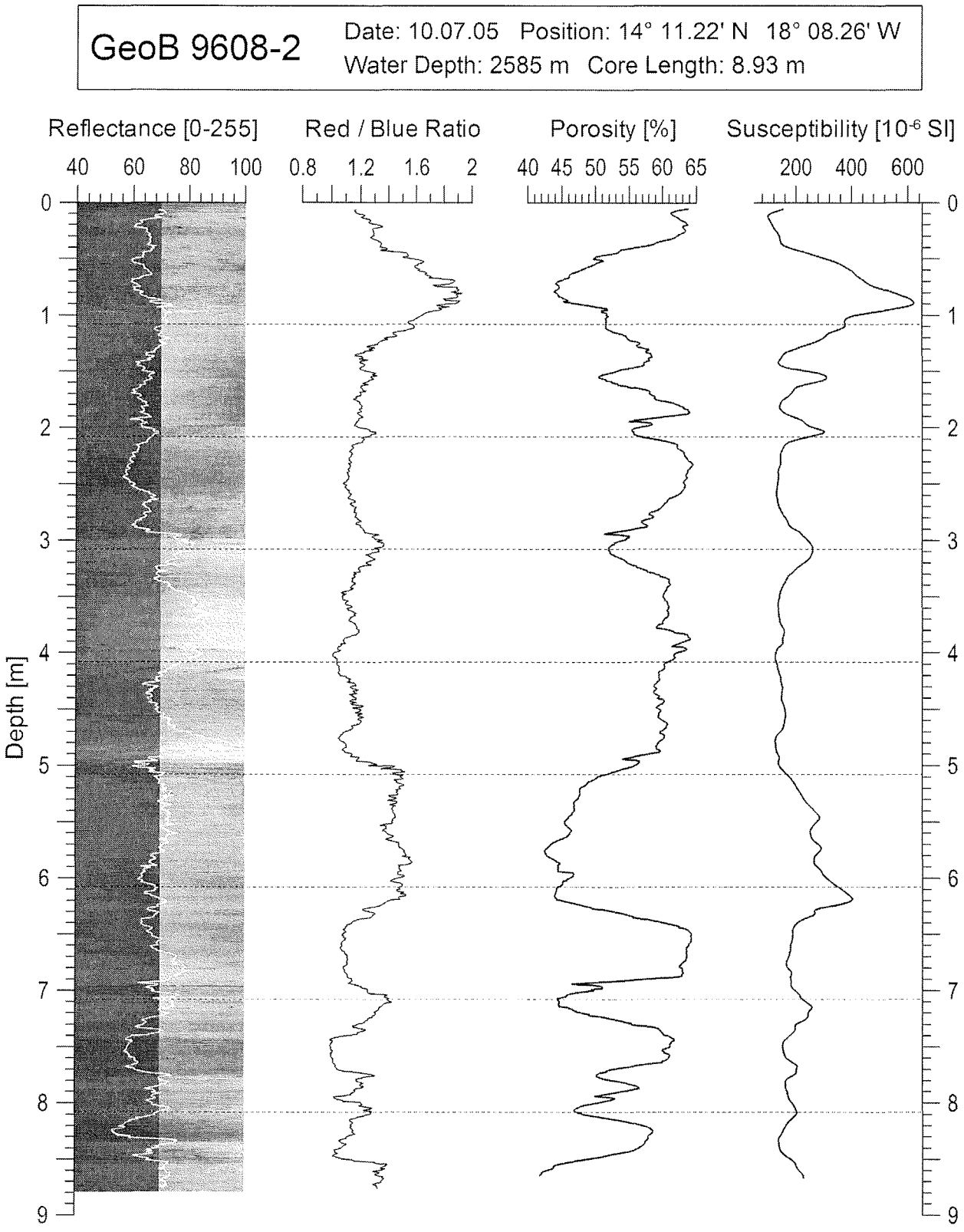

Physical properties of gravity core GeoB 9608-2. The dashed lines indicate the ends of the 1 m sections of the core.

GeoB 9609-2

Date: 10.07.05 Pos: 14°11.35´N 18°05.63´W
Water depth: 2785 m Core length: 530 cm

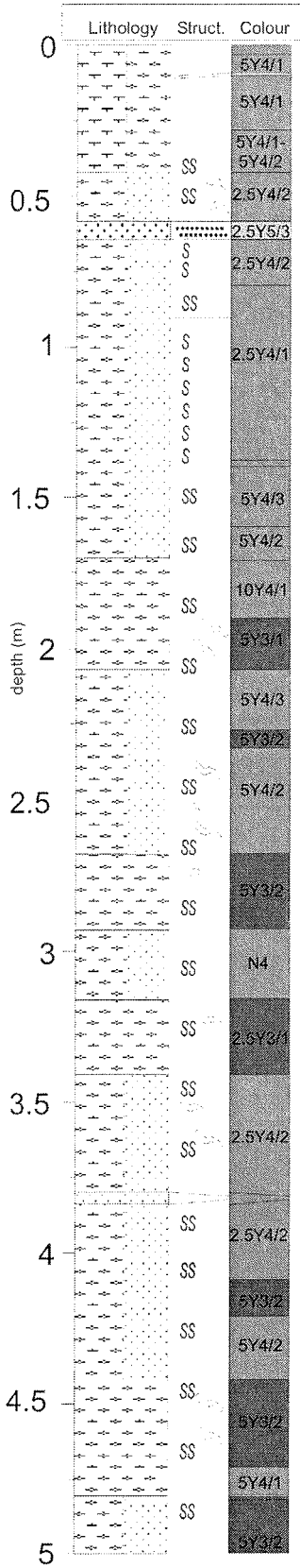

Comments

0-3 cm: olive grey to olive foram-bearing nanno mud; 5Y4/2 to 5Y4/3.
3-9 cm: dark grey foram-bearing nanno mud; 5Y4/1.
9-10 cm: greyish brown silt; 2.5Y5/2. ***Ts***
10-28 cm: dark grey foram-nanno silty mud; 5Y4/1.
28-42 cm: dark grey to olive grey foram-bearing siliceous nanno mud; 5Y4/1 to 5Y4/2.

42-58 cm: dark greyish brown foram-bearing siliceous silty mud; 2.5Y4/2.
58-64 cm: light olive brown very fine laminated sand; 2.5Y5/3. ***Ts***

64-79 cm: dark greyish brown foram-bearing silty mud; 2.5Y4/2.

79-138 cm: dark grey foram-bearing silty mud; 2.5Y4/1.

138-140 cm: dark grey foram-bearing silty mud; 5Y4/1.
140-160 cm: olive foram-bearing silty mud, mod. bioturb. with disperse tiny monosulph. spots; 5Y4/3.
160-171cm: olive grey foram-bearing silty mud, bioturb.; 5Y4/2.

171-190 cm: dark greenish grey foram-bearing mud, bioturb., open burrows; 10Y4/1.

190-207 cm: very dark grey foram-bearing mud, bioturb., open burrows 5Y3/1.

207-227 cm: olive foram-bearing silty mud, bioturb.; 5Y4/3.

227-233 cm: dark olive grey foram-bearing silty mud, bioturb.; 5Y3/2.

233-268 cm: olive grey foram-bearing silty mud, many burrows (*Zoophycos*); 5Y4/2.

268-293 cm: dark olive grey foram-bearing mud, mod. bioturb., rare monosulph. spots, single *Zoophycos*; 5Y3/2.

293-316 cm: dark grey foram-bearing silty mud, mod. bioturb.; N4.

316-339 cm: very dark grey foram-bearing mud, mod. bioturb. (several *Zoophycos*); 2.5Y3/1.

339-378/379cm: dark greyish brown foram-bearing silty mud, mod. bioturb. (several Zoophycos); 2.5Y4/2.

378/379-381/382 cm: olive brown silty layer; 2.5Y4/3. ***Turbidite Ts***
381/382-407 cm: dark greyish brown foram-bearing silty mud, mod. bioturb. (several Zoophycos), monosulph. spots in the lower part; 2.5Y4/2.

407-419 cm: dark olive grey foram-bearing silty mud with monosulph. spots; 5Y3/3.

419-440 cm: olive grey foram-bearing silty mud with monosulph. spots; 5Y4/2.

440-469 cm: dark olive grey foram-bearing mud, mod. bioturb. (several Zoophycos filled with fine sand and upper material); 5Y3/2.

469-479 cm: dark grey foram-bearing mud, mod. bioturb., single monosulph. spots; 5Y4/1.
479-519 cm: dark olive grey foram-bearing silty mud, mod. bioturb.; 5Y3/2.

GeoB 9609-2

Date: 10.07.05 Pos: 14°11.35´N 18°05.63´W
Water depth: 2785 m Core length: 530 cm

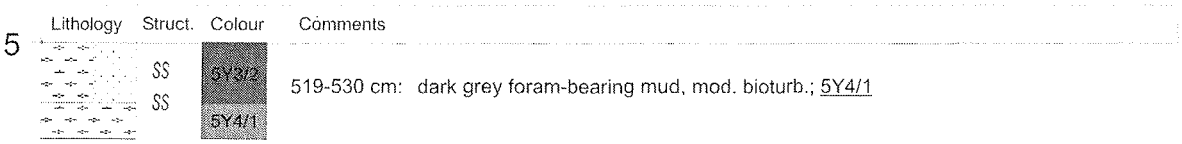

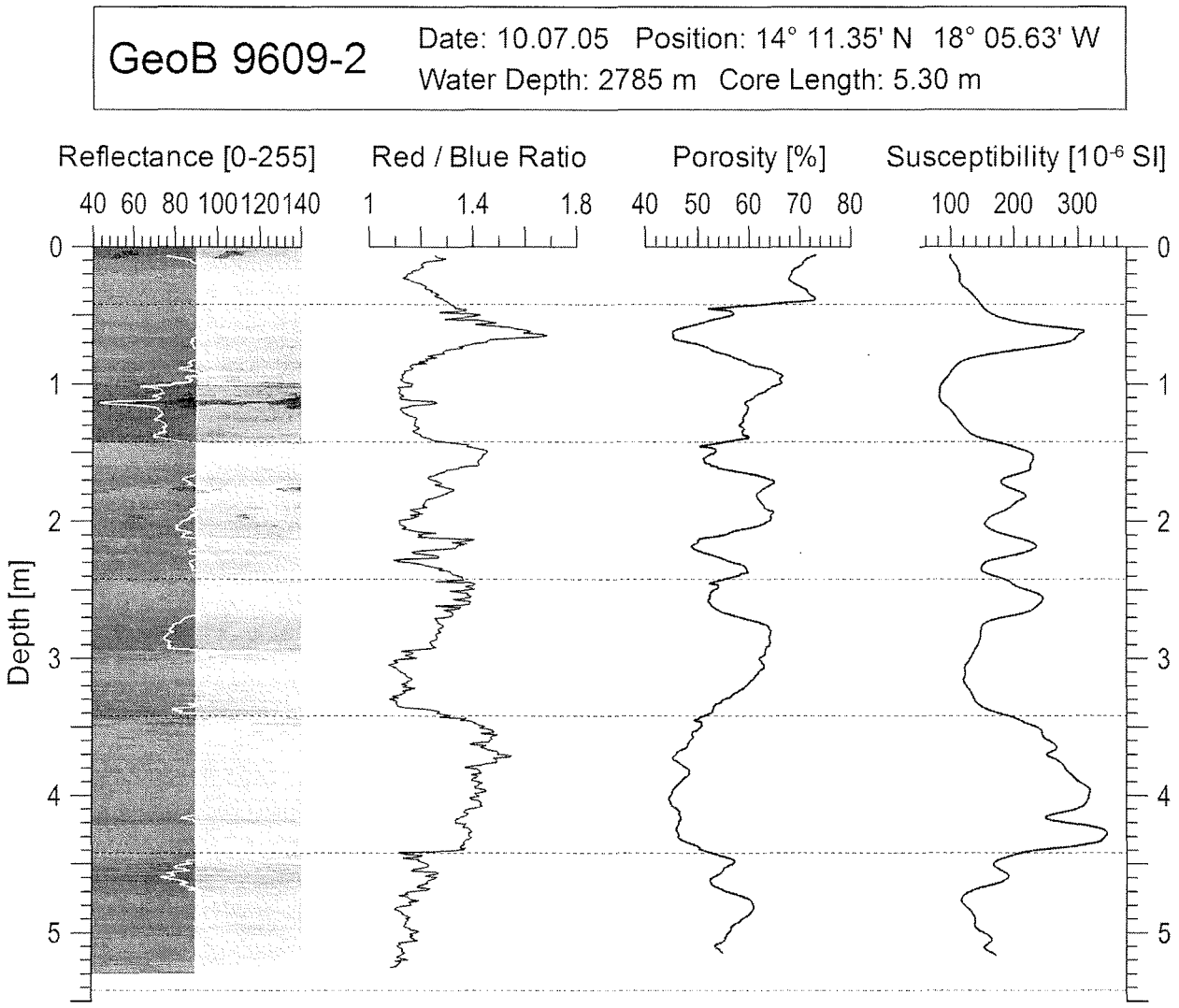

Physical properties of gravity core GeoB 9609-2. The dashed lines indicate the ends of the 1 m sections of the core.

GeoB 9610-1

Date: 12.07.05 Pos: 13°45.27´N 18°32.61´W
Water depth: 3752 m Core length: 254 cm

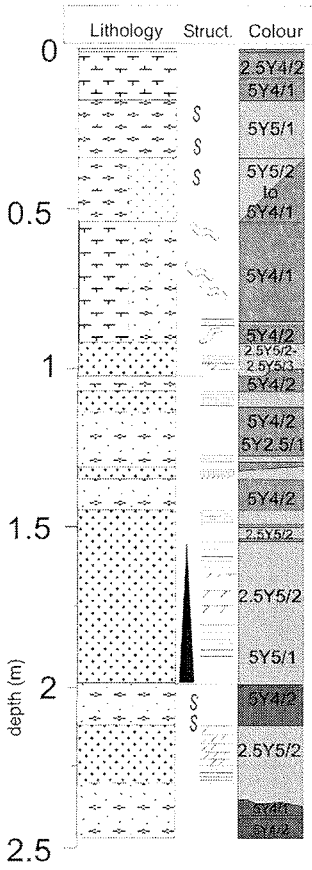

Comments

0-1 cm: brown mud; 10YR4/3.
1-9 cm: dark greyish brown foram-nanno mud to ooze; 2.5Y4/2.
9-16 cm: dark grey foram-nanno mud to ooze; 5Y4/1.
16-34 cm: grey foram-nanno silty mud, weakly bioturbated; 5Y5/1.
34-54 cm: olive grey to dark grey foram-bearing silty mud, weakly bioturbated; 5Y5/2 to 5Y4/1.
54-85 cm: grey siliceous silty nanno mud; 5Y4/1.
85-86 cm: greyish brown to light olive brown; 2.5Y5/2 to 2.5Y5/3. ***Turbidite siliciclast. Ts$_1$***
86-92 cm: olive grey silty siliceous nanno-bearing mud; 5Y4/2.
92-100/102 cm: greyish brown to light olive brown fine quartz sand; 2.5Y5/2 to 2.5Y5/3. ***Turbidite siliciclast. Ts$_2$***
100/102-107 cm: olive grey silty siliceous nanno-bearing mud; 5Y4/2.
107-112 cm: greyish brown to light olive brown fine quartz sand; 2.5Y5/2 to 2.5Y5/3
112-127 cm: black silty siliceous mud; 5Y4/2; 5Y2.5/1 in lenses.
127-129 cm: greyish brown to light olive brown fine quartz sand; 2.5Y5/2 to 2.5Y5/3.
129-144 cm: black silty siliceous mud; 5Y4/2, 5Y2.5/1 in lenses.
144-149 cm: greyish brown to light olive brown fine quartz sand; 2.5Y5/2 to 2.5Y5/3.
150-153.5 cm: greyish brown foram-quartz fine sand; 2.5Y5/2. ***Turbidite***
154.5-199 cm: grey to greyish brown foram quartz medium to fine sand; 2.5Y5/2 to 5Y5/1. ***Turbidite (complete Bouma sequence)***
199-212 cm: olive grey silty mud mottled by black monosulfid burrows; 5Y4/2.
212-235/237 cm: greyish brown fine to very fine foram quartz sand; 2.5Y5/2. ***complex almalgamated turbidite unit, basal part finer D-E units, upper part C mud; 4 DE-units;*** 5Y4/2.
235/237-240 cm: dark grey silty mud; 5Y4/1.
240-241 cm: greyish brown very fine sand. ***Turbidite D***
241-247 cm: olive grey silty mud; 5Y4/2.

GeoB 9611-1

Date: 12.07.05 Pos: 13°32.30´N 18°52.60´W
Water depth: 3983 m Core length: 140 cm

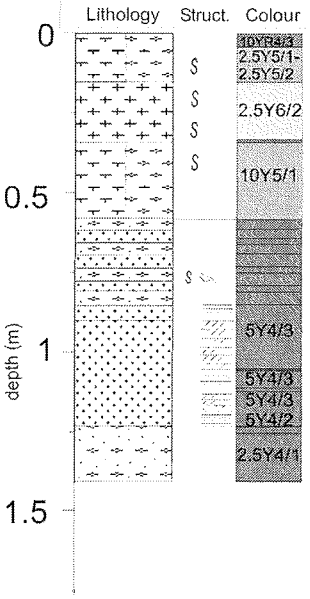

Comments

0-4 cm: brown foram-bearing nanno mud; 10YR4/3.
4-15 cm: grey to greyish foram-nanno mud, weakly bioturbated; 2.5Y5/1 to 2.5Y5/2.
15-33 cm: light brownish grey foram-nanno ooze, weakly bioturbated; 2.5Y6/2.
33-34 cm: dark greenish grey stiff foram-bearing nanno mud; 10Y4/1.
34-58 cm: greenish grey foram-bearing slightly silty nanno mud; 10Y5/1.
58-61 cm: olive silty mud; 5Y4/3.
61-64 cm: brown fine quartz sand; 10YR4/3. ***Turbidite*** Ts$_1$
64-66 cm: olive silty mud; 5Y4/3.
66-69 cm: brown fine quartz sand; 10YR4/3. ***Turbidite*** Ts$_2$
69-73 cm: olive silty mud; 5Y4/3.
73-75 cm: brown fine quartz sand; 10YR4/3. ***Turbidite*** Ts$_3$
75-79 cm: olive silty mud; 5Y4/3.
79-81 cm: brown fine quartz sand seperated by a mud band; 10YR4/3. ***Turbidite*** Ts$_4$ and Ts$_5$
81-85 cm: olive silty mud; 5Y4/3.
85-105 cm: brown fine quartz sand; 5Y4/3. ***Turbidite (D and C) Ts$_6$.***
105-105,5 cm: mud; 5Y4/1.
105,5-111 cm: brown fine quartz sand; 5Y4/3. ***Turbidite (D) Ts$_7$.***
111-112 cm: mud; 5Y4/1.
112-123 cm: brown fine quartz sand; 5Y4/3 to 5Y4/2. ***Turbidite (C and B) Ts$_8$.***
123-125 cm: olive brown silty mud; 2.5Y4/2.
125-140 cm: dark grey silty mud; 2.5Y4/1.

GeoB 9612-3

Date: 12.07.2005 Pos: 13°33.01´N 18°53.50´W
Water depth: 3893 m Core length: 863 cm

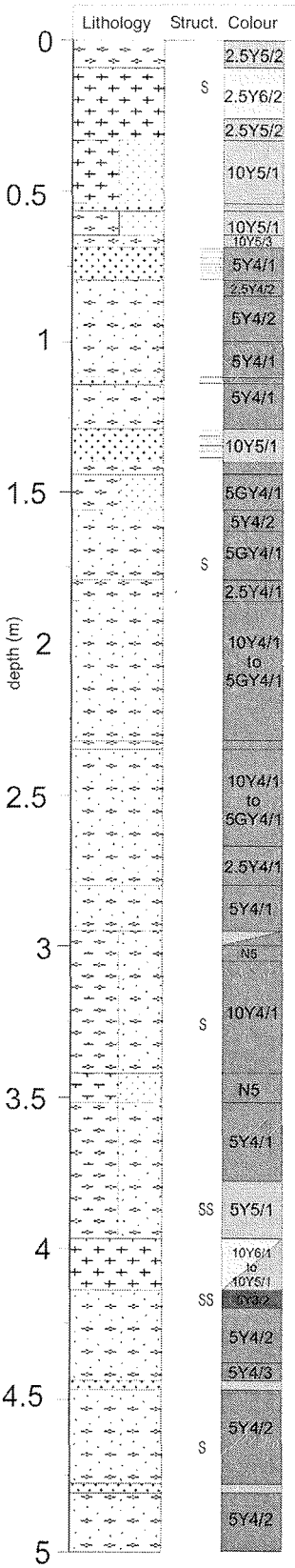

0-2 cm:	brown foram bearing nanno mud, 10YR4/2
2-9 cm:	gray to grayish brown foram-nanno mud, weakly bioturbated, 2.5Y5/1 to 2.5Y5/2
9-26 cm:	light brownish gray foram-nanno ooze, weakly bioturbated, 2.5Y6/2
26-33 cm:	grayish brown foram-nanno ooze, weakly bioturbated, 2.5Y5/2
33-54 cm:	dark greenish gray stiff foram bearing silty nanno ooze, 10Y5/1
54-56,5 cm:	brown very fine sand (**turbidite D**), 10YR5/3 to 10YR4/3
56,5-65 cm:	dark greenish gray silty foram bearing mud, 10Y5/1
65-69 cm:	brown silt and silty mud, very fine sand at 67 cm (**turbidite sand D**), 10YR5/3
69-80 cm:	dark grey to olive gray fine quartz foram laminated sand (**turbidite D**), 5Y4/1 to 5Y4/2
80-85 cm:	dark greenish brown silty mud, 2.5Y4/2 D 83-83,5 cm: grayish brown fine sand, 2.5Y5/2 D 84-84,5 cm: grayish brown fine sand, 2.5Y5/2
85-100 cm:	olive gray silty mud, with sponge spicules and radiolarians, 5Y4/2
100-112 cm:	dark gray silty mud, with sponge spicules, 5Y4/1
112-114 cm:	dark greenish gray laminated fine sand (**turbidite D**), 10Y4/1
114-129 cm:	dark gray to dark olive gray silty siliceous mud, moderately bioturbated by Chondrites, 5Y4/1 to 5Y3/2
129-134,5 cm:	greenish gray silty siliceous mud, 10Y5/1
134,5-141 cm:	greenish gray laminated fine quartz foram sand (**turbidite D**), 10Y5/1
141-145 cm:	dark gray foram bearing silty siliceous mud, 5Y4/1
145-157 cm:	dark greenish gray to very dark greenish gray foram bearing silty siliceous mud, 5GY4/1 to 5GY3/1
157-164 cm:	olive gray silty siliceous mud, 5Y4/2
164-180 cm:	dark greenish gray siliceous weakly silty mud, weakly bioturbated by Chondrites, 5GY4/1 to 10Y4/1
180-187 cm:	dark gray siliceous nanno and foram bearing mud, 2.5Y4/1
187-233 cm:	dark greenish gray siliceous silty nanno bearing mud with some forams, 10Y4/1 to 5GY4/1
233-236 cm:	dark gray siliceous nanno and foram bearing mud, 2.5Y4/1 237 cm: dark greenish stiff mud bands (**mud turbidite?**) 240 cm: dark greenish stiff mud bands (**mud turbidite?**) 260 cm: dark greenish stiff mud bands (**mud turbidite?**)
247-257 cm:	dark gray, see 187-233 cm, 10Y4/1 to 5GY4/1
257-265 cm:	dark greenish gray, see 187-233 cm, 10Y4/1 to 5GY4/1
265-278 cm:	dark gray to dark greenish brown, see 187-233 cm, 2.5Y4/1 to 2.5Y4/2
278-293 cm:	dark gray siliceous silty mud, 5Y4/1
293-298 cm:	greenish gray to dark greenish gray foram bearing siliceous silty mud, 10Y5/1 to 10Y4/1
298-305 cm:	gray to greenish gray foram-bearing siliceous silty mud, N5 to 10Y5/1
305-342 cm:	dark greenish gray foram bearing siliceous silty nanno mud, weakly bioturbated, some darker bands, 10Y4/1
342-352 cm:	gray foram nanno silty ooze, N5
352-378 cm:	dark gray foram bearing siliceous silty mud, 5Y4/1
378-397 cm:	dark gray foram bearing silty mud, moderately bioturbated by Chondrites, 5Y5/1
397-414 cm:	greenish gray siliceous nanno foram ooze, with quartz silt admixed, 10Y6/1 to 10Y5/1
414-420 cm:	dark olive gray silty siliceous mud, moderately bioturbated by Chondrites, 5Y3/2
420-438 cm:	olive gray silty mud, some forams, 5Y4/2
438-442,5 cm:	olive silty mud, 5Y4/3
442,5-445 cm:	brown very fine quartz sand (**turbidite D**), 10YR5/3
445-476 cm:	dark greenish brown silty mud, weakly bioturbated, disseminated very fine quartz sand in burrows at 469 and 489 cm (**turbidite D?**), 5Y4/2
476-479 cm:	brown very fine sand (**turbidite D**), 10YR5/3
479-570 cm:	background sediments: olive gray siliceous silty mud, weakly bioturbated, 5Y4/2
483-484 cm:	(**turbidite D**), 10YR5/3

GeoB 9612-3

Date: 12.07.2005 Pos: 13°33.01´N 18°53.50´W
Water depth: 3893 m Core length: 863 cm

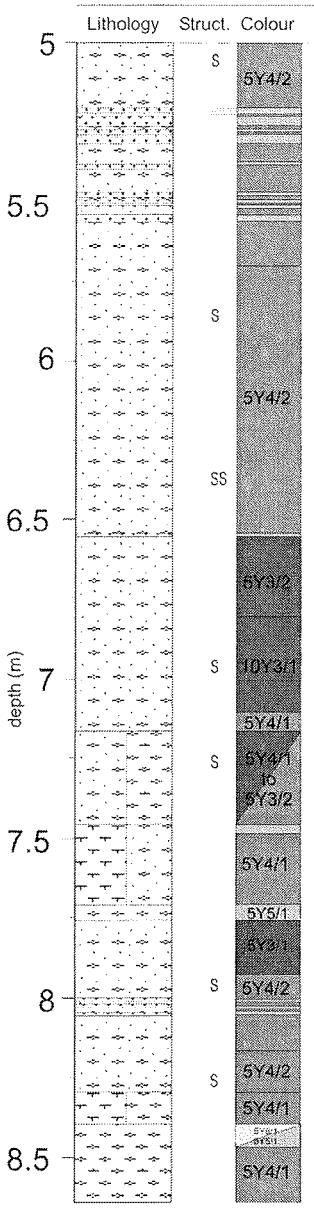

510/512-518 cm:	olive gray very fine quartz sand (**turbidite D**), 5Y4/2
520-522 cm:	laminated brown very fine quartz sand (**turbidite D**), 10YR5/3
523-525 cm:	brown very fine quartz sand (**turbidite D**), 10YR5/3
528-529 cm:	brown very fine quartz sand (**turbidite D**), 10YR5/3
534-537 cm:	brown very fine quartz sand (**turbidite D**), 10YR5/3
545-546 cm:	dark greenish gray mud, 5GY4/1
546-549 cm:	brown very fine quartz sand (**turbidite D**), 10YR5/3
554-555 cm:	brown very fine quartz sand (**turbidite D**), 10YR5/3
556-557 cm:	brown very fine quartz sand (**turbidite D**), 10YR5/3
558-560 cm:	brown very fine quartz sand (**turbidite D**), 10YR5/3
570-651 cm:	dark gray siliceous silty mud, weakly to moderately bioturbated throughout, indistinct colour banding with alternating somewhat lighter and darker layers, 5Y4/1
591 cm:	dark greenish gray 1-3 mm thick clay or mud layer, 5GY4/1
600 cm:	dark greenish gray 1-3 mm thick clay or mud layer, 5GY4/1
618 cm:	dark greenish gray 1-3 mm thick clay or mud layer, 5GY4/1
619 cm:	dark greenish gray 1-3 mm thick clay or mud layer, 5GY4/1
627 cm:	dark greenish gray 1-3 mm thick clay or mud layer, 5GY4/1
651-654 cm:	dark gray to olive gray siliceous silty mud, weakly bioturbated, 5Y4/1
654-655 cm:	brown very fine quartz sand, 10YR5/3
655-680 cm:	dark olive gray siliceous silty mud, 5Y3/2
680-710 cm:	very dark greenish gray siliceous silty mud, some nanno, few forams, weakly bioturbated throughout, 10Y3/1
710-716 cm:	dark gray siliceous silty nanno mud, 5Y4/1
716-743/745 cm:	dark gray to dark olive gray siliceous silty nanno and foram bearing mud, weakly bioturbated throughout, 5Y4/1 to 5Y3/2
743/745-748 cm:	gray siliceous silty nanno mud, 5Y5/1
748-770 cm:	dark gray siliceous silty nanno mud, 5Y4/1
770-775 cm:	gray silty foram bearing nanno mud, 5Y5/1
775-792 cm:	very dark gray silty mud, weakly bioturbated, 5Y3/1
792-816 cm:	olive gray silty siliceous mud, weakly bioturbated, 5Y4/2
802-803 cm:	brown very fine quartz sand (**turbidite**), 10YR5/3
805-806 cm:	brown very fine quartz sand (**turbidite**), 10YR5/3
807-808 cm:	brown very fine quartz sand (**turbidite**), 10YR5/3
816-821 cm:	see 792-816 cm, 5Y4/2
821-829 cm:	see 792-816 cm, 5Y4/2
829-839 cm:	dark gray nanno mud, 5Y4/1
839-846 cm:	gray silty siliceous foram nanno bearing mud, 5Y6/1 to 5Y5/1
846-863 cm:	dark gray silty siliceous foram and nanno bearing mud, 5Y4/1

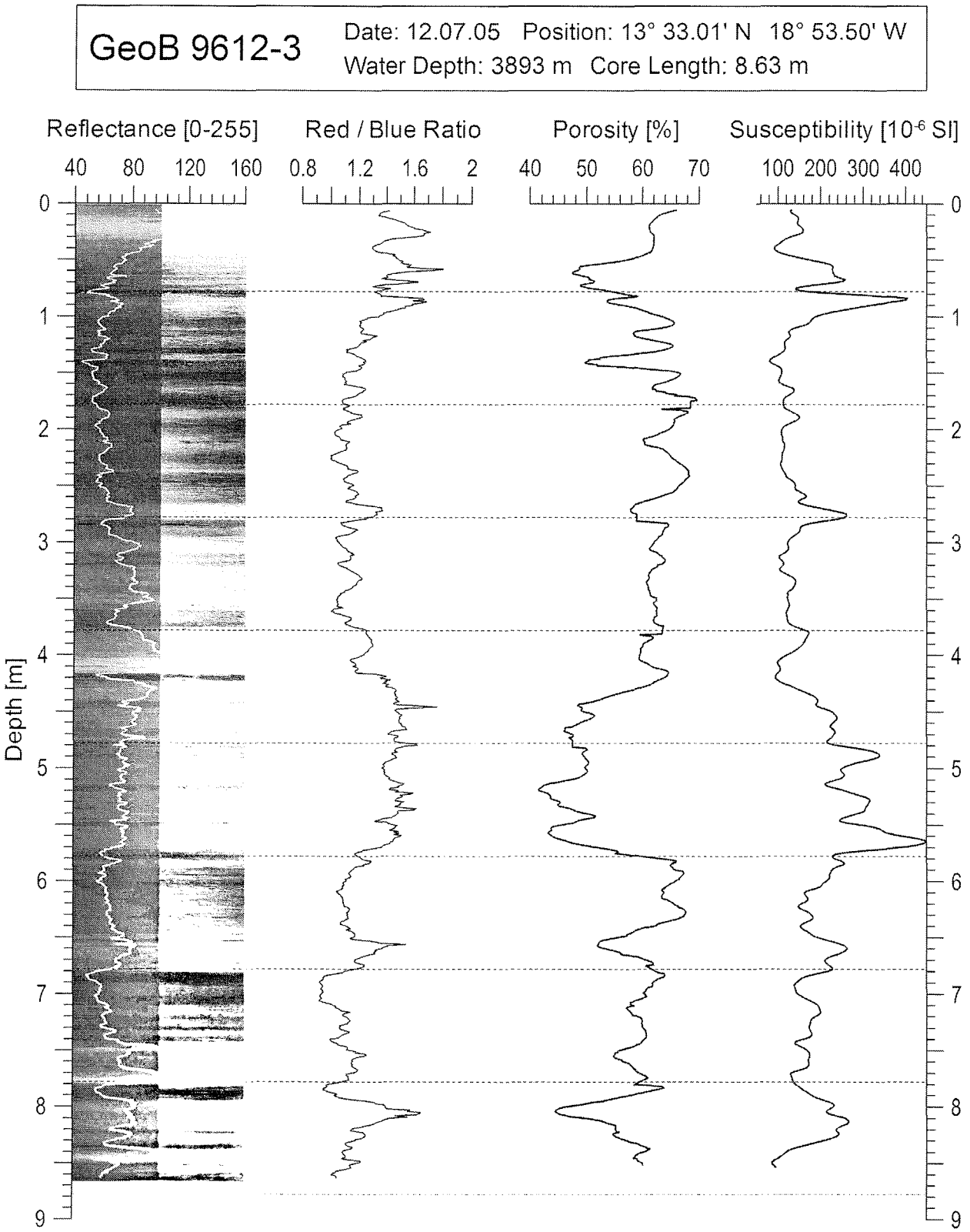

Physical properties of gravity core GeoB 9612-3. The dashed lines indicate the ends of the 1 m sections of the core.

GeoB 9613-2

Date: 13.07.05 Pos: 13°30.80´N 18°50.80´W
Water depth: 3936 m Core length: 972 cm

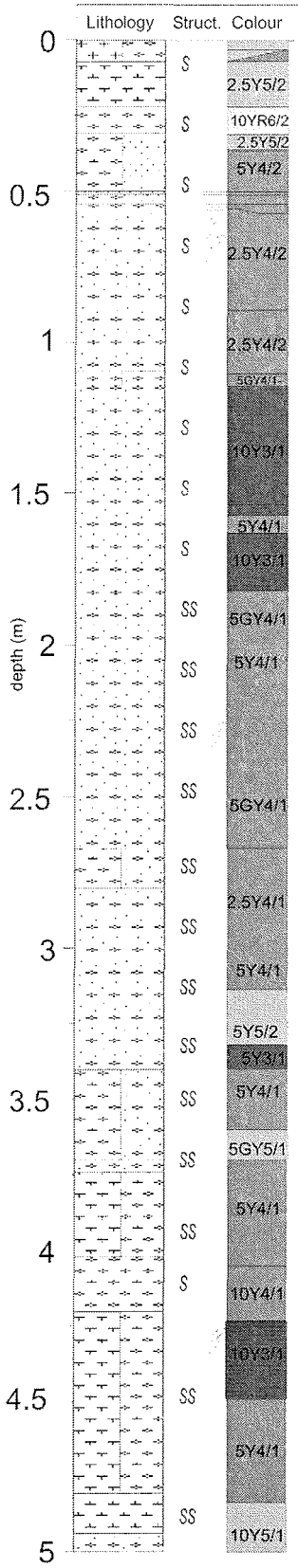

0-3 cm:	brown soft foram-nanno mud; 10YR5/3.
3-7 cm:	greyish brown to dark brown foram-nanno mud; 2.5Y5/2 to 2.5Y4/2.
7-22 cm:	greyish brown foram-nanno ooze, weakly bioturb.; 2.5Y5/2.
22-31 cm:	light brownish grey foram-bearing nanno mud, weakly bioturb.; 10YR6/2.
31-36 cm:	greyish brown foram-bearing silty mud; 2.5Y5/2.
36-36.5 cm:	dark greenish grey mud/clay; 5GY4/1.
36.5-49/50 cm:	olive grey foram-bearing silty nanno mud; 5Y4/2.
49/50-51 cm:	olive brown very fine sand and silt; 2.5Y4/3. ***Turbidite (D)***
51-54 cm:	olive grey foram-bearing silty nanno mud; 5Y4/2.
54-55/57 cm:	dark grey to olive grey very fine laminated sand; 5Y4/1 to 5Y5/2. ***Turbidite (D)***
55/57-89 cm:	dark greyish brown silty nanno-bearing mud, well developed Zoophycos; 2.5Y4/2.
89-110 cm:	dark grey to very dark grey silty mud with some nannos and few forams, weakly bioturb.; 2.5Y4/2.
	dark greenish gray 1-3 mm thick mud layer at 84 cm, 106 cm and 128 cm.
110-114 cm:	dark greenish grey foram-bearing silty nanno mud, weakly bioturb.; 5GY4/1.
114-157 cm:	very dark greenish grey silty mud, weakly bioturb.; 10Y3/1.
157-163 cm:	dark grey to olive grey silty mud, weakly bioturb.; 5Y4/1 to 5Y4/2.
163-182 cm:	very dark greenish grey silty mud, weakly bioturb.; 10Y3/1.
182-200 cm:	dark greenish grey silty mud, weakly bioturb.; 5GY4/1.
200-205 cm:	dark grey silty mud with some forams; 5Y4/1.
205-267 cm:	dark greenish grey silty mud, weakly bioturb.; 5GY4/1.
267-280 cm:	dark grey silty foram/nanno-bearing silty mud, weakly bioturb.; 2.5Y4/1.
	dark greenish grey stiff mud at 274 cm and 289 cm; 5GY4/1.
280-314 cm:	dark grey silty mud; 5Y4/1.
	dark greenish grey mm-thick mud layers at 294 cm, 296 cm, 306 cm, 328 cm and 335 cm; 5GY4/1.
314-332 cm:	olive grey silty mud; 5Y5/2.
332-340 cm:	very dark grey silty mud; 5Y3/1.
340-360 cm:	dark grey foram-bearing silty nanno mud; 5Y4/1.
360-370 cm:	greenish grey foram-bearing silty nanno mud; 5GY5/1.
370-374 cm:	very dark grey silty mud; 5Y3/1.
374-402 cm:	dark grey, foram-bearing nanno mud; 5Y4/1.
402-420 cm:	dark greenish grey foram-bearing mud, single monosulph. spots, mod. bioturb.; 10Y4/1.
420-446 cm:	very dark greenish grey foram-bearing nanno mud; 10Y3/1.
446-480 cm:	dark grey foram-bearing nanno mud; 5Y4/1.
480-494 cm:	greenish grey foram ooze, mod. bioturb. (open burrows); 10Y5/1.
494-500 cm:	dark grey to olive grey silty mud, mod. bioturb.; 5Y4/1 to 5Y4/2.

GeoB 9613-2

Date: 13.07.05 Pos: 13°30.80´N 18°50.80´W
Water depth: 3936 m Core length: 972 cm

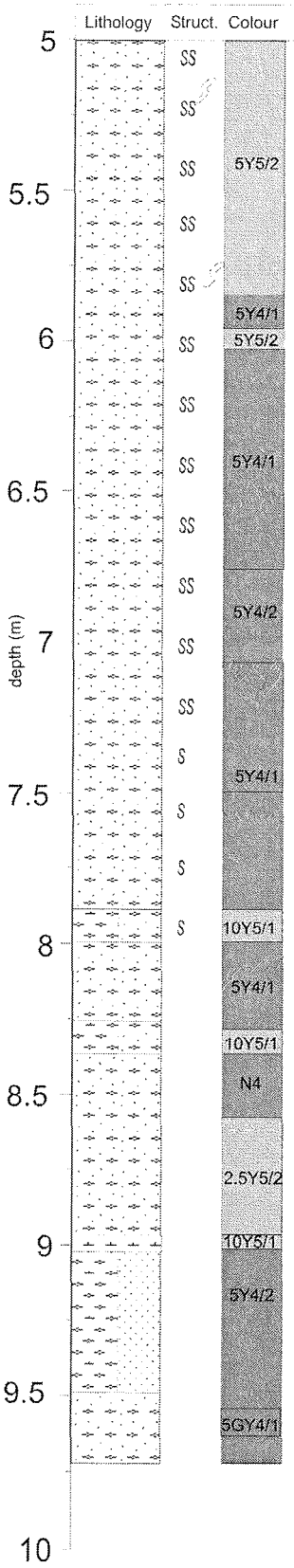

500-584 cm: olive grey to olive silty mud, weakly bioturb.; 5Y5/2 to 5Y5/3.

584-595 cm: dark grey to very dark grey silty mud, weakly bioturb.; 5Y4/1 to 5Y3/1.
595-602 cm: olive grey to olive silty mud, weakly bioturb.; 5Y5/2 to 5Y5/3.
602-675 cm: dark grey to very dark grey silty mud, weakly bioturb.; 5Y4/1 to 5Y3/1.

dark greenish grey mm-thick mud at 603 cm, 618 cm, 640 cm and 652 cm; 5GY4/1.
675-706 cm: olive grey silty mud, weakly bioturb; 5Y4/2.

706-749 cm: dark grey to very dark grey silty mud, weakly bioturb.; 5Y4/1 to 5Y3/1.

749-756 cm: olive grey silty mud, mod. bioturb.; 5Y4/2.
756-788 cm: dark grey to very dark grey silty mud, weakly bioturb.; 5Y4/1 to 5Y3/1.

788-797 cm: greenish grey foram-bearing silty nanno mud, weakly bioturb.; 10Y5/1.

797-826 cm: dark grey silty mud, few forams, weakly bioturb., faint monosulph. tubes; 5Y4/1.

826-834 cm: greenish grey foram-bearing silty nanno mud, weakly bioturb.; 10Y5/1.
834-855 cm: dark grey silty mud, few forams and some nannos, weakly bioturb.; N4.

855-864 cm: greyish brown silty mud; 2.5Y5/2.
864-865 cm: light brownish grey very fine sand/silt; 2.5Y6/2. ***Turbidite***
865-894 cm: greyish brown silty mud, weakly bioturb., faint monosulph. burrow tubes; 2.5Y5/2

894-901 cm: greenish grey foram-nanno ooze; 10Y5/1.

901-920 cm: dark grey foram-bearing silty nanno mud, weakly bioturb., faint monosulph. burrow tubes; 5Y4/1.
920-957 cm: dark grey to very dark grey silty nanno-bearing mud, weakly bioturb.; 5Y4/1 to 5Y3/1.

957-966 cm: dark greenish grey silty mud; 5GY4/1.
966-972 cm: dark grey to very dark grey silty mud, weakly bioturb.; 5Y4/1 to 5Y3/1.

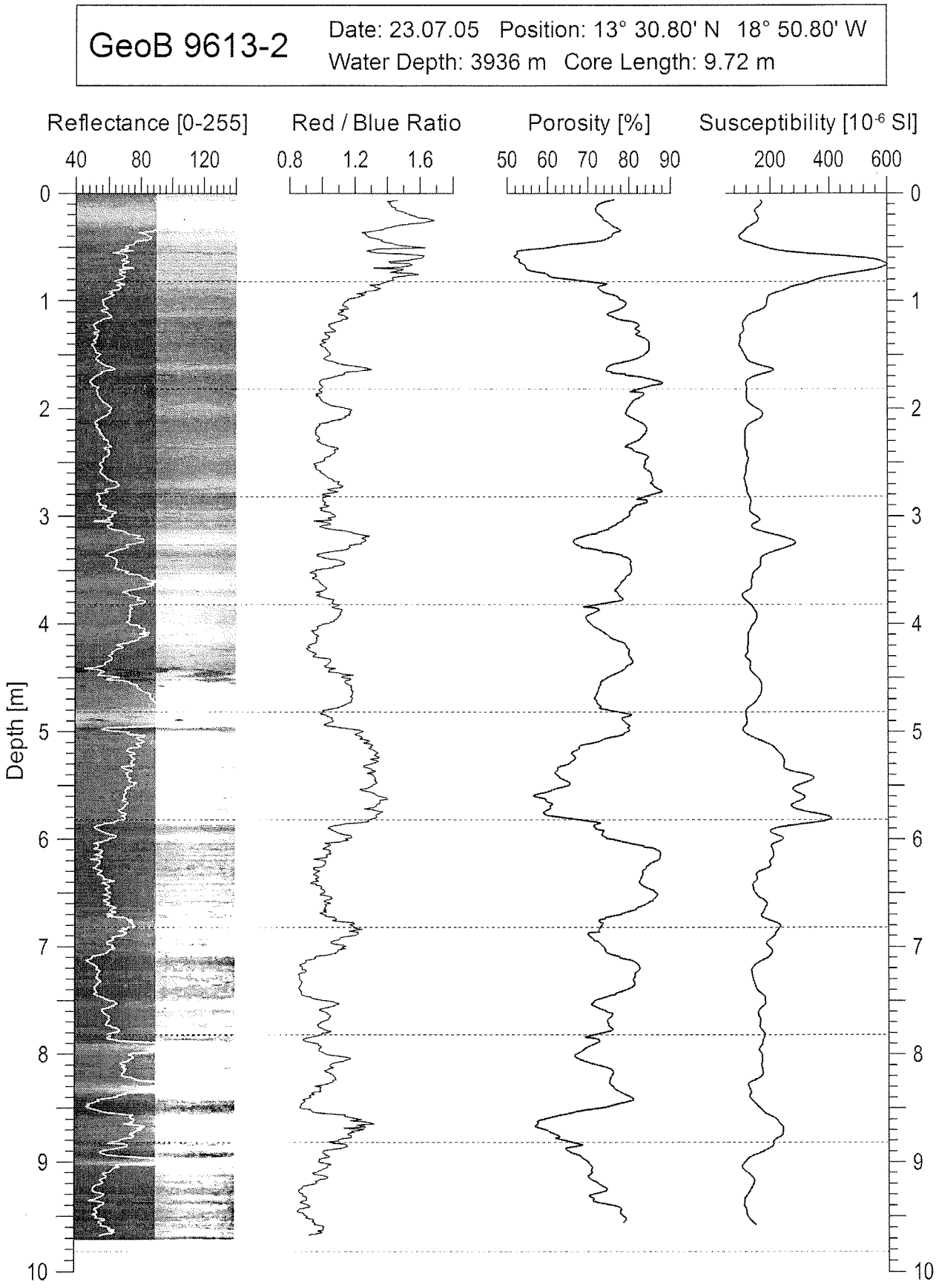

Physical properties of gravity core GeoB 9613-2. The dashed lines indicate the ends of the 1 m sections of the core.

GeoB 9614-1

Date: 13.07.05 Pos: 13°20.54´N 19°03.56´W
Water depth: 4090 m Core length: 467 cm

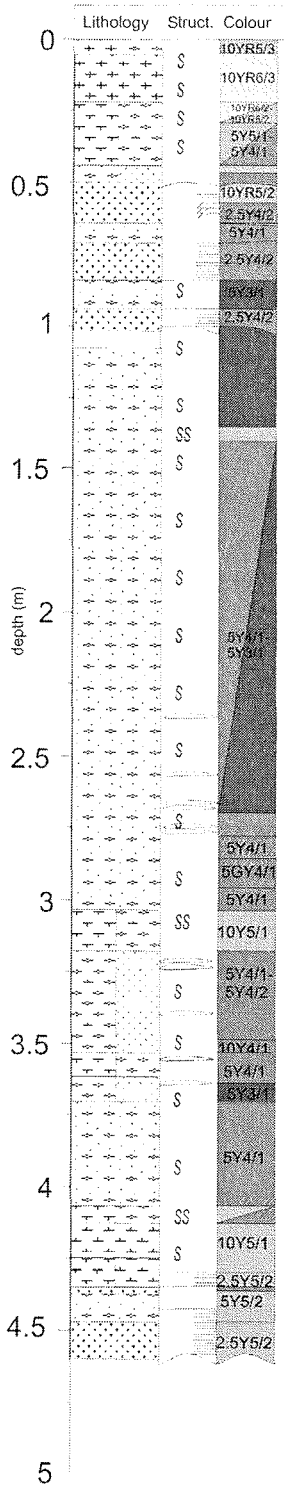

0-5 cm: brown soft foram-nanno mud, sponge spicules; 10YR5/3.
5-22 cm: pale brown foram-nanno ooze, weakly bioturb.; 10YR6/3.
22-29 cm: light brownish grey to greyish brown foram-bearing nanno mud, weakly bioturb.; 10YR6/2 to 10YR5/2.
29-44 cm: grey to dark grey foram-bearing nanno mud; 5Y5/1 to 5Y4/1.
3 mm-thick dark greenish grey stiff mud/clay at 30 and 35.5 cm; 5GY4/1.
44-46.5 cm: grey silty foram-bearing nanno mud; 5Y5/1.
46.5-50 cm: dark grey silty foram-bearing nanno mud; 5Y4/1.
50-57 cm: greyish brown very fine quartz sand; 10YR5/2. ***Turbidite Ts, (D)***
57-64 cm: dark greyish brown foram quartz fine sand; 2.5Y4/2. ***Turbidite Ts, (C)***
64-65 cm: greyish brown mud; 2.5Y4/2.
65-70/71 cm: grey silty mud; 5Y4/1.
70/71-84 cm: dark greyish brown laminated fine sand; 2.5Y4/2. ***Turbidite Ts_2 (D)***
84-94 cm: very dark grey silty siliceous mud: 5Y3/1.
94-100/103 cm: dark greyish brown fine quartz sand; 2.5YR4/2. ***Turbidite Ts,***
100/103-135 cm: very dark grey to black silty mud with some forams.

135-140 cm: dark grey to olive grey silty mud; 5Y4/1 to 5Y4/2.
140-270 cm: very dark grey to black silty mud, weakly bioturb.; 5Y4/1 to 5Y3/1.
dark greenish grey stiff mud/clay bands of several mm thickness at 244 cm, 254/255 cm, 268 cm and 269 cm.

270-278 cm: dark grey to olive grey silty mud, 5Y4/1 to 5Y4/2.
278- 285 cm: dark grey silty mud; 5Y4/1.
285-295 cm: dark greenish grey silty mud, some forams, weakly bioturb.; 5GY4/1.
295-304 cm: dark grey silty mud, some forams, weakly bioturb.; 5Y4/1.
304-317 cm: greenish grey foram-bearing nanno mud, weakly to mod. bioturb. (Zoophycos, Chondrites); 10Y5/1.
317-353 cm: dark grey to olive grey foram-bearing silty mud, weakly bioturb.; 5Y4/1 to 5Y4/2.
intercalations of: dark greenish grey 1-3 mm thick stiff clay/mud bands at 280 cm, 282 cm, 320 cm, 323 cm, 346 cm, 360 cm and 368 cm; 10GY4/1.
353-360 cm: dark greenish grey foram-nanno mud, weakly bioturb.; 10Y4/1.
360-368 cm: dark grey foram-bearing silty mud, weakly bioturb.; 5Y4/1.
368-384 cm: very dark grey silty mud, some forams, weakly bioturb.; 5Y3/1.
384-411 cm: dark grey siliceous silty (quartz) mud, weakly bioturb.; 5Y4/1.
411-417 cm: grey to dark grey foram-bearing nanno mud, mod. bioturb.; 5Y5/1 to 5Y4/1.
417-425 cm: greenish grey foram ooze; 10Y5/1.
425-434 cm: greenish grey foram-nanno ooze, weakly bioturb.; 10Y5/1.
2 mm-thick olive mud layer at 431 cm.
434-439 cm: greyish brown very fine quartz sand to silt; 2.5Y5/2. ***Turbidite Ts_4 (D)***
439-440.5 cm: dark greenish grey stiff mud/clay; 5GY4/1.
440.5-448 cm: olive grey silty mud, weakly bioturb.; 5Y5/2.
448-467 cm: greyish brown laminated very fine sand to silt; 2.5Y5/2. ***Turbidite Ts_5 (D)***

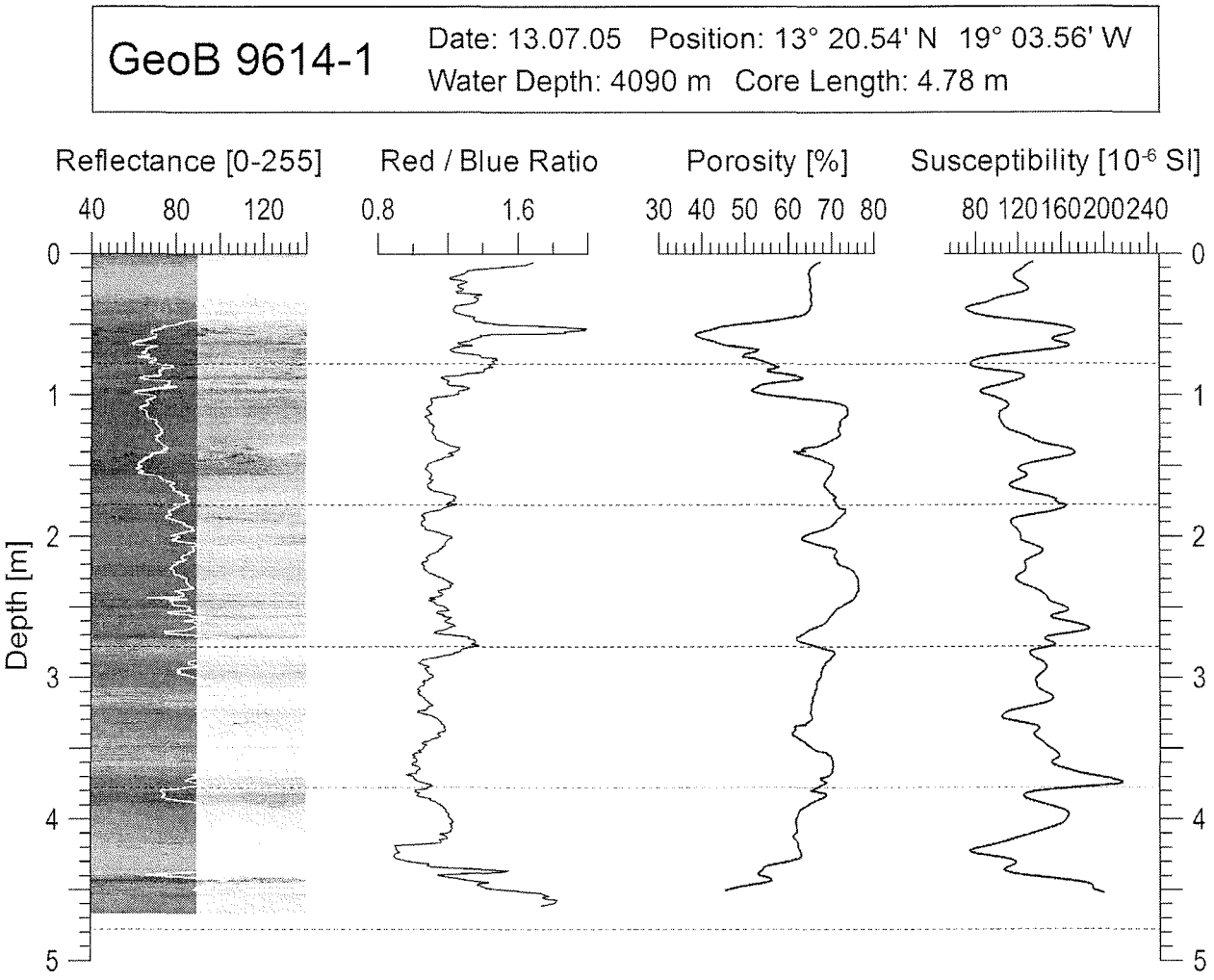

Physical properties of gravity core GeoB 9614-1. The dashed lines indicate the ends of the 1 m sections of the core.

GeoB 9615-1

Date: 14.07.05 Pos: 13°23.68´N 19°06.27´W
Water depth: 4180 m Core length: 930 cm

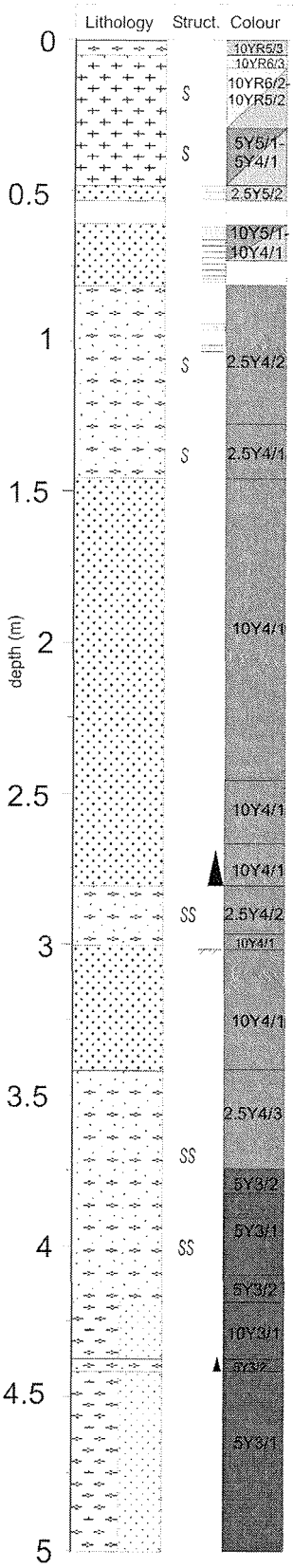

0-4 cm:	brown soft foram-nanno mud, 10YR5/3.
4-8 cm:	pale brown foram-nanno ooze, weakly bioturb., 10YR6/3.
8-21 cm:	light brownish grey to greyish brown foram nanno 00ze, weakly bioturb., 10YR6/2 to 10YR5/2.
21-28 cm:	light brownish grey to greyish brown, foram-bearing nanno mud, weakly bioturb. 10YR6/2 to 10YR5/2.
28/32 cm:	dark greenish grey, stiff mud, 5GY4/1.
28-47 cm:	grey to dark grey, foram-bearing nanno mud, weakly bioturb., 5Y5/1 to 5Y4/1.
47-52 cm:	greenish brown to light olive brown, very fine laminated sand, 2.5Y5/2 to 2.5Y5/3. **turbidite Ts1**
52-60 cm:	no description
60-72 cm:	greenish grey to dark greenish grey, laminated fine sand grading upward to very fine sand, 10Y5/1 to 10Y4/1. **turbidite Ts2 (D)**
72-72,5 cm:	dark greenish grey mud, 5GY4/1.
72,5-80 cm:	alternating layers of fine and very fine sand, laminated throughout, **turbidite Ts3**
80-126 cm:	dark greyish brown, silty mud, weakly bioturb., 2.5Y4/2.
84-85 cm:	light olive brown, very fine sand to silt layers, 2.5Y5/3. **turbidite Ts4 (D)**
88-89 cm:	light olive brown, very fine sand to silt layers, 2.5Y5/3. **turbidite Ts5 (D)**
94-95 cm:	light olive brown, very fine sand to silt layers, 2.5Y5/3. **turbidite Ts6 (D)**
102-103 cm:	light olive brown, very fine sand to silt layers, 2.5Y5/3. **turbidite Ts7 (D)**
126-144 cm:	dark grey, silty mud, weakly bioturb., 2.5Y4/1.
144-244 cm:	dark greenish grey, fine quartz sand, foram-bearing (matrix content?, eventually sandy debrite or turbidite D unit), grain size appear to be quite uinform, 10Y4/1.
244-265 cm:	dark greenish grey, fine to very fine quartz sand, mixed with forams, 10Y4/1. **turbidite Ts8**
265-279 cm:	dark greenish grey, fine to medium sand, with forams, 10Y4/1. **turbidite Ts8**
279-289 cm:	dark greyish brown, silty mud, moderatly bioturb. (Chondrites), 2.5Y4/2.
289-295 cm:	dark greyish brown to very dark greyish brown, silty mud, weakly bioturb., 2.5Y4/2 to 2.5Y4/3.
295-300 cm:	dark greenish grey, silty mud, 10Y4/1.
300-340 cm:	dark greenish grey,fine to very fine quatz sand, mixed with forams, laminated up to 303 cm, cross bedded above, 10Y4/1.
340-373 cm:	very dark greyish brown, silty mud, 2.5Y4/3.
373-381 cm:	dark olive grey, silty mud, bioturb., 5Y3/2.
381-408 cm:	very dark grey, silty mud,bioturb., 5Y3/1.
408-417 cm:	dark olive grey, silty mud,bioturb.; 5Y3/2.
417-436 cm:	very dark greenish grey, foram-bearing silty mud, single monsulph. spots, 10Y3/1.
436-440 cm:	dark olive grey, silty mud with fine sand on base, 5Y3/2. **turbidite Ts 9**
440-478 cm:	very dark grey, foram-bearing silty mud, 5Y3/1.
478-499 cm:	very dark grey, foram-bearing silty mud, 5Y3/1.
499-512 cm:	olive grey, silty mud, 5Y4/2.

GeoB 9615-1

Date: 14.07.05 Pos: 13°23.68´N 19°06.27´W
Water depth: 4180 m Core length: 930 cm

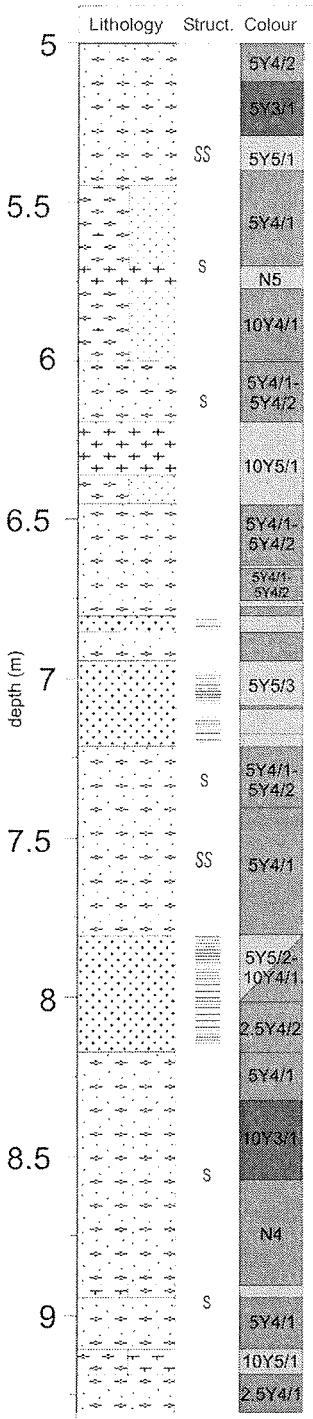

Comments	
512-529 cm:	very dark grey, silty mud, 5Y3/1.
529-540 cm:	grey, silty mud, bioturb., 5Y5/1.
540-545 cm:	dark grey, silty mud, weakly bioturb., 5Y4/1.
542 cm:	dark greenish grey, mud band, 5GY4/1.
545-570 cm:	dark grey, foram-bearing silty mud, weakly bioturb., 5Y4/1.
570-577 cm:	grey, foram-nanno ooze, weakly bioturb., N5.
577-600 cm:	dark greenish grey, foram-bearing silty mud, weakly bioturb., 10Y4/1.
600-619 cm:	dark grey to olive grey, silty mud, few forams, weakly bioturb., 5Y4/1 to 5Y4/2.
619-636 cm:	greenish grey, foram-nanno ooze, weakly bioturb., 10Y5/1.
636-645 cm:	greenish grey, foram-bearing silty nanno mud, weakly bioturb., 10Y5/1.
645-664 cm:	dark grey to olive grey, silty mud, weakly bioturb., 5Y4/1 to 5Y4/2.
664-665 cm:	light olive brown, very fine quartz sand, 5Y5/3. **turbidite Ts10**
665-675 cm:	dark grey to olive grey, silty mud, weakly bioturb., 5Y4/1 to 5Y4/2.
675-677 cm:	light olive brown, very fine quartz sand, 5Y5/3. **turbidite Ts11**
677-680 cm:	dark grey to olive grey, silty mud, weakly bioturb., 5Y4/1 to 5Y4/2.
680-685 cm:	light olive brown, very fine quartz sand, laminated throughout, 5Y5/3. **turbidite Ts12**
685-694 cm:	dark grey to olive grey, silty mud, weakly bioturb., 5Y4/1 to 5Y4/2.
694-708 cm:	light olive brown, very fine quartz sand and silt, laminated throughout, 5Y5/3. **turbidite Ts13**
708-709 cm:	dark grey, silty mud, weakly bioturb., 5Y4/1.
709-716 cm:	light olive brown, very fine quartz sand and silt, laminated throughout, 5Y5/3. **turbidite Ts14**
716-717 cm:	very dark grey, silty mud, 5Y3/1.
717-721 cm:	light olive brown, very fine quartz sand and silt, laminated throughout, 5Y5/3. **turbidite Ts15**
721-740 cm:	dark grey to olive grey, silty mud, weakly bioturb., 5Y4/1 to 5Y4/2.
740-780 cm:	dark grey, silty mud, moderatley bioturb., 5Y4/1.
755-757 cm:	dark greenish grey colored band
768-769 cm:	dark greenish grey colored band
780-801 cm:	olive grey to dark greenish grey, fine to very fine laminated quartz sand, 5Y5/2 to 10Y4/1. alternating layers of fine sand and very fine sand, **turbidite Ts16 (D)**
801-802 cm:	dark grey, silty mud, 5Y4/1.
802-817 cm:	dark greyish brown to greyish brown, laminated very fine sand and silt, 2.5Y4/2. **turbidite Ts 16 (D)**
817-832 cm:	dark grey, silty mud, weakly bioturb., 5Y4/1.
825/826 cm:	dark greenish grey, mm sized, mud layer, 5GY4/1.
832-857 cm:	very dark greenish grey, silty mud, weakly bioturb., 10Y3/1.
857-890 cm:	dark grey, silty mud, weakly bioturb., N4.
890-894 cm:	greenish grey, nanno mud to ooze, few forams, weakly bioturb., 10Y5/1.
894-910 cm:	very dark grey, silty mud, weakly bioturb., 5Y4/1.
910-918 cm:	greenish grey, foram-bearing nanno ooze, weakly bioturb., 10Y5/1.
918-930 cm:	dark grey, silty mud, weakly bioturb., 2.5Y4/1.

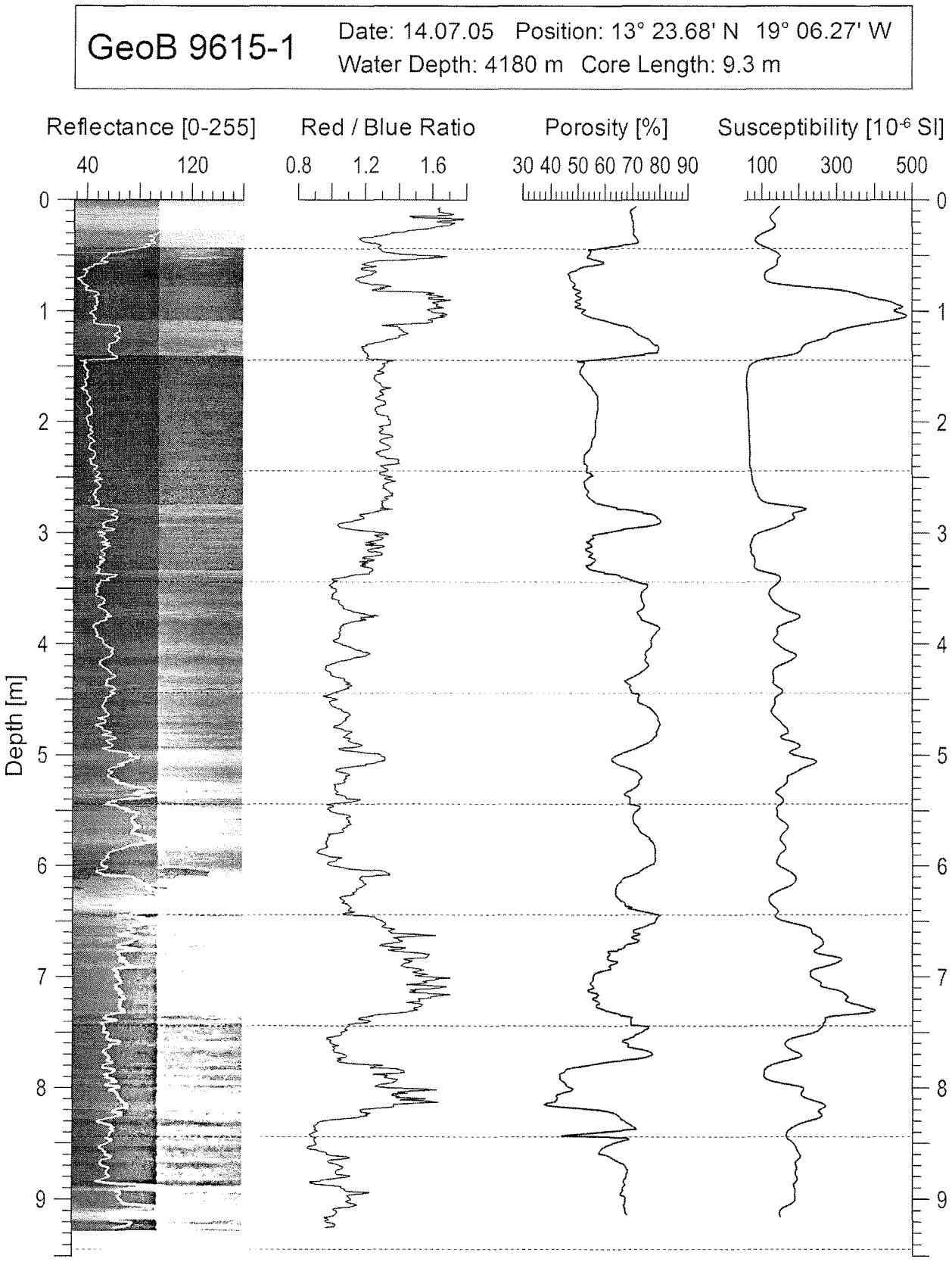

Physical properties of gravity core GeoB 9615-1. The dashed lines indicate the ends of the 1 m sections of the core.

GeoB 9621-3

Date: 17.07.05 Pos: 19°39.37´N 16°56.35´W
Water depth: 52 m Core length: 574 cm

0-61 cm: dark greenish grey, sandy, silty mud with abundant shells and shell fragments, intensive H_2S-smell, 10Y4/2.

61-62 cm: very dark grey, (foram-bearing) sandy, silty mud, sulfat reduction horizon (?), shell fragments, N3.

62-237 cm: dark greenish grey, sandy, silty mud with abundant shells and shell fragments, intensive H_2S-smell, 10Y4/2.

237-474 cm: dark greenish grey, sandy, silty mud, with less shell fragments, intensive H_2S-smell, 10Y4/2.

285 cm: plant fragment (wood fragment ?)

474-574 cm: core not opened, OSL-dating

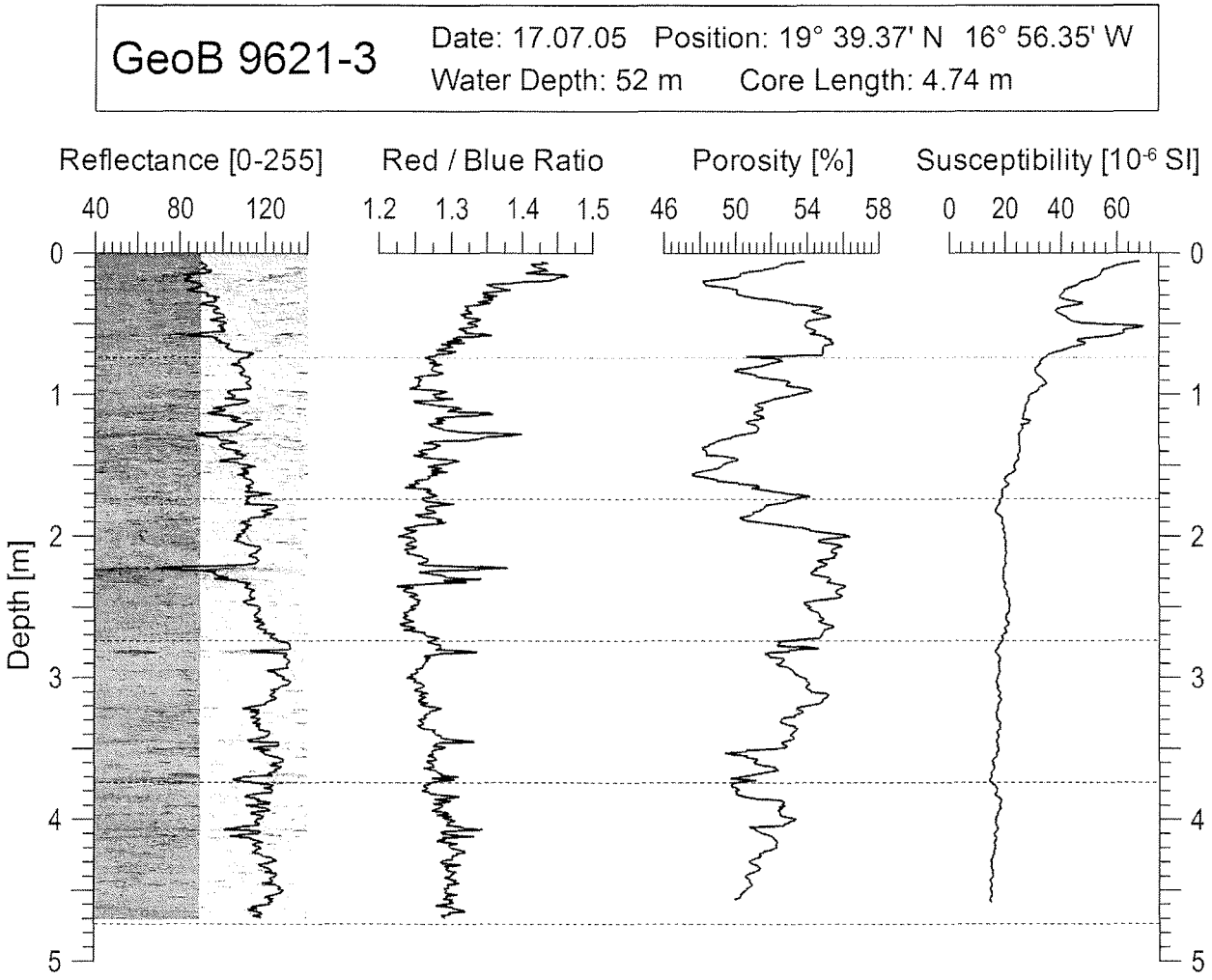

Physical properties of gravity core GeoB 9621-3. The dashed lines indicate the ends of the 1 m sections of the core.

GeoB 9622-3

Date: 18.07.05 Pos: 19°14.85´N 18°33.19´W
Water depth: 2879 m Core length: 1031 cm

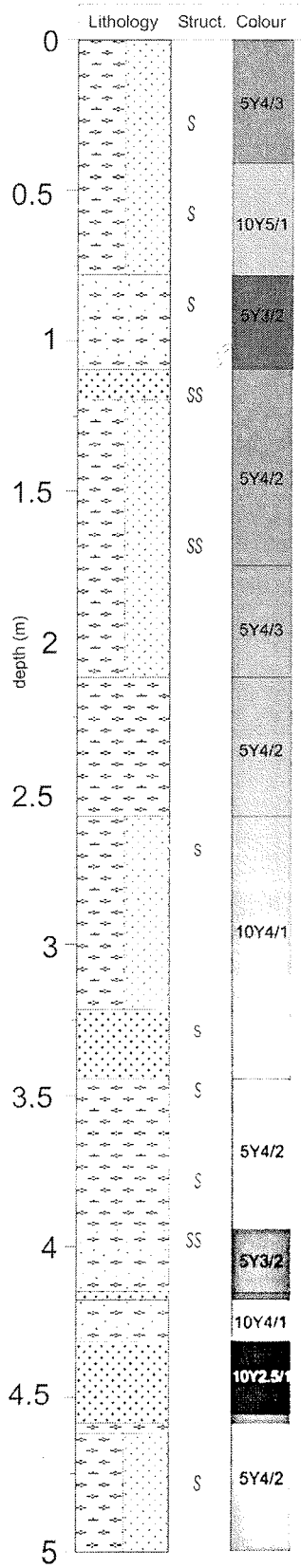

Comments

0-1 cm: olive brown foram-bearing silty mud, 2.5Y4/3.
1-41 cm: olive foram-bearing silty mud, weakly bioturb., 5Y4/3.

strong H_2S-smell over the complete core
41-78 cm: greenish grey foram-bearing silty mud, weakly bioturb., 10Y5/1.

78-109 cm: dark olive grey silty mud with burrows of *Zoophycea*, 5Y3/2.

109-119 cm: olive grey foram-bearing silty muddy fine sand, 5Y4/2. **turbidite Ts1**

119-174 cm: olive grey foram-bearing silty mud, bioturb., 5Y4/2.

5Y4/1

174-211 cm: olive foram-beraing silty mud, bioturb., 5Y4/3.

211-257 cm: olive grey foram-bearing mud, monosulph. spots, 5Y4/2.

257-321 cm: dark greenish grey foram-bearing silty mud, weakly bioturb., 10Y4/1.

321-344 cm: dark greenish grey fine sand, 10Y4/1. **turbidite Ts2**

344-394 cm: olive grey foram-bearing mud, weakly bioturb., monosuiph. spots, 5Y4/2.

394-415 cm: dark olive grey silty mud, bioturb. in the upper part, 5Y3/2.

415-417 cm: very dark grey quartz fine sand, 5Y3/1. **turbidite Ts3**
417-431 cm: dark greenish grey silty mud, 10Y4/1.

431-453 cm: greenish black quartz fine sand, 10Y2.5/1. **turbidite Ts4**

454-456 cm: black medium to fine sand (erosive contact or base?), 5Y2.5/1. **turbidite Ts4**
456-459 cm: very dark greenish grey foram-bearing mud, 10Y3/1.
459-552 cm: olive grey foram-bearing silty mud, weakly bioturb., 5Y4/2.

GeoB 9622-3

Date: 18.07.05 Pos: 19°14.85´N 18°33.19´W
Water depth: 2879 m Core length: 1031 cm

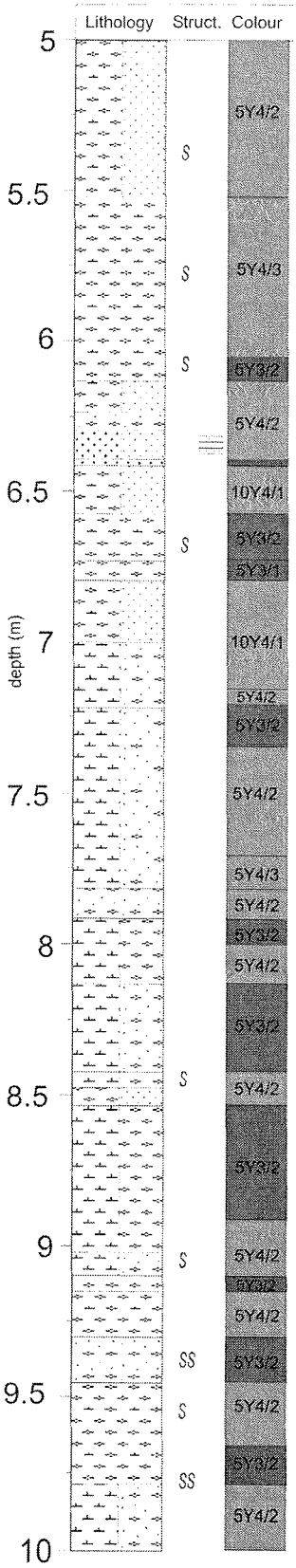

552-605 cm: olive foram-bearing mud, monosulph. spots, 5Y4/3.

605-613 cm: dark olive grey foram-bearing mud, weakly bioturb., 5Y3/2.

613-624 cm: olive grey foram-bearing silty mud, monosulph. spots, weakly bioturb., 5Y4/2.
624-629 cm: olive grey silty mud, 5Y4/2.
629-639 cm: olive grey fine (mm-sized) laminated fine sand/silt layers, 5Y4/2. **turbidite Ts5**
639-641 cm: very dark grey fine sand, 5Y3/1. **tubidite Ts5**
641-657 cm: dark greenish grey foram-bearing silty mud, monosulph. spots, 10Y4/1.
657-672 cm: dark olive grey foram-bearing mud, weakly bioturb., 5Y3/2.

672-679 cm: very dark grey mud, weakly bioturb., 5Y3/1.

679-680 cm: very dark greenish grey foram-bearing fine sand, 10Y3/1.
680-700 cm: dark greenish grey foram-bearing silty mud, 10Y4/1.

700-716 cm: dark greenish grey silty muddy foraminiferal ooze, 10Y4/1.
716-721 cm: olive grey silty muddy foraminiferal ooze, 5Y4/2.

721-735 cm: dark olive grey silty muddy foraminiferal ooze, 5Y3/2.

735-771 cm: olive grey muddy silty foraminiferal ooze, 5Y4/2.

771-782 cm: olive muddy silty foraminiferal ooze, 5Y4/3.
782-787 cm: olive grey silty mud, 5Y4/2.
787-788 cm: dark grey silt, 5Y4/1.
788-799 cm: dark olive grey muddy foraminiferal ooze, 5Y3/2.
799-813 cm: olive grey muddy foraminiferal ooze, monosulph. spots, 5Y4/2.

813-842 cm: dark olive grey silty muddy foraminiferal ooze, 5Y3/2.

842-848 cm: olive grey muddy foraminiferal ooze, 5Y4/2.
848-853 cm: olive grey foram-bearing silty mud, monosulph. spots, weakly bioturb., 5Y4/2.
853-891 cm: dark olive grey muddy foraminiferal ooze, monosulph. spots, 5Y3/2.

891-902 cm: olive grey muddy foraminiferal ooze, weakly bioturb., monosulph. spots, 5Y4/2.
902-910 cm: olive grey silty muddy foraminiferal ooze, 5Y4/2.
910-914 cm: dark olive grey mud, weakly biotrub., 5Y3/2.
914-915 cm: dark grey silt, 5Y3/1.
915-930 cm: olive grey foram-bearing mud, bioturb., 5Y4/2.
930-944 cm: dark olive grey silty mud, biotrub., 5Y3/2.
944-945 cm: dark olive grey foram sand, 5Y3/2.
945-966 cm: olive grey foram-bearing mud, weakly bioturb., 5Y4/2.

966-979 cm: dark olive grey foram-bearing mud, bioturb., 5Y3/2.
979-1031 cm: olive grey silty, muddy foraminiferal ooze, 5Y4/2.

GeoB 9622-3

Date: 18.07.05 Pos: 19°14.85´N 18°33.19´W
Water depth: 2879 m Core length: 1031 cm

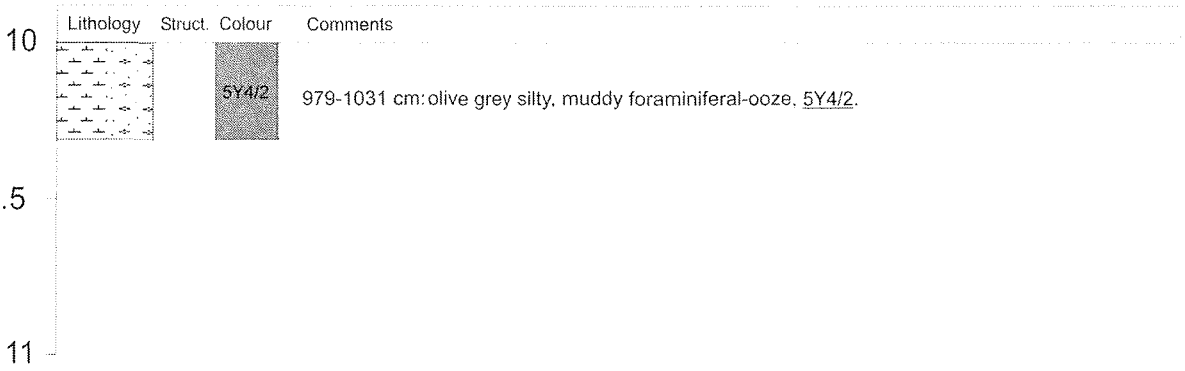

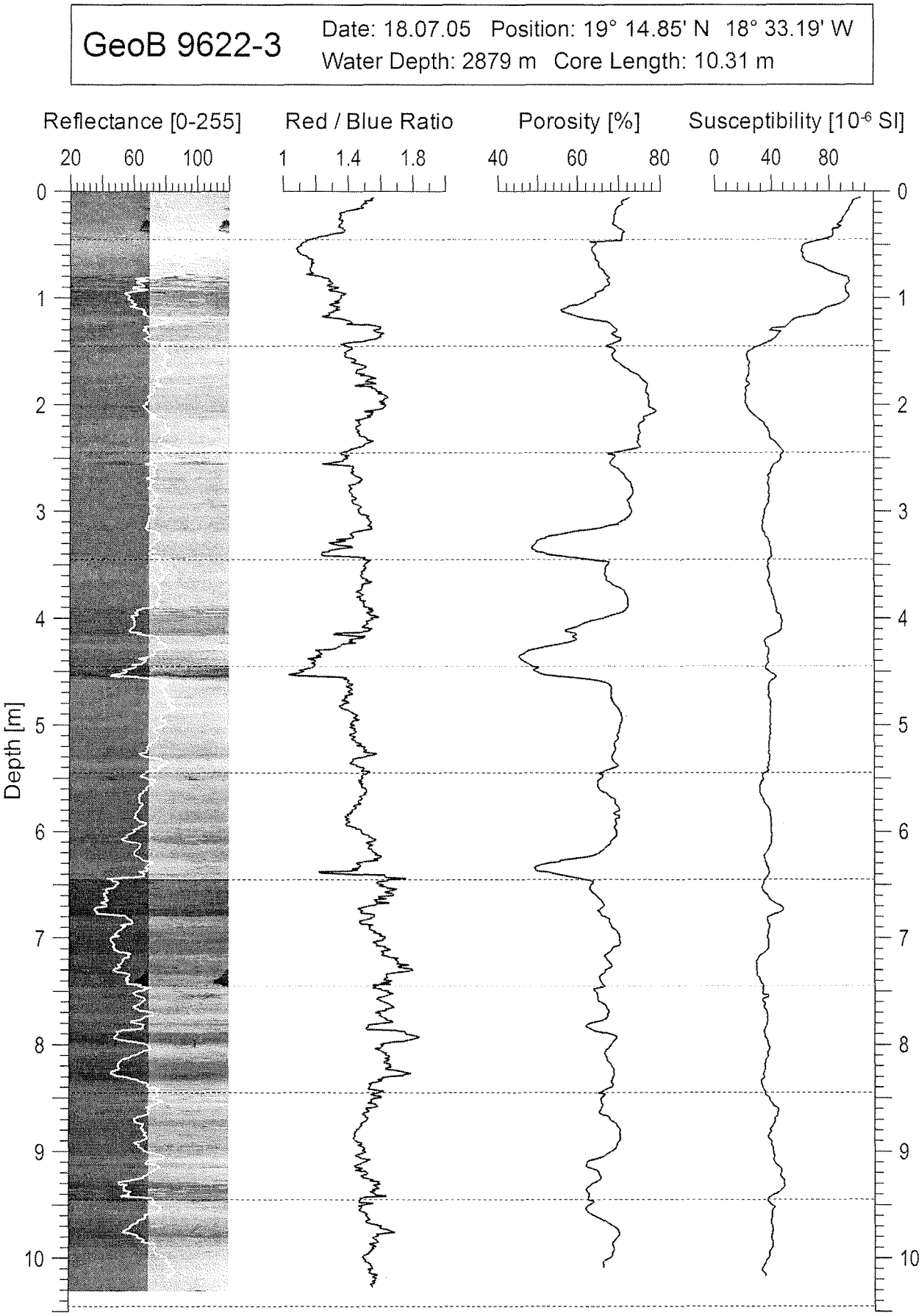

Physical properties of gravity core GeoB 9622-3. The dashed lines indicate the ends of the 1 m sections of the core.

GeoB 9624-1

Date: 20.07.2005 Pos: 20°30.63′N 20°39.51′W
Water depth: 3894 m Core length: 1118 cm

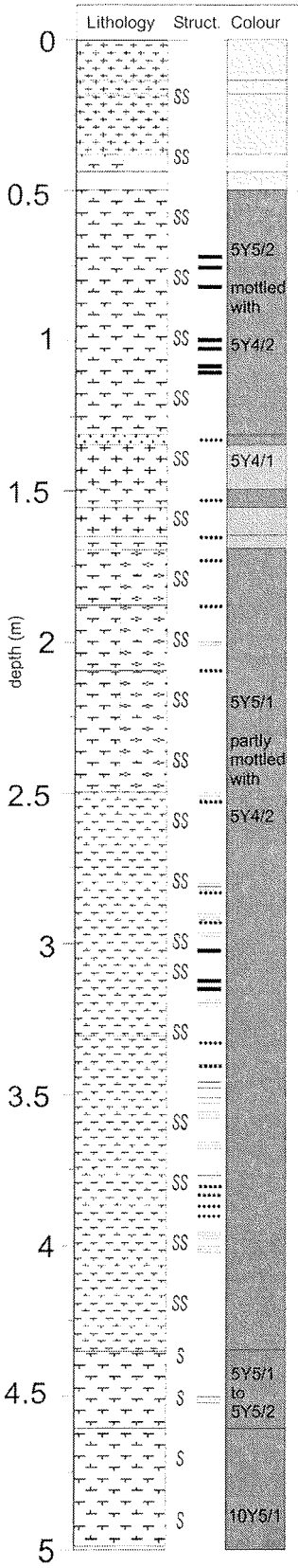

Comments

0-14 cm: light brown foram nanno ooze; 7.5Y6/3
14-18 cm: light brownish gray to dark gray mottled foram nanno ooze, weakly bioturbated; 10YR6/2
18-32 cm: light gray to light brownish gray foram nanno ooze, weakly bioturbated; 10Y7/1 to 10YR6/2
33 cm: 2 mm dark greenish gray mud layer; 5GY4/1
33-43 cm: light greenish gray foram bearing siliceous nanno mud; 10Y7/1 to 10Y6/1
43-51 cm: greenish gray foram bearing siliceous nanno mud; 10Y6/1
51-130 cm: (greenish) olive gray silty siliceous nanno bearing mud, moderately bioturbated, with dark olive gray layers (= bioturbated mud layers); 5Y5/2 mottled with 5Y4/2

weak dark green and gray coloured bands of mm-thick mud layers at: 72, 77, 81, 100, 102, 112, 115 cm: 5GY4/1

133-134 cm: "Ts"
130-144 cm:
144-150 cm: greenish gray silty siliceous foram nanno mud; 5Y5/1 (**A**)
150-156 cm: olive gray siliceous nanno mud; 5Y4/1 (**B**)
153 cm: light gray silty quartz sand (**Tm-Ts**)
156-160 cm: see A
160-163 cm: see B
163-167 cm: dark gray very fine quartz sand (**Turbidite D**)
173-174 cm: dark gray very fine quartz sand
164-188 cm: (greenish) olive gray siliceous foram bearing nanno mud, with olive gray coloured banding, mottled by moderate bioturbation (Chondrites, faint monosulfidic burrows)
188-190 cm: dark gray very fine quartz sand
190-210 cm: see 165-188 cm
205-207 cm: dark olive gray band
210-212 cm: dark gray very fine sand
212-222 cm: see A
222-225 cm: see B
225-250 cm: see 164-188 cm
250-252 cm: olive gray silty siliceous mud (**mud flow?**)
252-253 cm: dark gray very fine quartz sand (**turbidite D**)

couplets of thin basal dark gray very fine sand and olive gray siliceous mud at top at: 264-266, 282-283 cm

253-330 cm: background sediments: (greenish) olive gray siliceous foram-nanno bearing mud, with olive coloured mottling, moderately bioturbated throughout
294-295 cm: olive gray siliceous homogenous mud layer
319-320 cm: olive gray siliceous homogenous mud layer
dark greenish bands at: 301, 312, 316 cm

330-430 cm: background sediment: (greenish) olive gray siliceous nanno mud, moderately mottled by bioturbation, with olive gray burrow fillings throughout

dark gray fine to very fine quartz sand (**turbidite D; overspill fine sands**) at: 336-338, 342-344, 380-381, 383 (3 mm), 385 (2 mm), 387-388 cm

dark greenish gray stiff mm-thick mud at: 352, 357, 365 cm

olive gray siliceous homogenous nanno mud (**turbidite E, mud flows**) at: 342-344, 375-378, 399,5-400,5 cm

436-456 cm: gray to olive gray foram nanno ooze, weakly bioturbated

456-461 cm: olive gray siliceous nanno mud (**B**)
461-481 cm: greenish gray foram nanno ooze, weakly bioturbated (**A**) (faint burrows, Planolites)
481-482 cm: dark gray very fine quartz sand (**turbidite D**)
482-492 cm: see A
492-495 cm: see B
495-496 cm: very dark gray silt (**turbidite D**)
496-498 cm: see B
499,5-501,5 cm: see B

GeoB 9624-1

Date: 20.07.2005 Pos: 20°30.63´N 20°39.51´W
Water depth: 3894 m Core length: 1118 cm

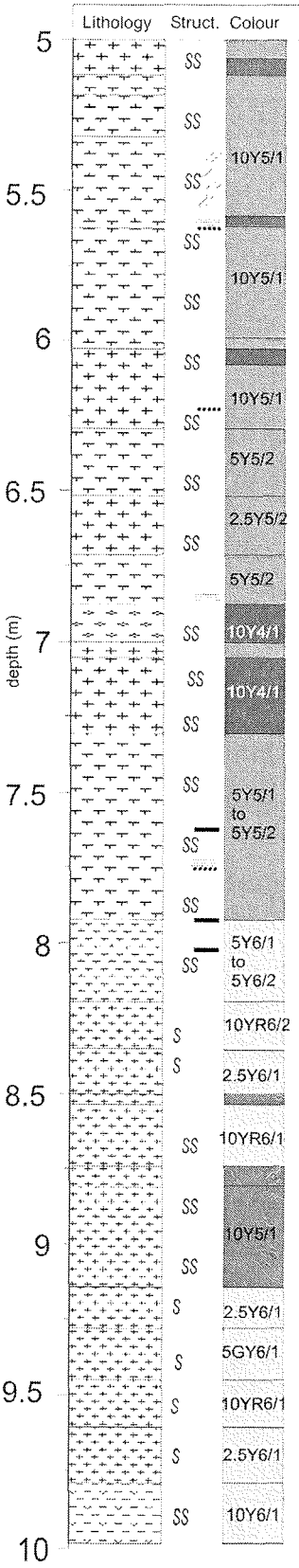

Comments	
501,5-505 cm:	see A
505-510 cm:	see B
510-530 cm:	greenish gray siliceous foram bearing nanno mud, moderately bioturbated (Planulites, faint monosulfidic burrows); 10Y5/1
517-518 cm:	see B
522-524 cm:	see B
530-560 cm:	greenish gray foram bearing siliceous nanno mud, moderately bioturbated by cm-sized tubes, faint monosulfidic burrows
560-564 cm:	dark gray fine to very fine quartz sand, laminated throughout (**turbidite D**)
564-605 cm:	greenish gray foram bearing siliceous nanno mud, moderately bioturbated by cm-sized tubes, faint monosulfidic burrows (olive gray filling); 10Y5/1
605-630 cm:	greenish gray foram nanno ooze, weakly to moderately bioturbated; 10Y5/1
630-651 cm:	olive gray siliceous nanno mud, moderately bioturbated; 5Y5/2
644 cm:	3-mm thick dark gray very fine quartz sand (**Ts, spillover turbidite**); 5Y4/1
651-670 cm:	grayish brown nanno foram ooze, moderately bioturbated; 2.5Y5/2
670-682 cm:	olive gray siliceous nanno mud, moderately bioturbated; 5Y5/2
682-683 cm:	olive gray siliceous mud; 5Y4/2
683-688 cm:	see 670-682 cm
688-700 cm:	dark greenish gray siliceous mud, moderately bioturbated; 10Y4/1
700-704 cm:	grayish brown nanno foram ooze, moderately bioturbated; 2.5Y5/2
704-762 cm:	dark greenish gray siliceous mud, moderately bioturbated; 10Y4/1
726-790 cm:	gray to olive gray nanno mud, few forams, moderately bioturbated, (burrows often with dark olive filling, stretched Planulites type, faint monosulfidic tubes); 5Y5/1 to 5Y5/2
766-767 cm:	diffuse olive gray siliceous mud layer
774-775,5 cm:	couplet of olive gray mud and very fine quartz sand (**Ts, spillover turbidites**)
791-823 cm:	gray to light olive gray foram bearing nanno mud, moderately bioturbated (faint monosulfidic tubes + deformed Planulites); 5Y6/1 to 5Y6/2
dark greenish mm-sized mud bands at: 791, 804 cm	
823-834 cm:	light brownish gray foram nanno ooze, weakly bioturbated; 10YR6/2
823-834 cm:	light brownish gray foram nanno ooze, weakly bioturbated; 10YR6/2
834-850 cm:	gray nanno foram ooze, weakly bioturbated; 2.5Y6/1
850-856 cm:	grayish brown foram nanno ooze, weakly bioturbated; 2.5Y5/2
856-875 cm:	light brownish gray foram nanno ooze, weakly bioturbated; 10YR6/2
875-880 cm:	grayish brown foram nanno ooze; 2.5Y5/1
880-913 cm:	greenish gray foram nanno ooze, moderately bioturbated (faint monosulfidic tubes, stretched mm-sized burrows); 10Y5/1
913-915 cm:	olive gray siliceous nanno mud
915-929 cm:	gray foram nanno mud, moderately bioturbated; 2.5Y6/1
929-945 cm:	greenish gray foram nanno mud, moderately bioturbated, 5GY6/1
945-958 cm:	light brownish gray nanno foram ooze, weakly bioturbated; 10YR6/2
958-978 cm:	gray foram nanno ooze, weakly bioturbated; 2.5Y6/1

GeoB 9624-1

Date: 20.07.2005 Pos: 20°30.63´N 20°39.51´W
Water depth: 3894 m Core length: 1118 cm

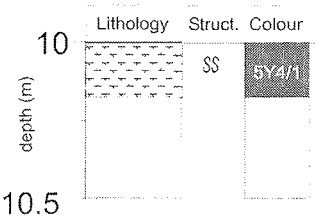

978-1017 cm: greenish gray foram bearing siliceous nanno mud, moderately bioturbated (olive gray fillings); 5GY5/1

1017-1019 cm: (layer)

1019-1118 cm: see 978-1017 cm

Next Page:

Physical properties of gravity core GeoB 9624-1. The dashed lines indicate the ends of the 1 m sections of the core.

GeoB 9624-1

Date: 19.07.05 Position: 20° 30.63' N 20° 39.51' W
Water Depth: 3894 m Core Length: 11.18 m

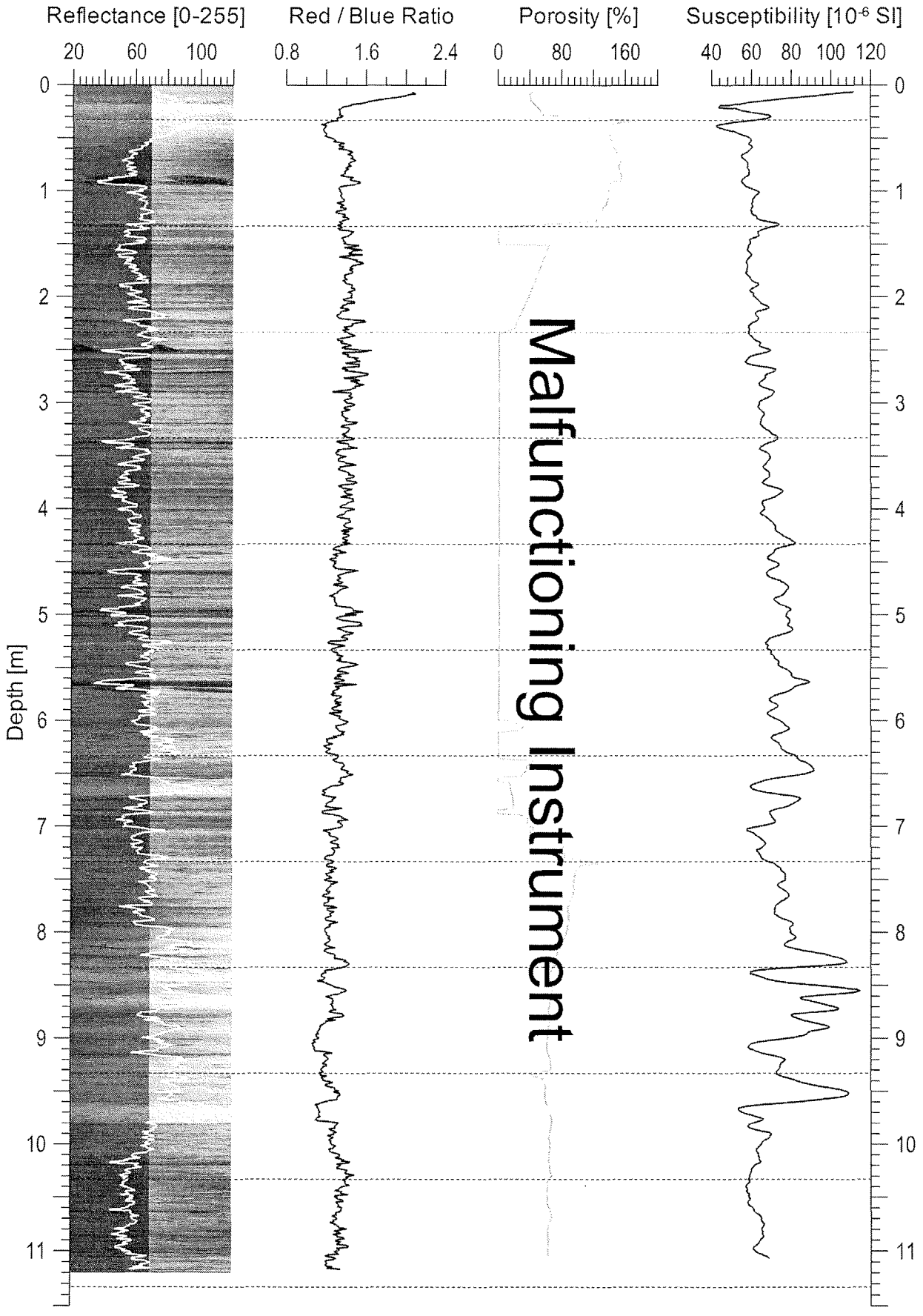

GeoB 9626-1

Date: 20.07.2005 Pos: 20°29.32´N 20°42.26´W
Water depth: 3926 m Core length: 420 cm

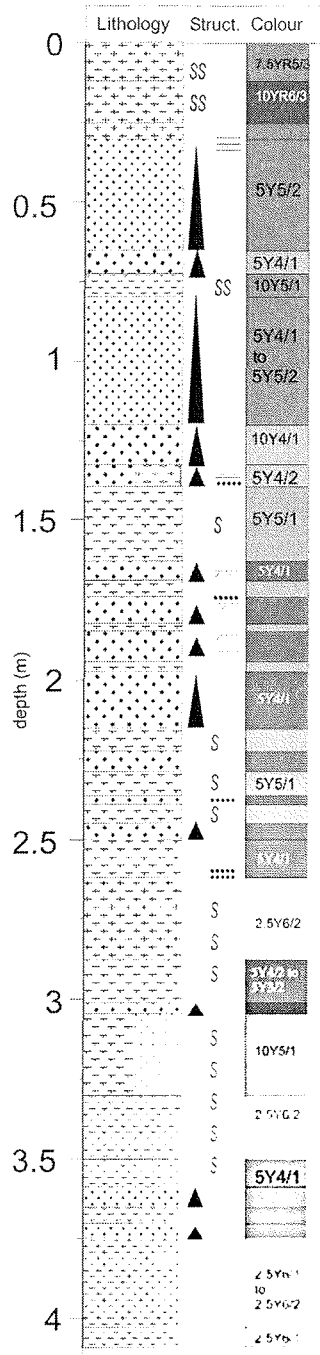

0-10 cm:	brown nanno foram ooze, weakly bioturbated; 7.5YR5/3
10-25 cm:	pale brown nanno foram ooze, weakly bioturbated; 10YR6/3
25-31 cm:	brown foram nanno ooze, weakly bioturbated; 10YR5/3
31-66 cm:	olive gray fine quartz sand, laminated at 31-43 cm, top brownish and greenish decolourized due to oxidation; 5Y5/2 (T,1)
	** flow structures formed during opening of the core*
66-74 cm:	dark gray (somewhat brownish) very fine quartz sand and silt; 5Y4/1 (T,2)
74-79 cm:	greenish gray nanno mud, few forams; 10Y5/1
79-121 cm:	alternation of thick layers of dark gray and greenish gray fine and very fine quartz sand; 5Y4/1 to 5Y5/2 (T,3)
121-131 cm:	dark greenish gray very fine quartz sand; 10Y4/1 (T,4)
137-141 cm:	couplets of olive gray nanno mud and dark very fine quartz sand; 5Y4/2 (T,5)
	** flow structures formed during opening of the core*
141-162 cm:	greenish gray siliceous nanno mud, some forams; 5Y5/1 (A)
162/164-169/168 cm:	dark gray fine quartz sand to very fine quartz sand; 5Y4/1 (B) (T,6)
168/169-173 cm:	see A
173-182 cm:	see B (T,6)
182-184 cm:	see A
184-190 cm:	see B (T,7)
190-195 cm:	see A
195-215 cm:	see B (T,8)
215-221 cm:	see A
221-228 cm:	see B (T,9)
228- 237 cm:	see A
237-239 cm:	dark gray very fine quartz sand (T,10)
239-248 cm:	greenish gray siliceous nanno mud, weakly to moderately bioturbated; 5Y5/1
248-250 cm:	olive gray siliceous nanno mud; 5Y4/2
250-260 cm:	olive gray homogenous siliceous nanno mud; 5Y4/1; with mm-thin layers of very fine sand at: 258,5, 260 cm; 5Y4/2 (T,11, 12)
260-288 cm:	grayish brown foram nanno ooze, moderately bioturbated; 2.5Y6/2
288-301 cm:	olive gray to dark olive gray siliceous nanno mud, moderately bioturbated at the top; 5Y4/2 to 5Y3/2
301-303 cm:	dark gray very fine quartz sand (T,13)
303-332 cm:	greenish gray siliceous silty nanno mud, moderately bioturbated; 10Y5/1
332-350 cm:	gray foram nanno ooze, weakly bioturbated; 2.5Y6/1
350-358 cm:	olive gray homogenous siliceous nanno mud, moderately bioturbated by Chondrites; 5Y4/2
358-367 cm:	dark gray very fine quartz sand; 5Y4/1 (turbidite D) (T,14)
367-372 cm:	olive gray siliceous nanno mud; 5Y4/2
372-375 cm:	dark gray very fine quartz sand, laminated throughout; 5Y4/1 (T,15)
375-404 cm:	gray to light brownish gray nanno foram ooze, weakly bioturbated; 2.5Y6/1 to 2.5Y6/2
404-407 cm:	gray siliceous nanno mud, weakly bioturbated; 2.5Y6/1

[404-420 cm: Duplication of top sequence by wave hieve during coring]

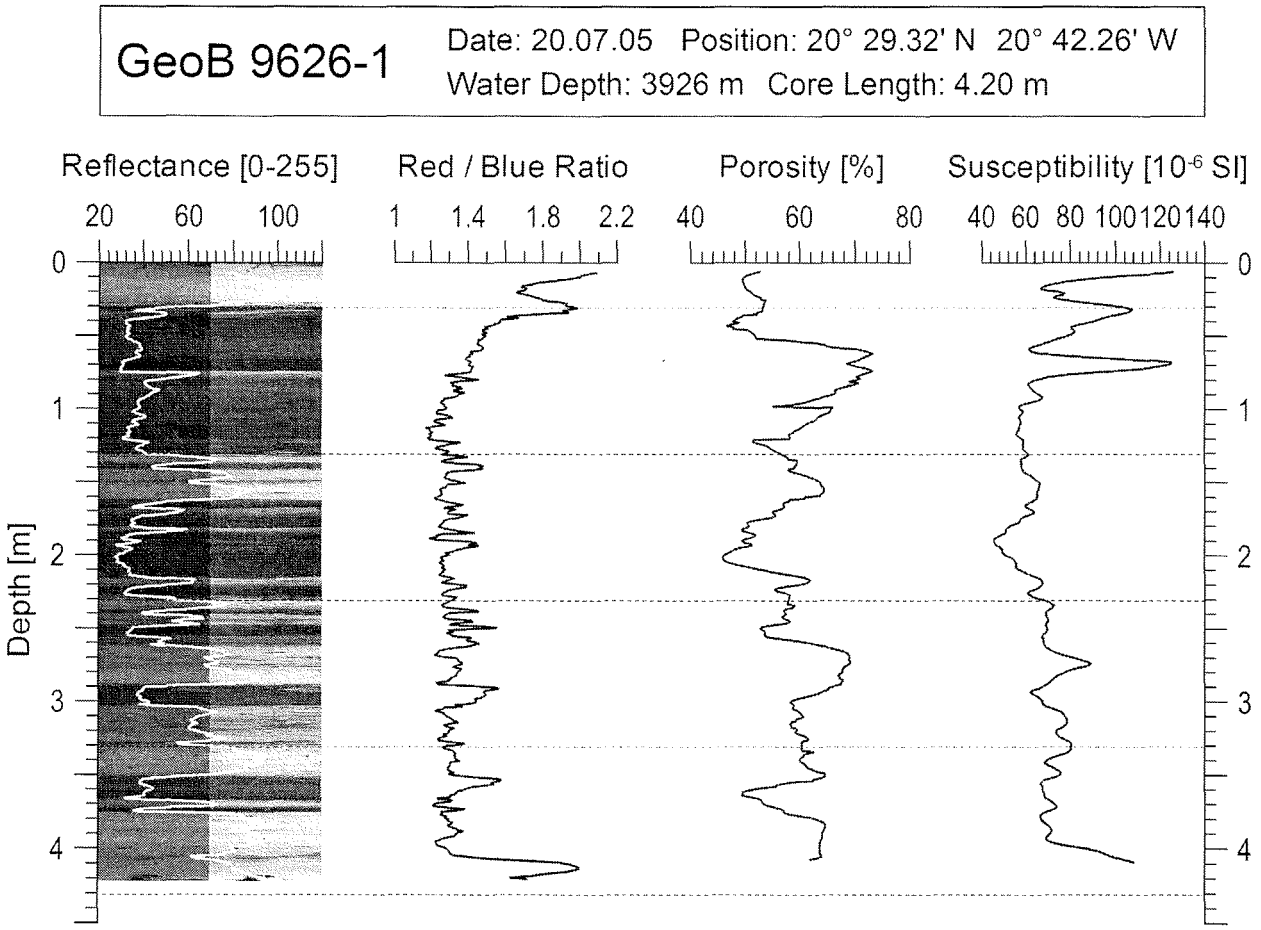

Physical properties of gravity core GeoB 9626-1. The dashed lines indicate the ends of the 1 m sections of the core.

GeoB 9627-1

Date: 21.07.2005 Pos: 20°39.52´N 20°56.06´W
Water depth: 4028 m Core length: 305 cm

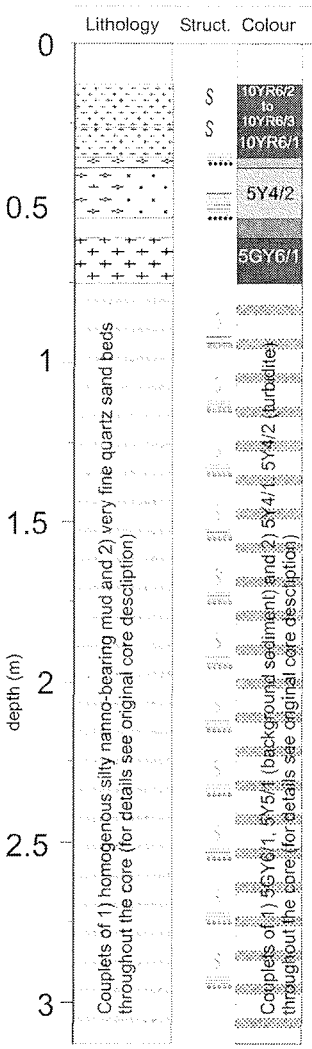

		Comments
12-26 cm:		light brownish gray topale brown foram nanno ooze, weakly bioturbated: 10YR6/2 to 10YR6/3
26-33 cm:		greenish gray foram nanno ooze, weakly bioturbated; 10Y6/1
33-39 cm:		dark greenish gray homogenous siliceous nanno bearing mud, moderately bioturbated by Chondrites; 5GY4/1 to 5Y4/1
39-40 cm:		dark gray fine quartz sand; 5Y4/1 (T_{vm}1)
40-43 cm:		olive gray foram bearing nanno mud; 5Y5/2
43-54 cm:		olive gray homogenous silty nanno bearing mud (mudflow), moderately bioturbated by Chondrites; 5Y4/2 (T_{vm}2)
54-55 cm:		dark gray very fine quartz sands **(B)**
55-57 cm:		greenish gray homogenous mud; 10Y5/1
57-65 cm:		greenish gray foram nanno ooze: 5GY6/1
65-72 cm:		olive gray homogenous silty nanno bearing mud; 5Y4/2 **(A)** (T_{vm}3)
72-76 cm:		see 57-65
76-79 cm:		see (A) (T_{vm}4)
79-81 cm:		see (B)
81-82 cm:		see (A) (T_{vm}5)
82-83 cm:		see (B)
83-89 cm:		see 57-65
89-91 cm:		see (A) (T_{vm}6)
91-97 cm:		see 57-65
97-99 cm:		see (A) (T_{vm}7)
99-102 cm:		
102-110 cm:		couplets of basal dark gray fine sand (1 cm) and overlying olive gray siliceous nanno bearing mud; 5Y4/2 (A_1) (= T_{vm}8)
110-115 cm:		olive gray homogenous siliceous nanno bearing mud; 5Y4/2 (A_2) (= T_{vm}9)
115-118 cm:		greenish gray foram bearing nanno mud; 5Y5/1 **(B)**
118-125 cm:		see A. (= T_{vm}10)
125-126 cm:		see B
126-135 cm:		see A_2 (= T_{vm}11)
135-138 cm:		see B
138-144,5 cm:		see A_1 (= T_{vm}12)
144,5-146 cm:		see A_2 (= T_{vm}13)
146-150 cm:		see B
150-155 cm:		see A_1 (= T_{vm}14)
155-157 cm:		see B
157-166 cm:		see A_2 (= T_{vm}15)
166-169 cm:		see A_1 (= still T_{vm}15)
169-173 cm:		see B
173-180 cm:		see A_2 (= T_{vm}16)
180-182 cm:		see A_1 (= still T_{vm}16)
182-186 cm:		see B
186-193 cm:		see A_2 (= T_{vm}17)
193-195 cm:		see A_2 (= T_{vm}18)
195-199 cm:		see B
200-208 cm:		dark gray fine quartz sand, laminated, overlayn by homogenous olive gray siliceous nanno bearing mud: 5Y4/1to 5Y4/2 (A_1) (= T_{vm}19)
208-211 cm:		see A_2 (= T_{vm}20)
211-213 cm:		greenish gray foram bearing nanno mud, weakly bioturbated; 5Y5/1 **(B)**
213-226 cm:		see A_1 (= T_{vm}21)
226-230 cm:		see B
230-238 cm:		see A_1 (= T_{vm}22)
238-239 cm:		see B
239-243 cm:		homogenous olive gray siliceous nanno bearing mud see (A_2) (= T_{vm}23)
243-245 cm:		see B
245-252 cm:		see A_2 (= T_{vm}24)
252-254 cm:		see B
254-258 cm:		see A_2 (= T_{vm}25)
258-260 cm:		see B
260-267 cm:		see A_2 (= T_{vm}26)
267-271 cm:		see B
271-274 cm:		see A_2 (= T_{vm}27)
274-276 cm:		see B
276-282 cm:		see A_2 (= T_{vm}28)
282-283 cm:		see A_2 (= T_{vm}29)
283-284 cm:		see B
284-295 cm:		see A_2 (= T_{vm}30)
295-300 cm:		see A_2 (= T_{vm}31-33)
300-305 cm:		see A_2 (= T_{vm}34)

GeoB 9627-1

Date: 21.07.05 Position: 20° 39.52' N 20° 56.06' W
Water Depth: 4028 m Core Length: 3.05 m

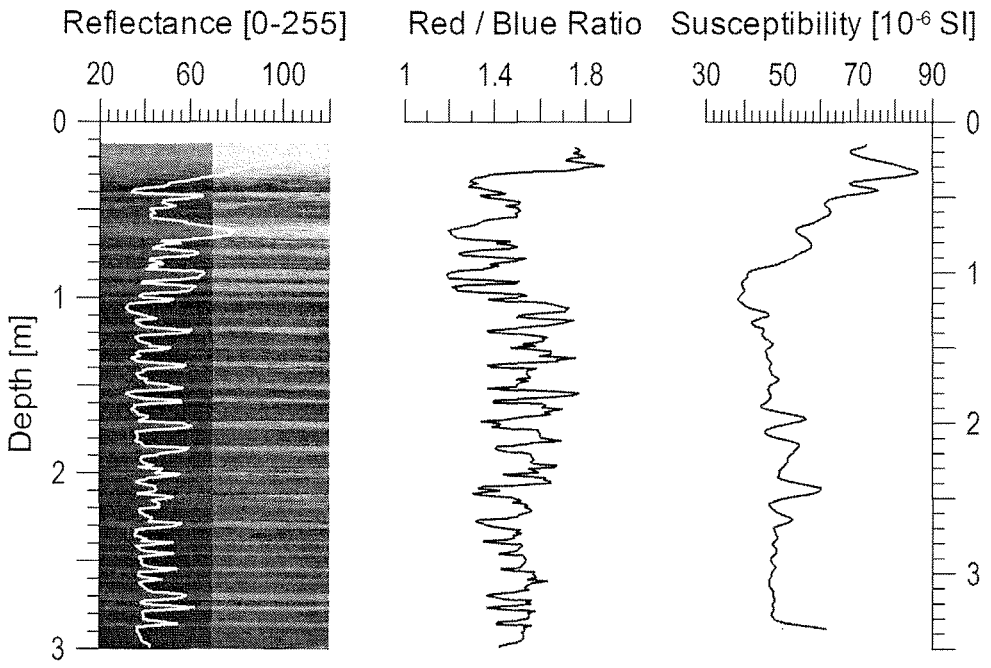

Physical properties of gravity core GeoB 9627-1. The dashed lines indicate the ends of the 1 m sections of the core.

GeoB 9628-1

Date: 21.07.2005 Pos: 20°37.46´N 20°37.30´W
Water depth: 3928 m Core length: 1054 cm

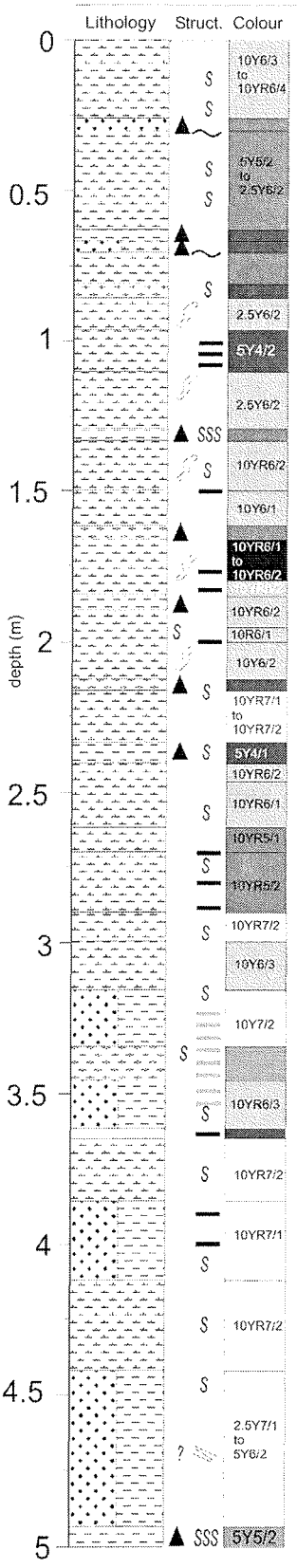

0-27 cm:	pale to light yellowish brown soft and wet foram ooze, slightly bioturbated, upper 8 cm more brownish; 10YR6/3 to 10YR6/4
27-30 cm:	brown soft fine sand turbidite, erosive base, increasingly bioturbated towards the top; 10YR5/3 (**T**,1)
30-64 cm:	olive gray to light brownish gray foram ooze, bioturbated, varying colours from brownish gray to greenish gray, some monosulfidic spots; 5Y5/2 to 2.5Y6/2
64-66 cm:	dark gray clay horizon, bare of forams, distorted by bioturbation; 2.5Y4/1 (**T_m1**)
66-68 cm:	dark grayish to olive brown foram bearing sand layer, erosional base (?), perhaps with genetic contact to T_m1; 2.5Y4/2 to 2.5Y4/3 (**T**,2)
68-79 cm:	see 30-64 cm
79-81 cm:	olive gray foram bearing mud horizon, bioturbated; 5Y4/2
81-96 cm:	see 30-64 cm, bioturbated, with large burrows filled with dark greenish T_m material; 2.5Y6/2
96-109 cm:	olive gray foram ooze, intercalated by three 1-cm thick pure mud turbidites, bare of forams, bioturbated; 5Y4/2 (**T_m3-5**)
109-129 cm:	light brownish gray foram ooze, some monosulf. spots, bioturbated; 2.5Y6/2
129-131 cm:	olive mud turbidite, bare of forams, strongly bioturbated, with a greenish faint up to 124 cm: 5Y5/3 (**T_m6**)
131-150 cm:	light brownish gray foram ooze, bioturbated by larger burrows containing mud turbidite material: 10YR6/2
150-152 cm:	reddish gray faint blackish horizon; 10R6/1 (**b1**)
152-161 cm:	see 131-150 cm; 10YR5/1 to 10YR5/2
161-164 cm:	gray to olive gray foram bearing mud turbidite, sharp base, not as darkish green as upper mud; 5Y5/1 to 5Y5/2 (**T_m7**)
164-181 cm:	grey to light brownish gray foram ooze, larger burrows with mud turbidite material, bioturbated, 2 blackish layers at 176-177, 180-181 cm; 10YR6/1 to 10YR6/2 (**b2, 3**)
181-186 cm:	light brownish gray traces of an bioturbated mud turbidite, some forams; 10YR6/2
186-213 cm:	light brownish gray foram ooze, bioturbated, some monosulf. spots, rare larger burrows; 10YR6/2
196-199 cm:	reddish gray faint blackish horizon; 10R6/1 (**b4**)
213-217 cm:	grayish brown to light olive brown foram bearing mud horizon, bioturbated; 2.5Y5/2 to 2.5Y5/3 (**T_m8**)
217-237 cm:	see 186-213 cm, light gray, larger monosulf. spots at the base; 10YR7/1 to 10YR7/2
237-241 cm:	dark gray clay horizon, bioturbated, greenish colour extends up to 228 cm; 5Y4/1 (**T_m9**)
241-263 cm:	light brownish gray to gray foram ooze, bioturbated, rare tiny monosulf. spots; 10YR6/1
263-291 cm:	gray to light brownish gray foram ooze; 10YR6/1 to 10YR5/2
267-268 cm:	blackish layer (**b5**)
291-300 cm:	light gray to light brownish gray foram bearing to foram ooze, 2 blackish layers at 282, 285 cm; 10YR6/3 (**b6, 7**)
223-268 cm:	0.5-cm thick greenish layers intercalated into the background, partly with regular spacing of 1 cm (**g**)
300-317 cm:	pale brown foram ooze, bioturbated, base probably sharp
317-333 cm:	light gray muddy foram sand, bioturbated; 10YR7/2
333-347 cm:	pale brown foram bearing mud, bioturbated
347-364 cm:	light gray muddy foram sand, bioturbated; 10YR6/3
280-468 cm:	single large monosulf. spots
366-381 cm:	light gray foram ooze, bioturbated, a brownish layer at the base
364-366 cm:	reddish gray, blackish layer, gradual at base and top, surrounded by a greenish faint (**b8**), greenish layers at 375, 388 cm; 10YR7/2
381-410 cm:	light gray muddy foram sand with blackish layers at 381-382, 397 cm; 10YR7/1 (**b9, 10**)
410-441 cm:	light gray foram ooze,bioturbated, many monosulf. spots, colours slightly varying from greenish to brownish taints; 10YR7/2
441-491 cm:	light gray to light olive gray muddy foram sand, decreasing foram content towards the base, abundant monosulf. spots, various colours, same greenish and blackish spots, "layering" somehow disturbed/stretched?, with several greenish coloured clouds; 2.5Y7/1 to 5Y6/2
492-499 cm:	olive gray to light olive gray clay horizon, strongly bioturbated; 5Y5/2 to 5Y6/2 (**T_m10**)

GeoB 9628-1

Date: 21.07.2005 Pos: 20°37.46´N 20°37.30´W
Water depth: 3928 m Core length: 1054 cm

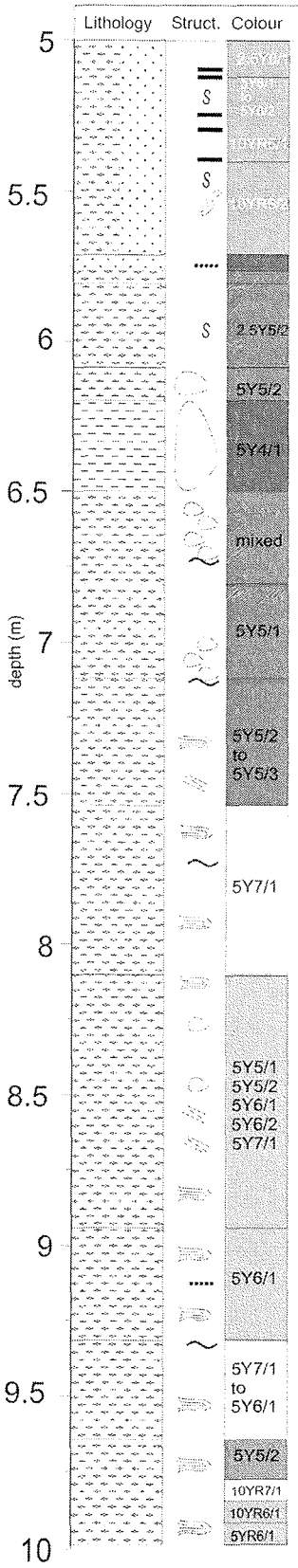

Comments	
499-573 cm:	see 441-491 cm, gray to light olive gray to light brownish gray, with defined greenish layers at: 507, 508, 525, 532, 545 cm, bioturbated, large burrows filled with greenish mud, Chondrite-like swarms at 500-505 cm, laterally stretched?, rare monosulf. spots; 2.5Y6/1, 5Y6/1 to 5Y6/2, 10YR6/1; 10YR6/2
574-576 cm:	dark grayish brown coarse silt layer, laterally somehow dislocated or massively bioturbated; 2.5Y4/2 (**T,3**)
576-580 cm:	olive gray foram bearing soft clayey mud, laterally stretched, Chondrites swarms; 5Y5/2
588 cm:	blackish horizon (**b11**)
580-607 cm:	grayish brown to gray relatively soft foram bearing mud, bioturbated; 2.5Y5/2
607-621/623 cm:	olive gray foram bearing to foram ooze, clearly stiffer, a single large burrow with greenish mud; 5Y5/2
621/623-648/652 cm:	dark gray homogenous clast of stiff olive homogenous clay, bioturbated by larger burrow filled with lighter material (with bright margins), convex surface; 5Y4/1 (**Debrite at 621-1013? cm**)
Debrite content:	1) olive gray silt layer. 2) dark gray sand layer (**T,?**), 3) olive gray pure clay (**T_m?**), 4) gray mud with forams, 4) gray mud with forams, 5) Matrix: unsorted coarse to medium sand. 6) Clasts: gray pure stiff clay, 7) gray slightly foram bearing mud: 5Y4/2, 5Y4/1, 5Y5/1, 5Y6/1
669-692 cm:	gray stiff foram bearing homogenous mud, is it a larger clast?, plenty of monosulf. spots; 5Y5/1
692-710 cm:	pleanty of laterally elongated lense-shaped clasts, in the lower part floating in a sandy matrix (1 dark gray, 2 gray, 3 gray, 4 light gray and light olive gray); 5Y4/1, 5Y5/1, 5Y6/1, 5Y7/1
700-710 cm:	(1 light gray, 2 light gray, 3 gray)
711-967 cm:	olive gray to olive different foram bearing mud layers, flow structures, faint monosulf. spots; 5Y5/2 to 5Y5/3
752-808 cm:	light gray relatively homogenous unit of stif foram bearing mud, abundant larger monosulf. spots; 5Y7/1
808-896 cm:	massive flow structures, single clasts floating in an imhomogenous matrix, faint tiny monosulf. spots, some layers are coloured like mud turbidites, shear surfaces at: 643-646, 661-646, 687-693 cm; Matrix: 5Y5/1, 5Y5/2, 5Y6/1; Clasts: 5Y5/2, 5Y7/1 *[For detailed internal structures see original core description!]*
896-929 cm:	relatively horizontally layered unit of foram bearing mud and thin foram mud, in the latter layers are underlain be thin black layer; 5Y6/1
929-967 cm:	light gray to gray massively flown unit of foram bearing muds of various colours, shear surfaces at 940, 947 cm; 5Y7/1 to 5Y6/1
967-1013 cm:	sequence of horizons of foram bearing mud, somehow laterally stretched; 5Y5/2 to 10YR6/2

GeoB 9628-1

Date: 21.07.2005 Pos: 20°37.46´N 20°37.30´W
Water depth: 3928 m Core length: 1054 cm

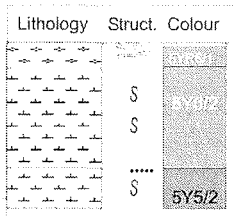

1013-1043 cm: light olive gray foram ooze, bioturbated, interlayered by blackish thin layers, faint monosulf. spots, but no clear bedding: 5Y6/2

**Not clear whether the section 1013-1043 cm is still part of the debrite unit above*

1043-1054 cm: foram ooze, similar to 1013-1043 cm: 5Y5/2; layer with slightly sitly foram sand at 1045-1046 cm: 5Y4/1 (**T,4**)

Next Page:

Physical properties of gravity core GeoB 9628-1. The dashed lines indicate the ends of the 1 m sections of the core.

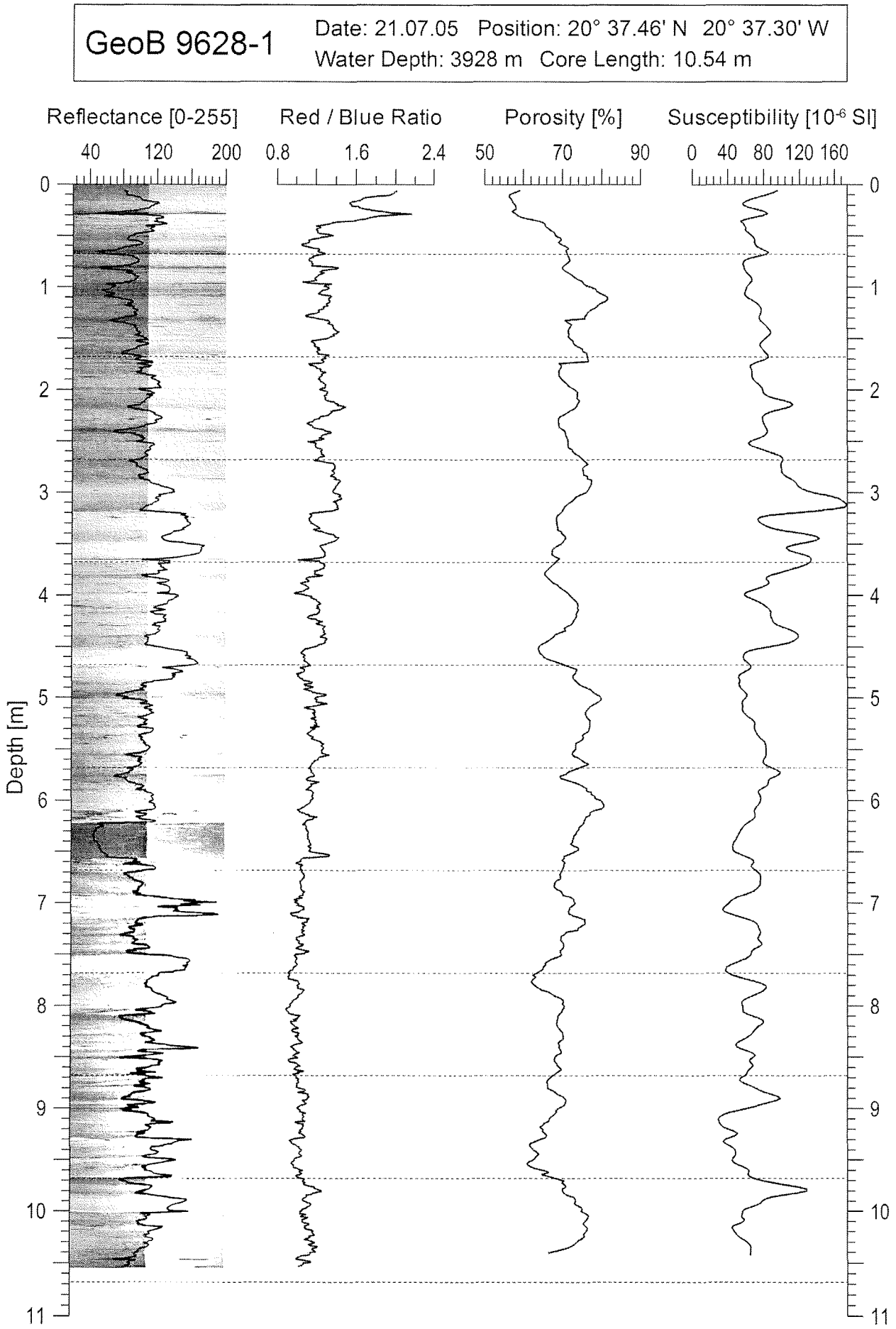
GeoB 9628-1
Date: 21.07.05 Position: 20° 37.46' N 20° 37.30' W
Water Depth: 3928 m Core Length: 10.54 m
Reflectance [0-255]
40 120 200
Red / Blue Ratio
0.8 1.6 2.4
Porosity [%]
50 70 90
Susceptibility [10-6 SI]
0 40 80 120 160
Depth [m]
0 1 2 3 4 5 6 7 8 9 10 11

4.3.1.4 Sampling procedure of Kasten Corer (Kastenlot) sediment profiles

Due to the high relevance of the shelf around the Gulf d'Arguin as a major source of material for the Cap Timiris Canyon, (and due to a mechanical damage of an actually available Vibrocorer) we decided to give the Kastenlot a try for a deeper penetration through coarser material. This Kasten Corer has a length of 3 m and a diameter of 30 cm. The weight load is 3.5 tons. Used at one single station, the Kasten Corer has penetrated the dense and shell-rich surface sediments for about 1.5 m but did not reach the underlying strata that would have been of relevance. The core was photographed and transparent, 50-cm long archive boxes have been taken downcore.

4.3.2 Sedimentology: shipboard results

4.3.2.1 The Dakar Canyon/Channel System

Our primary scientific targets have been to detect events and phenomena of sediment wasting inside and in the vicinity of the Dakar Canyon in the South East of Cap Verde which forms a major pathway and conduit for sediment transfer from the shelf to the deep sea. In order to re-construct the variability, frequency and history of sediment dynamics the following coring strategy was followed. Three cores (GeoB 9604-9606, see Fig. 4.1.2 for location) were positioned on the upper continental slope at about 2000m water depth where a potential slide just south of the Dakar Canyon had been detected by hydroacoustic profiling. In addition, the canyon itself was crossed by coring traverses at the middle and lower slope. At the middle slope three cores were recovered: (1) in the area close to the thalweg, e.g. Core GeoB 9607-3 (3004 m water depth), (2) on a southern terrace, e.g. Core GeoB 9609-2 (2785 m water depth), and (3) on the northern flank at 2586 m water depth, e.g. Core GeoB 9608-2 (see Fig. 4.1.4 for location). In addition, one core was taken from a deeper location at the southern terrace of the Dakar Canyon in 3752 m water depth (GeoB 9610-1). The second traverse crossing the canyon at the lower continental slope comprises Cores GeoB 9612-3 from the levee on the northern flank at 3893 m water depth, GeoB 9611-1 from the canyon floor at 3983 m water depth and GeoB 9613 from the southern flank, where the Dakar Slide appears closely beneath the seafloor in the hydroacoustic profiles (see Fig. 4.1.5 for location). Further downstream, where the Dakar Channel shallows and widens considerably, two cores were taken along another traverse, e.g. GeoB 9615-1 from the channel floor remnant at 4108 m water depth and GeoB 9614 from a small depression incised into Dakar Slide at the southern flank of the remnant of Dakar channel (see Fig. 4.1.6).

A surprising result, when opening cores GeoB 9604, 9605 and 9606, was that we found no indication for sliding or any other features of mass wasting and downslope

movement. With regard to the recovery between 8.0 and 9.5 m, respectively, we should have definitely penetrated into the transparent unit displayed in the hydroacoustic records. Instead, we found a continuous hemipelagic succession in both cores. The only exception is a single thin (8 cm thick) turbidite bed in Core GeoB 9604. Hence, we have no explanation for the unusual hydroacoustic character of these sediments, even more, since the same lithologic sequences display alternating parallel reflectors at one location (GeoB 9605-1, 1912 m water depth) and a transparent layer at the other locations (GeoB 9604-3, 1925m water depth and GeoB 9606-2, 2287 m water depth). The succession of hemipelagic sediments is characterised by pronounced alternations in sediment colour and less by changes in sediment composition. Rhythmic alternations of dark olive grey to very dark olive grey sediment packages and light grey to greenish grey units are evident at the first view. In contrast, lithologic changes are less pronounced comprising alternations of hemipelagic foram-nanno mud and weakly siliceous hemipelagic mud. Additionally, foram nanno oozes occurring at distinct levels provide a useful tool for a first rough lithologic correlation. Most typical sedimentary structures are rhythmic alternations in bioturbation type and intensity. The darker slightly siliceous sediments are stronger affected by bioturbation, often displaying well developed large Zoophycos burrows, which extend for more than a metre downcore. As a first working hypothesis, climatically induced changes in upwelling intensity and humidity in the hinterland with variable supply of fluvial suspension load and dust could have caused the observed rhythmical changes in sediment character.

The character of lithologic changes in the background sediments in the cores along the traverse at the middle slope remained the same as discussed above. A typical succession is revealed by the record of Core GeoB 9608-2 at the southern flank of the canyon in 2586 m water depth. The presumably Holocene-aged section is represented by 50-cm thick, brownish grey foram nanno ooze and foraminiferal mud. An additional carbonate-rich unit of comparable thickness occurs at about 2 m subbottom depth, and three thin (10-20 cm) carbonate layers are intercalated between 3.5 m and 5 m core depth. The remaining section of the 9-m long core reveals alternations of hemipelagic foram-bearing terrigenous mud with siliceous terrigenous mud. No indications for turbidity current activity or other types of downslope mass movement were found in this core. In the 200-m deeper located terrace Core GeoB 9609-2 (2785 m water depth) the changes in background sediment character are even more subtle with exception of colour changes and bioturbation style. Since forams appear to be even more diluted in this core (compared to Core GeoB 9608-2), high accumulation rates might be expected. Three thin turbidites are recorded in the terrace core giving evidence that a suspension cloud has filled the canyon above the terrace level during this time, but did not overspill the flanks. The 7.8-m long Core GeoB 9607-3 from the floor of the Dakar Canyon recovered, below the ~60cm thick Holocene top sequence, 3-m of terrigenous

hemipelagic mud with intercalation of 12 fine-grained siliciclastic turbidites admixed with fine shell debris of molluscs. Four of these turbidite beds are 5 to 25 cm thick, whereas the rest is less than 2 cm thick. The structural inventory comprises, according to the Bouma classification, BCDE or CDE sequences in the thick beds, and DE sequences in the thin layers. At 3-m core depth, a 25 cm thick turbidite bed cuts erosive into a more than 4.5 m thick debrite. The basal 3.5 m display a succession of two slide blocks with only weak indications of internal deformation and typical sheared mud-clast carpets at their base. The top of the debrite is formed by a 1-m thick unit of a dark olive grey sandy mud matrix into which abundant mollusc shells and deep-water coral fragments and cm-sized mud clasts of variable colour, composition and stage of consolidation are admixed. The composition of this debrite provides an indication that slide blocks eroded from the side walls of the canyon were mixed with slumped material from positions higher up-stream in the canyon. The deep-water corals as well as the mollusc shells might either have derived from a deep-water reef belt higher up on the slope or grew on terraces within the canyon. All together it appears more probable that a bigger debris flow was canalized through the canyon and filled it partly up than that a local collapse of the side walls of the canyon occurred.

Despite a rather poor recovery (2.5 m), Core GeoB 9610 positioned on a terrace in the canyon at 3750 m water depth further downstream also displays a high turbidite activity in post-Holocene times. The lower 1.5 metres contain 14 turbidites indicating a period with high frequency flooding events on this terrace. Even more interesting, the sequence of turbidite events may correlate roughly with the turbidity record of Core GeoB 9611-1 recovered from the canyon floor further downstream, in which 8 turbidites are recognised in the 1-m long section below the Holocene top. The 8.8-m long core GeoB 9612-3 taken at the levee on the northern flank of the Canyon at this traverse contains 24 spill-over turbidites with a typical DE Bouma succession. In addition, 10-thin mm-sized greenish mud layers are observed which we interpret as deposits of over-spilling mud clouds. It is most interesting that the turbidites occur in bundles evidencing alternating periods of high turbidity activity and periods of quietness.

Further downstream, where the Dakar Channel shallows and widens considerably, Cores GeoB 9615-1 from the floor of the channel in 4108 m water depth and GeoB 9614 at the northern flank in 4090 m water depth also reflect this bundled turbidite activity. The cores can be correlated by typical carbonate-rich horizons. In addition, correlation is also possible to the levee Core GeoB 9612 further upstream. Turbidite beds are generally thicker and occur in higher frequency at the remnant of the channel floor than within the small the depression on the southern flank, indicating that the channel remnant remained the major conduit for flows despite its widening and shallowing.

In conclusion, the collected cores during M65/2 cruise provide a unique chance to reconstruct the temporal evolution of turbidite activity in the Dakar Canyon/Channel system in detail including estimates of flow volumes of individual events.

4.3.2.2 The Timiris Canyon/Channel System

Main scientific targets in the area of the Timiris Canyon have been to improve our knowledge about sediment dynamics in the already explored part of the canyon and to extend the investigation further downstream to more distal parts. The following coring strategy was chosen.

At first, we took a series of five giant box cores from the outermost part of the shelf ahead the tributary system of the canyon. These should provide a better data base about the sediment provenance in the source area of turbidites passing the canyon. Furthermore based on sediment acoustic profiling, the two 1.5 and 5.0-m long Cores GeoB 9618 (90 m water depth, see Fig. 4.2.15 for location) and GeoB 9621 (52 m water depth, see Fig. 4.2.15 for location) were taken from this area to be able to reconstruct the Holocene land-ocean coupling and its implications for the canyon activity. These cores show homogeneous muddy fine-sand successions rich in *in-situ* preserved bivalves.

Coring in a cut-off loop at 2881 m water depth (GeoB 9622, see Fig. 4.2.14 for location), which was mapped during the M58/2 expedition in 2003 already and which is today situated 100 m above the active channel floor, was intended by: (1) to supply information about sediment dynamics for periods older than the last deglacial transition, which presently is not available, (2) to decipher flow events in the canyon in recent and past times that reached above the level of the cut-off loop. Further downstream at the transition to the deep-sea basin, the canyon changes its morphology and starts to become wider and shallower. Here, cores were taken along a traverse crossing the channel area, e.g. GeoB 9624-1 on the northern levee in 3894 m water depth, GeoB 9623-2 on a northern terrace, GeoB 9625-1 on the channel floor in 3990m water depth, and GeoB 9626-1 from the floor of a smaller associated channel which incises into the southern flank of the main channel at 3926 m water depth (see Fig. 4.1.8 for location). Additional cores were taken further downstream where the channel area widens to more than 14 km. Core GeoB 9627-1 was recovered at the margin of the channel flat (see Fig. 4.1.9 for location). The final core (Core GeoB 9628-1, see Fig. 4.1.10 for location) recovered from the Timiris region and also the final core taken during this cruise was positioned at the margin of the Cap Blanc Slide. Primary target was to penetrate into the slide and date the slide by establishing an age model for the hemipelagic sediment cover over the slide.

Background sediments in the 10.45-m long Core GeoB 9622 from the cut-off loop at 2881 m water depth appear to be rather homogenous at a first glance. Below 40 cm of greyish brown foram nanno ooze presumably of Holocene age, a 6-m thick unit of light olive grey moderately bioturbated foram-bearing slightly siliceous mud is observed. At 7 m core depth, an obvious shift in background sedimentation occurs with a clear dominance of light olive grey foram nanno ooze. This shift correlates with a change in turbidite intercalation. No turbidite activity in the Holocene section is evident. In following 6 m of the core, 5 thick (5-30 cm) and partly coarse siliciclastic turbidite beds are found evidencing that huge shelf-derived sand suspensions have been drained through the canyon, the level of the sand cloud being well above the elevation of the cut-off loop. In contrast to this, in the lower section only a single cm-sized siliciclastic turbidite layer and a 5-cm thick mud cloud spill-over is recognised.

Interestingly, a similar pattern is also recognised in the 11.33-m long Core GeoB 9624-1, which was taken further downstream at 3894 m water depth on the northern levee of the main Timiris Channel where the channel becomes wider and flattens considerably. Here the upper 6 m of the core contains numerous spill-over turbidites below 50-cm thick greyish brown foram nanno ooze, whereas only few turbidites are found in the lower 5 m of the core. Four types of over-spill turbidites are recognised, e.g. (1) thin (1-3 cm thick) dark grey fine to very fine laminated quartz sand layers which correspond to Bouma sequence D, (2) several cm-thick olive grey homogenous slightly siliceous and nanno-bearing mud interpreted as mud cloud over-spills, (3) couplets of a thin basal dark grey very fine quartz-sand and thicker olive grey mud tops, and (4) mm thick dark greenish grey mud layers also interpreted as mud cloud over-spills. Within the upper 6 m, 16 olive grey mud cloud over-spills, three very fine sand/mud couplets, 15 dark greenish grey thin mud over-spills, and 18 very fine sand over-spills were detected, whereas in the lower 5 m of the core only two olive grey mud over-spills, one couplet, three dark greenish grey thin mud over-spills and 6 very fine sand over-spills occur. All together this clearly documents a consistent shift in the frequency of these events.

The 1.96-m long Core GeoB 9623-2 from the northern terrace of the main channel at 3940 m water depth displays, beneath the 40-cm thick Holocene foram nanno ooze without turbidites, two thick (30 and 70 cm) coarse siliciclastic turbidite beds admixed with debris of mollusc shells indicating an outer shelf/upper slope environment as source area. In the lower section of this short core, three over-spill couplets and three olive grey mud over-spills are found. Coring on the channel floor was not successful; however, a 4-m long Core GeoB 9626-1 was retrieved from the floor of a small channel incised into the southern levee of the channel at 3926 m water depth. Again directly underlying the Holocene section, a series of two thick coarse siliciclastic turbidite beds admixed with shell debris occurs. Below this, 7 several-cm thick turbidites of the same

type are observed. Then with the shift to carbonate-rich background sediments, thickness and frequency of turbidite events decreases. The final core taken in the Timiris system, the 3.12-m long Core GeoB 9627 was positioned further downslope at 4028 m water depth on the northern flank of the channel, where the channel area widens to more than 14 km. This core documents 34 mud-cloud over-spill events, which often are amalgamated indicating an interaction of mud clouds derived from different directions.

The final core of the cruise M65-2, the Core GeoB 9628-1 was recovered from the margin of the Cap Blanc Slide complex at 3028 m water depth. The 10.68-m long core penetrated into the slide at 6.3 m subbottom depth and contains below a 50-cm thick cover a clast-rich olive grey matrix-rich debrite unit which is underlain by tilted, stretched, folded and sheared glide blocks consisting of close alternations of pale light greenish grey to brownish grey mud layers. The basal core segment represents either a non-deformed, non-tilted glide block or is the autochthonous base of the Cap Blanc Slide. No clear glide plane could be identified.

In summary, coring in the Timiris Canyon was very successful. We have collected a set of spectacular cores, which enable us to reconstruct the frequency, dynamics and volumes of turbidite activity during the last glacial interglacial cycle, and, at least at some locations, much further back in time.

4.4 Physical Properties Studies

(D. Heslop, M. Höcker)

4.4.1 Methods

The sediment series recovered during METEOR Cruise M65/2 with the gravity corer were subject to laboratory geophysical studies. Shipboard measurements on the segmented cores were made using a GEOTEK Multi-Sensor Core Logger (MSCL) and routinely comprised three basic physical parameters:

- electric resistivity R_s (to determine density and porosity),
- magnetic volume susceptibility κ, and,
- Light reflectance

These properties are closely related to lithology and grain size of the sediments. Electric resistivity and magnetic volume susceptibility yield medium-resolution core logs and act as a basis for other detailed investigations. The characteristic sensor response width for these parameters is approximately 5-8 cm and measurements were performed at a spacing of 1 cm on the archive halves of the cores. In addition, oriented cube samples for subsequent shore based rock and paleomagnetic studies were taken from the work halves of the cores at 5 cm intervals. If turbidites or debris flows were sampled, the sampling density was usually reduced to 20 cm. Archive halves of all sampled cores were optically scanned to obtain high resolution digital photographs and light reflectance curves with a resolution of 0.01 cm (see section 4.3).

Magnetic Volume Susceptibility

The magnetic volume susceptibility, κ, of a material is defined by the equations

$$B = \mu_0 \cdot \mu_r \cdot H = \mu_0 \cdot (1 + \kappa) \cdot H = \mu_0 \cdot H + \mu_0 \cdot \kappa \cdot H = B_0 + M$$

with the magnetic induction B, the absolute and relative permeabilities μ_0 and μ_r, the magnetizing field H and the volume magnetization M. As can be seen from the third term, κ is a dimensionless physical quantity. It represents the amount to which a material is magnetized by an external magnetic field.

For marine sediments the magnetic susceptibility may vary from an absolute minimum value of around $-15 \cdot 10^{-6}$ (produced by diamagnetic minerals such as pure carbonate or silicate) to a maximum of some $10000 \cdot 10^{-6}$ for basaltic debris rich in (titano-) magnetite. In most cases κ is primarily determined by the concentration of ferrimagnetic minerals, while paramagnetic matrix components such as clays are of minor importance. High magnetic susceptibilities indicate high concentrations of lithogenics / high iron (bio-)mineralization or low carbonate / opal productivity. Low values of magnetic

susceptibility, on the other hand, can also be a result of post-depositional reduction of magnetic minerals. In cores with a low level of disturbance, magnetic susceptibility serves for the mutual correlation of sedimentary sequences which were deposited under similar global or regional conditions.

The GEOTEK MSCL equipment is mounted with a commercial BARTINGTON M.S.2 susceptibility meter with a 140 mm loop sensor. Due to the sensor's size, it integrates the response signal over a core interval of ~8 cm. Consequently, sharp susceptibility changes in the sediment column appear smoothed in the κ core log and thin layers may not be resolved appropriately by the whole-core susceptibility measurement.

Electrical Resistivity, Porosity, and Density

The electrical sediment resistivity R_s was determined using a noncontact sensor. An integrated fast resistance thermometer simultaneously provides data for a temperature correction. A platinum resistance thermometer (PRT) was used to measure the temperature of a reference section whilst resistivity logging took place. For absolute calibration of the resistivity sensor a series of saline solutions were measured prior to the commencement of logging. This calibration is applied to the measured voltage data during post-processing.

For each measured core its porosity ϕ was calculated according to the empirical Archie's equation,

$$R_s/R_w = k \cdot \phi^{-m}$$

which approximates the ratio of sediment resistivity R_s to pore water resistivity R_w by a power function of porosity ϕ. Following a recommendation by BOYCE (1968), suitable for sea water saturated clay-rich sediments, values of k=1.30 and m=1.45 are used here. During M65/2 and the previous leg M65/1 a number of problems were encountered with the noncontact sensor. The measured voltage data recorded by the sensor would make sudden (and unexplainable) jumps of the order 10-100mV. In most cases these jumps could be easily identified as a step in the data and corrected for during post-processing.

Light Reflectance

The digital imaging module of the GEOTEK MSCL consists of a camera containing three 1024 pixel CCD arrays. The camera is mounted ~40 cm above the surface of the sediment and measures the light reflected from two fluorescent tubes which illuminate the core from a height of ~ 5 cm. Archive halves of the core sections were prepared to give a smooth surface to reduce shadow effects from micro-topographic features. All cores were scanned at a resolution setting of 100, corresponding to 10 rows of pixels for

every 1mm in core depth. For the individual cores the lightest part of the sediment was selected in order to determine an aperture which allows the entire core to be measured on the same setting without saturating any of the colour channels. Before measuring each core a white-black calibration which measures the response of the camera to a white tile of known reflectance (white calibration) and taking the average response of the camera whilst the lens cap was in place (black calibration) was performed. Prepared test cards consisting of stripes of known colour and grayscales were measured before and after each core, to calibrate the final segment images to true colour and to determine the magnitude of any drift in the camera. Drift of the camera is assumed to be linear drift with depth and was thus compensated for using a correction factor.

Post-processing software was employed in order that end-caps, cavities at the top and bottom of the segments and other disturbances could be removed from the raw image data. During post-processing spurious colour stripes caused by a non-uniform response of the camera's colour channels were filtered out of the image data by normalising the means of the individual columns of pixels to the same value. The median value of each row of pixels was chosen to represent the sediment colour for each line (the median was selected in preference to the mean value because of its resistance to the influence of outlying values). From each processed core, depth series were constructed for the red, green and blue channels, in addition, total intensity (mean value of the three channels) and the ratio of the red to blue channels were calculated. An enhanced core image was produced by manually adjusting the brightness and contrast of the original core image in order to extenuate the layers within the sediment.

4.4.2 Shipboard Results

4.4.2.1 Sampling Sites and Recovery

The Gravity Coring stations investigated during Cruise M65/2 were split into 2 main working areas around the Dakar and Cap Timiris Canyons (Working Area A and B respectively). These coring locations were specifically chosen to investigate sedimentation processes and pathways at the tropical continental margin.

Working Area A

Working Area A focused on locations along the Dakar Canyon. After recovery of a first reference core (GeoB9601-3, 1920m water depth) to the north of the working area, a second reference core, GeoB9602-3 containing a number of turbidites was taken to the south of the Dakar Canyon at a water depth of 3981m. This was followed by 3 further cores, GeoB9604-3, GeoB9605-1and GeoB9606-2 taken at shallower depths on the levee at locations based on Parasound investigations. Three cores provided a profile across the canyon at a water depth of ~3000m including a core from within the deepest

portion of the canyon (GeoB9607-3), a reference site on the levee (GeoB9608-2) and a core from the terrace (GeoB9609-2). The deepest part of the canyon was investigated with 3 further cores, two within the canyon itself (GeoB9610-1 & GeoB9611-1) and a reference core from the levee (GeoB9612-3). Finally for Working Area A, three cores (GeoB9613-2, GeoB9614-1 & GeoB9615-1) were taken at the lowest part of the canyon at a water depth of ~4000m to recover material from a complex of slides.

Working Area B

The first deep-water gravity core location (GeoB9622-3) in Working Area B was situated over an abandoned arm of the Cap Timiris Canyon at a water depth of 2879m in an area that had apparently been subjected to a high level of sliding. Previous to this a core had been taken on the shelf (GeoB9621-3) in a water depth of only 52m. The remaining cores in Working Area B focused on sampling the Cap Timiris Canyon at water depths of ~4000m in the region of the Cap Blanc slide. A core from the levee (GeoB9624-1) at the base of the canyon contained pelagic sedimentation with small overspill turbidites. A small side gully off the Cap Timiris Canyon was sampled with core GeoB9626-1 and found to contain brown Holocene material with a number of turbidites. The open portion of the main path of the canyon was sampled at a water-depth of 4028m by core GeoB9627-1. Finally core GeoB9628-1 recovered sediment from above the Cap Blanc slide complex and contained pelagic sediment on top of a large debrite.

4.4.2.2 General Results

The general characteristics of the physical properties of the cores from the two working areas were found to be quite different and will therefore be discussed in two separate subsections.

Working Area A (Dakar Canyon)

The majority of the cores recovered from Working Area A showed a consistent pattern in their physical properties. This behaviour is exemplified by the first core taken on the cruise; GeoB9601-3 at a location off Senegal. In general it is found that where magnetic susceptibility is high, porosity is low, Red/Blue colour ratio is high and vice versa. One remarkable feature of these cores is a peak in magnetic susceptibility that is found in the upper portion of the sediment. This peak is mirrored by a low in porosity, in some cases ~40%, and a corresponding high in Red/Blue ratio. This feature was also observed in cores taken during M65/1, however an explanation of its origin is still lacking. Magnetic susceptibility gives extremely limited information about the type of magnetic minerals contained within the sediment but such high values would indicate the presence of magnetite (Fe_3O_4). The working hypothesis is that the Senegal shelf

and margin sediments have alternating magnetite-reducing (green) and magnetite-preserving (brown) layers which correspond to warm and cold climatic periods respectively. Comparison to the ship-board geochemical data obtained by XRF analysis, shows that maxima in magnetic susceptibility correspond to minima in iron content. This relationship demonstrates that the variations in magnetic susceptibility cannot be solely attributed to changes in the concentration of a magnetic mineral assemblage, but instead the composition of the assemblage must also be varying, with minerals with a higher κ occurring in the peaks in magnetic susceptibility. Currently, although there is a clear correlation between a number of the cores in Working Area A, there is no obvious correlation of the physical properties logs to existing climate records. Therefore the hypothesis of climatically controlled iron preservation and reduction will only be testable once a more detailed rock-magnetic investigation of the sediments has been performed.

A number of cores in Working Area A contained a large number of turbidites (for example, core GeoB9612-3 was found to contain a total of 23). A number of the turbidites were thin, 1cm or less, making them difficult to resolve in physical properties logs where the magnetic susceptibility and resistivity sensors integrate the signal over ~5-8 cm of the core. In general however, it was found that the turbidites had no consistent pattern in their physical properties indicating that the material from which they were composed had originated from a number of different sources.

Box and Whisker plots are used to show the general characteristics of the physical properties of the cores from Working Area A (Figs. 4.4.1-4.4.3). No clear relationship exists between core location and physical properties. This however is not surprising as the cores were taken in locations where extremely different sedimentary environments occur within close proximity to each other (as discussed in Sampling Sites and Recovery), for example moving from continuous deep sea sedimentation to the flank of a canyon and then to the centre of a canyon. There is therefore no reason to assume that simply because two cores are located within a small area that they will show the same, or even similar, patterns in their physical properties.

Box and whisker plots representing the physical properties (magnetic susceptibility, porosity and Red\Blue colour ratio) of the gravity cores taken during M65/2 in working Area A are shown in Figures 4.4.1-4.4.3. The limits of each box represent the values of the 75th and 25th percentiles of the core data, whilst the cross-bar contained within the box gives the median value. The whiskers show the full span of the data-set, i.e. the minimum and maximum values. The cores in Working Area A have been divided into 3 subgroups based upon their locations. Although the cores within each group are located in similar areas they can represent extremely different sedimentological environments. It

is however possible to define some basic patterns in the physical properties of the cores. Following the general relationship of high magnetic susceptibility, low porosity and high Red\Blue ratio it is found that there are consistent differences between cores taken from at the top of the canyon and those taken at the base. In general the cores at the base of the canyon have lower magnetic susceptibility, higher porosity and lower Red\Blue ratio than those at the top. This may indicate that the material causing the large peaks in magnetic susceptibility may be terrestrial in origin and is not transported the full length of the canyon to the distal coring locations.

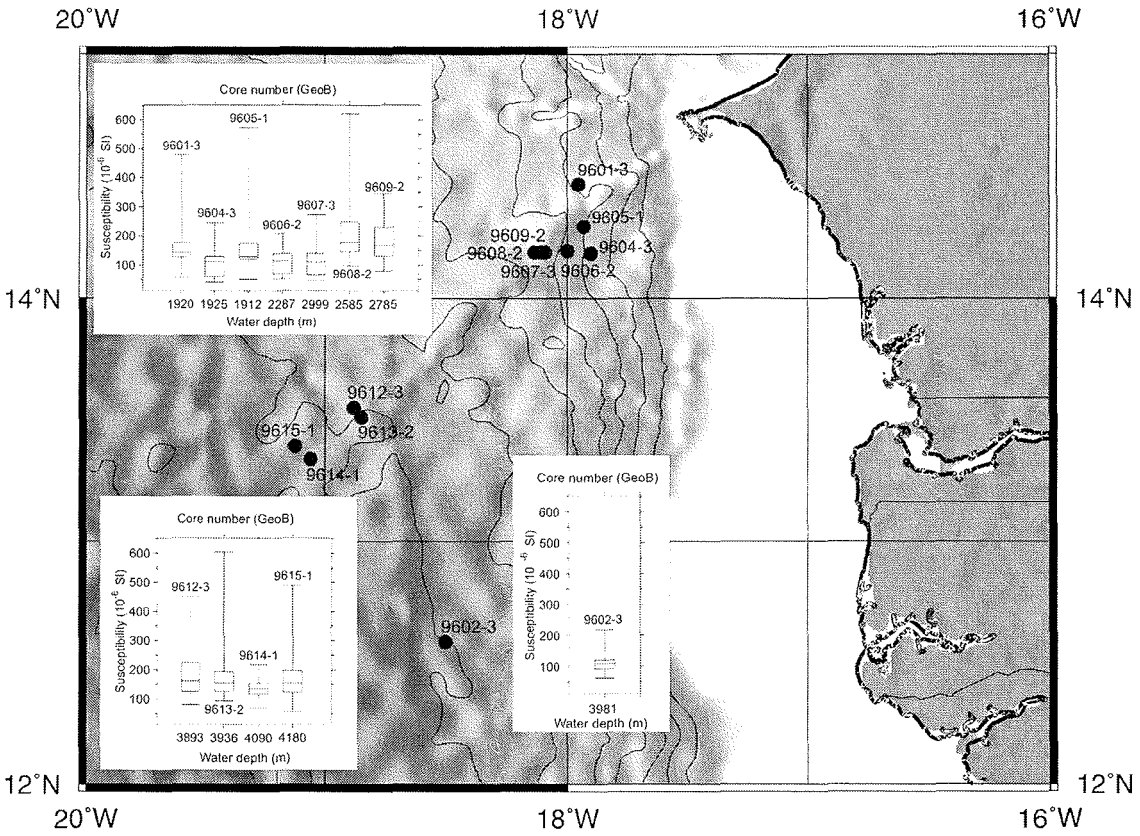

Figure 4.4.1: Magnetic Susceptibility values for the gravity cores in Working Area A. All core names are prefixed with GeoB.

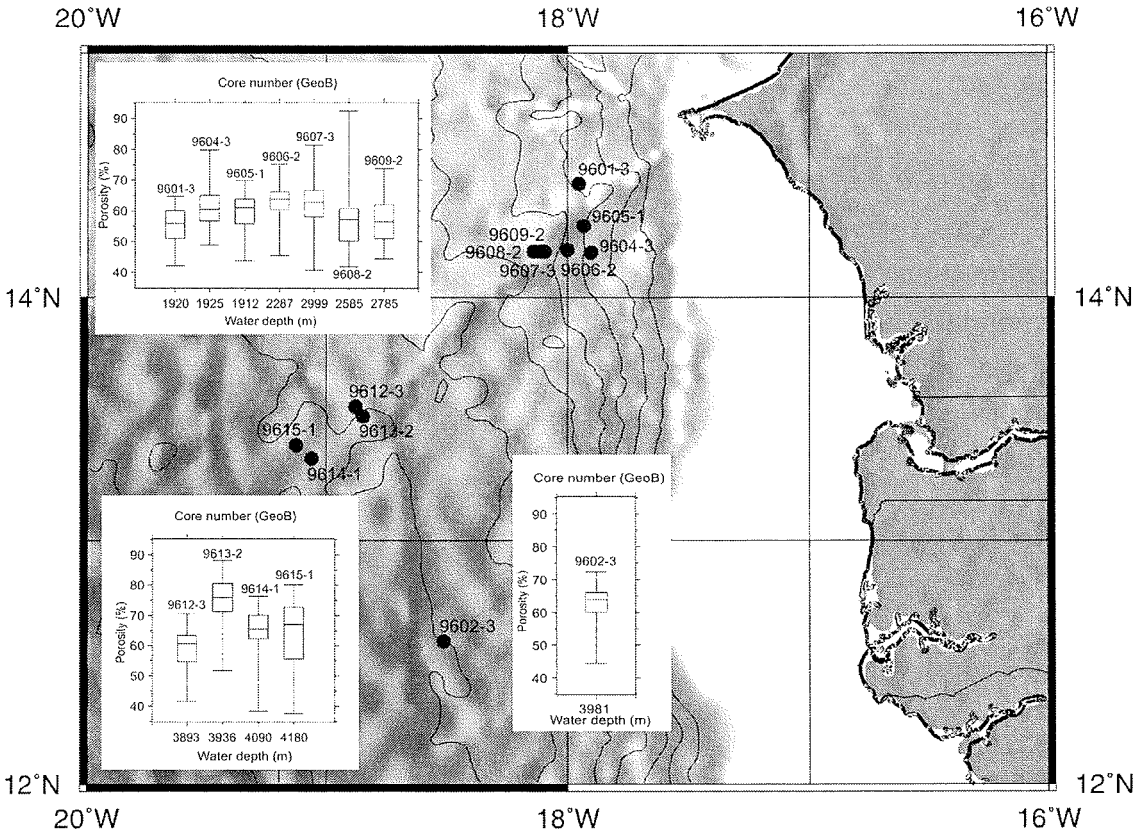

Figure 4.4.2: Porosity values for the gravity cores in Working Area A. All core names are prefixed with GeoB.

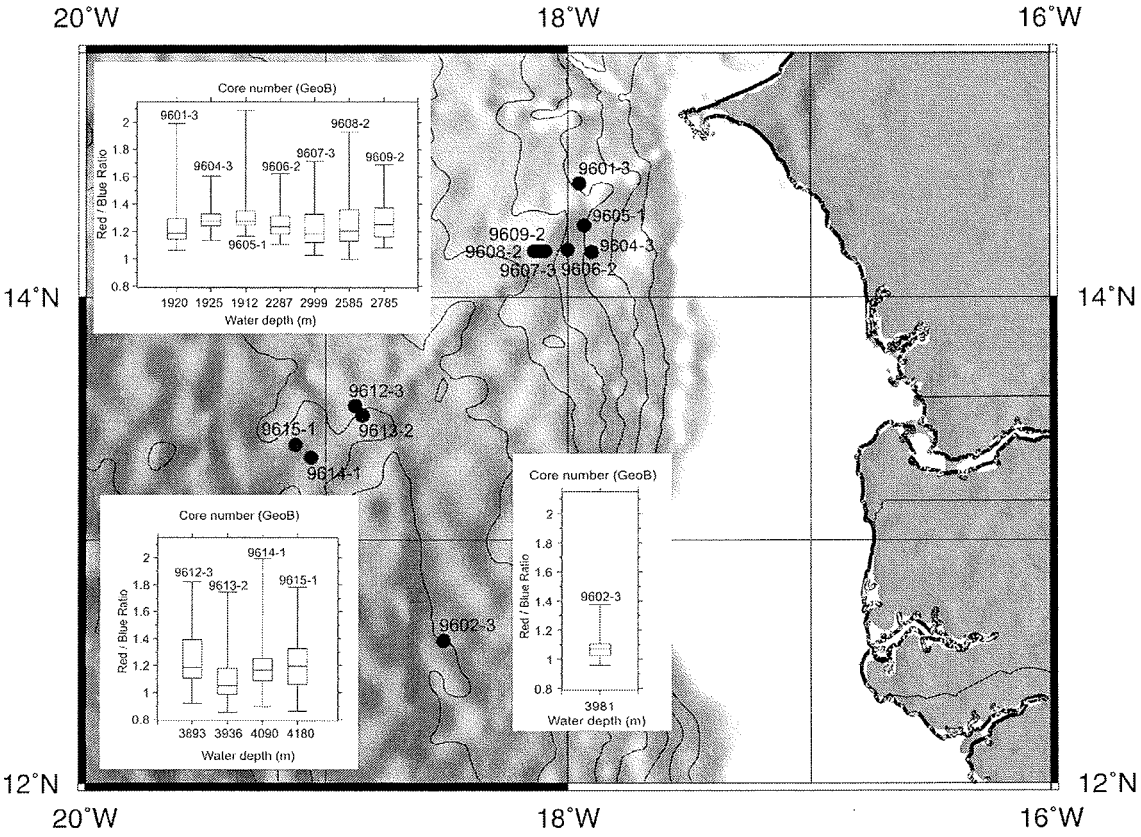

Figure 4.4.3: Red\Blue ratio values for the gravity cores in Working Area A. All core names are prefixed with GeoB.

Working Area B (Cap Timiris Canyon)

Core GeoB9621-3 was taken at a location on the shelf away from the main working area and not surprisingly it was found to have quite different physical properties to the other cores. Visual inspection revealed that the core had a high carbonate content and a uniform lithology, this was confirmed by low values in magnetic susceptibility and an almost constant value of the Red\Blue colour ratio. Box and whisker plots representing the physical properties (magnetic susceptibility, porosity and Red\Blue colour ratio) of the gravity cores taken during M65/2 in working Area B around the Cap Timiris Canyon are shown in Figures 4.4.4-4.4.6. The limits of each box represent the values of the 75th and 25th percentiles of the core data, whilst the cross-bar contained within the box gives the median value. The whiskers show the full span of the data-set, i.e. the minimum and maximum values. Although the cores within each group are located in similar areas they can represent extremely different sedimentological environments.

The peak of high magnetic susceptibility that occurred in a number of the cores in Working Area A was found to be absent in the cores from Working Area B. In addition the median magnetic susceptibility of the cores from working area B was substantially lower than the cores in Working Area A. Pooled core data from Working Areas A and B are compared in Figure 4.4.7 with a box and whisker plot of the same form as those displayed in the previous figures. There are two possible explanations for this discrepancy given the present data sets. Firstly, the transport of highly magnetic material from an unknown source to Area A may not extend to Area B. Secondly, visual examination and the reflected light scans of the cores from working Area B revealed a high carbonate content. Biogenic carbonate can act to dilute the concentration of terrigenous material in the sediment and therefore reduce the overall magnetic susceptibility. A number of cores have values of magnetic susceptibility, porosity and Red\Blue ratio that reach extremes (high values in magnetic susceptibility, low values in porosity and high values in Red\Blue ratio) in the top ~1m of the core but then maintain almost constant values for the deeper material.

As with Working Area A, a number of the cores in Working Area B contained a large number of turbidites. These are easily identifiable from the reflected light scans and in cores such as GeoB9627-1, the Red\Blue ratio provides clearly alternating values between the turbidites and the background sediment. Because of the limited resolution of the magnetic susceptibility and resistivity instruments it is difficult to study the turbiditic layers in detail. However, in the cores containing a large number of turbidites there is no clear relationship between the turbiditic layers and changes in magnetic susceptibility and porosity.

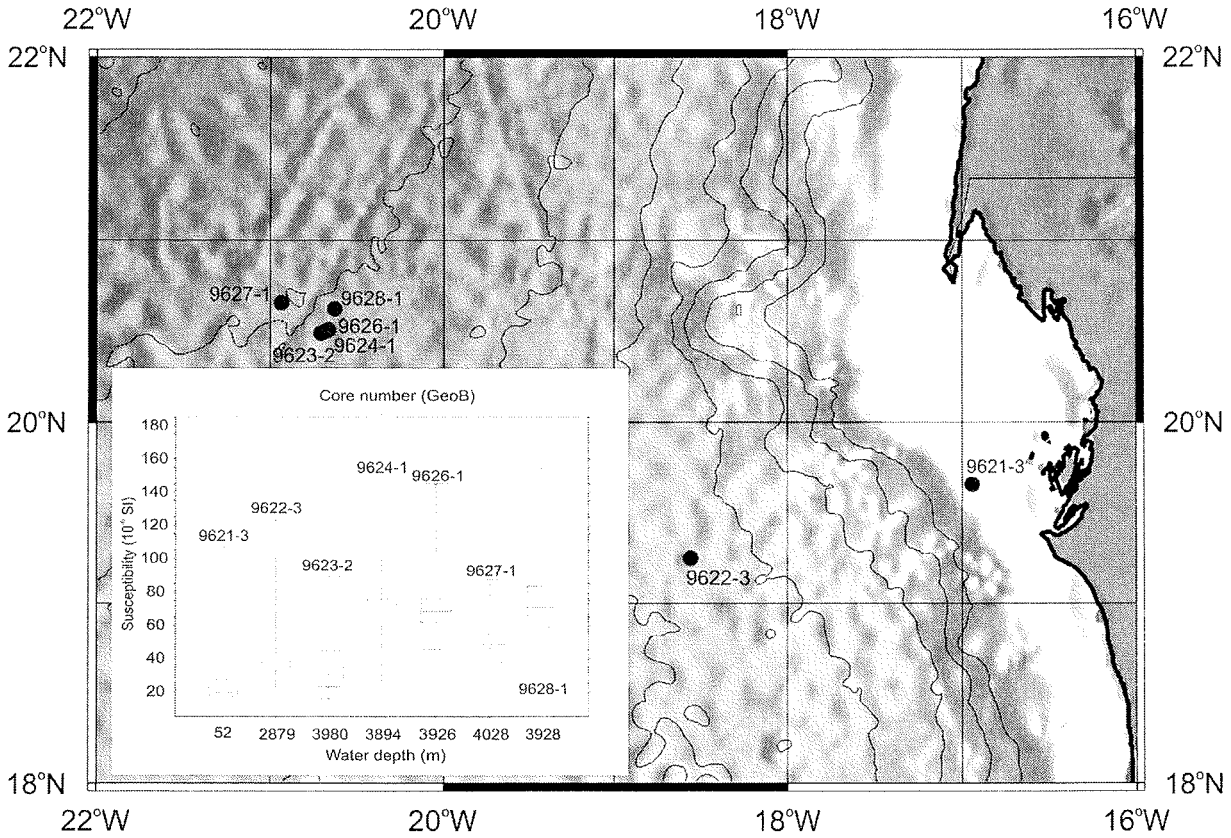

Figure 4.4.4: Magnetic Susceptibility values for the gravity cores in Working Area B. All core names are prefixed with GeoB.

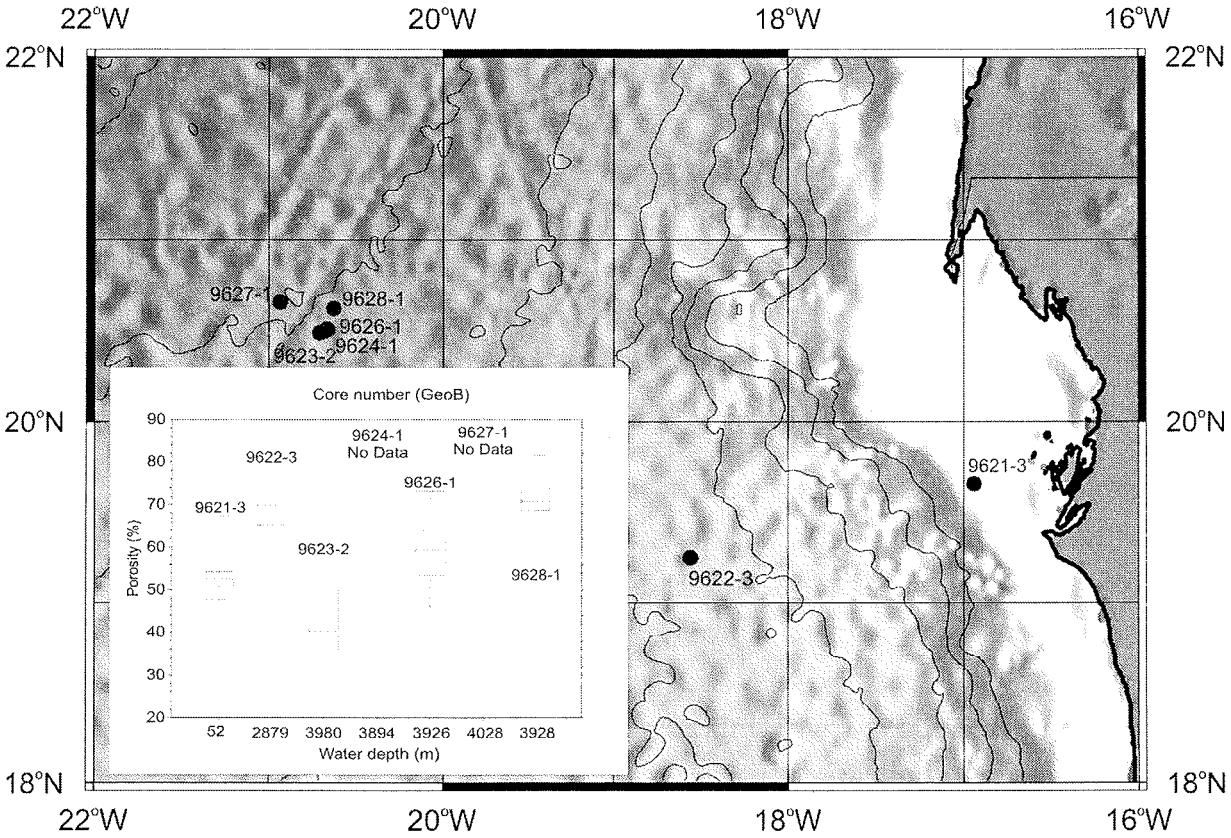

Figure 4.4.5 Porosity values for the gravity cores in Working Area B. All core names are prefixed with GeoB.

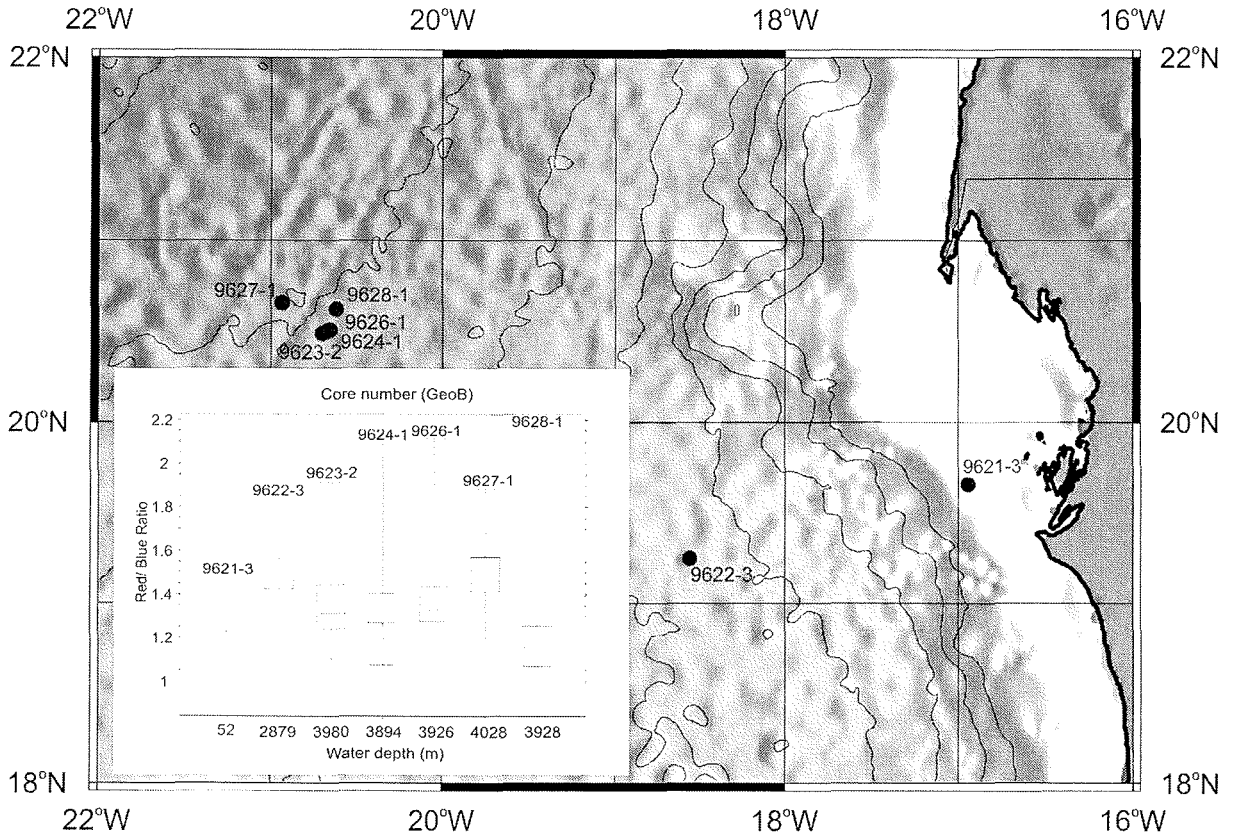

Figure 4.4.6 Red\Blue colour ratio values for the gravity cores in Working Area B. All core names are prefixed with GeoB.

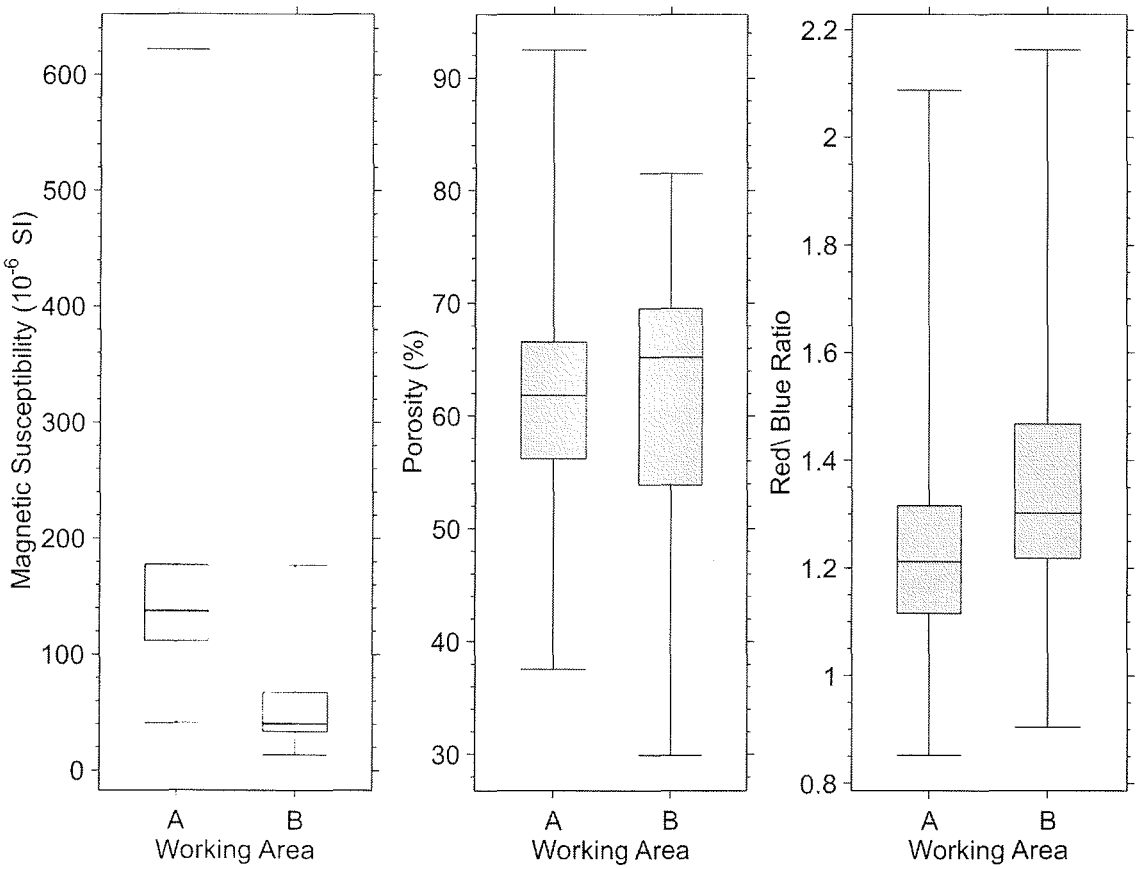

Figure 4.4.7: Comparison of the pooled core data from Working Areas A and B

4.5 Sediment and Pore Water Geochemistry

(K. Enneking, J. Hoffmann, M.Kölling, L. Schnieders, H.D. Schulz)

4.5.1 Scientific questions

An onboard XRF method for analyzing sediment solid phase samples that had been successfully used on cruises M57-1, M58-1 and M58-2 should be used to allow a rapid evaluation of the major element composition one to three days after coring using a portable XRF analytical device (XEPOS®, SPEKTRO A.I. GmbH. & Co. KG., Kleve). The onboard investigations mainly aimed at a stratigraphic interpretation of the element content profiles.

The analysis of pore water samples on this cruise included only a few parameters (alkalinity, ammonium and sulphate) on pore water samples, which were extracted with the new rhizon technique (see below) in a sufficient volume from either the closed or open core. So, since no separate core was taken for pore water analyses, the same core could be used by the three groups, the geology, geophysics and the geochemistry group.

Since the pore water profiles may be interpreted as result of normal decay of organic matter in stratified sediments a mass flow event will appear in the pore water profile as deviation from a normal steady state situation. Steady state pore water concentration profiles usually show linear gradients with either a flux from the bottom water into the sediment (sulphate) or a flux from the sediment into the bottom water (ammonium, phosphate, alkalinity). In non-steady state situations as induced by a mass flow event the pore water profile has significant changes in gradients that may be modeled. Fitting the model data to the measured concentrations allows estimating the age of very young (< 500 a) events. Dating of such geologically very young events cannot be done by means of an element stratigraphy.

4.5.2 Core material sampled for XRF and pore water analyses

In total twelve cores from the gravity corer and six cores from the multicorer were analysed with the XRF. Samples from seven more gravity cores and from seven more multicorers were collected, dried and stored for analysis in the home lab. Pore water was analysed from 19 cores from the multicorer and seven cores from the gravity corer. The pore water analysis started always as soon as the core was on deck.

Table 4.5.1: Samples of the geochemistry group on RV "Meteor" Cruise M 65-2.

Tab. 4.5.1
Samples Geochemistry Group
PW = pore water

Meteor M65 / 2
Dakar/Senegal - Las Palmas/Canaries
02th July 2005 - 26th July 2005

GeoB #	board #	devices dev.	devices type	coordinates latitude	coordinates longitude	time UTC start/contact	time UTC end	water depth [m]	waters	remarks	area / waters	samples XRF		samples PW	
9601	333			14°27'80" N	17°57'04" W	19:03	23:53	1924	Senegal	southwest off Dakar on undisturbed hemipelagic sediments	slope off Dakar				
		-2	MUC	14°27'79" N	17°57'01" W	20:46		1924		20-24 cm		12	m	3	m
		-3	GC 12	14°27'81" N	17°59'98" W	22:37		1920		755 cm; hemipelagic sediments, no turbidites		188	m	17	m
9602	335			12°35'25" N	18°30'42" W	16:10	23:05	3977	Senegal	reference core on the levee	southern part of working area, close to the border of Guinea Bissau, Diola Canyon				
		-2	MUC	12°35'23" N	18°30'36" W	18:34		3986		34-38 cm		18	m	-	-
		-3	GC 12	12°35'26" N	18°30'37" W	21:35		3981		495 cm; hemipelagic sediments, some spillover turbidites		121	m	14	m
9603	336			12°34'02" N	18°30'10" W	23:17	05:30	4078	Senegal	canyon thalweg					
		-2	MUC	12°34'02" N	18°30'08" W	23:21		4083		40 cm		10	m	1	m
		-3	GC 6	12°34'11" N	18°30'10" W	03:56		4085		barrel bent, no core		-	-	-	-
9604	338			14°10'96" N	17°54'06" W	12:12	16:48	1927	Seneg./Gambia	area with missing upper part of the sediments according to parasound	area with small debris flows at the continental slope, according to parasound somtimes the upper meters of sediment are missing				
		-2	MUC	14°11'07" N	17°54'04" W	14:11		1920		33 cm		8	m	-	-
		-3	GC 12	14°11'01" N	17°54'10" W	16:12		1925		831 cm; only one small turbidite in hemipelagic sediments		208	m	18	m
9605	339			14°17'57" N	17°55'79" W	17:35	20:51	1920	Seneg./Gambia	close to GeoB 9604 in undisturbed sediments					
		-1	GC 12	14°17'60" N	17°55'80" W	18:12		1920		790 cm; hemipelagic sediments, no turbidites		198	m	16	m
		-2	MUC	14°17'60" N	17°55'80" W	19:58		1915		30 cm		15	m	4	m
9606	340			14°11'63" N	17°59'88" W	21:46	01:32	2288	Seneg./Gambia	close to GeoB 9604, between many little slides according to parasound					
		-1	MUC	14°11'61" N	17°59'85" W	22:37		2286		34 cm		20	m	5	m
		-2	GC 12	14°11'63" N	17°59'82" W	00:44		2287		951 cm; normal hemipelagic sediments without turbidites		236	m	19	m
9607	342			14°11'27" N	18°06'65" W	07:21	13:46	2997	Seneg./Gambia	thalweg of Dakar Canyon	profile through the Dakar Canyon at a water depth of 3000 m				
		-2	MUC	14°11'23" N	18°06'63" W	10:18		3000		48 cm		20	b	5	m
		-3	GC 12	14°11'29" N	18°06'65" W	12:56		3004		784 cm; core with many turbidites and debris flow		192	m	21	m
9608	343			14°11'22" N	18°08'26" W	14:25	19:30	2585	Seneg./Gambia	reference core on the levee					
		-2	GC 12	14°11'19" N	18°08'29" W	16:01		2586		908 cm; hemipelagic sediments, no turbidites		223	m	18	m
		-3	MUC	14°11'18" N	18°08'28" W	18:10		2590		34-43 xm		19	b	-	-
9609	344			14°11'32" N	18°05'60" W	19:49	00:11	2769	Seneg./Gambia	position on a 'terrace' between thalweg and levee					
		-1	MUC	14°11'32" N	18°05'62" W	20:48		2776		35-39 cm		19	b	-	-
		-2	GC 6	14°11'35" N	18°05'63" W	23:08		2785		542 cm; core not sampled		-	-	-	-
9610	347			13°45'23" N	18°32'75" W	08:25	10:12	3752	Seneg./Gambia	thalweg of Dakar Canyon	deeper parts of the Dakar Canyon, water depth 3700-3900 m				
		-1	GC 3	13°45'27" N	18°32'68" W	09:47		3752		254 cm; short core with many turbidites		58	m	15	m
9611	348			13°32'32" N	18°52'65" W	13:43	16:34	3981	Seneg./Gambia	thalweg of Dakar Canyon, further downstream					
		-1	GC 3	13°32'30" N	18°52'60" W	15:18		3983		147 cm; short core, many turbidites between hemipelagic sediments		36	m	8	m
9612	349			13°33'07" N	18°52'64" W	16:52	22:35	3958	Seneg./Gambia	reference core on the levee					
		-2	MUC	13°32'98" N	18°52'70" W	19:14		3922		10-11 cm		10	b	1	m
		-3	GC 12	13°33'01" N	18°53'50" W	22:15		3893		878 cm; hemipelagic sediments with many overspill turbidites		216	m	18	m

Table 4.5.1 continued: Samples of the geochemistry group on RV "Meteor" Cruise M 65-2.

Tab. 4.5.1 continued
Samples Geochemistry Group
PW = pore water

Meteor M65 / 2
Dakar/Senegal - Las Palmas/Canaries
02th July 2005 - 26th July 2005

GeoB #	board #	devices dev.	devices type	coordinates latitude	coordinates longitude	time UTC start/contact	time UTC end	water depth [m]	waters	remarks	area / waters	samples XRF		samples PW	
9613	351			13°30'82" N	18°50'83" W	14:28	19:38	3933	Seneg./Gambia	on top of slide complex according to parasound	lowest part of the Dakar Canyon, water depth of ca. 4000 m; Canyon partly covered by slide or debris flow				
		-1	GC 12	13°30'80" N	18°50'80" W	17:57		3936		982 cm normal pelagic sediments with only few turbidites		242	b	22	m
9614	352			13°23'60" N	19°03'65" W	21:28	22:30	4096	Seneg./Gambia	broader thalweg of the channel over an older slide complex					
		-1	GC 12	13°23'64" N	19°03'60" W	22:21		4090		478 cm, only 4 turbidites in normal pel. sediments, slide not reached		118	b	11	m
9615	353			13°23'68" N	19°06'27" W	00:12	02:13	4088	Seneg./Gambia	in prolongation of the canyon, sediment fills small depressions					
		-1	GC 12	13°23'65" N	19°06'25" W	01:14		4108		944 cm; pel. sed. with many turb. and thick, hogeneous sand layer		230	m	19	m
9621	362			19°39'37" N	16°56'37" W	15:29	17:05	52	Mauretania	outer shelf	outer shelf				
		-2	MUC	19°39'37" N	16°56'37" W	16:01		53		32-34 cm		18	b	-	-
		-3	GC 6	19°39'37" N	16°56'36" W	16:31		52		574 cm; sandy mud with many shells, not sampled		2	m	-	-
9622	364			19°14'58" N	18°33'19" W	02:55	08:32	2879	Mauretania	cut off loop of Cap Timiris Canyon	middle part of Cap Timiris Canyon				
		-2	MUC	19°14'87" N	18°33'20" W	04:45		2878		32-39 cm		20	b	5	m
		-3	GC 12	19°14'87" N	18°33'21" W	07:16		2881		1045 cm; hemipel. sed., turb., at 4.55 mbsf young slide, (pore water)		191	m	21	m
9623	367			20°30'40"N	20°40'06"W	06:00	09:58	3939	Mauretania	position on a 'terrace' between thalweg and levee	Lowest part of Cap Timiris Canyon (CTC), water depth of ca. 4000 m, close to the area where the canyon is covered by the Cap Blanc Slide, and where the canyon branches out.				
		-2	GC 12	20°30'38"N	20°39'96"W	08:12		3940		barrel bent, good core, brown layer on top, pel. sed., overspill turb.		48	b	8	m
9624	368			20°30'63"N	20°39'51" W	10:08	15:45	3890	Mauretania	reference core on the levee					
		-1	GC 12	20°30'64"N	20°39'53" W	11:08		3894		8-10 cm		4	b	-	-
		-2	MUC	20°30'64"N	20°39'55" W	13:59		3890		1133 cm; pel. sed. with many overspill turb., brown layer (cf.9623)		246	b	23	m
9626	370			20°29'32" N	20°42'26" W	18:34	20:45	3928	Mauretania	little gully close to the canyon					
		-1	GC 6	20°29'31" N	20°42'24" W	19:33		3926		431 cm; brown layer (cf.9623), many turb., small layers of pel. sed.		106	b	9	m
9627	371			20°39'52" N	20°56'06" W	08:11	10:23	4026	Mauretania	little elevation in broad thalweg with sediments on top (parasound)					
		-1	GC 6	20°39'50" N	20°56'03" W	09:14		4028		312 cm; brown layer (cf.9623), many turb., small layers of pel. sed.		74	b	7	m
9628	372			20°37'46" N	20°37'30" W	12:25	16:20	3935	Mauretania	sedim. on top of Cap Blanc Slide Complex according to parasound					
		-1	GC 12	20°38'55" N	20°37'62" W	13:27		3941		1068 cm; upper 6.2 m pel. sed. without turb., debrite, last 30 cm pel. (?)		264	b	20	m
												3390	all	328	m
												1991	m		

m = measured
b = in bags

Table 4.5.2: Overview over geochemical sample treatment on RV "Meteor" Cruise M65-2.

Tab. 4.5.2
Samples Geochemistry Group
Overview sample treatment

Meteor M65 / 2
Dakar/Senegal - Las Palmas/Canaries
02th July 2005 - 26th July 2005
PW = pore water, GC = gravity corer, MUC = multicorer

			PW		Sediment MUC						Sediment GC					
Location	Muc	GC	sampled	analyzed	sampled	dried	ground	measured	in vials	in bags	sampled	dried	ground	measured	in vials	in bags
GeoB 9601	-2	-3	x	x	x	x	x	x	x	-	x	x	x	x	x	x
GeoB 9602	-2	-3	x	x	x	x	x	x	x	-	x	x	x	x	x	x
GeoB 9603	-2	barrel bent	no PW	no PW	x	x	x	x	x	-	-	-	-	-	-	-
GeoB 9604	-2	-3	x	x	x	x	x	x	x	-	x	x	x	x	x	-
GeoB 9605	-2	-1	x	x	x	x	x	x	x	-	x	x	x	x	x	-
GeoB 9606	-1	-2	x	x	x	x	x	x	x	-	x	x	x	x	x	-
GeoB 9607	-2	-3	x	x	x	x	-	-	-	x	x	x	x	x	x	-
GeoB 9608	-3	-2	x	x	x	x	-	-	-	x	x	x	x	x	x	-
GeoB 9609	-1	-2	no PW	no PW	x	x	-	-	-	x	not sampled			-	-	-
GeoB 9610	-	-1	x	x	-	-	-	-	-	-	x	x	x	x	x	-
GeoB 9611	-	-1	x	x	-	-	-	-	-	-	x	x	x	x	x	-
GeoB 9612	-2	-3	x	x	x	x	-	-	-	x	x	x	x	x	x	-
GeoB 9613	-	-1	x	x	-	-	-	-	-	-	x	x	-	-	-	x
GeoB 9614	-	-1	x	x	-	-	-	-	-	-	x	x	-	-	-	x
GeoB 9615	-	-1	x	x	-	-	-	-	-	-	x	x	x	x	x	-
GeoB 9621	-2	-3	no PW	no PW	x	x	-	-	-	x	mainly shells, only 2 samples at 125 and 255 cm					
GeoB 9622	-2	-3	x	x	x	x	-	-	-	x	x	x	x	x	x	-
GeoB 9623	-	-2	x	x	-	-	-	-	-	-	x	x	-	-	-	x
GeoB 9624	-	-1	x	x	x	x	-	-	-	x	x	x	-	-	-	x
GeoB 9625	-	empty barrel	-	-	-	-	-	-	-	-	-	-	-	-	-	-
GeoB 9626	-	-1	x	x	-	-	-	-	-	-	x	x	-	-	-	x
GeoB 9627	-	-1	x	x	-	-	-	-	-	-	x	x	-	-	-	x
GeoB 9628	-	-1	x	x	-	-	-	-	-	-	x	x	-	-	-	x

4.5.3 Methods of pore water sampling and analysis

We used during this cruise only the new rhizon technique for the extraction of pore water from the fresh cores. It is possible to use them directly after coring at the still closed core liners (Fig. 4.5.1) or by inserting them into the sediment of the working half shell of the split core (Fig. 4.5.2). In most cases we used the first way because we wanted to extract the pore water as fast as possible. In some few cases it was necessary to open the core directly after coring, so that extraction of pore water from the open core was necessary.

Rhizons were originally developed to gain pore water samples which were then used to analyse the moisture of water in unsaturated soils (Meijboom and van Nordwijk 1992). A rhizon is supposed to function like an artificial root of a plant, hence its name is derived from 'rhiza', the Greek word for root. The device consists of thin tubes of various lengths (several cm) measuring approx. 2.5 mm in diameter. They are closed on one end and possess a connector on the other, over which a negative pressure is built up inside the tube. The tube material consists of a hydrophilic porous polymer, with a pore diameter of about 0.1µm. The actually quite instable tube is reinforced by an inserted piece of wire made of inert metal or durable plastic, allowing it to easily penetrate the soil or a sediment from the outside. In case of hard soils or sediments, a hole must first be punctured with a similarly shaped piece of metal or durable plastic.

The special property of the hydrophilic porous polymer is that, after short soaking in water, it becomes permeable to water — but not to air — once a vacuum is applied inside. Wherever the rhizon and the pore water come into contact, the negative pressure will draw the water into the interior, without allowing air to enter or destroy the vacuum. The water thus drawn inside will be simultaneously filtered through the 0.1µm – wide pores, permitting its analysis without further treatment.

Seeberg-Elverfeldt et al. (2005) applied rhizons for the first time in marine environments and obtained very good results. The method of extracting pore water with rhizons not only seems to be easier, but better as well. Rhizons are manufactured and distributed by Rhizosphere Research Products (Dolderstraat 62, NL-6706 JG Wageningen, The Netherlands) or Eijkelkamp (P.O. Box 4, NL-6987 ZG Giesbeek, The Netherlands). Their price is markedly higher as compared to filters used for pressing pore water out of a sediment sample, however, they can be used more than just once. Special sizes and connectors will be supplied, if a larger number of pieces is ordered.

From the water samples (usually 10 – 20 ml) the concentrations of alkalinity (titration with a sample volume of 1.5 ml and 0.01 m HCl), ammonium (flow injection technique,

Fig. 4.5.1: Extraction of pore water samples with rhizons from a still closed core only few minutes after taking the core aboard.

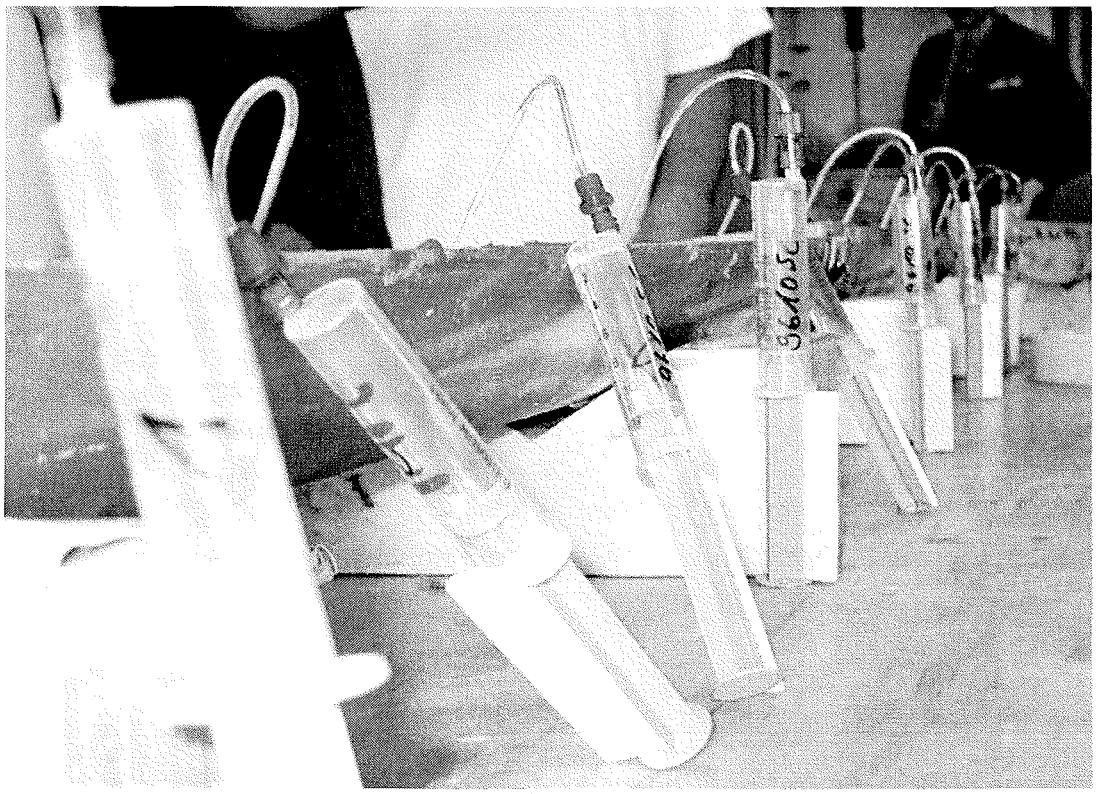

Fig. 4.5.2: If a core for other reasons has to be opened immediately, it is still possible to extract pore water with rhizons. The extraction does not affect other measurements or samples.

Hall and Aller, 1992), and sulphate were analysed. The analyses for sulphate were done nephelometrically/photometrically directly after a precipitation of barium sulphate with a test technique of Merck®. For analysing these three parameters usually only 2 – 3 ml of pore water were used. From these parameters comprising the major products of the anoxic degradation of organic matter, the degree of early diagenesis in a marine sediment was deductable with sufficient reliability. Other parameters can be measured after the cruise in the remaining pore water sample, from which a part was acidified and another part was diluted 1:10 with deionized water. A total of 328 pore water samples was extracted and analysed during the cruise M65-2.

Fig. 4.5.3 shows a concentration profile of ammonium measured during the cruise. It documents as well the applicability of rhizons for sampling marine pore water as the high accuracy of the flow injection technique for the measurements of ammonium in small volumes of marine pore water.

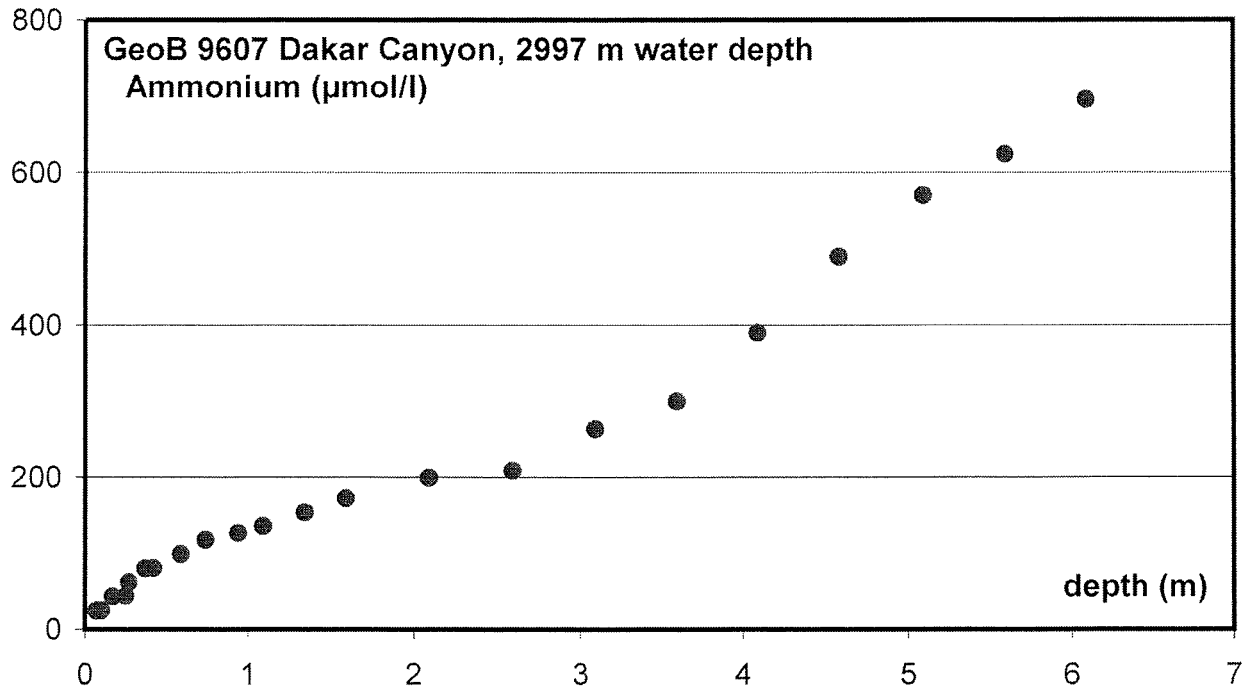

Fig. 4.5.3: Profile of ammonium concentrations in pore water of the core from location GeoB 9607. Samples were extracted with rhizons, ammonium was analysed with the flow injection technique (Hall and Aller, 1992).

4.5.4 Methods of XRF sediment analysis

The XRF spectrometer XEPOS® (SPECTRO A.I. GmbH. & Co. KG, Kleve) had been successfully tested on M57 and M58 cruises to perform elemental analyses on dried

and ground sediment samples. A method for powdered samples with a measuring time of 7.5 minutes per sample was used, which represents a compromise between measuring time and accuracy.

This method allows processing an 8 m core at a depth resolution of 4 cm in net measuring time of 24 h so that first results may be used immediately for planning further sampling sites. Reference measurements were performed after each series of samples using the MAG-1 sediment standard as a pressed tablet.

Sampling was performed by pressing U-channels (dimensions: 320(360)x16x10 mm LxWxH, material: titanium) into the sediment of the working half shell of the split core and separating the filled U-channel from the core using a plastic wire. The sediment in the U-channel was cut into 4 cm samples resulting in a sample size of approximately 5-6 cm^3 wet sediment. The samples, still remaining within the titanium U-channels, were dried in a drying furnace at 200°C and manually ground to a uniform grain size.

Due to the extensive help with grinding and overnight measurements from other groups twelve of the nineteen sampled cores from the gravity corer were directly measured on board.

Overall more than 1990 samples (total number of samples 3390, see Tab. 4.5.1 and 4.5.2) were analysed for 22 elements. With the rapid method used, the results for the elements Mg, Al, Si, P, S, Cl, K, Ca, Ti, V, Cr, Mn, Fe, Ni, Cu, Zn, Br, Rb, Sr, Ba, Pb, U are well above the background. As on the previous cruises M57 and M58, the XEPOS® XRF did not show errors due to the unusual ambient conditions on a ship. Some few samples which showed extremely high values for the aluminium content were at normal values in a repeated measurement. We will have to find the reason for this after the cruise.

4.5.5 First results

Pore water analyses

The three parameters sulphate, alkalinity and ammonium were absolutely sufficient to document the main processes of early diagenesis. The parameters also were sufficient to recognize whether a pore water profile had been in a quasi steady state situation for at least some centuries, or whether young disturbances might have happened.

In Fig. 4.5.4 the pore water concentration profiles of two characteristic situations are given. On the right side of this figure, a 'normal' steady state situation for a sediment

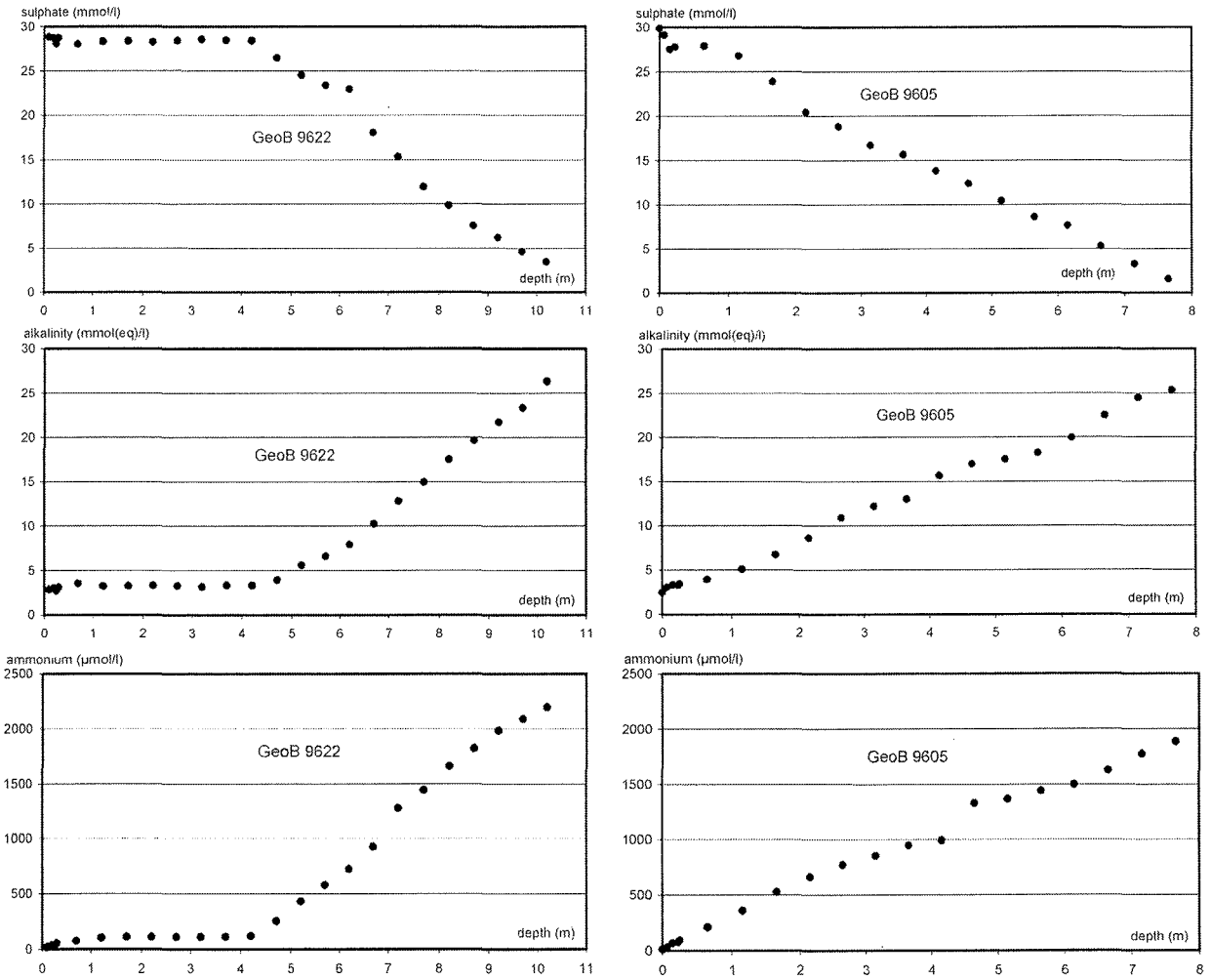

Fig. 4.5.4: Pore water concentration profiles in a normal steady state situation (right half of diagram) and in the non-steady state situation of a young slide event (left half of diagram).

with high content of reactive organic matter and corresponding high reaction rates is shown. In this situation nearly linear gradients of the constituents alkalinity and ammonium lead from very low seawater concentration two the high concentrations in deeper pore water. These linear gradients document diffusive fluxes from deeper parts of the sediment column to the sediment surface. The flux of sulphate goes into the opposite direction and transports the seawater sulphate down to a sulphate-methane reaction zone in a depth of about 8 m below the sediment surface, where sulphate and methane consume each other in a 1:1 reaction. From this gradient therefore not only the downward flux of sulphate, but also the upward flux of methane can be calculated. Most other locations had similar concentration profiles with usually somewhat lower gradients.

The left half of fig. 4.5.4 shows a not normal, non-steady state profile of pore water concentrations. In a depth of about 4.5 m below sediment surface a former sediment

surface is revealed by the pore water profiles. The concentration profiles between 4.5 and 10 m are just nearly identical with those of the location GeoB 9605 in the right half of the figure. Such highly reactive concentration profiles are characteristic e.g. for turbidite sequences, which received reactive organic matter directly from the shelf. The upper part of the concentration profile, however, is characteristic for a sediment with very low contents of reactive organic matter, as it is sedimented as pelagic mud on the levees of the channel. We therefore have to postulate, that the upper part of 0.0 – 4.5 m was transported as a slide on top of the older sediment column of 4.5 – 10 m. This slide event necessarily is quite young (between 10 and 20 years), otherwise the diffusion would have smoothed much more the sharp kinks in the profiles around 4.5 m. We know a similar profile from the deep sea fan of the river Congo, where also an intact layer of pelagic slope sediments slid down from a higher location, and ended on top of a series of young, organic rich turbidites (Zabel and Schulz, 2001).

XRF analyses of the sediment solid phase

A total of 12 cores with together about 1800 samples from the gravity corer was already measured onboard. With 22 elements per sample, this is a data set with about 40,000 values which will later, after a more detailed evaluation, be available in the Pangaea Data Base. In this first cruise report we show only the four major constituents Fe, Ca, Si, Al. In all cores shaded areas mark the depths, where turbidites were documented in the sedimentological description (cf. chapter 4.3 of this report).

Sediment porosity calculated from chloride content

In the dried sediment samples always a very well measurable content of chlorine is present, which results from the chloride of the pore water. Since the chloride concentration of seawater is quite constant, and since practically no chlorine containing minerals are known, this chlorine content of a sample represents directly the original pore volume of the sample. Especially for silt and clay dominated sediments with a low permeability, this chlorine content can be used to calculate the sediment porosity (Fig. 4.5.17). It is essential, that when the sample is taken, still the total pore volume is saturated with pore water, which certainly is the case for most marine sediments. Only samples of well permeable sediments like pure sand, will only contain a part of the original amount of water. In such samples the calculation via the chlorine content will probably underestimate the real porosity.

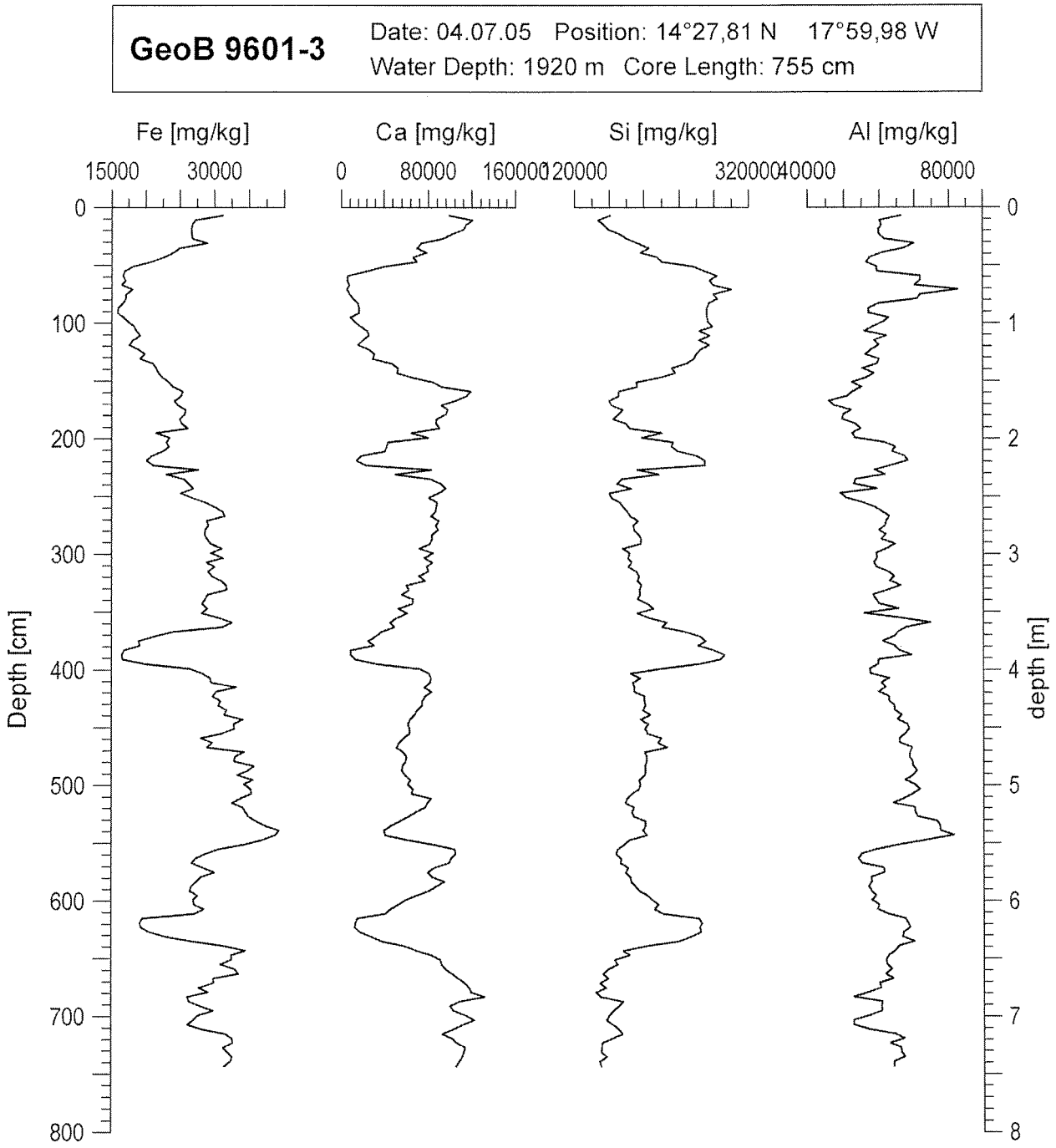

Fig. 4.5.5: Gravity corer GeoB 9601. XRF sediment element profiles of major components iron, calcium, silicium and aluminium measured onboard during cruise M65-2.

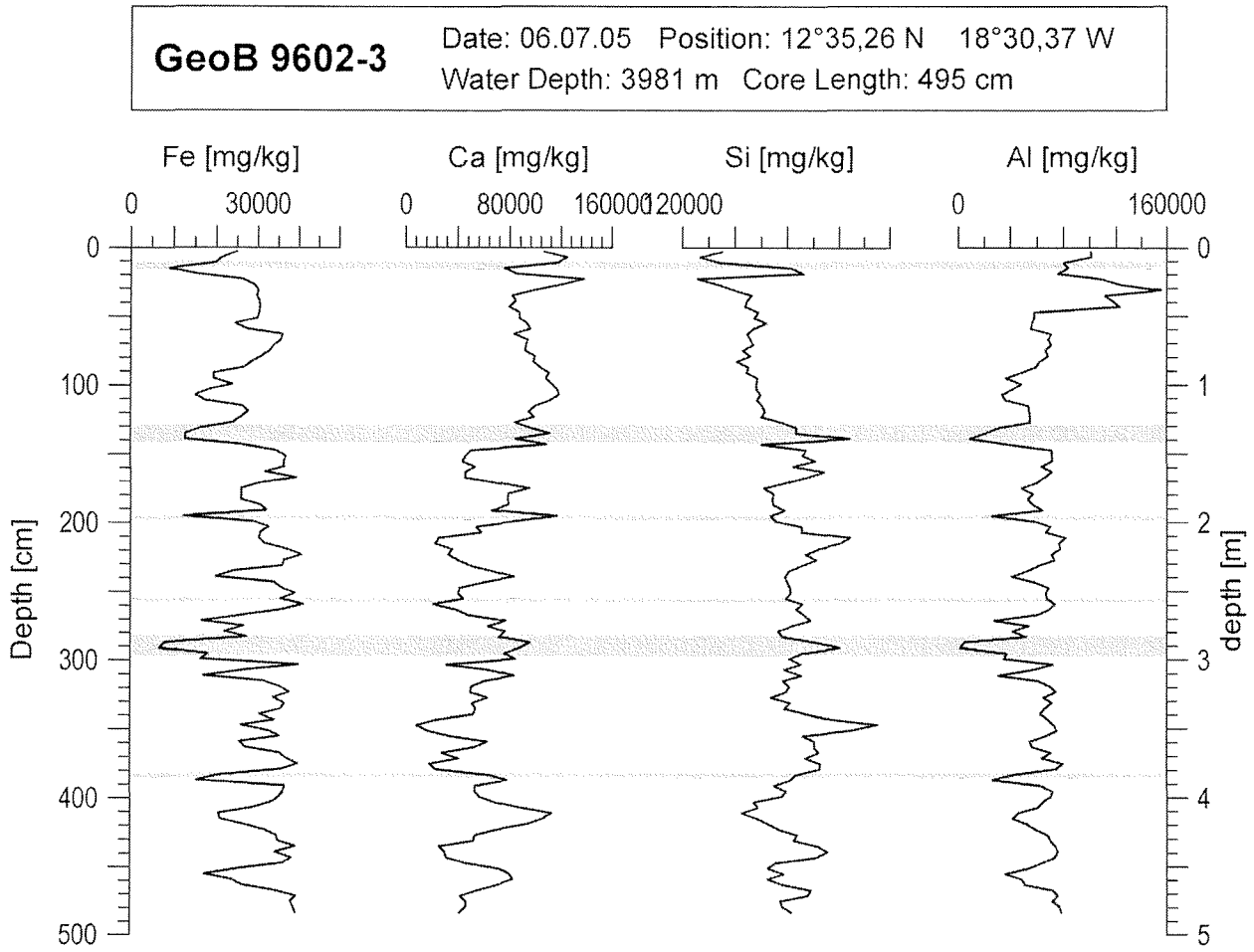

Fig. 4.5.6: Gravity corer GeoB 9602. XRF sediment element profiles of major components iron, calcium, silicium and aluminium measured onboard during cruise M65-2. The shaded areas describe turbidite layers following the sedimentological description (cf. chapter 4.3 of this report).

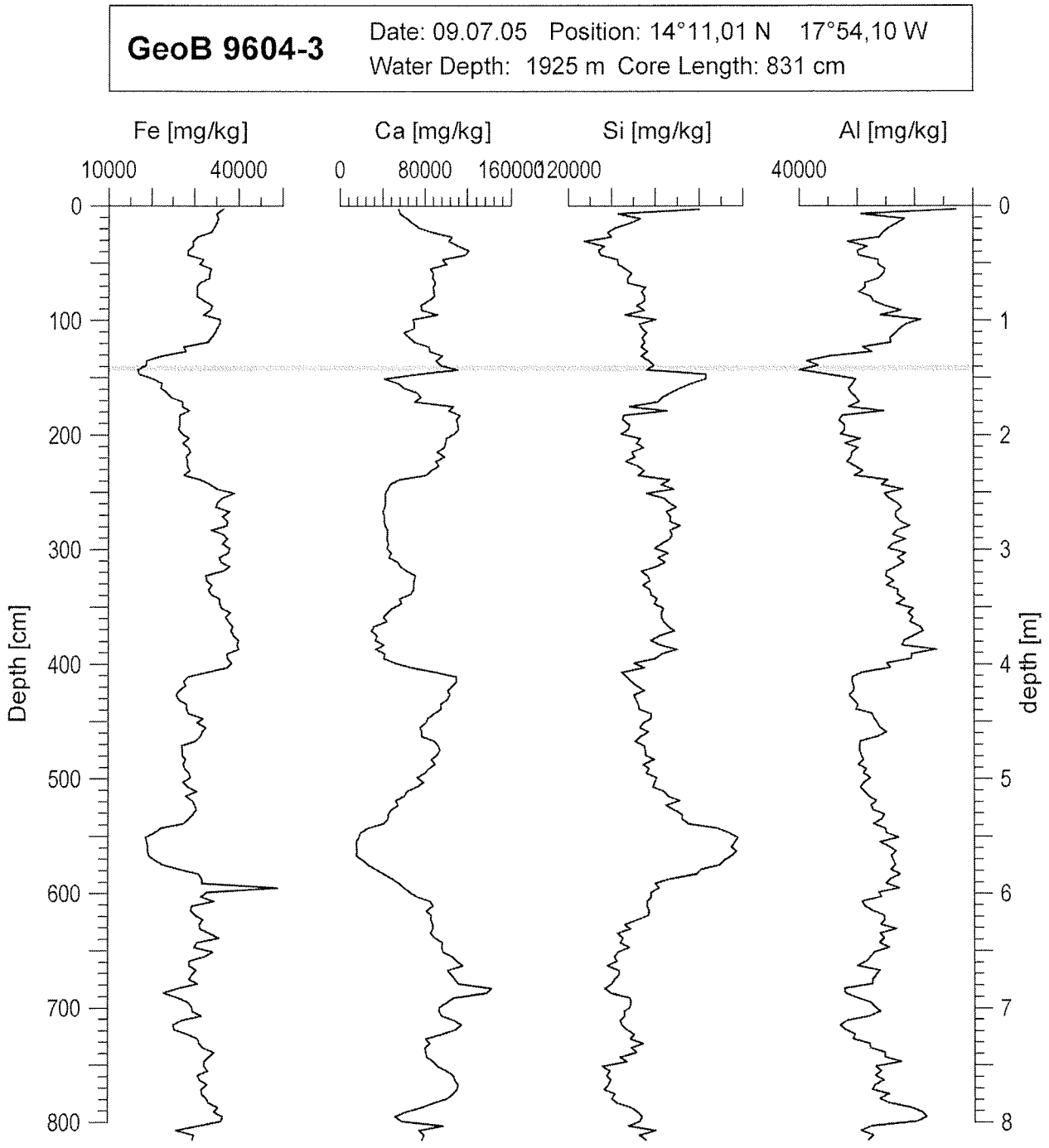

Fig. 4.5.7: Gravity corer GeoB 9604. XRF sediment element profiles of major components iron, calcium, silicium and aluminium measured onboard during cruise M65-2. The shaded areas describe turbidite layers following the sedimentological description (cf. chapter 4.3 of this report).

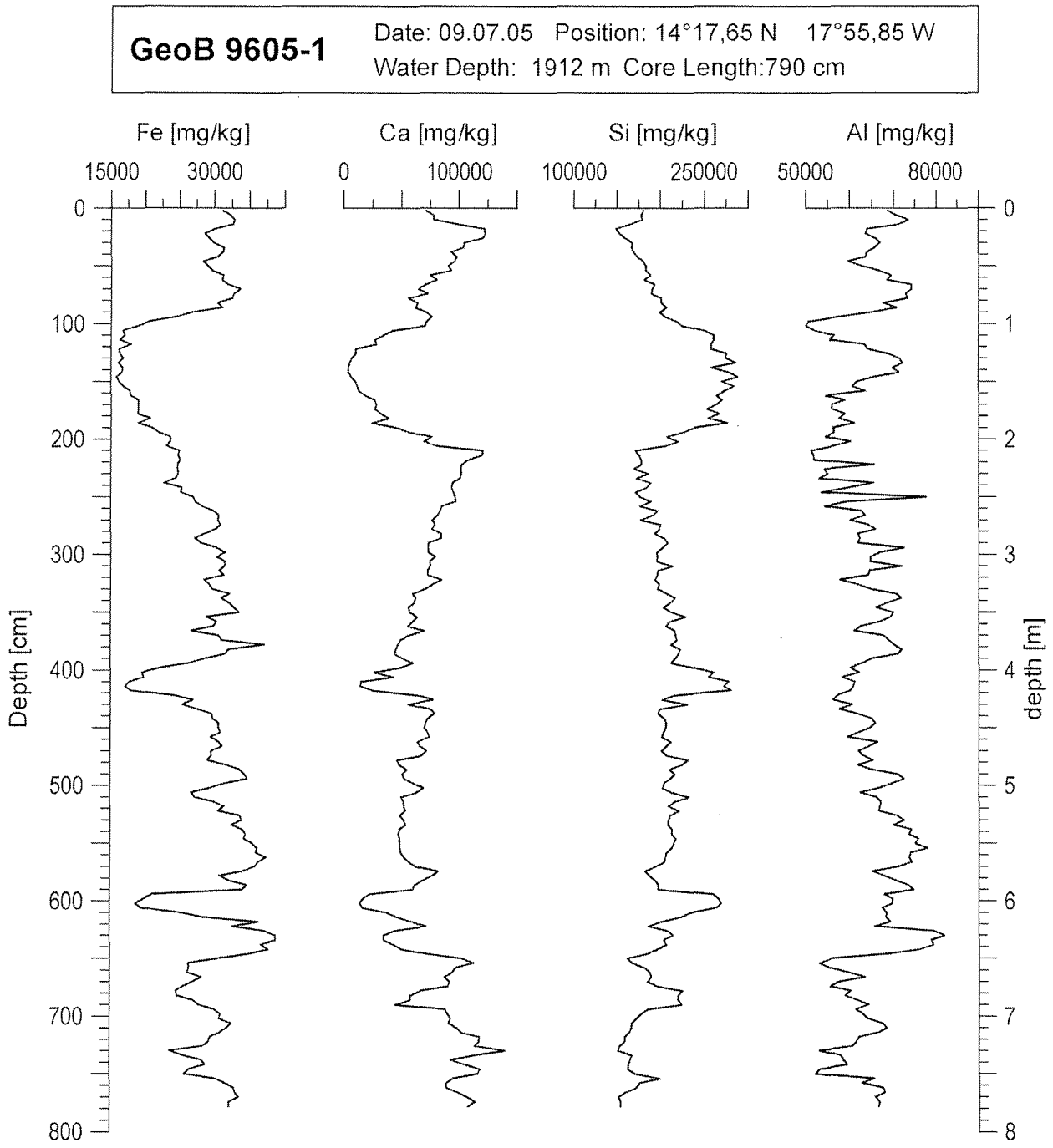

Fig. 4.5.8: Gravity corer GeoB 9605. XRF sediment element profiles of major components iron, calcium, silicium and aluminium measured onboard during cruise M65-2.

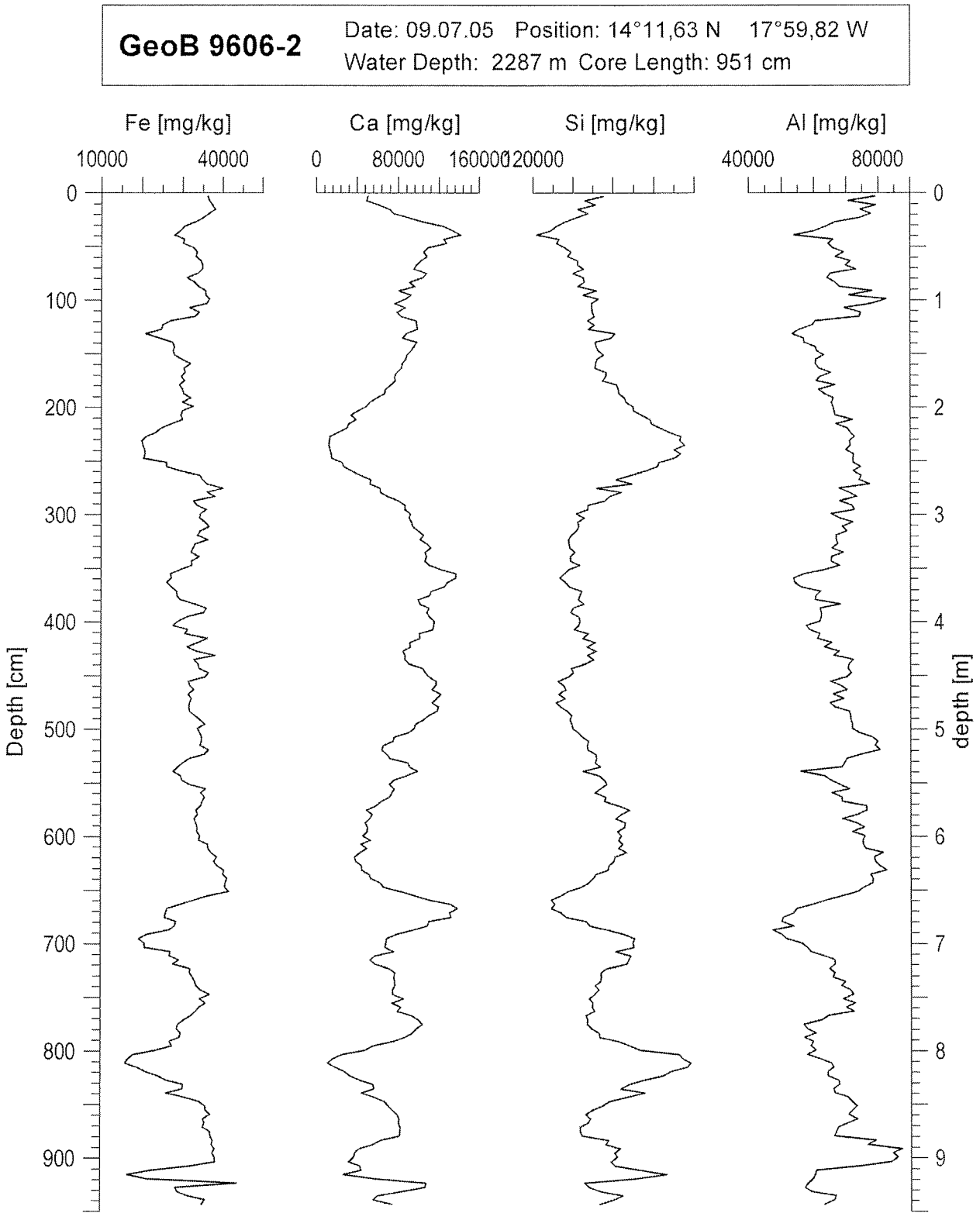

Fig. 4.5.9: Gravity corer GeoB 9606. XRF sediment element profiles of major components iron, calcium, silicium and aluminium measured onboard during cruise M65-2.

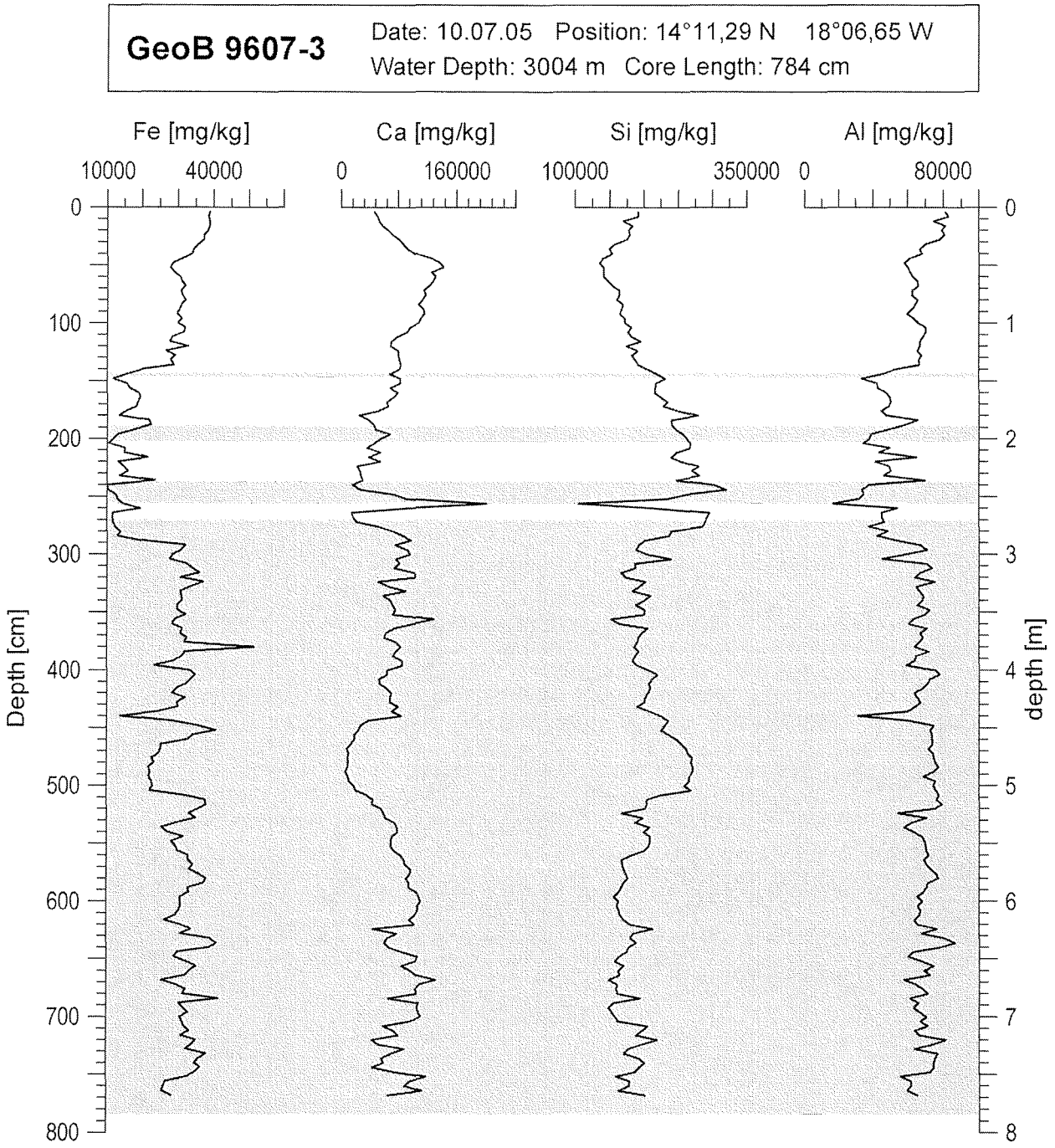

Fig. 4.5.10: Gravity corer GeoB9607. XRF sediment element profiles of major components iron, calcium, silicium and aluminium measured onboard during cruise M65-2. The shaded areas describe turbidite layers following the sedimentological description (cf. chapter 4.3 of this report).

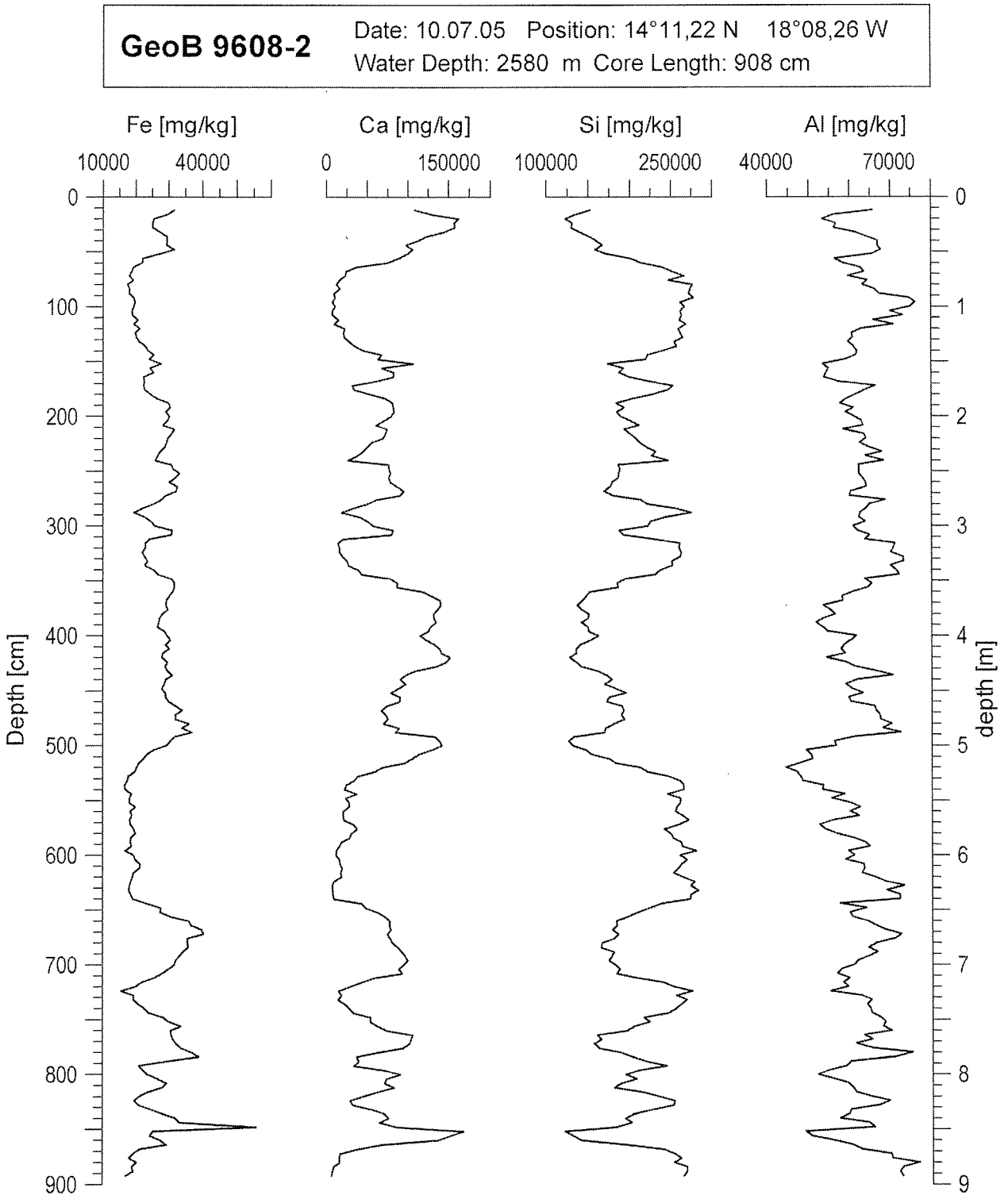

Fig. 4.5.11: Gravity corer GeoB 9608. XRF sediment element profiles of major components iron, calcium, silicium and aluminium measured onboard during cruise M65-2.

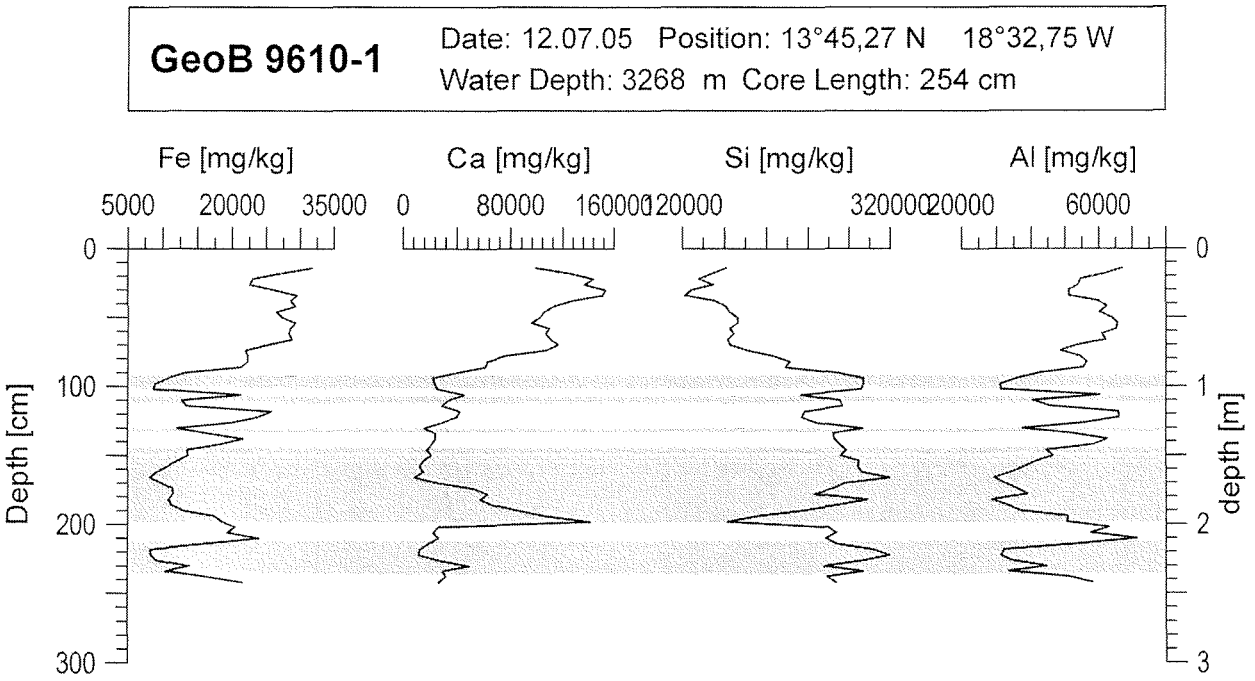

Fig. 4.5.12: Gravity corer GeoB 9610. XRF sediment element profiles of major components iron, calcium, silicium and aluminium measured onboard during cruise M65-2. The shaded areas describe turbidite layers following the sedimentological description (cf. chapter 4.3 of this report).

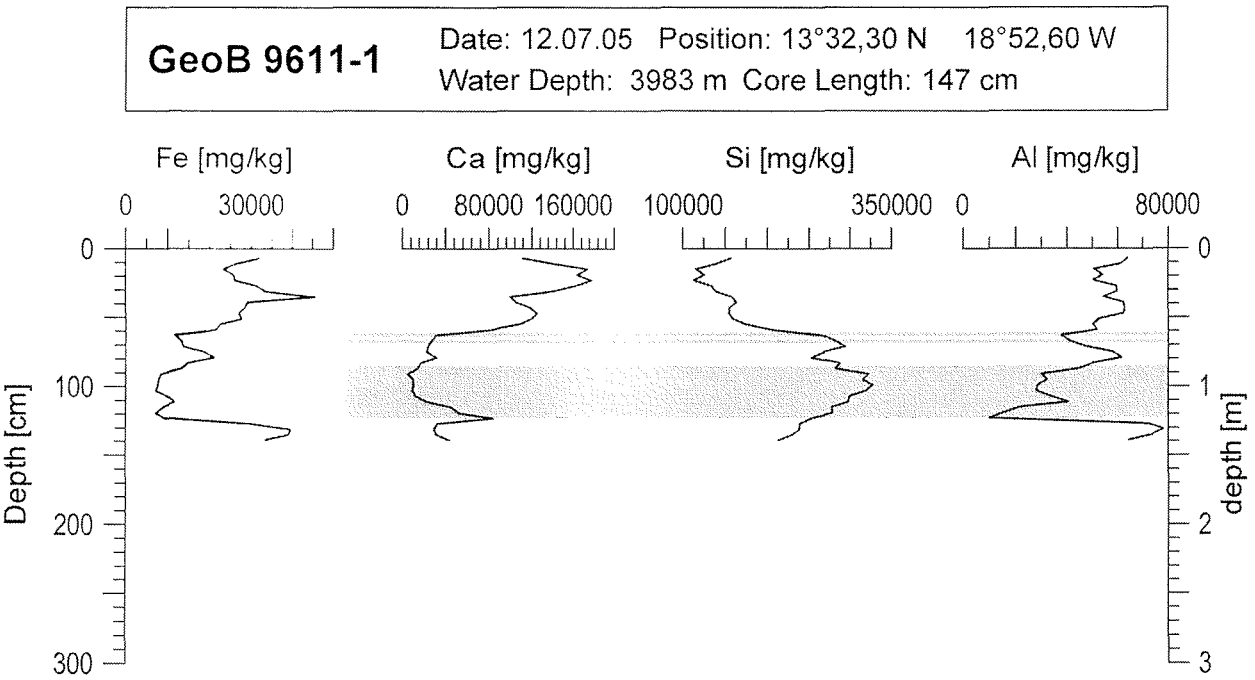

Fig. 4.5.13: Gravity corer GeoB 9611. XRF sediment element profiles of major components iron, calcium, silicium and aluminium measured onboard during cruise M65-2. The shaded areas describe turbidite layers following the sedimentological description (cf. chapter 4.3 of this report).

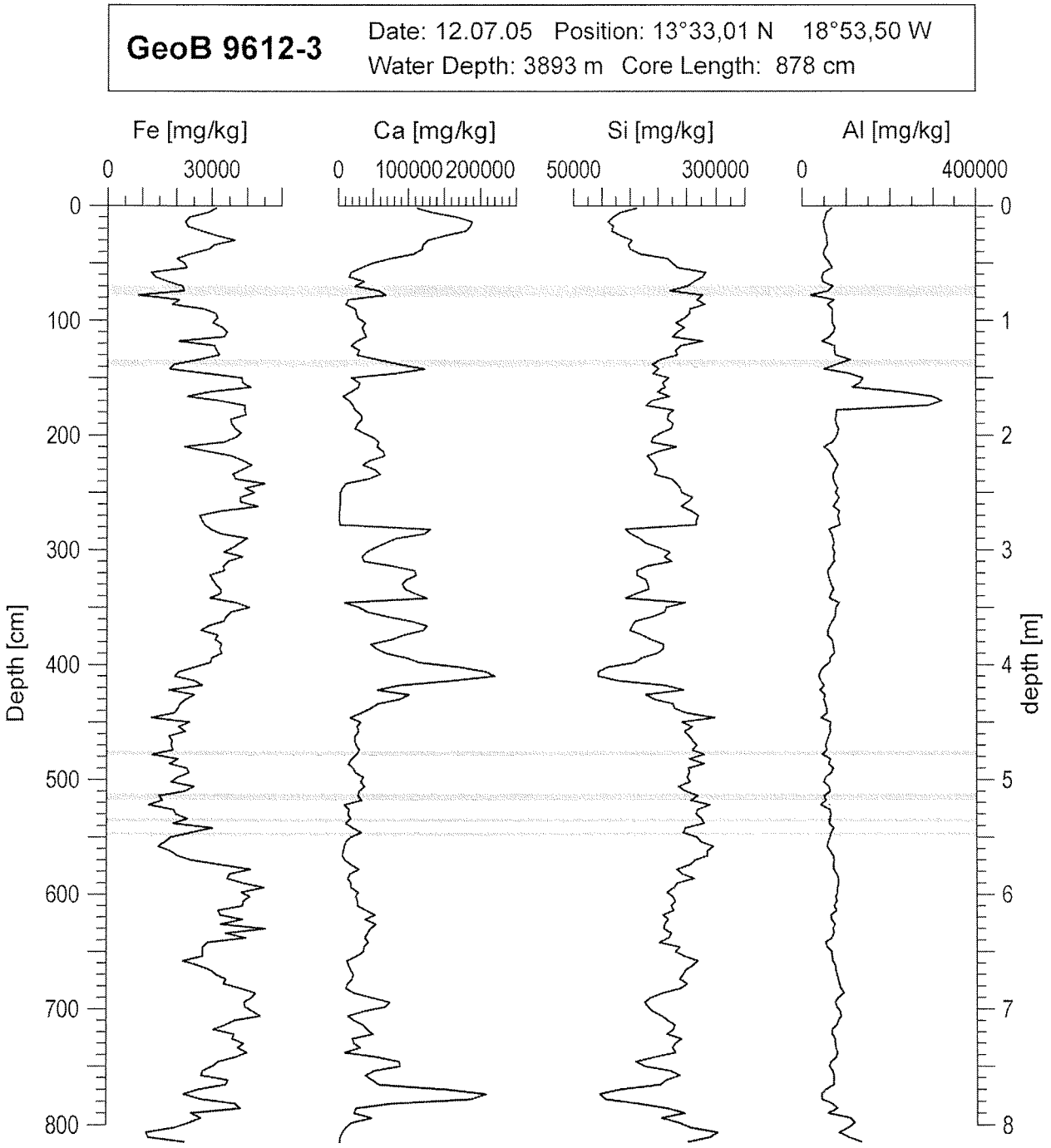

Fig. 4.5.14: Gravity corer GeoB 9612. XRF sediment element profiles of major components iron, calcium, silicium and aluminium measured onboard during cruise M65-2. The shaded areas describe turbidite layers following the sedimentological description (cf. chapter 4.3 of this report).

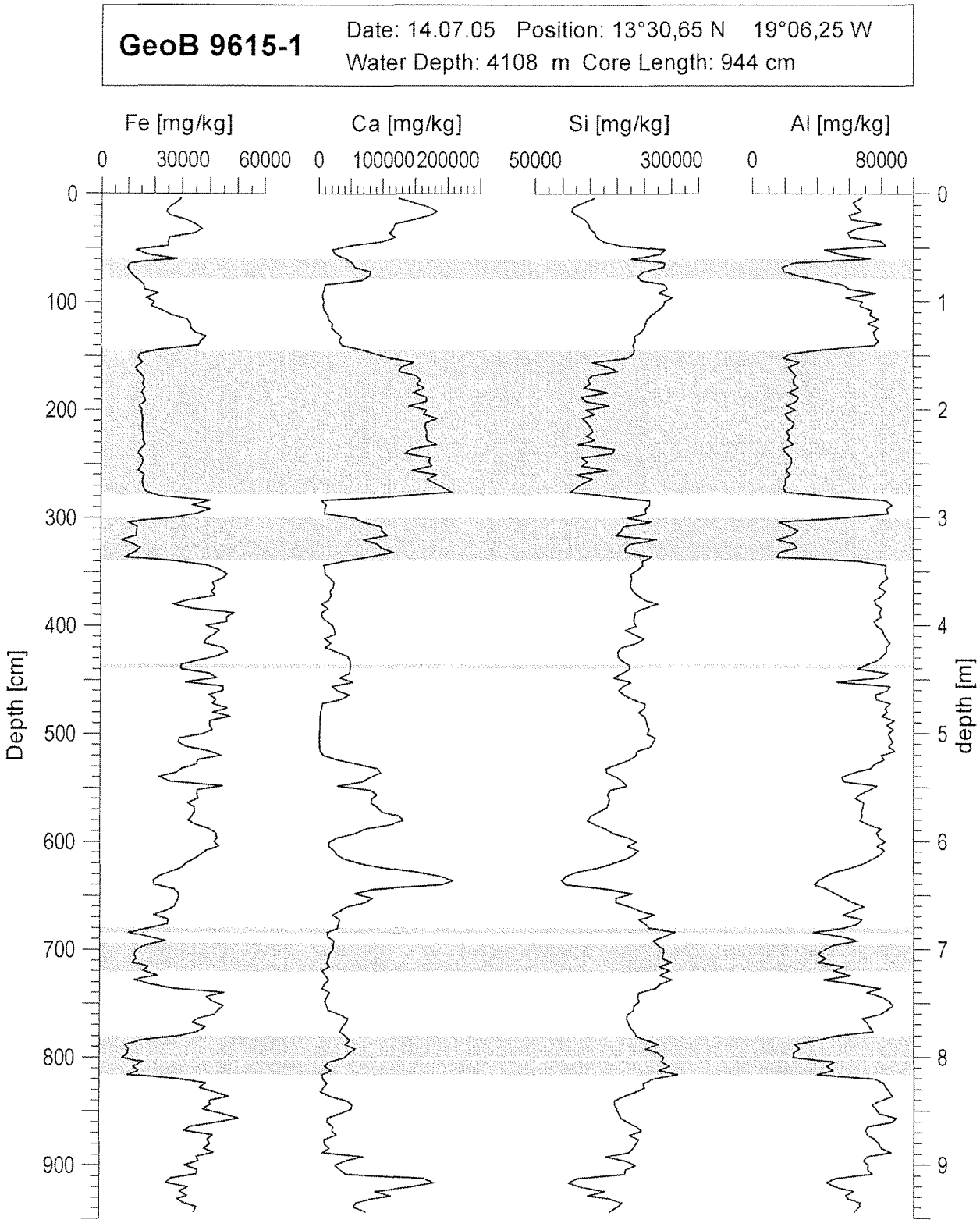

Fig. 4.5.15: Gravity corer GeoB 9615. XRF sediment element profiles of major components iron, calcium, silicium and aluminium measured onboard during cruise M65-2. The shaded areas describe turbidite layers following the sedimentological description (cf. chapter 4.3 of this report).

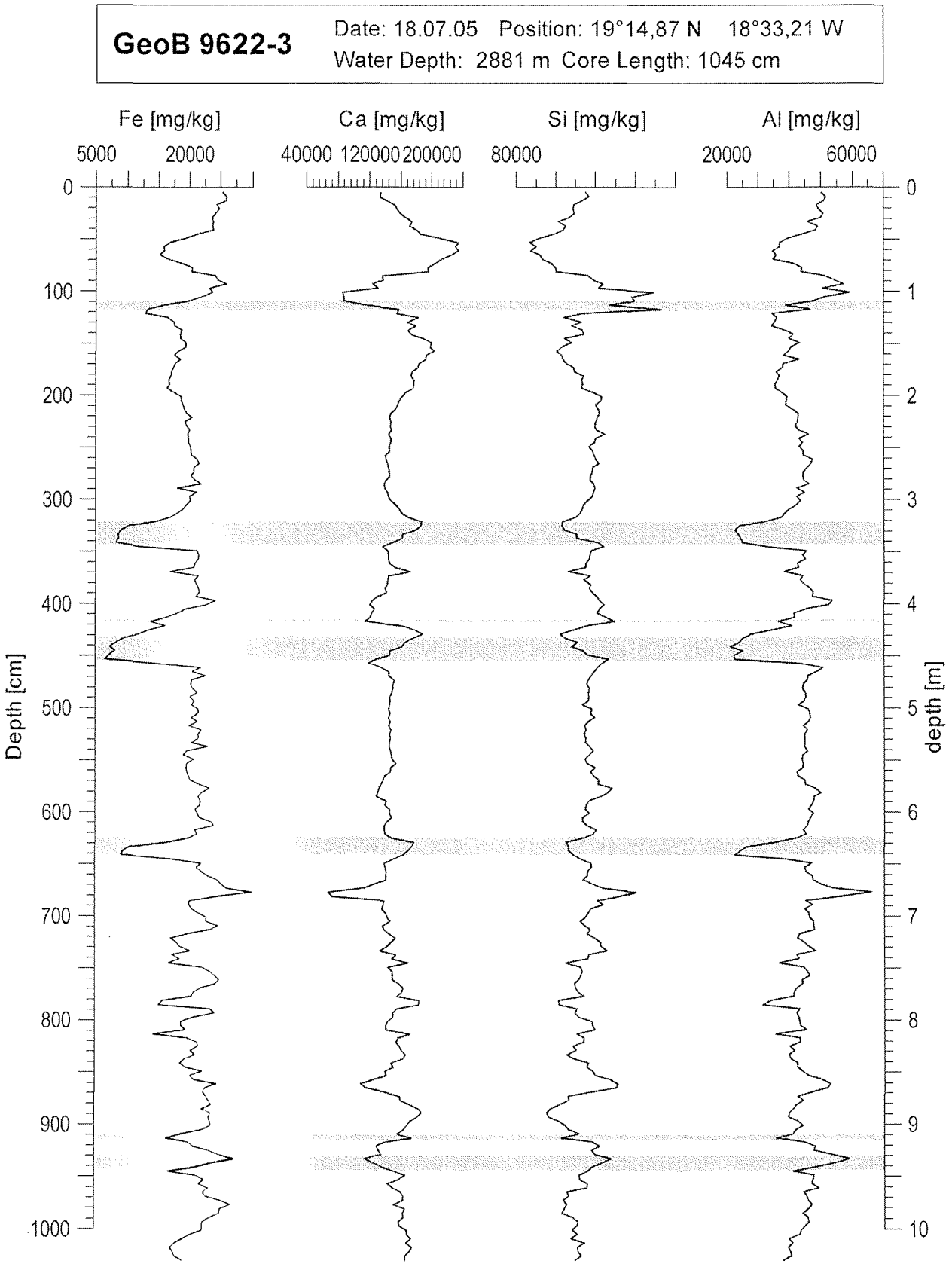

Fig. 4.5.16: Gravity corer GeoB 9622. XRF sediment element profiles of major components iron, calcium, silicium and aluminium measured onboard during cruise M65-2. The shaded areas describe turbidite layers following the sedimentological description (cf. chapter 4.3 of this report).

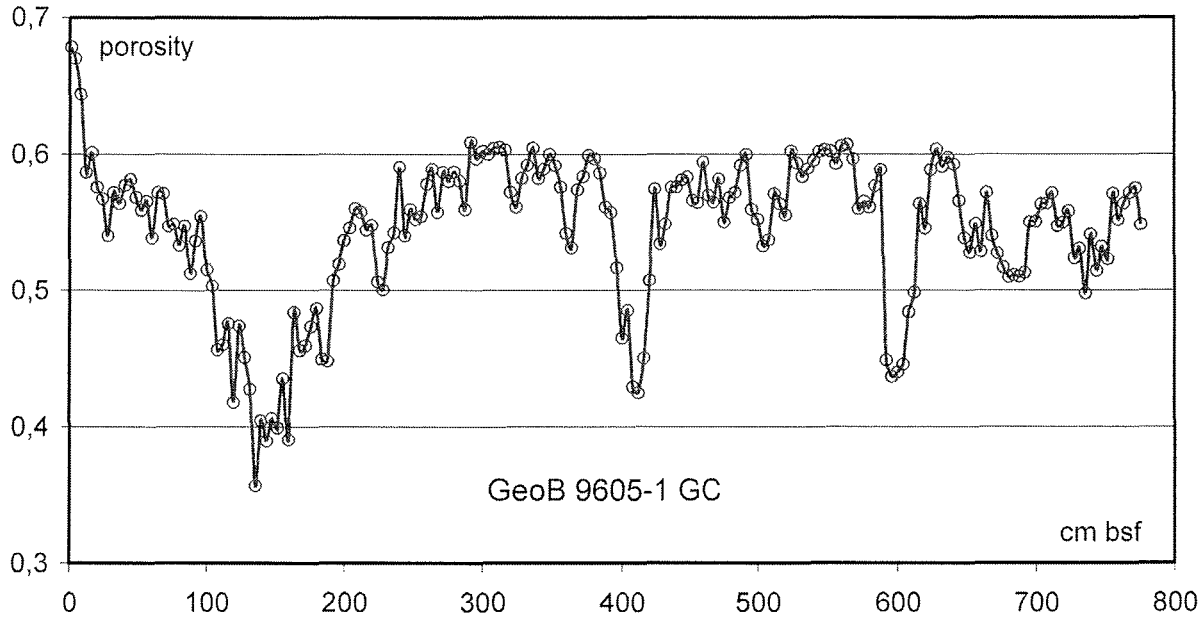

Fig. 4.5.17: Profile of sediment porosity as calculated from the chlorine profile.

Correlation of cores from different locations

The major aim of the XRF element analysis was to measure profiles of element contents, which could be used to correlate cores with other cores, for which a reliable age model was known. For this area we used already in cruise M58 especially the published age model of the core CD 53-30 (Matthewson et al., 1995), which we also transferred via the carbonat/calcium profiles to our core GeoB 7919-5. This core was also treated with the same sampling and XRF measuring technique which we used during this cruise, so that for a correlation and deducation of an age model for a new core all 22 measured elements could be used. In practise in this area especially the profiles of Sr contents were most useful for the correlation of cores. The other element profiles were in most cases only used for the verification of correlations, which were achieved via Sr profiles.

As an example fig. 4.5.18 shows a correlation between GeoB 7919-5 and the new core GeoB 9608-2. It gives the new core a maximum age of about 230 kyrs which results in a mean sedimentation rate of close to 4 cm per kyr. The correlation of this core was especially good feasible, since it did not contain any turbiditic sequences.

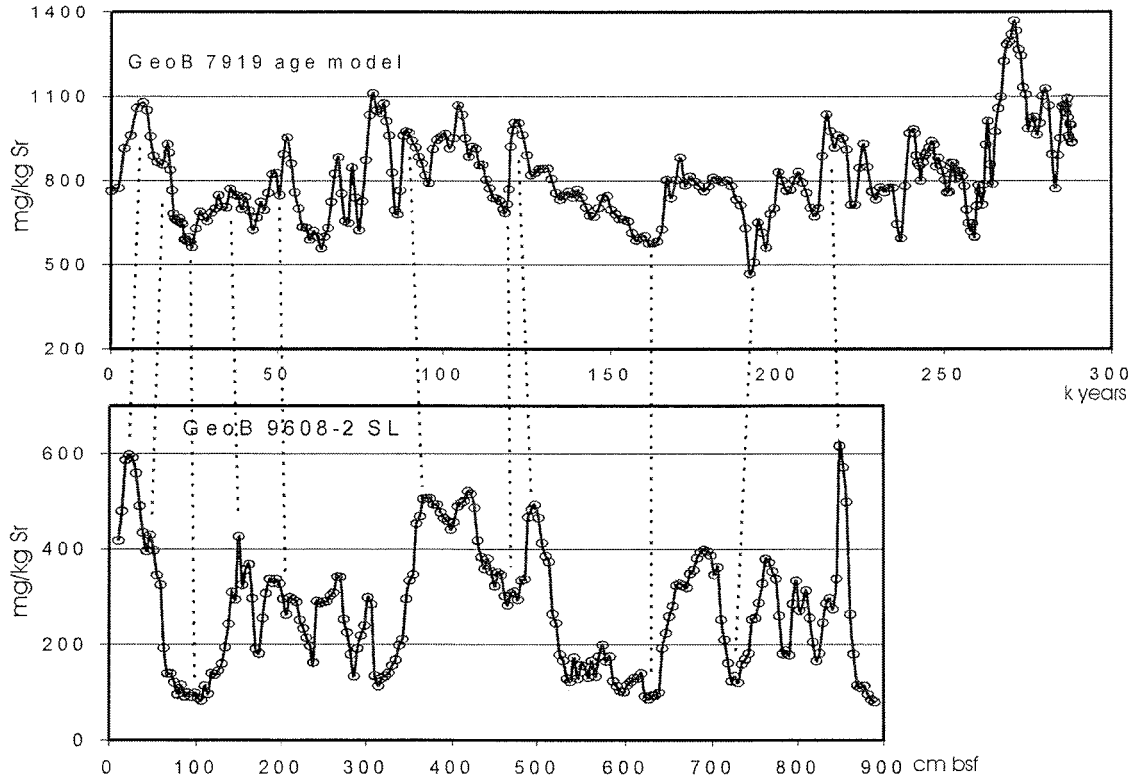

Fig. 4.5.18: Correlation with GeoB 7919-5 and deduction of an age model for cor GeoB 9608. In this case the correlation was especially easy, since the core did not contain turbidites.

More difficult are correlations with cores, which contain tubiditic sequences. With the assumption that these turbidites probably in most cases were not erosive, we cut all samples containing turbiditic material out of the data file. For this procedure we followed the core description of the sedimentology group. Since our samples always had a length of 4 cm, necessarily some of them contained in parts turbiditic material and in other parts normal (hemi)pelagic sediments. These 'mixed' samples were also taken out of the data file, accepting that thus also normal sediments were lost from the file. These parts of the core will be resampled in Bremen together with the sedimentology group, when we have a refined knowledge of the turbidite sequences.

Fig. 4.5.19 and fig. 4.5.20 show the correlations and age model for cores, from which the turbiditic sequences have been cut out. Since the depth scale of such 'turbidite free' cores is after this procedure not identical with the original depth scale of the core, these figures contain also a diagram which relates the new, turbidite free depth scale to the original depth scale of the core. In this diagram, the horizontal parts of the curve always represent the turbidites, whereas the parts with a linear rise of the curve describe the normal (hemi)pelagic sediments. Core GeoB 9612 (Fig. 4.5.19) contained only few

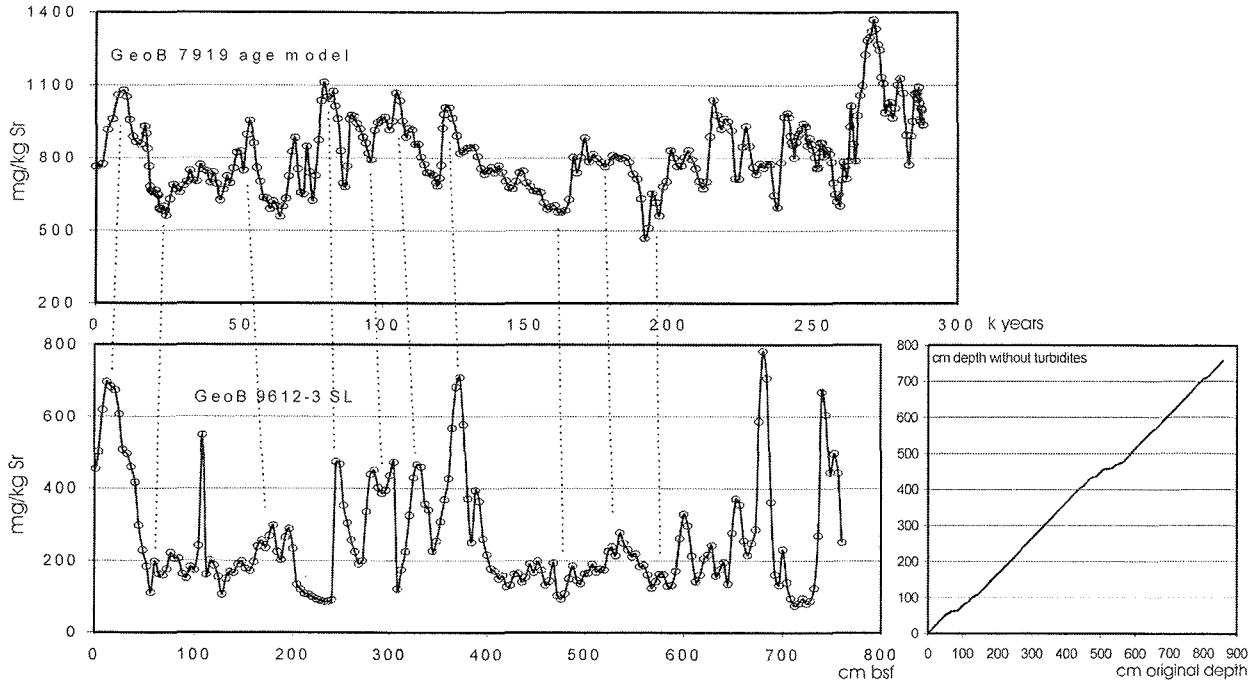

Fig. 4.5.19: Correlation with GeoB 7919-5 and deduction of an age model for cor GeoB 9612. A diagram is added, which relates the new 'turbidite free' depth scale to the original depth scale of the core. The core contained only few turbidites.

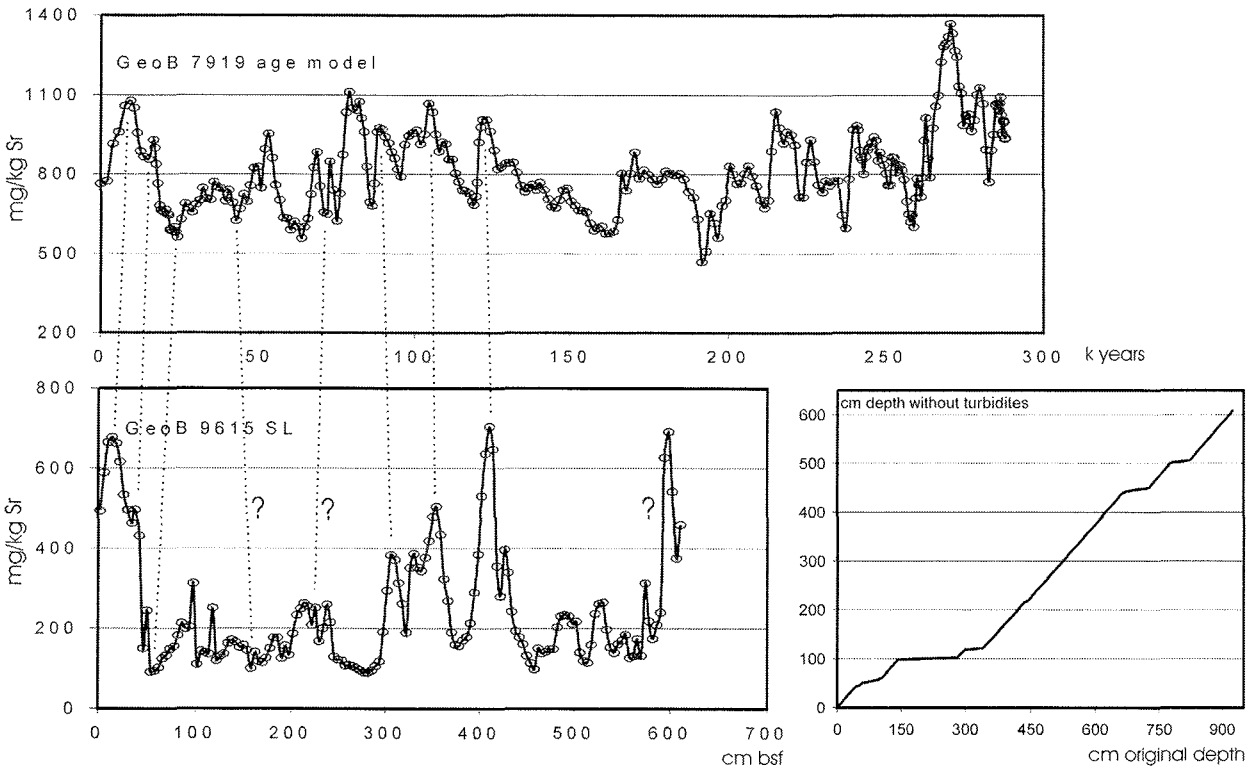

Fig. 4.5.20: Correlation with GeoB 7919-5 and deduction of an age model for cor GeoB 9615. A diagram is added, which relates the new 'turbidite free' depth scale to the original depth scale of the core. The core contained many turbidite sequences.

turbidites, which obviously had not been erosive, so that the correlation and the establishment of an age model was not very problematic. Core GeoB 9615 (Fig. 4.5.20) contained much more turbidites, which is documented by the large horizontal parts of its depth/depth diagram. However, also for this core a correlation with GeoB 7919-5 seemed to be possible, although some question marks remained in Fig. 4.5.20.

Two short cores from the thalweg of the Dakar Canyon (GeoB 9610 and GeoB 9611 in Figs. 4.5.21 and 4.4.22) are characterized by a (hemi)pelagic sedimentation in their upper 50 – 70 cm. In both cores in the lower parts the sediments of the last glacial maximum (LGM) could be reached and well documented by the Sr profiles. The very reliable age models prove that in these parts of the Dakar Canyon the turbidite activity ended around 15 – 16 kyrs bp.

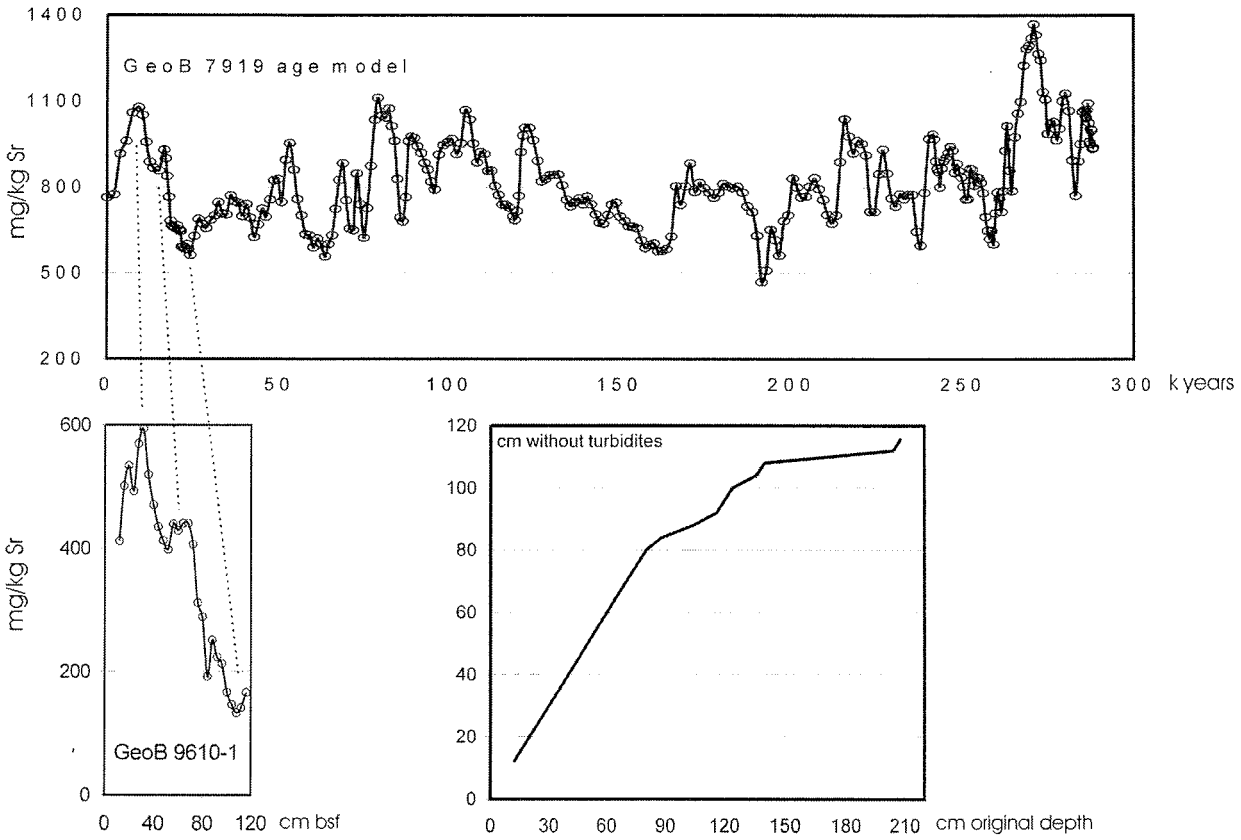

Fig. 4.5.21: Correlation with GeoB 7919-5 and deduction of an age model for cor GeoB 9610. A diagram is added, which relates the new 'turbidite free' depth scale to the original depth scale of the core. This short core from the thalweg of the Dakar Canyon contained thick turbiditic sequences especially in its lower part.

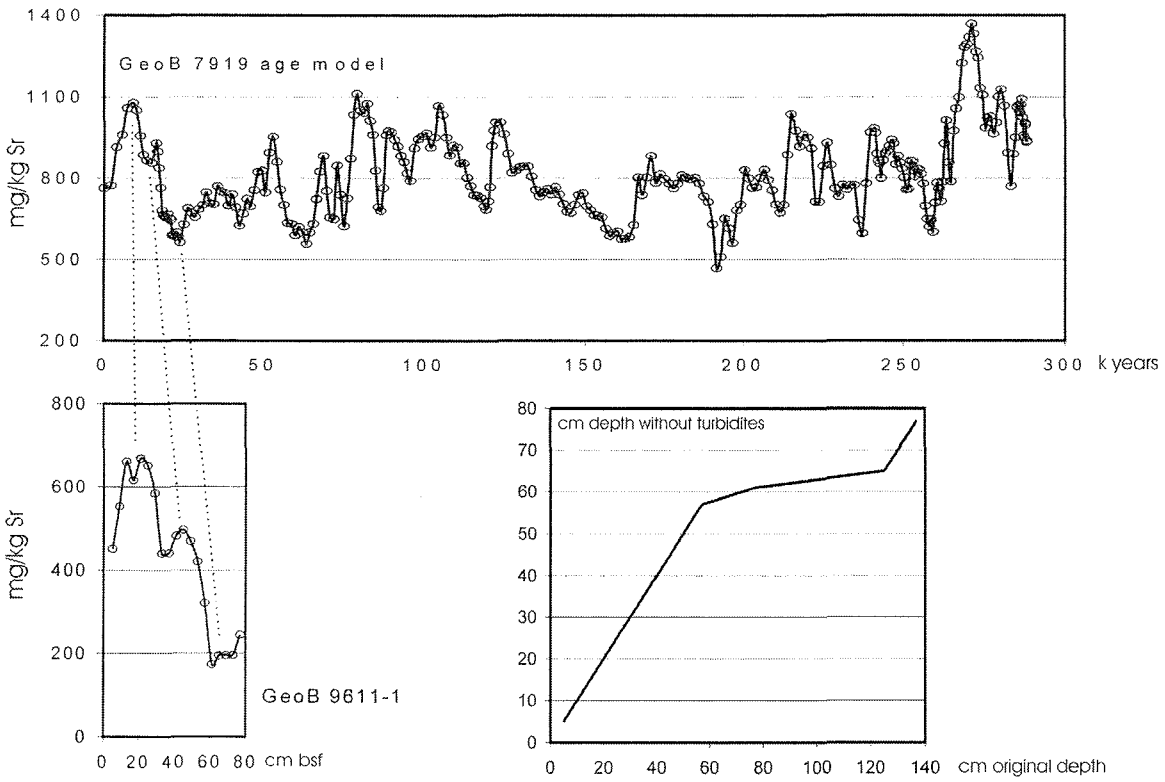

Fig. 4.5.22: Correlation with GeoB 7919-5 and deduction of an age model for cor GeoB 9611. A diagram is added, which relates the new 'turbidite free' depth scale to the original depth scale of the core. This short core from the thalweg of the Dakar Canyon contained thick turbiditic sequences especially in its lower part.

4.6 Micro-Paleontology

(M. Beld, A. Hübner)

4.6.1 Introduction

The successful use of proxy parameters in palaeoceanographic application lies in the use of species compositions of microfossils and the stable isotopes and their elemental composition. To use this constructively detailed information is needed about their transition and the imprint of environmental conditions of the Atlantic Ocean in fossil sediments has to be known. In contrast to the regions north of the research area almost no background information is available about the distribution and ecology of organic- and calcareous-walled dinoflagellate cysts in the study area.

Dinoflagellates are a diverse group of eukaryotic, primarily unicellular organisms having two distinctive flagella giving the organism a (species-) characteristic spiral motion (Fensome et al., 1993). They live in the upper part of the water column with, as result of their small size (the majority of species have sizes between 10 – 60 µm), their migration ability being limited to several meters only. Together with diatoms and coccolithophorids, dinoflagellates constitute the majority of the marine eukaryotic phytoplankton and are, therefore, important as primary producers. Organic- and calcareous-walled dinoflagellate cysts are useful tools in reconstructing paleoceanographic conditions. They can be used to obtain important information about surface water conditions such as SST, SSS, stratification of the upper water column and nutrient content (Vink et al., 2001) as well as oxygen concentrations of deep ocean bottom waters (Zonneveld et al., 2005).

Individual dinoflagellate species degrade with a different degradation rate according to a higher order degradation process (Zonneveld, 1997). This information may be used to separate the aerobic degradation signal from the productivity signal in fossil sediments. To asses the species-specific degradation constants of the individual cyst species, it is essential to possess information about the degradation rates of the cysts in relation to the exposed oxygen concentration, oxygen exposure time (sedimentation rates) and bio productivity in the upper water column.

The isotopic composition of the wall of the calcareous dinoflagellate cyst Thoracosphaera heimii reflects the temperature conditions of the upper water column where it is formed; the deep chlorophyll maximum. The wide geographic and stratigraphic distribution of T. heimii cysts in sediments, the stable position of this cyst within the water column and the high resistance of T. heimii against calcite dissolution

emphasize its potential for a wide usability in paleotemperature reconstructions (Zonneveld, 2003). To use the stable isotope composition of calcareous dinoflagellate cysts T.heimii to estimate the role and influence of tropical surface water masses as well as the variability of the intermediate and deep water circulation of the region on climate change, detailed information of the cyst distribution in surface sediments, surface waters as well as the isotopic composition of T.heimii cysts in situ, is required.

The objectives to be addressed during Leg 65-2 are:

- Compare the stable isotopic composition of the calcareous din cyst T. heimii and stable isotopes of the water-mass in which the cysts are formed

- Determine species-specific degradation rates of organic walled dinoflagellate cyst species.

- Establish a relationship between the geographic distribution of organic- and calcareous dinoflagellate cyst in modern sediments in relation to environmental conditions in de upper water column.

- Set-up of a 'degradation-experiment' in the Atlantic ocean focussing on how digenesis alters the signal of organic temperature- and productivity proxies.

4.6.2 Multicorer

To assess these scientific questions 11 multi cores and 5 box cores have been collected (Tabs. 4.6.1, 4.6.2). The surface sediments (0-1 cm) have been collected and have been stored in dark 125 ml NALGENE HDPE bottles together with bottom water. The lower part of the core has been collected to carry out high resolution studies and sediments will be used to establish unicellular cultures at the University of Bremen. Culture material will also be used to determine the organic bio-molecular character of the cyst walls of individual cyst species. During the cruise water and surface sediments were scanned for living cyst in order to create cultures.

Table 4.6.1. Multi core data

MUC Nr.	Date	Ground contact [UTC]	Geographic Position (N)	(W)	Water depth [m]	Length of the core [cm]	°C of water	Notes
9601-2	04.07.05	20.46	14°27.79	17°57.01	1924	24	11.1	Top sediment layer was one day in container at 5°C
9602-2	06.07.05	18.34	12°35.27	18°30.39	3988	36	10.0	Both in freezer
9605-2	09.07.05	19.58	14°17.60	17°55.80	1915	30	9.6	Both in Freezer
9606-1	09.07.05	22.37	14°11.61	17°59.81	2286	34	9.6	Both in freezer
9607-2	10.07.05	10.18	14°11.23	18°06.63	3000	48	8.0	Both in freezer
9608-3	10.07.05	18.10	14°11.18	18°08.28	2590	38	8.3	Both in freezer
9609-1	10.07.05	20.48	14°11.32	18°05.62	2776	37	8.5	Both in freezer
9612-2	12.07.05	19.14	13°32.98	18°53.50	3922	10	10.2	One small core, MUC problem
9621-2	17.07.05	16.01	19°39.37	16°56.37	53	32	20.1	Both in freezer
9622-2	18.07.05	04.45	19°14.87	18°33.20	2878	40	8.5	Both in freezer
9624-2	20.07.05	13.09	20°30.64	20°39.53	3890	10	13.4	One large core, MUC problems

Table 4.6.2. Box core data

Box core Nr.	Date	Ground contact [UTC]	Geographic Position (N)	(W)	Water depth [m]
9616-1	16-07-05	10.12	20°03.31	17°32.96	90
9617-3	16.07.05	11.50	20°05.32	17°32.15	80
9618-1	16.07.05	12.37	20°04.79	17°33.08	90
9619-1	16-07-05	13.16	20°05.16	17°34.06	84
9620-2	16.07.05	14.10	20°06.88	17°34.01	90

4.6.3 Water Sampling

To isolate T. heimii from the deep chlorophyll maximum water samples were taken (Tab. 4.6.3, Figure 4.6.1) to measure the δ13 C and δ18O values of the surface water and the calcareous dinoflagellate cysts using a 180 litre Rosette (Fig. 4.6.2) and CTD to estimate the chlorophyll maximum at all water depths. The water that was taken from the upper thermo cline with the Rosette was filtered over a 100, 75 and 20 µm sieve and a filter with mesh size of 10µm. The material in the size fraction between 20 µm and 10µm (mostly T. heimii) was dried and stored for further analysis at the University of Bremen.

Table 4.6.3: Rosette water samples

sample	Date	Time [UTC]	Geographic Position (N)	(W)	Water depth [m]	Water sample depth [m]	Water-temp. [°C]	Salinity [^{0}/oo]	Vol. [L]
9601-4	04.07.05	19.35	14°27.58	17°57.00	1924	60	17.53	35.81	170
9603-1	06.07.05	00.42	12°34.02	18°30.10	4090	40	20.18	35.85	180
9604-1	09.07.05	15.00	14°11.14	17°54.05	1927	50	21.55	36.10	180
9608-1	10.07.05	14.41	14°11.24	18°08.25	2589	60	19.18	36.03	180
9612-1	12.07.05	17.08	9608-1	18°52.70	3956	47	20.02	36.01	180
9617-1	16.07.05	11.30	20°05.32	17°32.17	80	10	22.29	35.87	180
9620-1	16.07.05	14.00	20°06.89	17°34.07	92	10	24.10	36.13	180
9621-1	17.07.05	15.35	19°39.37	16°56.37	53	7	23.41	35.88	180
9622-1	18.07.05	03.12	19°14.85	18°33.19	2879	40	16.90	36.09	180
9623-1	21.07.05	06.17	20°30.48	20°40.06	3940	40	20.86	36.12	180
9629-4	22.07.05	13.39	21°18.96	20°46.34	4174	45	18.59	35.77	170
9630-4	23.07.05	11.05	20°44.17	18°42.64	2735	30	20.01	35.93	180

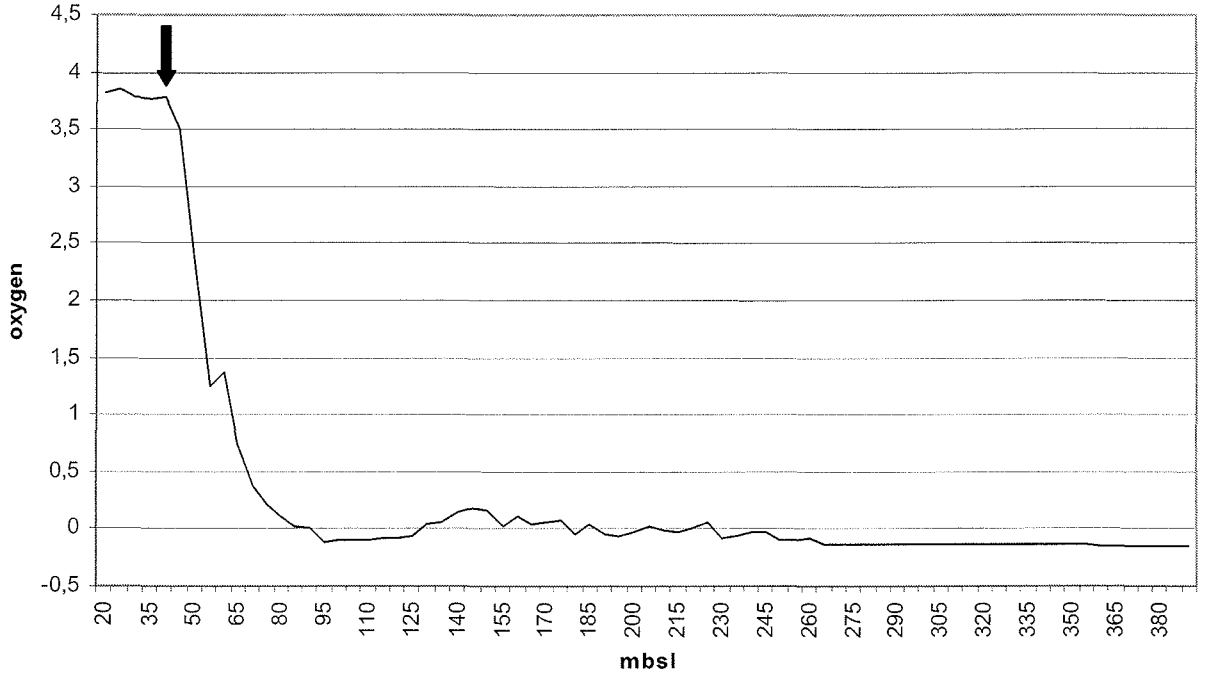

Figure 4.6.1: Station 9604. Example of oxygen content of Atlantic ocean water. Oxygen minimum zone and thus chlorophyll maximum at 50 mbsl (not yet calibrated).

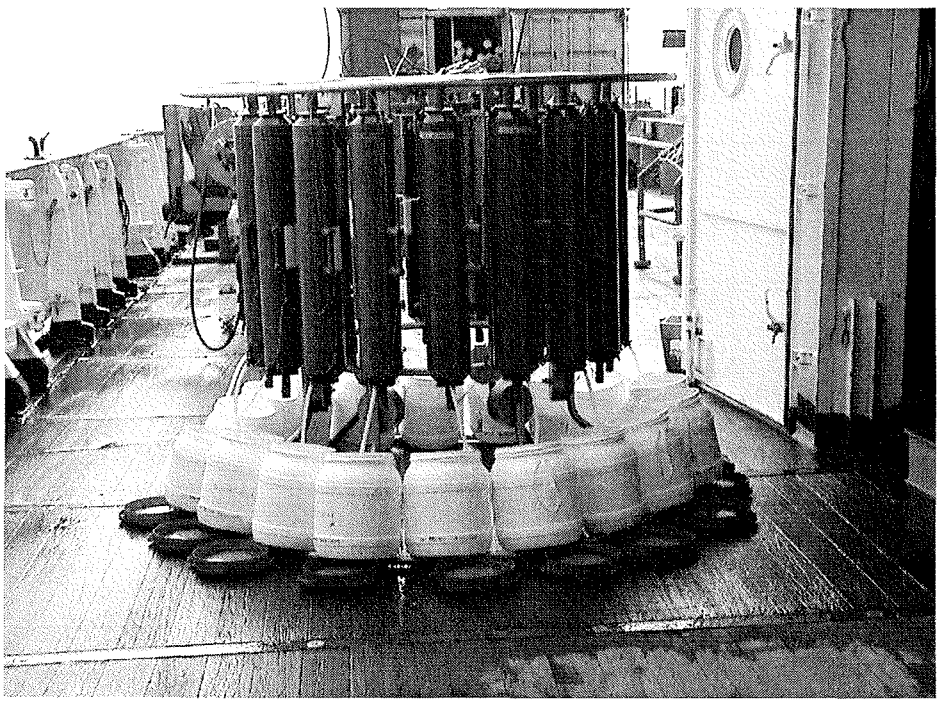

Fig. 4.6.2: The 180 litre Rosette.

4.6.4 Degradation experiment

Sediment derived from the oxygen minimum zone on the shelf of Walvis Bay in Namibia were placed on both moorings deployed during Meteor-Cruise M65/2 (see section 4.7.1) in the Atlantic water masses offshore NW Africa, characterized by different oxygen concentrations ranging from oxygen-poor till oxygen-rich. The collected sediment is recently produced and therefore with minimal digenesis. The objective is to examine how different organic productivity and temperature proxies give a varying signal to changes in degradation. Changes in Tex 86, the amount of dinoflagellates and chemical proxies will be studied. Previous studies show that in oxygen-rich water Protoperidiniums spp. degrade from the sediment, while sediment placed in oxygen-poor water show no changes in dinoflagellate abundance.

This experiment can be used to study the degradation rate of the individual dinoflagellate species and use them as a proxy to determine the oxygen concentrations of bottom-water masses in the past.

4.7 Particle transport and fluxes off Cap Blanc (Mauretania)

(N. Nowald, C. Reuter, G. Fischer)

4.7.1 Particle fluxes measured with sediment traps

One aim of this part of the cruise was to recover and redeploy the moorings CB-15/16 located about 200 nm off Cap Blanc (Mauretania) This mesotrophic study site operated since 1988 is located in the outer part of the Cap Blanc filament in about 4100 m water depth. Another mooring named CBi-2 was deployed during a RV POSEIDON cruise 80 nm further to the east; this system was also planned to be exchanged. This eutrophic study site is close to DSDP site 658 in the coastal upwelling off Mauretania in about 2700 m water depth. Both sites CB and CBi are influenced by the NE trade winds being part of the North Atlantic climate system. They are characterized by enhanced supply of terrigenous material, mainly dust particles. The spatial and temporal distribution of productivity and biomass and the supply of dust particles to the ocean will be monitored by satellite imagery (SeaWiFS, MODIS) and shall be compared to the patterns of deep ocean particles fluxes.

The data of deployments and recoveries of the moorings are listed in Table 4.7.1 together with the sampling data of the traps. On July 22, we successfully recovered mooring CB-15 which was deployed by RV POSEIDON in April 2004. It was redeployed as CB-16 with a similar configuration. CB-15 provided two complete sample sets of each 20 cups showing relatively low fluxes at both trap levels and lower seasonality compared to most records of the previous years. In the early morning of July 23, we recovered the 1500 m long mooring array CBi-2 in the coastal part of the Cap Blanc filament which was equipped with two traps and one current meter. A mooring with similar configuration was redeployed in the afternoon of the same day. We obtained two complete sets of sediment trap samples. First estimates of particle fluxes show much higher fluxes and a stronger seasonality at this site compared to the more open-ocean site CB. Particle fluxes from the year before (site CBi-1) reached values of almost 1000 mg m^{-2} d^{-1} in winter and springtime being about twice as high compared to site CB-14. This fits to the general pattern of primary production and biomass distribution taken from the SeaWiFS or MODIS sensors. It is planned to recover and redeploy both mooring arrays with RV POSEIDON in early fall 2006.

Table 4.7.1: Data for recoveries and redeployments of the sediment trap mooring arrays during M65-2.

Mooring	Position	Water depth (m)	Interval	Instr.	Depth (m)	Intervals (no x days)
Mooring recoveries						
Cap Blanc mesotrophic:						
CB-15	21°17,9' N	4162	17.04.04-	SMT 230	1246	20 x 23
	20°47,8' W		21.07.05	SMT 234	3624	20 x 23
				RCM 8	1269	
Cap Blanc eutrophic:						
CBi-2	20°44.7' N	2714	18.04.04-	SMT 230	1296	2 x 22, 18x 23
	18°42.1' W		20.07.05	SMT 230	1876	2 x 22, 18x 23
				RCM8	1320	
Mooring deployments						
Cap Blanc mesotrophic:						
CB-16	21°16.85'N	4160	25.07.05-	SMT 230	1205	20 x 21.5
	20°47.80'W		26.09.06	SMT 230	3633	20 x 21.5
				RCM 8	1258	
Cap Blanc eutrophic:						
CBi-3	20°45.55'N	2693	25.07.05-	SMT 230	1277	20 x 21.5
18°41.85'W		26.09.06	SMT 234	1855	20 x 21.5	
				RCM8	1320	

Instruments used:
SMT 230 = Titanium particle sediment trap 243, Aquatec Meerestechnik, Kiel
RCM 8 = Aanderaa current meter, RCM 8

4.7.2 Particle distribution measured with optical systems (ParCa)

The photographic particle camera system ParCa was deployed at 3 sites for the in-situ measurement of the vertical size distribution and concentration of particulate matter in the ocean. The system was designed and improved in consideration of similar systems used by Honjo et al. (1984) or Asper (1987). ParCa consists of a modified Nikon Coolpix 995 digital camera with adapted software. A strobe fires a collimated light beam of 12 cm width, illuminating a sample volume of 0,007 m^3. Power Source is a 24V/38 Ah rechargeable lead battery designed for the use to full ocean depth. ParCa can operate in depths down to 3000 m and all devices are mounted in a 200 kg galvanised frame. Communication with the ship is done by a microcontroller and an additionally installed SeaBird telemetry unit, providing full control of the entire system via the ships coaxial wire. ParCa was deployed together with a SeaBird SBE 19 CTD. Datasets are extracted from the images using a digital image analysis software. The aim of the deployments was to continue the optical measurements in the region off Cap Blanc/NW-Africa, carried out since 2001. Camera profiles acquired at the mooring sites CB-i (GeoB 9630) and CB (GeoB 9629) (Fig. 4.7.1 a-b) are presented here.

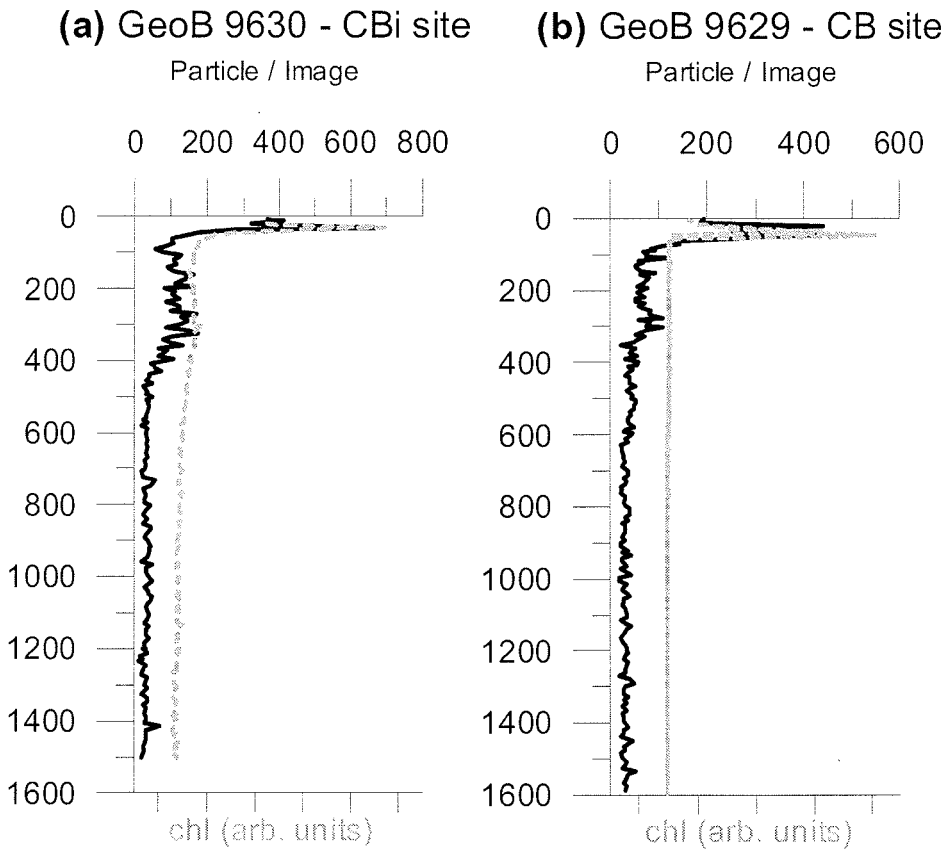

Fig 4.7.1 a-b: Particle abundance and chlorophyll maxima (dashed line) at sites GeoB 9630 and GeoB 9629.

Profile GeoB 9630

Highest particle concentrations in the surface water are seen at the coastal near site GeoB 9630 (Fig. 4.7.1a). A distinct particle maximum is observed at 30 m water depth, reaching values of almost 700 particles/image. Below this maximum, the concentration of particulate matter decreases rapidly down to 100 particles/images at a depth of 70 m. Between 70 m and 400 m depth, concentrations remain almost constant around 100 particles/image. At 400 m, another decrease in the particle concentrations is observed. The abundance of particulate matter decreases down to 50 particles/image. No significant changes in the particle abundance are seen in the water column below. The chlorophyll concentration profile follows the concentration curve of the particle abundance well. The particle maximum at 30 m, coincides with the chlorophyll maximum in the same depth. The rapid decrease in the particle concentration between 50 m and 70 m is likewise seen in the chlorophyll measurements. The second decrease in the particle concentrations around 400 m, again matches the chlorophyll concentration decrease.

Profile GeoB 9629

The concentration profile of site GeoB 9629 (Fig. 4.7.1b) looks very similar to that of GeoB 9630. Two particle maxima are seen at 20 m and 50 m depth, reaching values of around 440 particles/image. Particle abundance decreases rapidly from 440 particles/image at 50 m, down to 80 particles/image at 90 m. Another decrease in the particle abundance from 80 particles/image to 50 particles/image is seen at 350 m water depth, with no changes in the abundance of particulate matter below this depth. While the particle concentration profile shows a maximum at 20 m depth, no similar chlorophyll maximum is seen at the same depth. However, the second particle maximum at 50 m depth coincides with the chlorophyll maximum. Below 60 m water depth, the chlorophyll concentrations remain constant down the remaining profile.

4.7.3 CTD-O_2-chlorophyll-fluorescence probe

Thirteen CTD/O_2/chlorophyll-fluorescence profiles were taken with a self-contained SEABIRD SBE-19 profiler equipped with a conductivity-temperature-depth probe plus oxygen sensor and a CHELSEA-fluorometer. The sensors were calibrated prior to the cruise by the manufacturer except the CHELSEA-fluorometer. The chlorophyll-fluorescence probe was used to detect the chlorophyll maximum (for the sampling of dinoflagellates); absolute values could not be derived. At the sediment trap mooring sites, however, we took water samples for the classical determination of chlorophyll (see chapter below) to obtain information about the absolute values. The calibration coefficients from the calibration have been used to process down- or upcast data on board shortly after data retrieval. However, the oxygen values seem to be much too low (around 1.5-2.0 ml/l) due to alteration of the membrane. Using a sampling rate of 2 samples/dbar, the CTD was deployed 10 m above the rosette (ROS) or the particle camera (ParCa) (Table 4.7.2). Profiles with the CTD were taken between 150m and 2000 m depth. The raw data were recovered on board and standard plots (mostly upcast plots) were immediately produced to evaluate the stratification of the water column and the depth of the chlorophyll maximum.

The profiles show a chlorophyll maximum mostly in the depth range of 40-50 m (see also Fig. 4.7.1) which was within the upper thermocline in the tropical-subtropical open ocean off Senegal and The Gambia. These maxima also generally coincided with the decline of the oxygen content, that means they were located within the nutricline. The deepest chlorophyll fluorescence maximum with about 70 m water depth was obtained

at site 9608 within the deeper part of the major shallow thermocline. Only at the two coastal upwelling sites 9617 and 9621 off Mauretania, a shallow chlorophyll maximum between 0 and 15 m water depth was recorded in the non-stratified water column. At the mesotrophic mooring site CB, the chlorophyll maximum was located between 35 and 45 m water depth in the upper thermocline, pycnocline and nutricline. There, oxygen was relatively low between 100 and 600 m water depths. At the more coastal site CBi, the chlorophyll maximum was slightly shallower at about 30 m.

Table. 4.7.2: List of CTD-O_2-chlorophyll-fluorescence profiles taken during M65-2 (ROS=rosette, water sampler; ParCa=particle camera)

Station GeoB	water depth (m)	profile depth (m)	attached to...	remark
9601-1	1924	150	ROS	
9602-1	3977	400	ROS	
9603-1	4087	400	ROS	
9604-1	1921	400	ROS	
9608-1	2589	400	ROS	
9612-1	3956	400	ROS	
9617-1	80	60	ROS	
9621-1	53	53	ROS	
9622-1	2879	400	ROS	
9623-1	3940	400	ROS	
9628-2	3941	1000	ParCa	
9629-1	4177	2000	ParCa	mooring site CB15/16
9630-1	2717	1500	ParCa	mooring site Cbi-2/3

4.7.4 Sampling for chlorophyll-a measurements

For the determination of chlorophyll-a concentrations in the surface waters, seawater from the shipboard installed seawater pump ("Membranpumpe") was sampled when sailing (Table 4.7.3). Half a liter or one liter of seawater were filtered onto a glass microfibre filter (Whatman, GF/F, 25 mm diameter). The samples were frozen at dark and will be analyzed by means of photometry at the laboratory in Bremen. The chlorophyll-a data should give information – together with older data - on the seasonal and regional variability in biomass distribution in the offshore region off Cap Blanc, in particular in the large filament. The results from the samples from the shipboard pump will be compared with satellite-derived chlorophyll concentration maps (SeaWiFS, MODIS) and may serve as calibration of these data. At the two mooring sites CBi and CB off Cap Blanc, two depth profiles were taken using water from the rosette (Table 4.7.3). Data from the depth profiles at the two mooring sites will be compared to optical

data of particle distribution in the water column and to the continuous records of chlorophyll fluorescence taken from the CTD profiles (see chapters above).

Table 4.7.3. Sampling locations for chlorophyll-a measurements (upper part: shipboard membrane pump, lower part: rosette). T-S-data were taken from the ships' thermosalinograph.

No.	Date 2005	Time (UTC)	Location LAT LONG	Water-depth (m)	Salinity (‰)	Water-Temp. (°C)	Sample volume (l)	Station
1	15.07	08:35	18°34.0 N 18°18.0 W	2837	36.31	25.3	0.5	
2	15.07	18:42	19°32.7 N 16°57.8 W	102	36.06	24.1	1.0	
3	16.07	08:25	19°57.8 N 17°32.6 W	155	36.02	24.5	1.0	
4	17.07	08:40	19°39.6 N 17°24.2 W	1331	36.09	24.9	1.0	
5	18.07	08:45	19°15.7 N 18°33.2 W	3150	36.24	26.4	1.0	
6	19.7	08:20	20°13.1 N 20°36.6 W	3755	36.08	23.5	1.0	
7	20.7	07:55	20°30.2 N 20°39.9 W	3945	36.12	23.7	0.5	~CB-15/16
8	21.7	08:20	20°39.5 N 20°56.1 W	4034	36.11	23.9	0.5	~CB-15/16

St. No.	Date 2005	Time (UTC)	Location LAT LONG	Water-Depth (m)	Sampling Depth (m)	Sample volume (l)	Station
9629-3	22.07	13:00	21°18.8 N 20°45.9 W	4177	10	0.5	~CB-15/16
					20	0.5	
					40	1.0	
					50	1.0	
					60	1.0	
9630-3	23.07	11:15	18°42.4 N 20°44.1 W	2730	10	0.5	~CBi-2/3
					20	0.5	
					40	1.0	
					50	1.0	
					60	1.0	

4.8 Wildlife Observations

(R.B. Wynn)

List of confirmed bird and cetacean species observed at sea during the cruise

Cory's Shearwater	*Calonectris diomedea*
Fea's Petrel	*Pterodroma fea*
Bulwer's Petrel	*Bulweria bulwerii*
Wilson's Storm-petrel	*Oceanites oceanicus*
Leach's Storm-petrel	*Oceanodroma leucorhoa*
Madeiran Storm-petrel	*Oceanodroma castro*
Northern Gannet	*Morus bassanus*
Brown Booby	*Sula leucogaster*
Arctic Skua	*Stercorarius parasiticus*
Long-tailed Skua	*Stercorarius longicaudus*
Sandwich Tern	*Sterna sandvicensis*
Common Tern	*Sterna hirundo*
Roseate Tern	*Sterna dougalii*
Royal Tern	*Sterna maxima*
Bridled Tern	*Sterna anaethetus*
Black Tern	*Chlidonias niger*
Common Swift	*Apus apus*
Alpine Swift	*Apus melba*
Plain Swift	*Apus unicolor*
White-rumped Swift	*Apus caffer*
Little Swift	*Apus affinis*
Barn Swallow	*Hirundo rustica*
Bottle-nosed Dolphin	*Tursiops truncatus*
Short-finned Pilot Whale	*Globicephala macrorhynchus*
Minke Whale	*Balaenoptera acutorostrata*

July 4th: Passage from Dakar Harbour, Senegal to 14°28'N/17°57'W (60 km WSW of Dakar, Senegal)

Water depth = 0-2000 m

The cruise started in Dakar with Yellow-billed Kites flying around the ship and scavenging fish in the harbour. Once the cruise was underway, the initial passage across the shelf into deep water was surprisingly quiet. At least 20 Royal Terns and four Black Terns were noted, and also about 15 storm-petrel sp. that were too distant to identify (suspected to be Madeiran Storm-petrels). The highlight was a group of four Bottle-nosed Dolphins seen close inshore. Sea surface temperature (SST) data showed that the waters over the shelf were about 1°C cooler than those offshore, indicating weak upwelling. During the evening, while arriving on station over the margin of Dakar Canyon, a larger group of oceanic dolphins comprising 10's of animals was seen distantly, and 100-500 flying fish were noted. Surprise of the day was an Alpine Swift

seen moving south, while seabirds seen offshore included a Wilson's Storm-petrel and two Black Terns.

July 5th: Passage from 14°03'N/17°52'W (90 km SW of Dakar, Senegal) to 13°18'N/17°51'W (110 km W of southern Senegal)
Water depth = 2000-2500 m
The day was spent undergoing southward passage along the upper slope. Two large groups of distant unidentified dolphins were seen, comprising 100's of animals, and also a distant pod containing 10's of Short-finned Pilot Whales. Seabirds included 35 Black Terns, mostly in two groups of 10 and 16 seen feeding over tuna shoals. All birds were in first-summer plumage except for a single second-summer/adult. In addition, a single Brown Booby attempted to land on the ship. Good numbers of flying fish and tuna were seen throughout the day, and also a single large dorado. The calm weather meant it was possible to see patches of plankton 'soup' in the surface waters.

July 6th: On station at 12°35'N/18°30'W (180 km off southern Senegal)
Water depth = 4000 m
A tropical storm with torrential rain and strong winds prevented any observations for much of the day. In the late afternoon single Little Swift and Plain Swift were seen flying around the ship, and appeared to roost on board. The Little Swift was relocated during the night clinging to a window wiper on the bridge deck! Equally surprising was a Royal Tern that appeared exhausted as it flew alongside the ship and then flopped onto the water. It quickly became waterlogged but was rescued by a crewman with a long landing net! It was boxed, force-fed some defrosted squid, and left to dry out overnight. Presumably, it had become weakened and disoriented by the storm. The two swifts could also have been forced offshore by the rain, or alternatively could have been early migrants returning south from the Cape Verde Islands. Finally, a Common Tern was seen flying around the ship in the afternoon.

July 7th: Passage from 12°40'N/18°30'W (180 km off southern Senegal) to 13°12'N/18°13'W (160 km off southern Senegal)
Water depth = 3500-4000 m
The Royal Tern was still alive and well in the morning, and after its release flew strongly around the ship before settling on the mast structure for several hours. It had apparently departed by late afternoon. At least six Plain Swifts were around the ship during the morning, including one stranded on the working deck that was successfully re-launched into the air from the bridge deck. A White-rumped Swift flying over mid-morning was the fourth swift species recorded since leaving Dakar! Seabirds included a single Common Tern and eight Black Terns. The Black Terns, when seen in flocks in calm weather, fly 20-30 m above the sea searching for tuna boils. In the evening a distant group of

dolphins was seen (note that all of the dolphins seen offshore so far have been at long range, preventing firm identification).

July 8th: Passage from 13°45'N/18°16'W (150 km SW of Dakar, Senegal) to 13°56'N/18°13'W (130 km SW of Dakar, Senegal)
Water depth = 3000-3500 m
The only seabird noted was a first-summer Common Tern that spent several hours hunting small fish around the front of the ship.

July 9th: Passage from 14°38'N/17°47'W (30 km SW of Dakar, Senegal) to station at 14°11'N/17°53'W (80 km SSW of Dakar, Senegal)
Water depth = 1200-2000 m
The day began over the upper part of Dakar Canyon, in sight of the Dakar Peninsula. However, there were still very few seabirds to be seen, with just 13 Black Terns noted. A slight temperature dip of about 0.5°C over the canyon may indicate weak upwelling. The surprise of the day was an Oleander Hawk-moth found on deck in the afternoon.

July 10th: On station at 14°11'N/18°06'W (100 km SW of Dakar, Senegal)
Water depth = 3000 m
During the morning sample survey not a single seabird, fish or otherwise was recorded. The only wildlife observations related to an influx of migrant moths, with about 25 individuals of at least 10 species recorded.

July 11th: Passage from 13°18'N/19°01'W (220 km SW of Dakar, Senegal) to 13°14'N/18°58'W (200 km SW of Dakar, Senegal)
Water depth = 4000 m
Two storm-petrel sp. were seen during the morning, together with a distant group of 10-100 dolphin sp. Another five or so migrant moths were found on deck.

July 14th: Passage from 14°25'N/19°05'W (170 km W of Dakar, Senegal) to 16°04'N/19°02'W (220 km NW of Dakar, Senegal)
Water depth = 3000-3500 m
A day of passage took the ship north of Dakar for the first time, and there was a marked change in the variety of seabirds recorded. Two Cory's Shearwaters, three Bulwer's Petrels, three Fea's Petrels, three Madeiran Storm-petrels and eight storm-petrel sp. were seen, as well as about 70 Short-finned Pilot Whales and three turtle sp. Good numbers of Flying fish were seen again, but Tuna were totally absent in this area. SST began to drop as the ship moved northwards. Before this date all midnight values taken during the cruise were in the range of 27.7-28.8°C, however, by mid-evening SST had dropped to 27.0°C and by the early hours of the 15th it was down to 24.2°C.

July 15th: Passage from 18°42'N/18°02'W (180 km SW of Cap Timiris, Mauritania) to 19°35'N/16°56'W (50 km W of Cap Timiris, Mauritania)
Water depth = 100-2600 m
During the day the Western Palearctic zoogeographical recording area was entered for the first time as the ship progressed north. The day began with a typical scatter of open ocean seabirds, including seven Leach's, seven Wilson's and five Madeiran Storm-petrels, seven Bulwer's Petrels, three Cory's Shearwaters and 18 Black Terns. A single Arctic Skua in second-summer plumage was the only indication of the approaching shelf edge. Cetaceans included 20-30 Short-finned Pilot Whales, a group of 10-50 spinner dolphins, and a further three groups of dolphin sp. totalling 100's of animals. Also of note were a turtle sp. and two Hammerhead Sharks. Flying fish were still abundant but only three fishing boats were seen, none of which was accompanied by seabirds.

Around midday the winds began blowing steadily offshore, providing a reminder that we were now in the active Trade Wind belt and the start of the upwelling zone. The shelf break was reached at about 1700 hrs, and SST suddenly dropped from 26.5°C to 24.9°C within an hour (a decrease of 1.5°C). An indication of the changing water temperature was shown by the marked reduction in Flying fish recorded, and also the arrival of a flotilla of at least a dozen fishing boats scattered across the sea (exploiting the fish stocks associated with the upwelling). A comparison of midnight SST indicated that the upwelled waters were about 3°C cooler than the surrounding water. The change in seabird density was staggering; up to mid-afternoon no more than 20 birds per hour were recorded, but after the upwelling zone was reached this instantly rose to 1000+ per hour. The dominant species was Wilson's Storm-petrel, particularly around the front itself at the shelf edge. Over 1000 were estimated in the first hour of passage though the upwelling zone, including a group of over 200 sitting on the sea. The largest numbers of Black Terns, literally 100's of birds, were not counted until the outer shelf was reached, and the vast majority of these were congregated around, or flying between, trawlers in the act of recovering their catches. Roughly 90% were in first-summer plumage. Other species seen included 10's of Royal Terns, Common Terns and Cory's Shearwaters (all of the race diomedea where noted) and also single first-summer Sandwich and Roseate Terns. Surprisingly, the only skua noted was an immature Arctic Skua, seen harassing terns around one of the fishing boats. In general, the vast majority of seabirds on the outer shelf were associating with active fishing boats, and even those birds seen away from the boats themselves were on the move rather than feeding (most of the birds seen passing the RV Meteor did so to the rear of the ship). Only the Wilson's Storm-petrels seemed to be unaffected by human fishing activities. Despite careful scanning, no other species of storm-petrels were observed.

July 16th: Passage from 20°01'N/17°31'W (125 km NW of Cap Timiris, Mauritania) to 20°05'N/17°32'W (125 km NW of Cap Timiris, Mauritania)
Water depth = 50-250 m
A calm start to the day provided good conditions for observations. A transect on the outer shelf began with 100's of Wilson's Storm-petrels and Black Terns, but really came alive at 0820 hrs when the shelf edge was reached. Several huge flocks of resting and feeding Wilson's Storm-petrels were roughly lined up just upslope from the shelf edge, with a conservative estimate of some 2000 birds present in this small area. The true figure was probably much higher as just one of the flocks was counted in a photograph, and actually contained at least 600 birds. Most birds were sitting on the sea but those closest to the survey line took to the air en masse as the ship approached to within 100 m. A small number of Cory's Shearwaters were associated with the flocks at the shelf edge, and a sub-adult Gannet was seen sitting on the sea. At least three immature Arctic Skuas were also noted around the shelf edge, including one being harassed by a Long-tailed Skua. It seems likely that this dense concentration of birds was a result of the calm conditions, with nutrient-rich upwelled waters remaining concentrated at the shelf edge, rather than being mixed and dispersed across the outer shelf and upper slope. Most birds appeared to be flocking at the interface between these cool upwelled waters and the warmer surface waters. This interface marked a change in SST of about 1°C over a distance of <5 km.

As the ship headed back onto the flat outer shelf, numbers of Wilson's Storm-petrels and Black Terns decreased markedly, although hundreds of birds were still scattered over the area. A significant decrease in Wilson's Storm-petrels occurred towards the end of a survey line at 0930 hrs, when SST increased by 1°C, even though water depth remained constant. This increased SST may represent the transition out of the upwelled water mass. Very few of the Black Terns seen appeared to be feeding, but instead appeared to be commuting (between active trawlers?) at a height of ~10 m. Between 0900-1000 hrs nearly all birds seen were moving NW, roughly parallel with the shelf edge, although the significance of this movement is unclear. The only feeding flock comprised about 40 birds seen at 1642 hrs. A quick age survey earlier in the day found that about 80-85% were birds in their first-summer plumage, with the remainder being second-summer or adult birds.

Other seabirds seen during the day included small numbers of Common and Sandwich Terns, and also a single Bridled Tern. A juvenile Swallow rested on the ship for a few minutes in the afternoon, and a butterfly sp. was also seen.

July 17th: Passage from 19°53'N/17°26'W (110 km WNW of Cap Timiris, Mauritania) to 19°39'N/17°24'W (100 km WNW of Cap Timiris, Mauritania)
Water depth = 1500-50 m
An initial passage from deep water onto the shelf provided a good opportunity to quantify the changing concentration of seabirds across this transect. At water depths >1000 m, numbers of Black Terns and Wilson's Storm-petrels were seen at a rate of 10's per hour, with only a couple of (probably non-active) fishing boats seen and small numbers of Flying fish. Most of the Black Terns were seen in a loose flock of up to 45 birds that circled repeatedly around the ship. As the uppermost slope and outer shelf was reached, numbers of Black Terns and Wilson's Storm-petrels increased to 100's per hour, and small numbers of Cory's Shearwaters, Common Terns and Royal Terns appeared at the shelf edge. An immature Long-tailed Skua was seen harassing a dark immature Arctic Skua. The number of trawlers increased to five and Flying fish disappeared.

The highest density of birds was present on the outer shelf in association with up to 16 trawlers, with 1000's of Black Terns concentrated in huge flocks around active boats and 100's of Wilson's Storm-petrels scattered loosely across the whole area. At times a steady stream of Black Terns could be watched passing across the back of our ship as they moved between trawlers. The largest single flock, containing 1000's of birds, was associated with a pair of trawlers working in tandem. There was some evidence for feeding independent of human fishing activity, for example about 700 Black Terns were watched actively feeding in a linear flock on the outer shelf at 1230 hrs, even though five trawlers were in the vicinity. This flock was almost totally made up of the one species, and no skuas were in attendance (skuas were notable for their absence for most of the day). Three-figure counts of Royal Terns and Cory's Shearwaters were made in certain areas, and both species were strongly associated with trawlers, e.g. 270 Royal Terns flying around (and perched on two trawlers) at 1448 hrs, and 130 Cory's Shearwaters following trawlers at the shelf edge between 1740 and 1755 hrs. The latter species was usually seen in loose flocks of up to 80 birds, and at times would follow the ship for long periods. All birds were of the race diomedea where this could be determined. Other species recorded included 10's of Common and Sandwich Terns and a total of six Bridled Terns (including one attempting to steal food from a Black Tern), although only one distant skua sp. was seen. A Leach's Storm-petrel was found in the after deck laboratory in the early afternoon and was released successfully; it had presumably come on board during the previous night when the lights were on and the ship was working in deeper waters offshore.

Towards the end of the day the wind and sea state began to steadily increase and observations became more difficult. Overall it was much windier than the previous day,

presumably leading to more mixing/dispersal of the upwelled waters and probably explaining why there were no marked concentrations of Wilson's Storm-petrels at the shelf edge. In addition, the huge concentrations of terns around active trawlers ensured that lower numbers of birds were actually seen away from the boats themselves, possibly even fewer than in areas where no trawlers were operating. Towards the end of the day, during passage westwards into deeper water, nearly all of the Black Terns seen were heading back towards the shelf, possibly as part of a pre-roost movement.

Estimated totals for the commonest seabird species recorded in the Mauritania upwelling zone, from July 15th-17th, included 10,000 Wilson's Storm-petrels, 10,000 Black Terns, 700 Royal Terns, 350 Cory's Shearwaters and 100 Common Terns.

July 20th: On station at 20°30'N/20°40'W (380 km W of Cap Blanc, Mauritania)
Water depth = 4000 m
After a couple of days of strong winds and rough seas, the weather became calmer and some observations were made. The only seabirds noted were two distant petrel sp., but migrant land birds included two Swallows and up to eight Common Swifts, several of which appeared to roost on the ship overnight. These birds had probably been displaced by the same weather system that had pushed large amounts of reddish Saharan dust westwards out to sea. The highlight of the day was a group of two or three Minke Whales feeding around the ship in the evening for at least two hours. One of the animals surfaced within 25 m of the starboard side and then dived before resurfacing close by on the port side. The typical dive sequence consisted of 5-10 blows at 12-15 second intervals, before a dive of 2-10 minutes duration. On rising, a low and fairly bushy blow up to 3 m high was seen, accompanied by a loud exhalation (if the animals were close enough to hear). The twin blowholes sat behind a single longitudinal ridge and prominent splashguard. The latter was sometimes still visible as the tall, falcate dorsal fin appeared. The back was dark blackish and sleek in appearance, and on at least one animal a paler area could be seen extending up onto the upper flank in front of the dorsal fin. Before a dive, the tail stock was clearly arched, but the flukes were never seen.

July 21st: Passage from 20°39'N/20°55'W (380 km W of Cap Blanc, Mauritania) to 20°32'N/20°32'W (370 km W of Cap Blanc Mauritania)
Water depth = 4000 m
Another three Common Swifts were seen around the ship during the morning, and an exhausted bird was picked up in the early afternoon. Unfortunately it was too weak to fly, and despite attempts to give it water, it soon became moribund and died the following day. The only seabirds noted were a single Bulwer's Petrel and up to 11

Leach's/Madeiran Storm-petrels. Other wildlife included small numbers of Flying fish, at least two shark sp., and a distant small rorqual sp.

July 22nd: Passage from 21°15'N/20°40'W (380 km WNW of Cap Blanc, Mauritania) to 21°13'N/20°32'W (375 km WNW of Cap Blanc, Mauritania)
Water depth = 4000 m
An hour of survey in the evening produced two Leach's/Madeiran Storm-petrels and 10-100 Flying fish

July 23rd: Passage from 20°53'N/18°40'W (160 km W of Cap Blanc, Mauritania) to 21°05'N/18°39'W (160 km WNW of Cap Blanc, Mauritania)
Water depth = 2500-3000 m
An hour of survey in the late afternoon in rough weather produced just three storm-petrel sp. and a few Flying fish.

July 24th: Passage from 24°06'N/18°12'W (220 km offshore Western Sahara) to 24°45'N/17°39'W (200 km offshore Western Sahara)
Water depth = 2500-3000 m
The only seabirds seen during the day were a Bulwer's Petrel, three Cory's Shearwaters and one Leach's/Madeiran Storm-petrel. A group of cetaceans seen in the early evening contained 10-20 Short-finned Pilot Whales and 5+ dolphin sp. Good numbers of Flying fish were still present.

July 25th: Passage from 26°34'N/17°04'W (150 km SE of Hierro, Canary Islands) to 26°40'N/17°07'W (140 km SE of El Hierro)
Water depth = 3500-4000 m
Slightly more seabirds were recorded as the ship steamed north towards the Canary Islands. A total of 32 Cory's Shearwaters and four Bulwer's Petrels were seen during the afternoon, together with small numbers of Flying fish. Most of the Cory's Shearwaters were seen as single birds, unlike in the Mauritania upwelling zone where most were gathered in loose flocks. Other birds noted included a single Racing Pigeon and two Plain Swifts.

5 Weather and Meteorological Conditions during the Cruise

(Th. Truscheit)

When R/V Meteor left the port of Dakar/Senegal at noon on July 4th 2005, clouds in the highest level prevailed, so it was a sunny and very warm day.

For the territorial waters of Guinea-Bissau no permission for research was given by the local government. Originally the working area "A" was planed to extend to the territorial waters of Guinea but the chief scientist decided that the border Senegal to Guinea-Bissau was the southern most point of working.

The working area "A" was located in the main axis of the ITC. Regularly powerful cloud clusters which developed over the continent were moving westward, crossing the position of R/V Meteor. While R/V Meteor was in the ITC, the wind was blowing from different directions, rarely less than Beaufort 4 to 5 and just seldom more than this. The only exception in the first 14 days of the cruise was July 6th 2005. Early in the morning of that day a really powerful cloud cluster was approaching the position of R/V Meteor. Very heavy showers of rain and thunderstorm started at approximately 9 o'clock and was accompanied by gusts of Beaufort 12 (up to 70 kts) .

When Meteor shifted to working area "B", it was outside of the main axis of the ITC. A very last part of a cloud cluster was crossing the position on July 16th 2005. After crossing, the cloud cover decreased to blue sky for the next days. Accompanied by that the wind increased up to Beaufort 7 on July 18th. In spite of the blue sky the visibility became poorer because of a lot of dust from the Sahara being in the atmosphere. Until July 21st the wind decreased to Beaufort 1, temporarily to calm for a short while. On this day also the Sahara dust dwindled away and the visibility became better. A wind force of Beaufort 1 continued until the next day before it increased again to Beaufort 5 from northern directions. These last two days of scientific work - mooring at position 21.17,9°N 20.47,8°W on Friday 22nd and at position 20.44°N 18.42°W on Saturday 23rd – were accompanied by light to moderate wind up to Beaufort 5 from northern direction and thinning cloud cover or blue sky at times. The last two days of the cruise were just been for transit from the last mooring position to Las Palmas.

The transit to Las Palmas started at noon on July 23rd with a blue sky and the wind blows from north eastern direction with Beaufort 5 with a swell also from northern direction up to 2.5 meters.

Even though for the weather conditions during the cruise it was not important, nevertheless it was an interesting phenomenon. In the south westerly current of the

upper atmosphere the "Kármán-Wirbel", called after the Hungarian T. Kármán, could be observed leeward of the Canary Islands. The pasted satellite picture of NOAA-12 shows this phenomenon very impressively.

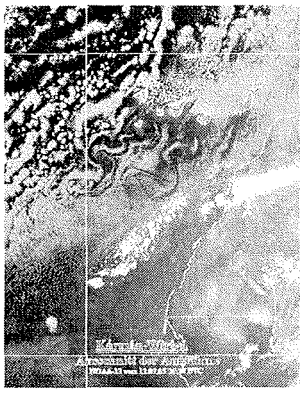

The cruise ended early in the morning of July 26th 2005 in Las Palmas/Canary Islands.

6 References

Antobreh, A.A., Krastel, S. (2005): Morphology, seismic characteristics and development of Cap Timiris Canyon, offshore Mauritania: a newly discovered canyon preserved off a major arid climatic region. Marine and Petroleum Geology doi:10.1016/j.marpetgeo.2005.06.003

Asper, V.L. (1987) Measuring the flux and sinking speed of marine snow aggregates. Deep Sea Research, 34, 1-17.

Boyce, RE (1968) Electrical resistivity of modern marine sediments from the Bering Sea. J. Geophys. Res. 73, 4759-4766.

Grant J.A., Schreiber, R. (1990) Modern swath sounding and sub-bottom profiling technology for research applications: The Atlas Hydrosweep and Parasound systems. Marine Geophys. Res. 12, 9-19.

Hall, P.O.J., Aller, R.C. (1992) Rapid, small-volume, flow injection analysis for CO_2 and NH_4^+ in marine and freshwaters. Limnology and Oceanography, 35, 1113-1119.

Honjo, S., Doherty, K.W., Agrawal, Y.C., Asper, V.L. (1984) Direct optical assessment of large amorphous aggregates (marine snow) in the deep ocean: Deep Sea Research I, 31, 67-76.

Krastel, S., Hanebuth, T.J.J., Wynn, R.B., Antobreh, A.A., Henrich, R., Holz, C., Kölling, M., Schulz, H.D., Wien, K. (2004) Cap Timiris Canyon: A newly discovered channel-system off Mauritania. EOS Transactions, 45/42, p. 417, 423

Matthewson, A.P., Shimmield, G.B., Kroon, D., Fallick, A.E. (1995) A 300 kyr high-resolution aridity record of the North African continent. Paleoceanography, 10(3), 677-692.

Meijboom, F.W., van Nordwijk, M. (1992) Rhizon Soil Solution Samplers as artificial roots. In: Kutschera, L., Hübl, E., Lichtenegger, E., Persson, H. and Sobotnik, M., (Eds.): Root Ecology and its practical Application.- Proc 3rd ISSR Symp., Verein für Wurzelforschung, Klagenfurt, Austria, 793-795.

Seeberg-Elverfeldt, J., Schlüter, M., Feseker, T., Kölling M. (2005) Rhizon sampling of pore waters near the sediment/water interface of aquatic systems. Limnology and Oceanography: Methods, 3, 361-371.

Schulz, H.D. and Cruise Participants (2003) Report and preliminary results of METEOR Cruise M 58/1, Dakar-Las Palmas, 15.04.2003-12.05.2003. Bereichte Fachbereich aus dem Fachbereich Geowissenschaften der Universität Bremen, 215, pp. 186.

Spieß V. (1993) Digitale Sedimentechographie - Neue Wege zu einer hochauflösenden Akustostratigraphie, Berichte aus dem Fachbereich Geowissenschaften der Universität Bremen, 35, pp. 199.

Zabel M., Schulz H.D. (2001) Importance of submarine landslides for non steady state conditions in pore water systems – lower Zaire (Congo) deep-sea fan. Marine Geology, 176, 87-99.

Acknowledgements

The great success of the work was very much depended on the close cooperation with Captain Jacobi and his crew. The scientific party gratefully acknowledges the close and friendly cooperation and the very efficient technical assistance. We also appreciate the most valuable help of the Leitstelle Meteor, Hamburg, in planning and realization of the cruise. The work was funded by the Deutsche Forschungsgemeinschaft within the scope of the DFG Research Center Ocean Margins (RCOM) at Bremen University.

Publications of this series:

No. 1 **Wefer, G., E. Suess and cruise participants**
Bericht über die POLARSTERN-Fahrt ANT IV/2, Rio de Janeiro - Punta Arenas, 6.11. - 1.12.1985.
60 pages, Bremen, 1986.

No. 2 **Hoffmann, G.**
Holozänstratigraphie und Küstenlinienverlagerung an der andalusischen Mittelmeerküste.
173 pages, Bremen, 1988. (out of print)

No. 3 **Wefer, G. and cruise participants**
Bericht über die METEOR-Fahrt M 6/6, Libreville - Las Palmas, 18.2. - 23.3.1988.
97 pages, Bremen, 1988.

No. 4 **Wefer, G., G.F. Lutze, T.J. Müller, O. Pfannkuche, W. Schenke, G. Siedler, W. Zenk**
Kurzbericht über die METEOR-Expedition No. 6, Hamburg - Hamburg, 28.10.1987 - 19.5.1988.
29 pages, Bremen, 1988. (out of print)

No. 5 **Fischer, G.**
Stabile Kohlenstoff-Isotope in partikulärer organischer Substanz aus dem Südpolarmeer (Atlantischer Sektor). 161 pages, Bremen, 1989.

No. 6 **Berger, W.H. and G. Wefer**
Partikelfluß und Kohlenstoffkreislauf im Ozean.
Bericht und Kurzfassungen über den Workshop vom 3.-4. Juli 1989 in Bremen.
57 pages, Bremen, 1989.

No. 7 **Wefer, G. and cruise participants**
Bericht über die METEOR - Fahrt M 9/4, Dakar - Santa Cruz, 19.2. - 16.3.1989.
103 pages, Bremen, 1989.

No. 8 **Kölling, M.**
Modellierung geochemischer Prozesse im Sickerwasser und Grundwasser.
135 pages, Bremen, 1990.

No. 9 **Heinze, P.-M.**
Das Auftriebsgeschehen vor Peru im Spätquartär. 204 pages, Bremen, 1990. (out of print)

No. 10 **Willems, H., G. Wefer, M. Rinski, B. Donner, H.-J. Bellmann, L. Eißmann, A. Müller, B.W. Flemming, H.-C. Höfle, J. Merkt, H. Streif, G. Hertweck, H. Kuntze, J. Schwaar, W. Schäfer, M.-G. Schulz, F. Grube, B. Menke**
Beiträge zur Geologie und Paläontologie Norddeutschlands: Exkursionsführer.
202 pages, Bremen, 1990.

No. 11 **Wefer, G. and cruise participants**
Bericht über die METEOR-Fahrt M 12/1, Kapstadt - Funchal, 13.3.1990 - 14.4.1990.
66 pages, Bremen, 1990.

No. 12 **Dahmke, A., H.D. Schulz, A. Kölling, F. Kracht, A. Lücke**
Schwermetallspuren und geochemische Gleichgewichte zwischen Porenlösung und Sediment im Wesermündungsgebiet. BMFT-Projekt MFU 0562, Abschlußbericht. 121 pages, Bremen, 1991.

No. 13 **Rostek, F.**
Physikalische Strukturen von Tiefseesedimenten des Südatlantiks und ihre Erfassung in Echolotregistrierungen. 209 pages, Bremen, 1991.

No. 14 **Baumann, M.**
Die Ablagerung von Tschernobyl-Radiocäsium in der Norwegischen See und in der Nordsee.
133 pages, Bremen, 1991. (out of print)

No. 15 **Kölling, A.**
Frühdiagenetische Prozesse und Stoff-Flüsse in marinen und ästuarinen Sedimenten.
140 pages, Bremen, 1991.

No. 16 **SFB 261 (ed.)**
1. Kolloquium des Sonderforschungsbereichs 261 der Universität Bremen (14.Juni 1991):
Der Südatlantik im Spätquartär: Rekonstruktion von Stoffhaushalt und Stromsystemen.
Kurzfassungen der Vorträge und Poster. 66 pages, Bremen, 1991.

No. 17 **Pätzold, J. and cruise participants**
Bericht und erste Ergebnisse über die METEOR-Fahrt M 15/2, Rio de Janeiro - Vitoria,
18.1. - 7.2.1991. 46 pages, Bremen, 1993.

No. 18 **Wefer, G. and cruise participants**
Bericht und erste Ergebnisse über die METEOR-Fahrt M 16/1, Pointe Noire - Recife,
27.3. - 25.4.1991. 120 pages, Bremen, 1991.

No. 19 **Schulz, H.D. and cruise participants**
Bericht und erste Ergebnisse über die METEOR-Fahrt M 16/2, Recife - Belem, 28.4. - 20.5.1991.
149 pages, Bremen, 1991.

No. 20 **Berner, H.**
Mechanismen der Sedimentbildung in der Fram-Straße, im Arktischen Ozean und in der Norwegischen See. 167 pages, Bremen, 1991.

No. 21 **Schneider, R.**
Spätquartäre Produktivitätsänderungen im östlichen Angola-Becken: Reaktion auf Variationen im Passat-Monsun-Windsystem und in der Advektion des Benguela-Küstenstroms.
198 pages, Bremen, 1991. (out of print)

No. 22 **Hebbeln, D.**
Spätquartäre Stratigraphie und Paläozeanographie in der Fram-Straße. 174 pages, Bremen, 1991.

No. 23 **Lücke, A.**
Umsetzungsprozesse organischer Substanz während der Frühdiagenese in ästuarinen Sedimenten.
137 pages, Bremen, 1991.

No. 24 **Wefer, G. and cruise participants**
Bericht und erste Ergebnisse der METEOR-Fahrt M 20/1, Bremen - Abidjan, 18.11.- 22.12.1991.
74 pages, Bremen, 1992.

No. 25 **Schulz, H.D. and cruise participants**
Bericht und erste Ergebnisse der METEOR-Fahrt M 20/2, Abidjan - Dakar, 27.12.1991 - 3.2.1992.
173 pages, Bremen, 1992.

No. 26 **Gingele, F.**
Zur klimaabhängigen Bildung biogener und terrigener Sedimente und ihrer Veränderung durch die Frühdiagenese im zentralen und östlichen Südatlantik. 202 pages, Bremen, 1992.

No. 27 **Bickert, T.**
Rekonstruktion der spätquartären Bodenwasserzirkulation im östlichen Südatlantik über stabile Isotope benthischer Foraminiferen. 205 pages, Bremen, 1992. (out of print)

No. 28 **Schmidt, H.**
Der Benguela-Strom im Bereich des Walfisch-Rückens im Spätquartär. 172 pages, Bremen, 1992.

No. 29 **Meinecke, G.**
Spätquartäre Oberflächenwassertemperaturen im östlichen äquatorialen Atlantik.
181 pages, Bremen, 1992.

No. 30 **Bathmann, U., U. Bleil, A. Dahmke, P. Müller, A. Nehrkorn, E.-M. Nöthig, M. Olesch, J. Pätzold, H.D. Schulz, V. Smetacek, V. Spieß, G. Wefer, H. Willems**
Bericht des Graduierten Kollegs. Stoff-Flüsse in marinen Geosystemen.
Berichtszeitraum Oktober 1990 - Dezember 1992. 396 pages, Bremen, 1992.

No. 31 **Damm, E.**
Frühdiagenetische Verteilung von Schwermetallen in Schlicksedimenten der westlichen Ostsee.
115 pages, Bremen, 1992.

No. 32 **Antia, E.E.**
Sedimentology, Morphodynamics and Facies Association of a mesotidal Barrier Island Shoreface (Spiekeroog, Southern North Sea). 370 pages, Bremen, 1993.

No. 33 **Duinker, J. and G. Wefer (ed.)**
Bericht über den 1. JGOFS-Workshop. 1./2. Dezember 1992 in Bremen. 83 pages, Bremen, 1993.

No. 34 **Kasten, S.**
Die Verteilung von Schwermetallen in den Sedimenten eines stadtbremischen Hafenbeckens.
103 pages, Bremen, 1993.

No. 35 **Spieß, V.**
Digitale Sedimentographie. Neue Wege zu einer hochauflösenden Akustostratigraphie.
199 pages, Bremen, 1993.

No. 36 **Schinzel, U.**
Laborversuche zu frühdiagenetischen Reaktionen von Eisen (III) - Oxidhydraten in marinen Sedimenten.189 pages, Bremen, 1993.

No. 37 **Sieger, R.**
CoTAM - ein Modell zur Modellierung des Schwermetalltransports in Grundwasserleitern.
56 pages, Bremen, 1993. (out of print)

No. 38 **Willems, H. (ed.)**
Geoscientific Investigations in the Tethyan Himalayas. 183 pages, Bremen, 1993.

No. 39 **Hamer, K.**
Entwicklung von Laborversuchen als Grundlage für die Modellierung des Transportverhaltens von Arsenat, Blei, Cadmium und Kupfer in wassergesättigten Säulen. 147 pages, Bremen, 1993.

No. 40 **Sieger, R.**
Modellierung des Stofftransports in porösen Medien unter Ankopplung kinetisch gesteuerter Sorptions- und Redoxprozesse sowie thermischer Gleichgewichte. 158 pages, Bremen, 1993.

No. 41 **Thießen, W.**
Magnetische Eigenschaften von Sedimenten des östlichen Südatlantiks und ihre paläozeanographische Relevanz. 170 pages, Bremen, 1993.

No. 42 **Spieß, V. and cruise participants**
Report and preliminary results of METEOR-Cruise M 23/1, Kapstadt - Rio de Janeiro, 4.-25.2.1993. 139 pages, Bremen, 1994.

No. 43 **Bleil, U. and cruise participants**
Report and preliminary results of METEOR-Cruise M 23/2, Rio de Janeiro - Recife, 27.2.-19.3.1993 133 pages, Bremen, 1994.

No. 44 **Wefer, G. and cruise participants**
Report and preliminary results of METEOR-Cruise M 23/3, Recife - Las Palmas, 21.3. - 12.4.1993 71 pages, Bremen, 1994.

No. 45 **Giese, M. and G. Wefer (ed.)**
Bericht über den 2. JGOFS-Workshop. 18../19. November 1993 in Bremen.
93 pages, Bremen, 1994.

No. 46 **Balzer, W. and cruise participants**
Report and preliminary results of METEOR-Cruise M 22/1, Hamburg - Recife, 22.9. - 21.10.1992. 24 pages, Bremen, 1994.

No. 47 **Stax, R.**
Zyklische Sedimentation von organischem Kohlenstoff in der Japan See: Anzeiger für Änderungen von Paläoozeanographie und Paläoklima im Spätkänozoikum.
150 pages, Bremen, 1994.

No. 48 **Skowronek, F.**
Frühdiagenetische Stoff-Flüsse gelöster Schwermetalle an der Oberfläche von Sedimenten des Weser Ästuares. 107 pages, Bremen, 1994.

No. 49 **Dersch-Hansmann, M.**
Zur Klimaentwicklung in Ostasien während der letzten 5 Millionen Jahre:
Terrigener Sedimenteintrag in die Japan See (ODP Ausfahrt 128). 149 pages, Bremen, 1994.

No. 50 **Zabel, M.**
Frühdiagenetische Stoff-Flüsse in Oberflächen-Sedimenten des äquatorialen und östlichen Südatlantik. 129 pages, Bremen, 1994.

No. 51 **Bleil, U. and cruise participants**
Report and preliminary results of SONNE-Cruise SO 86, Buenos Aires - Capetown, 22.4. - 31.5.93 116 pages, Bremen, 1994.

No. 52 **Symposium: The South Atlantic: Present and Past Circulation.**
Bremen, Germany, 15 - 19 August 1994. Abstracts. 167 pages, Bremen, 1994.

No. 53 **Kretzmann, U.B.**
^{57}Fe-Mössbauer-Spektroskopie an Sedimenten - Möglichkeiten und Grenzen.
183 pages, Bremen, 1994.

No. 54 **Bachmann, M.**
Die Karbonatrampe von Organyà im oberen Oberapt und unteren Unteralb (NE-Spanien, Prov. Lerida): Fazies, Zyklo- und Sequenzstratigraphie. 147 pages, Bremen, 1994. (out of print)

No. 55 **Kemle-von Mücke, S.**
Oberflächenwasserstruktur und -zirkulation des Südostatlantiks im Spätquartär.
151 pages, Bremen, 1994.

No. 56 **Petermann, H.**
Magnetotaktische Bakterien und ihre Magnetosome in Oberflächensedimenten des Südatlantiks.
134 pages, Bremen, 1994.

No. 57 **Mulitza, S.**
Spätquartäre Variationen der oberflächennahen Hydrographie im westlichen äquatorialen Atlantik.
97 pages, Bremen, 1994.

No. 58 **Segl, M. and cruise participants**
Report and preliminary results of METEOR-Cruise M 29/1, Buenos-Aires - Montevideo, 17.6. - 13.7.1994
94 pages, Bremen, 1994.

No. 59 **Bleil, U. and cruise participants**
Report and preliminary results of METEOR-Cruise M 29/2, Montevideo - Rio de Janiero 15.7. - 8.8.1994. 153 pages, Bremen, 1994.

No. 60 **Henrich, R. and cruise participants**
Report and preliminary results of METEOR-Cruise M 29/3, Rio de Janeiro - Las Palmas 11.8. - 5.9.1994. Bremen, 1994. (out of print)

No. 61 **Sagemann, J.**
Saisonale Variationen von Porenwasserprofilen, Nährstoff-Flüssen und Reaktionen in intertidalen Sedimenten des Weser-Ästuars. 110 pages, Bremen, 1994. (out of print)

No. 62 **Giese, M. and G. Wefer**
Bericht über den 3. JGOFS-Workshop. 5./6. Dezember 1994 in Bremen.
84 pages, Bremen, 1995.

No. 63 **Mann, U.**
Genese kretazischer Schwarzschiefer in Kolumbien: Globale vs. regionale/lokale Prozesse.
153 pages, Bremen, 1995. (out of print)

No. 64 **Willems, H., Wan X., Yin J., Dongdui L., Liu G., S. Dürr, K.-U. Gräfe**
The Mesozoic development of the N-Indian passive margin and of the Xigaze Forearc Basin in southern Tibet, China. – Excursion Guide to IGCP 362 Working-Group Meeting "Integrated Stratigraphy". 113 pages, Bremen, 1995. (out of print)

No. 65 **Hünken, U.**
Liefergebiets - Charakterisierung proterozoischer Goldseifen in Ghana anhand von Fluideinschluß - Untersuchungen. 270 pages, Bremen, 1995.

No. 66 **Nyandwi, N.**
The Nature of the Sediment Distribution Patterns in ther Spiekeroog Backbarrier Area, the East Frisian Islands. 162 pages, Bremen, 1995.

No. 67 **Isenbeck-Schröter, M.**
Transportverhalten von Schwermetallkationen und Oxoanionen in wassergesättigten Sanden. - Laborversuche in Säulen und ihre Modellierung -. 182 pages, Bremen, 1995.

No. 68 **Hebbeln, D. and cruise participants**
Report and preliminary results of SONNE-Cruise SO 102, Valparaiso - Valparaiso, 95.
134 pages, Bremen, 1995.

No. 69 **Willems, H. (Sprecher), U.Bathmann, U. Bleil, T. v. Dobeneck, K. Herterich, B.B. Jorgensen, E.-M. Nöthig, M. Olesch, J. Pätzold, H.D. Schulz, V. Smetacek, V. Speiß. G. Wefer**
Bericht des Graduierten-Kollegs Stoff-Flüsse in marine Geosystemen.
Berichtszeitraum Januar 1993 - Dezember 1995.
45 & 468 pages, Bremen, 1995.

No. 70 **Giese, M. and G. Wefer**
Bericht über den 4. JGOFS-Workshop. 20./21. November 1995 in Bremen. 60 pages, Bremen, 1996. (out of print)

No. 71 **Meggers, H.**
Pliozän-quartäre Karbonatsedimentation und Paläozeanographie des Nordatlantiks und des Europäischen Nordmeeres - Hinweise aus planktischen Foraminiferengemeinschaften.
143 pages, Bremen, 1996. (out of print)

No. 72 **Teske, A.**
Phylogenetische und ökologische Untersuchungen an Bakterien des oxidativen und reduktiven marinen Schwefelkreislaufs mittels ribosomaler RNA. 220 pages, Bremen, 1996. (out of print)

No. 73 **Andersen, N.**
Biogeochemische Charakterisierung von Sinkstoffen und Sedimenten aus ostatlantischen Produktions-Systemen mit Hilfe von Biomarkern. 215 pages, Bremen, 1996.

No. 74 **Treppke, U.**
Saisonalität im Diatomeen- und Silikoflagellatenfluß im östlichen tropischen und subtropischen Atlantik. 200 pages, Bremen, 1996.

No. 75 **Schüring, J.**
Die Verwendung von Steinkohlebergematerialien im Deponiebau im Hinblick auf die Pyritverwitterung und die Eignung als geochemische Barriere. 110 pages, Bremen, 1996.

No. 76 **Pätzold, J. and cruise participants**
Report and preliminary results of VICTOR HENSEN cruise JOPS II, Leg 6, Fortaleza - Recife, 10.3. - 26.3. 1995 and Leg 8, Vitoria - Vitoria, 10.4. - 23.4.1995.
87 pages, Bremen, 1996.

No. 77 **Bleil, U. and cruise participants**
Report and preliminary results of METEOR-Cruise M 34/1, Cape Town - Walvis Bay, 3.-26.1.1996.
129 pages, Bremen, 1996.

No. 78 **Schulz, H.D. and cruise participants**
Report and preliminary results of METEOR-Cruise M 34/2, Walvis Bay - Walvis Bay, 29.1.-18.2.96
133 pages, Bremen, 1996.

No. 79 **Wefer, G. and cruise participants**
Report and preliminary results of METEOR-Cruise M 34/3, Walvis Bay - Recife, 21.2.-17.3.1996.
168 pages, Bremen, 1996.

No. 80 **Fischer, G. and cruise participants**
Report and preliminary results of METEOR-Cruise M 34/4, Recife - Bridgetown, 19.3.-15.4.1996. 105 pages, Bremen, 1996.

No. 81 **Kulbrok, F.**
Biostratigraphie, Fazies und Sequenzstratigraphie einer Karbonatrampe in den Schichten der Oberkreide und des Alttertiärs Nordost-Ägyptens (Eastern Desert, N'Golf von Suez, Sinai). 153 pages, Bremen, 1996.

No. 82 **Kasten, S.**
Early Diagenetic Metal Enrichments in Marine Sediments as Documents of Nonsteady-State Depositional Conditions. Bremen, 1996.

No. 83 **Holmes, M.E.**
Reconstruction of Surface Ocean Nitrate Utilization in the Southeast Atlantic Ocean Based on Stable Nitrogen Isotopes. 113 pages, Bremen, 1996.

No. 84 **Rühlemann, C.**
Akkumulation von Carbonat und organischem Kohlenstoff im tropischen Atlantik: Spätquartäre Produktivitäts-Variationen und ihre Steuerungsmechanismen. 139 pages, Bremen, 1996.

No. 85 **Ratmeyer, V.**
Untersuchungen zum Eintrag und Transport lithogener und organischer partikulärer Substanz im östlichen subtropischen Nordatlantik. 154 pages, Bremen, 1996.

No. 86 **Cepek, M.**
Zeitliche und räumliche Variationen von Coccolithophoriden-Gemeinschaften im subtropischen Ost-Atlantik: Untersuchungen an Plankton, Sinkstoffen und Sedimenten. 156 pages, Bremen, 1996.

No. 87 **Otto, S.**
Die Bedeutung von gelöstem organischen Kohlenstoff (DOC) für den Kohlenstoffffluß im Ozean. 150 pages, Bremen, 1996.

No. 88 **Hensen, C.**
Frühdiagenetische Prozesse und Quantifizierung benthischer Stoff-Flüsse in Oberflächensedimenten des Südatlantiks. 132 pages, Bremen, 1996.

No. 89 **Giese, M. and G. Wefer**
Bericht über den 5. JGOFS-Workshop. 27./28. November 1996 in Bremen. 73 pages, Bremen, 1997.

No. 90 **Wefer, G. and cruise participants**
Report and preliminary results of METEOR-Cruise M 37/1, Lisbon - Las Palmas, 4.-23.12.1996. 79 pages, Bremen, 1997.

No. 91 **Isenbeck-Schröter, M., E. Bedbur, M. Kofod, B. König, T. Schramm & G. Mattheß**
Occurrence of Pesticide Residues in Water - Assessment of the Current Situation in Selected EU Countries. 65 pages, Bremen 1997.

No. 92 **Kühn, M.**
Geochemische Folgereaktionen bei der hydrogeothermalen Energiegewinnung. 129 pages, Bremen 1997.

No. 93 **Determann, S. & K. Herterich**
JGOFS-A6 "Daten und Modelle": Sammlung JGOFS-relevanter Modelle in Deutschland. 26 pages, Bremen, 1997.

No. 94 **Fischer, G. and cruise participants**
Report and preliminary results of METEOR-Cruise M 38/1, Las Palmas - Recife, 25.1.-1.3.1997, with Appendix: Core Descriptions from METEOR Cruise M 37/1. Bremen, 1997.

No. 95 **Bleil, U. and cruise participants**
Report and preliminary results of METEOR-Cruise M 38/2, Recife - Las Palmas, 4.3.-14.4.1997. 126 pages, Bremen, 1997.

No. 96 **Neuer, S. and cruise participants**
Report and preliminary results of VICTOR HENSEN-Cruise 96/1. Bremen, 1997.

No. 97 **Villinger, H. and cruise participants**
Fahrtbericht SO 111, 20.8. - 16.9.1996. 115 pages, Bremen, 1997.

No. 98 **Lüning, S.**
Late Cretaceous - Early Tertiary sequence stratigraphy, paleoecology and geodynamics of Eastern Sinai, Egypt. 218 pages, Bremen, 1997.

No. 99 **Haese, R.R.**
Beschreibung und Quantifizierung frühdiagenetischer Reaktionen des Eisens in Sedimenten des Südatlantiks. 118 pages, Bremen, 1997.

No. 100 **Lührte, R. von**
Verwertung von Bremer Baggergut als Material zur Oberflächenabdichtung von Deponien - Geochemisches Langzeitverhalten und Schwermetall-Mobilität (Cd, Cu, Ni, Pb, Zn). Bremen, 1997.

No. 101 **Ebert, M.**
Der Einfluß des Redoxmilieus auf die Mobilität von Chrom im durchströmten Aquifer. 135 pages, Bremen, 1997.

No. 102 **Krögel, F.**
Einfluß von Viskosität und Dichte des Seewassers auf Transport und Ablagerung von Wattsedimenten (Langeooger Rückseitenwatt, südliche Nordsee). 168 pages, Bremen, 1997.

No. 103 **Kerntopf, B.**
Dinoflagellate Distribution Patterns and Preservation in the Equatorial Atlantic and Offshore North-West Africa. 137 pages, Bremen, 1997.

No. 104 **Breitzke, M.**
Elastische Wellenausbreitung in marinen Sedimenten - Neue Entwicklungen der Ultraschall Sedimentphysik und Sedimentechographie. 298 pages, Bremen, 1997.

No. 105 **Marchant, M.**
Rezente und spätquartäre Sedimentation planktischer Foraminiferen im Peru-Chile Strom. 115 pages, Bremen, 1997.

No. 106 **Habicht, K.S.**
Sulfur isotope fractionation in marine sediments and bacterial cultures. 125 pages, Bremen, 1997.

No. 107 **Hamer, K., R.v. Lührte, G. Becker, T. Felis, S. Keffel, B. Strotmann, C. Waschkowitz, M. Kölling, M. Isenbeck-Schröter, H.D. Schulz**
Endbericht zum Forschungsvorhaben 060 des Landes Bremen: Baggergut der Hafengruppe Bremen-Stadt: Modelluntersuchungen zur Schwermetallmobilität und Möglichkeiten der Verwertung von Hafenschlick aus Bremischen Häfen. 98 pages, Bremen, 1997.

No. 108 **Greeff, O.W.**
Entwicklung und Erprobung eines benthischen Landersystemes zur *in situ*-Bestimmung von Sulfatreduktionsraten mariner Sedimente. 121 pages, Bremen, 1997.

No. 109 **Pätzold, M. und G. Wefer**
Bericht über den 6. JGOFS-Workshop am 4./5.12.1997 in Bremen. Im Anhang: Publikationen zum deutschen Beitrag zur Joint Global Ocean Flux Study (JGOFS), Stand 1/1998. 122 pages, Bremen, 1998.

No. 110 **Landenberger, H.**
CoTReM, ein Multi-Komponenten Transport- und Reaktions-Modell. 142 pages, Bremen, 1998.

No. 111 **Villinger, H. und Fahrtteilnehmer**
Fahrtbericht SO 124, 4.10. - 16.10.199. 90 pages, Bremen, 1997.

No. 112 **Gietl, R.**
Biostratigraphie und Sedimentationsmuster einer nordostägyptischen Karbonatrampe unter Berücksichtigung der Alveolinen-Faunen. 142 pages, Bremen, 1998.

No. 113 **Ziebis, W.**
The Impact of the Thalassinidean Shrimp *Callianassa truncata* on the Geochemistry of permeable, coastal Sediments. 158 pages, Bremen 1998.

No. 114 **Schulz, H.D. and cruise participants**
Report and preliminary results of METEOR-Cruise M 41/1, Málaga - Libreville, 13.2.-15.3.1998. Bremen, 1998.

No. 115 **Völker, D.J.**
Untersuchungen an strömungsbeeinflußten Sedimentationsmustern im Südozean. Interpretation sedimentechographischer Daten und numerische Modellierung. 152 pages, Bremen, 1998.

No. 116 **Schlünz, B.**
Riverine Organic Carbon Input into the Ocean in Relation to Late Quaternary Climate Change. 136 pages, Bremen, 1998.

No. 117 **Kuhnert, H.**
Aufzeichnug des Klimas vor Westaustralien in stabilen Isotopen in Korallenskeletten. 109 pages, Bremen, 1998.

No. 118 **Kirst, G.**
Rekonstruktion von Oberflächenwassertemperaturen im östlichen Südatlantik anhand von Alkenonen. 130 pages, Bremen, 1998.

No. 119 **Dürkoop, A.**
Der Brasil-Strom im Spätquartär: Rekonstruktion der oberflächennahen Hydrographie während der letzten 400 000 Jahre. 121 pages, Bremen, 1998.

No. 120 **Lamy, F.**
Spätquartäre Variationen des terrigenen Sedimenteintrags entlang des chilenischen Kontinentalhangs als Abbild von Klimavariabilität im Milanković- und Sub-Milanković-Zeitbereich. 141 pages, Bremen, 1998.

No. 121 **Neuer, S. and cruise participants**
Report and preliminary results of POSEIDON-Cruise Pos 237/2, Vigo – Las Palmas, 18.3.-31.3.1998. 39 pages, Bremen, 1998

No. 122 **Romero, O.E.**
Marine planktonic diatoms from the tropical and equatorial Atlantic: temporal flux patterns and the sediment record. 205 pages, Bremen, 1998.

No. 123 **Spiess, V. und Fahrtteilnehmer**
Report and preliminary results of RV SONNE Cruise 125, Cochin – Chittagong, 17.10.-17.11.1997. 128 pages, Bremen, 1998.

No. 124 **Arz, H.W.**
Dokumentation von kurzfristigen Klimaschwankungen des Spätquartärs in Sedimenten des westlichen äquatorialen Atlantiks. 96 pages, Bremen, 1998.

No. 125 **Wolff, T.**
Mixed layer characteristics in the equatorial Atlantic during the late Quaternary as deduced from planktonic foraminifera. 132 pages, Bremen, 1998.

No. 126 **Dittert, N.**
Late Quaternary Planktic Foraminifera Assemblages in the South Atlantic Ocean: Quantitative Determination and Preservational Aspects. 165 pages, Bremen, 1998.

No. 127 **Höll, C.**
Kalkige und organisch-wandige Dinoflagellaten-Zysten in Spätquartären Sedimenten des tropischen Atlantiks und ihre palökologische Auswertbarkeit. 121 pages, Bremen, 1998.

No. 128 **Hencke, J.**
Redoxreaktionen im Grundwasser: Etablierung und Verlagerung von Reaktionsfronten und ihre Bedeutung für die Spurenelement-Mobilität. 122 pages, Bremen 1998.

No. 129 **Pätzold, J. and cruise participants**
Report and preliminary results of METEOR-Cruise M 41/3, Vítoria, Brasil – Salvador de Bahia, Brasil, 18.4. - 15.5.1998. Bremen, 1999.

No. 130 **Fischer, G. and cruise participants**
Report and preliminary results of METEOR-Cruise M 41/4, Salvador de Bahia, Brasil – Las Palmas, Spain, 18.5. – 13.6.1998. Bremen, 1999.

No. 131 **Schlünz, B. und G. Wefer**
Bericht über den 7. JGOFS-Workshop am 3. und 4.12.1998 in Bremen. Im Anhang: Publikationen zum deutschen Beitrag zur Joint Global Ocean Flux Study (JGOFS), Stand 1/ 1999. 100 pages, Bremen, 1999.

No. 132 **Wefer, G. and cruise participants**
Report and preliminary results of METEOR-Cruise M 42/4, Las Palmas - Las Palmas - Viena do Castelo; 26.09.1998 - 26.10.1998. 104 pages, Bremen, 1999.

No. 133 **Felis, T.**
Climate and ocean variability reconstructed from stable isotope records of modern subtropical corals (Northern Red Sea). 111 pages, Bremen, 1999.

No. 134 **Draschba , S.**
North Atlantic climate variability recorded in reef corals from Bermuda. 108 pages, Bremen, 1999.

No. 135 **Schmieder, F.**
Magnetic Cyclostratigraphy of South Atlantic Sediments. 82 pages, Bremen, 1999.

No. 136 **Rieß, W.**
In situ measurements of respiration and mineralisation processes – Interaction between fauna and geochemical fluxes at active interfaces. 68 pages, Bremen, 1999.

No. 137 **Devey, C.W. and cruise participants**
Report and shipboard results from METEOR-cruise M 41/2, Libreville – Vitoria, 18.3. – 15.4.98. 59 pages, Bremen, 1999.

No. 138 **Wenzhöfer, F.**
Biogeochemical processes at the sediment water interface and quantification of metabolically driven calcite dissolution in deep sea sediments. 103 pages, Bremen, 1999.

No. 139 **Klump, J.**
Biogenic barite as a proxy of paleoproductivity variations in the Southern Peru-Chile Current. 107 pages, Bremen, 1999.

No. 140 **Huber, R.**
Carbonate sedimentation in the northern Northatlantic since the late pliocene. 103 pages, Bremen, 1999.

No. 141 **Schulz, H.**
Nitrate-storing sulfur bacteria in sediments of coastal upwelling. 94 pages, Bremen, 1999.

No. 142 **Mai, S.**
Die Sedimentverteilung im Wattenmeer: ein Simulationsmodell. 114 pages, Bremen, 1999.

No. 143 **Neuer, S. and cruise participants**
Report and preliminary results of Poseidon Cruise 248, Las Palmas - Las Palmas, 15.2.-26.2.1999.
45 pages, Bremen, 1999.

No. 144 **Weber, A.**
Schwefelkreislauf in marinen Sedimenten und Messung von *in situ* Sulfatreduktionsraten.
122 pages, Bremen, 1999.

No. 145 **Hadeler, A.**
Sorptionsreaktionen im Grundwasser: Unterschiedliche Aspekte bei der Modellierung des Transportverhaltens von Zink. 122 pages, 1999.

No. 146 **Dierßen, H.**
Zum Kreislauf ausgewählter Spurenmetalle im Südatlantik: Vertikaltransport und Wechselwirkung zwischen Partikeln und Lösung. 167 pages, Bremen, 1999.

No. 147 **Zühlsdorff, L.**
High resolution multi-frequency seismic surveys at the Eastern Juan de Fuca Ridge Flank and the Cascadia Margin – Evidence for thermally and tectonically driven fluid upflow in marine sediments. 118 pages, Bremen 1999.

No. 148 **Kinkel, H.**
Living and late Quaternary Coccolithophores in the equatorial Atlantic Ocean: response of distribution and productivity patterns to changing surface water circulation. 183 pages, Bremen, 2000.

No. 149 **Pätzold, J. and cruise participants**
Report and preliminary results of METEOR Cruise M 44/3, Aqaba (Jordan) - Safaga (Egypt) – Dubá (Saudi Arabia) – Suez (Egypt) - Haifa (Israel), 12.3.-26.3.-2.4.-4.4.1999. 135 pages, Bremen, 2000.

No. 150 **Schlünz, B. and G. Wefer**
Bericht über den 8. JGOFS-Workshop am 2. und 3.12.1999 in Bremen. Im Anhang:
Publikationen zum deutschen Beitrag zur Joint Global Ocean Flux Study (JGOFS), Stand 1/ 2000.
95 pages, Bremen, 2000.

No. 151 **Schnack, K.**
Biostratigraphie und fazielle Entwicklung in der Oberkreide und im Alttertiär im Bereich der Kharga Schwelle, Westliche Wüste, SW-Ägypten. 142 pages, Bremen, 2000.

No. 152 **Karwath, B.**
Ecological studies on living and fossil calcareous dinoflagellates of the equatorial and tropical Atlantic Ocean. 175 pages, Bremen, 2000.

No. 153 **Moustafa, Y.**
Paleoclimatic reconstructions of the Northern Red Sea during the Holocene inferred from stable isotope records of modern and fossil corals and molluscs. 102 pages, Bremen, 2000.

No. 154 **Villinger, H. and cruise participants**
Report and preliminary results of SONNE-cruise 145-1 Balboa – Talcahuana, 21.12.1999 – 28.01.2000.
147 pages, Bremen, 2000.

No. 155 **Rusch, A.**
Dynamik der Feinfraktion im Oberflächenhorizont permeabler Schelfsedimente. 102 pages, Bremen, 2000.

No. 156 **Moos, C.**
Reconstruction of upwelling intensity and paleo-nutrient gradients in the northwest Arabian Sea derived from stable carbon and oxygen isotopes of planktic foraminifera. 103 pages, Bremen, 2000.

No. 157 **Xu, W.**
Mass physical sediment properties and trends in a Wadden Sea tidal basin. 127 pages, Bremen, 2000.

No. 158 **Meinecke, G. and cruise participants**
Report and preliminary results of METEOR Cruise M 45/1, Malaga (Spain) - Lissabon (Portugal),
19.05. - 08.06.1999. 39 pages, Bremen, 2000.

No. 159 **Vink, A.**
Reconstruction of recent and late Quaternary surface water masses of the western subtropical Atlantic Ocean based on calcareous and organic-walled dinoflagellate cysts. 160 pages, Bremen, 2000.

No. 160 **Willems, H. (Sprecher), U. Bleil, R. Henrich, K. Herterich, B.B. Jørgensen, H.-J. Kuß, M. Olesch, H.D. Schulz,V. Spieß, G. Wefer**
Abschlußbericht des Graduierten-Kollegs Stoff-Flüsse in marine Geosystemen.
Zusammenfassung und Berichtszeitraum Januar 1996 - Dezember 2000. 340 pages, Bremen, 2000.

No. 161 **Sprengel, C.**
Untersuchungen zur Sedimentation und Ökologie von Coccolithophoriden im Bereich der Kanarischen Inseln: Saisonale Flussmuster und Karbonatexport. 165 pages, Bremen, 2000.

No. 162 **Donner, B. and G. Wefer**
Bericht über den JGOFS-Workshop am 18.-21.9.2000 in Bremen:
Biogeochemical Cycles: German Contributions to the International Joint Global Ocean Flux Study.
87 pages, Bremen, 2000.

No. 163 **Neuer, S. and cruise participants**
Report and preliminary results of Meteor Cruise M 45/5, Bremen – Las Palmas, October 1 – November 3, 1999. 93 pages, Bremen, 2000.

No. 164 **Devey, C. and cruise participants**
Report and preliminary results of Sonne Cruise SO 145/2, Talcahuano (Chile) - Arica (Chile), February 4 – February 29, 2000. 63 pages, Bremen, 2000.

No. 165 **Freudenthal, T.**
Reconstruction of productivity gradients in the Canary Islands region off Morocco by means of sinking particles and sediments. 147 pages, Bremen, 2000.

No. 166 **Adler, M.**
Modeling of one-dimensional transport in porous media with respect to simultaneous geochemical reactions in CoTReM. 147 pages, Bremen, 2000.

No. 167 **Santamarina Cuneo, P.**
Fluxes of suspended particulate matter through a tidal inlet of the East Frisian Wadden Sea (southern North Sea). 91 pages, Bremen, 2000.

No. 168 **Benthien, A.**
Effects of CO_2 and nutrient concentration on the stable carbon isotope composition of C37:2 alkenones in sediments of the South Atlantic Ocean. 104 pages, Bremen, 2001.

No. 169 **Lavik, G.**
Nitrogen isotopes of sinking matter and sediments in the South Atlantic. 140 pages, Bremen, 2001.

No. 170 **Budziak, D.**
Late Quaternary monsoonal climate and related variations in paleoproductivity and alkenone-derived sea-surface temperatures in the western Arabian Sea. 114 pages, Bremen, 2001.

No. 171 **Gerhardt, S.**
Late Quaternary water mass variability derived from the pteropod preservation state in sediments of the western South Atlantic Ocean and the Caribbean Sea. 109 pages, Bremen, 2001.

No. 172 **Bleil, U. and cruise participants**
Report and preliminary results of Meteor Cruise M 46/3, Montevideo (Uruguay) – Mar del Plata (Argentina), January 4 – February 7, 2000. Bremen, 2001.

No. 173 **Wefer, G. and cruise participants**
Report and preliminary results of Meteor Cruise M 46/4, Mar del Plata (Argentina) – Salvador da Bahia (Brazil), February 10 – March 13, 2000. With partial results of METEOR cruise M 46/2. 136 pages, Bremen, 2001.

No. 174 **Schulz, H.D. and cruise participants**
Report and preliminary results of Meteor Cruise M 46/2, Recife (Brazil) – Montevideo (Uruguay), December 2 – December 29, 1999. 107 pages, Bremen, 2001.

No. 175 **Schmidt, A.**
Magnetic mineral fluxes in the Quaternary South Atlantic: Implications for the paleoenvironment.
97 pages, Bremen, 2001.

No. 176 **Bruhns, P.**
Crystal chemical characterization of heavy metal incorporation in brick burning processes.
93 pages, Bremen, 2001.

No. 177 **Karius, V.**
Baggergut der Hafengruppe Bremen-Stadt in der Ziegelherstellung. 131 pages, Bremen, 2001.

No. 178 **Adegbie, A. T.**
Reconstruction of paleoenvironmental conditions in Equatorial Atlantic and the Gulf of Guinea Basins for the last 245,000 years. 113 pages, Bremen, 2001.

No. 179 **Spieß, V. and cruise participants**
Report and preliminary results of R/V Sonne Cruise SO 149, Victoria - Victoria, 16.8. - 16.9.2000.
100 pages, Bremen, 2001.

No. 180 **Kim, J.-H.**
Reconstruction of past sea-surface temperatures in the eastern South Atlantic and the eastern South Pacific across Termination I based on the Alkenone Method. 114 pages, Bremen, 2001.

No. 181 **von Lom-Keil, H.**
Sedimentary waves on the Namibian continental margin and in the Argentine Basin – Bottom flow reconstructions based on high resolution echosounder data. 126 pages, Bremen, 2001.

No. 182 **Hebbeln, D. and cruise participants**
PUCK: Report and preliminary results of R/V Sonne Cruise SO 156, Valparaiso (Chile) - Talcahuano (Chile), March 29 - May 14, 2001. 195 pages, Bremen, 2001.

No. 183 **Wendler, J.**
Reconstruction of astronomically-forced cyclic and abrupt paleoecological changes in the Upper Cretaceous Boreal Realm based on calcareous dinoflagellate cysts. 149 pages, Bremen, 2001.

No. 184 **Volbers, A.**
Planktic foraminifera as paleoceanographic indicators: production, preservation, and reconstruction of upwelling intensity. Implications from late Quaternary South Atlantic sediments. 122 pages, Bremen, 2001.

No. 185 **Bleil, U. and cruise participants**
Report and preliminary results of R/V METEOR Cruise M 49/3, Montevideo (Uruguay) - Salvador (Brasil), March 9 - April 1, 2001. 99 pages, Bremen, 2001.

No. 186 **Scheibner, C.**
Architecture of a carbonate platform-to-basin transition on a structural high (Campanian-early Eocene, Eastern Desert, Egypt) – classical and modelling approaches combined. 173 pages, Bremen, 2001.

No. 187 **Schneider, S.**
Quartäre Schwankungen in Strömungsintensität und Produktivität als Abbild der Wassermassen-Variabilität im äquatorialen Atlantik (ODP Sites 959 und 663): Ergebnisse aus Siltkorn-Analysen. 134 pages, Bremen, 2001.

No. 188 **Uliana, E.**
Late Quaternary biogenic opal sedimentation in diatom assemblages in Kongo Fan sediments. 96 pages, Bremen, 2002.

No. 189 **Esper, O.**
Reconstruction of Recent and Late Quaternary oceanographic conditions in the eastern South Atlantic Ocean based on calcareous- and organic-walled dinoflagellate cysts. 130 pages, Bremen, 2001.

No. 190 **Wendler, I.**
Production and preservation of calcareous dinoflagellate cysts in the modern Arabian Sea. 117 pages, Bremen, 2002.

No. 191 **Bauer, J.**
Late Cenomanian – Santonian carbonate platform evolution of Sinai (Egypt): stratigraphy, facies, and sequence architecture. 178 pages, Bremen, 2002.

No. 192 **Hildebrand-Habel, T.**
Die Entwicklung kalkiger Dinoflagellaten im Südatlantik seit der höheren Oberkreide. 152 pages, Bremen, 2002.

No. 193 **Hecht, H.**
Sauerstoff-Optopoden zur Quantifizierung von Pyritverwitterungsprozessen im Labor- und Langzeit-in-situ-Einsatz. Entwicklung - Anwendung – Modellierung. 130 pages, Bremen, 2002.

No. 194 **Fischer, G. and cruise participants**
Report and Preliminary Results of RV METEOR-Cruise M49/4, Salvador da Bahia – Halifax, 4.4.-5.5.2001. 84 pages, Bremen, 2002.

No. 195 **Gröger, M.**
Deep-water circulation in the western equatorial Atlantic: inferences from carbonate preservation studies and silt grain-size analysis. 95 pages, Bremen, 2002.

No. 196 **Meinecke,G. and cruise participants**
Report of RV POSEIDON Cruise POS 271, Las Palmas - Las Palmas, 19.3.-29.3.2001. 19 pages, Bremen, 2002.

No. 197 **Meggers, H. and cruise participants**
Report of RV POSEIDON Cruise POS 272, Las Palmas - Las Palmas, 1.4.-14.4.2001. 19 pages, Bremen, 2002.

No. 198 **Gräfe, K.-U.**
Stratigraphische Korrelation und Steuerungsfaktoren Sedimentärer Zyklen in ausgewählten Borealen und Tethyalen Becken des Cenoman/Turon (Oberkreide) Europas und Nordwestafrikas. 197 pages, Bremen, 2002.

No. 199 **Jahn, B.**
Mid to Late Pleistocene Variations of Marine Productivity in and Terrigenous Input to the Southeast Atlantic. 97 pages, Bremen, 2002.

No. 200 **Al-Rousan, S.**
Ocean and climate history recorded in stable isotopes of coral and foraminifers from the northern Gulf of Aqaba. 116 pages, Bremen, 2002.

No. 201 **Azouzi, B.**
Regionalisierung hydraulischer und hydrogeochemischer Daten mit geostatistischen Methoden. 108 pages, Bremen, 2002.

No. 202 **Spieß, V. and cruise participants**
Report and preliminary results of METEOR Cruise M 47/3, Libreville (Gabun) - Walvis Bay (Namibia), 01.06 - 03.07.2000. 70 pages, Bremen 2002.

No. 203 **Spieß, V. and cruise participants**
Report and preliminary results of METEOR Cruise M 49/2, Montevideo (Uruguay) - Montevideo, 13.02 - 07.03.2001. 84 pages, Bremen 2002.

No. 204 **Mollenhauer, G.**
Organic carbon accumulation in the South Atlantic Ocean: Sedimentary processes and glacial/interglacial Budgets. 139 pages, Bremen 2002.

No. 205 **Spieß, V. and cruise participants**
Report and preliminary results of METEOR Cruise M49/1, Cape Town (South Africa) - Montevideo (Uruguay), 04.01.2000 - 10.02.2000. 57 pages, Bremen, 2003.

No. 206 **Meier, K.J.S.**
Calcareous dinoflagellates from the Mediterranean Sea: taxonomy, ecology and palaeoenvironmental application. 126 pages, Bremen, 2003.

No. 207 **Rakic, S.**
Untersuchungen zur Polymorphie und Kristallchemie von Silikaten der Zusammensetzung $Me_2Si_2O_5$ (Me:Na, K). 139 pages, Bremen, 2003.

No. 208 **Pfeifer, K.**
Auswirkungen frühdiagenetischer Prozesse auf Calcit- und Barytgehalte in marinen Oberflächen-sedimenten. 110 pages, Bremen, 2003.

No. 209 **Heuer, V.**
Spurenelemente in Sedimenten des Südatlantik. Primärer Eintrag und frühdiagenetische Überprägung. 136 pages, Bremen, 2003.

No. 210 **Streng, M.**
Phylogenetic Aspects and Taxonomy of Calcareous Dinoflagellates. 157 pages, Bremen 2003.

No. 211 **Boeckel, B.**
Present and past coccolith assemblages in the South Atlantic: implications for species ecology, carbonate contribution and palaeoceanographic applicability. 157 pages, Bremen, 2003.

No. 212 **Precht, E.**
Advective interfacial exchange in permeable sediments driven by surface gravity waves and its ecological consequences. 131 pages, Bremen, 2003.

No. 213 **Frenz, M.**
Grain-size composition of Quaternary South Atlantic sediments and its paleoceanographic significance. 123 pages, Bremen, 2003.

No. 214 **Meggers, H. and cruise participants**
Report and preliminary results of METEOR Cruise M 53/1, Limassol - Las Palmas – Mindelo, 30.03.2002 - 03.05.2002. 81 pages, Bremen, 2003.

No. 215 **Schulz, H.D. and cruise participants**
Report and preliminary results of METEOR Cruise M 58/1, Dakar – Las Palmas, 15.04..2003 - 12.05.2003. Bremen, 2003.

No. 216 **Schneider, R. and cruise participants**
Report and preliminary results of METEOR Cruise M 57/1, Cape Town – Walvis Bay, 20.01. – 08.02.2003. 123 pages, Bremen, 2003.

No. 217 **Kallmeyer, J.**
Sulfate reduction in the deep Biosphere. 157 pages, Bremen, 2003.

No. 218 **Røy, H.**
Dynamic Structure and Function of the Diffusive Boundary Layer at the Seafloor. 149 pages, Bremen, 2003.

No. 219 **Pätzold, J., C. Hübscher and cruise participants**
Report and preliminary results of METEOR Cruise M 52/2&3, Istanbul – Limassol – Limassol, 04.02. – 27.03.2002. Bremen, 2003.

No. 220 **Zabel, M. and cruise participants**
Report and preliminary results of METEOR Cruise M 57/2, Walvis Bay – Walvis Bay, 11.02. – 12.03.2003. 136 pages, Bremen 2003.

No. 221 **Salem, M.**
Geophysical investigations of submarine prolongations of alluvial fans on the western side of the Gulf of Aqaba-Red Sea. 100 pages, Bremen, 2003.

No. 222 **Tilch, E.**
Oszillation von Wattflächen und deren fossiles Erhaltungspotential (Spiekerooger Rückseitenwatt, südliche Nordsee). 137 pages, Bremen, 2003.

No. 223 **Frisch, U. and F. Kockel**
Der Bremen-Knoten im Strukturnetz Nordwest-Deutschlands. Stratigraphie, Paläogeographie, Strukturgeologie. 379 pages, Bremen, 2004.

No. 224 **Kolonic, S.**
Mechanisms and biogeochemical implications of Cenomanian/Turonian black shale formation in North Africa: An integrated geochemical, millennial-scale study from the Tarfaya-LaAyoune Basin in SW Morocco. 174 pages, Bremen, 2004. Report online available only.

No. 225 **Panteleit, B.**
Geochemische Prozesse in der Salz- Süßwasser Übergangszone. 106 pages, Bremen, 2004.

No. 226 **Seiter, K.**
Regionalisierung und Quantifizierung benthischer Mineralisationsprozesse. 135 pages, Bremen, 2004.

No. 227 **Bleil, U. and cruise participants**
Report and preliminary results of METEOR Cruise M 58/2, Las Palmas – Las Palmas (Canary Islands, Spain), 15.05. – 08.06.2003. 123 pages, Bremen, 2004.

No. 228 **Kopf, A. and cruise participants**
Report and preliminary results of SONNE Cruise SO175, Miami - Bremerhaven, 12.11 - 30.12.2003. 218 pages, Bremen, 2004.

No. 229 **Fabian, M.**
Near Surface Tilt and Pore Pressure Changes Induced by Pumping in Multi-Layered Poroelastic Half-Spaces.
121 pages, Bremen, 2004.

No. 230 **Segl, M. , and cruise participants**
Report and preliminary results of POSEIDON cruise 304 Galway – Lisbon, 5. – 22. Oct. 2004, 27 pages, Bremen 2004

No. 231 **Meinecke, G. and cruise participants**
Report and preliminary results of POSEIDON Cruise 296, 42 pages, Bremen 2005.

No. 232 **Meinecke, G. and cruise participants**
Report and preliminary results of POSEIDON Cruise 310, 49 pages, Bremen 2005.

No. 233 **Meinecke, G. and cruise participants**
Report and preliminary results of METEOR Cruise 58/3, Bremen 2005.

No. 234 **Feseker, T.**
Numerical Studies on Groundwater Flow in Coastal Aquifers. 219 pages. Bremen 2004.

No. 235 **Sahling, H. and cruise participants**
Report and preliminary results of R/V POSEIDON Cruise P317/4, Istanbul-Istanbul , 16 October - 4 November 2004. 92 pages, Bremen 2004.

No. 236 **Meinecke, G. und Fahrtteilnehmer**
Report and preliminary results of POSEIDON Cruise 305, Las Palmas (Spain) - Lisbon (Portugal), October 28th – November 6th, 2003. 43 pages, Bremen 2005.

No. 237 **Ruhland, G. and cruise participants**
Report and preliminary results of POSEIDON Cruise 319, Las Palmas (Spain) - Las Palmas (Spain), December 6th – December 17th, 2004. 50 pages, Bremen 2005.

No. 238 **Chang, T.S.**
Dynamics of fine-grained sediments and stratigraphic evolution of a back-barrier tidal basin of the German Wadden Sea (southern North Sea). 102 pages, Bremen 2005.

No. 239 **Lager, T.**
Predicting the source strength of recycling materials within the scope of a seepage water prognosis by means of standardized laboratory methods. 141 pages, Bremen 2005.

No. 240 **Meinecke, G.**
DOLAN - Operationelle Datenübertragung im Ozean und Laterales Akustisches Netzwerk in der Tiefsee. Abschlußbericht. 42 pages, Bremen 2005.

No. 241 **Guasti, E.**
Early Paleogene environmental turnover in the southern Tethys as recorded by foraminiferal and organic-walled dinoflagellate cysts assemblages. 203 pages, Bremen 2005.

No. 242 **Riedinger, N.**
Preservation and diagenetic overprint of geochemical and geophysical signals in ocean margin sediments related to depositional dynamics. 91 pages, Bremen 2005.

No. 243 **Ruhland, G. and cruise participants**
Report and preliminary results of POSEIDON cruise 320, Las Palmas (Spain) - Las Palmas (Spain), March 08th - March 18th, 2005. 57 pages, Bremen 2005.

No. 244 **Inthorn, M.**
Lateral particle transport in nepheloid layers – a key factor for organic matter distribution and quality in the Benguela high-productivity area. 127 pages, Bremen, 2006.

No. 245 **Aspetsberger, F.**
Benthic carbon turnover in continental slope and deep sea sediments: importance of organic matter quality at

different time scales. 136 pages, Bremen, 2006.

No. 246 **Hebbeln, D. and cruise participants**
Report and preliminary results of RV SONNE Cruise SO-184, PABESIA, Durban (South Africa) – Cilacap (Indonesia) – Darwin (Australia), July 08th - September 13th, 2005. 142 pages, Bremen 2006.

No. 247 **Ratmeyer, V. and cruise participants**
Report and preliminary results of RV METEOR Cruise M61/3. Development of Carbonate Mounds on the Celtic Continental Margin, Northeast Atlantic. Cork (Ireland) – Ponta Delgada (Portugal), 04.06. – 21.06.2004. 64 pages, Bremen 2006.

No. 248 **Wien, K.**
Element Stratigraphy and Age Models for Pelagites and Gravity Mass Flow Deposits based on Shipboard XRF Analysis. 100 pages, Bremen 2006.

No. 249 **Krastel, S. and cruise participants**
Report and preliminary results of RV METEOR Cruise M65/2, Dakar - Las Palmas, 04.07. - 26.07.2005. 185 pages, Bremen 2006.